Thermal Stability of Al_2O_3/Silicone Composites as High-Temperature Encapsulants

Yiying Yao

Dissertation submitted to the faculty of the Virginia Polytechnic Institute and State University in partial fulfillment of the requirement for the degree of

Doctor of Philosophy

In

Materials Science and Engineering

Guo Quan Lu, Committee Chair

Khai D. Ngo

Abby R. Whittington

Carlos T.A. Suchicital

September 22, 2014

Blacksburg, VA

Keywords: High-temperature packaging, power electronic packaging, encapsulant, thermal stability, silicone elastomer, composites, thermal degradation, weight loss, dielectric strength, hydrogen bond, chain mobility

Thermal Stability of Al_2O_3/Silicone Composites as High-Temperature Encapsulants

Yiying Yao

Abstract

Conventional microelectronic and power electronic packages based on Si devices usually work below 150°C. The emergence of wide-bandgap devices, which potentially operate above a junction temperature of 250°C, results in growing research interest in high-density and high-temperature packaging. There are high-temperature materials such as encapsulants on the market that are claimed for capability of continuous operation at or above 250°C. With an objective of identifying encapsulants suitable for packaging wide-bandgap devices, some of commercial high-temperature encapsulants were obtained and evaluated at the beginning of this study.

The evaluation revealed that silicone elastomers are processable for various types of package structure and exhibit excellent dielectric performance in a wide temperature range (25 - 250°C) but are insufficiently stable against long-term aging (used by some manufacturers, e.g., P^2SI, to evaluate polymer stability) at 250°C. These materials cracked during aging, causing their dielectric strength to decrease quickly (as soon as 3 days) and significantly (60 - 70%) to approximately 5 kV/mm, which is below the value required by semiconductor packaging. The results of this evaluation clearly suggested that silicone needs higher thermal stability to reliably encapsulate wide-bandgap devices.

Literature survey then investigated possible methods to improve silicone stability. Adding fillers is reported to be effective possibly due to the interaction between filler

surface and polymer chains. However, the interaction mechanism is not clearly documented. In this study, the effect of Al_2O_3 filler on thermal stability was first investigated by comparing the performance of unfilled and Al_2O_3-filled silicones in weight-loss measurements and dielectric characterization. All test results on composites filed with Al_2O_3 micro-rods indicated that thermal stability increased with increasing filler loading. Thermogravimetric analysis (TGA) test demonstrated that the temperature of degradation onset increased from 330 to 379°C with a 30 wt% loading of Al_2O_3 rods. In isothermal soak test, unfilled and 30-wt%-filled silicones lost 10% of polymer weight in 700 and 1800 hours, respectively. The dielectric characterization found that both Weibull parameters, characteristic dielectric strength (E_0, representing the electric field at which 62.3% of samples are electrically broken down) and shape parameter (β, representing the spread of data. The larger the β, the narrower the distribution) can reflect the thermal stability of polymers. Both of them were influenced by microstructure evolution, to which β was found to be more sensitive than E_0. The characteristic dielectric strength of unfilled silicone decreased significantly after 240 hours of aging at 250°C, whereas that of Al_2O_3/silicone composites exhibited no significant change within 560 hours. The shape parameter of Al_2O_3-filled silicone decreased slower than that of unfilled silicone, also indicating the positive effect of Al_2O_3 micro-rods on thermal stability.

Improved thermal stability can be explained by restrained chain mobility caused by interfacial hydrogen bonds, which are formed between hydroxyl groups on Al_2O_3 surface and silicone backbone. In this study, the effect of hydrogen bonds was investigated by dehydrating Al_2O_3 micro-rods at high temperature in N_2 to partially destroy the bonds. Removal of hydrogen bonds impaired thermal stability by increasing the initial weight-

loss rate from 0.025 to 0.036 wt%/hour. The results explained the importance of interfacial hydrogen bond, which effectively reduced the average chain mobility, hindered the formation of degradation products, and led to higher thermal stability.

The main discoveries of this study are listed below:

1. Al_2O_3 micro-rods were found to efficiently improve the thermal stability of silicone elastomer used for high-temperature encapsulation.

2. Characteristic dielectric strength and shape parameter obtained from Weibull distribution reflected the change of material microstructure caused by thermal aging. The shape parameter was found to be more sensitive to microscale defects, which were responsible for dielectric breakdown at low electric field.

3. Hydrogen bonds existing at filler/matrix interface were proven to be responsible for the improvement of thermal stability because they effectively restrained the average chain mobility of the silicone matrix.

Happiness

Is a Point of View

Acknowledgements

This work is supported by the office of naval research (under award No. N00014-07-1-0777), Rolls Royce, and the high-density integration (HDI) mini-consortium of the center for power electronics systems (CPES).

I would like to express my greatest gratitude to my advisors Dr. Guo-Quan Lu and Dr. Khai Ngo for support and guidance in my studies. I would also like to thank Dr. Dushan Boroyevich and Dr. Fred Wang for their support over the years. I'm very grateful to the technical support from Dr. Justin Barone and Mr. Devin Ridgley of the Department of Biological Systems Engineering and Dr. Robert Moore, Dr. Bruce Orler, and Ms. Amanda Hudson of the Department of Chemistry of Virginia Tech. I am also grateful to my colleagues: Dr. Puqi Ning, Dr. Wenli Zhang, Dr. Thomas Lei, Dr. Kewei Xiao, Li Jiang, Hanguang Zheng, Yi Yan, and many others. Special thanks go to those who make me stronger than I could ever imagine.

Finally, but also most importantly, my deepest gratitude and love belong to my dearest husband, Dr. Zheng Chen, who supports me as a colleague and walks me through my difficult days.

Table of Contents

List of Figures

List of Tables

Chapter 1. Introduction

1.1. Introduction

1.1.1.Encapsulation in power electronic module

Components on circuit boards or in electronic modules are commonly covered with polymeric encapsulants (Fig. 1-1) to protect them against adverse environmental conditions (e.g., moisture, contaminants, mobile ions, radiations, and mechanical damages) and to increase their reliability [1, 2]. Moisture can cause corrosion of integrated circuit (IC) devices and is also responsible for electro-oxidation and metal migration in the packages [2]. Mobile ions can destroy the semiconductor devices by re-

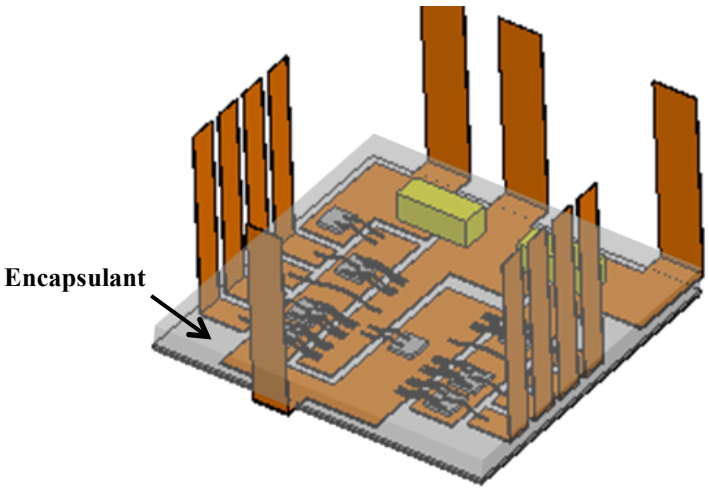

Fig. 1-1. High-temperature SiC module with encapsulation.

depositing on p-n junctions [2] and degrading oxide layers (Na^+ and K^+) [3] or by dissolving aluminum metallization (Cl^-) [2]. With low content of moisture and ions (typically a few ppm or less), polymeric encapsulants improve the manufacturing yields and the reliability of the electronic modules. In power electronics, a high dielectric strength (> 10 kV/mm or 250 V/mil for most encapsulants) is required to prevent breakdown in the package [4]. A relatively high thermal conductivity (> 1 W/m-K) is also preferred to conduct the heat away from the components.

1.1.2.Operation temperature of encapsulants for conventional packages

The fundamental limitation to use semiconductor devices at high temperature is their increasing density of intrinsic carriers with increasing temperature. The increase in carrier density produces an increase of leakage current in p-n diodes, a decrease of gain in bipolar transistors, shifts in the threshold voltage of MOSFETs, etc. [4]. Si-based power devices usually cannot operate above 175°C. Conventional encapsulants designed for such devices work also in the same temperature range (typically, -55 to 175°C).

1.1.3.Wide-bandgap devices with high-temperature capability

Wide-bandgap semiconductors, such as silicon carbide (SiC) and gallium nitride (GaN), offer multiple advantages for high-temperature power electronics.

Taking SiC as an example, it has a bandgap energy of 3.2 eV (4H-SiC), which is approximately three times of that of Si (1.1 eV). The wide bandgap guarantees a negligibly small concentration of intrinsic carrier compared to that of the dopants and therefore a small leakage current even at high temperature (> 800°C) [5]. SiC also has a high critical electric field (2.0 MV/cm for SiC compared to 0.3 MV/cm for Si), which significantly increases the blocking capability and thus reduces on-state resistance by

allowing thin and highly doped drift layers [6, 7]. Moreover, the high thermal conductivity of SiC (490 W/m-K for SiC compared to 150 W/m-K for Si) improves heat transfer within the device and reduces the risk of device overheating even at high ambient temperature. For example, heat transfer in SiC is approximately three times quicker than in Si due to the difference in their thermal conductivity. All these advantages of SiC enable high-temperature power devices with maximum junction temperature (T_{jmax}) > 300°C [5]. Commercial high-temperature SiC power transistors with T_{jmax} up to 250°C are already available on the market [8, 9]. The emergence of such high-temperature devices results in growing research interest in high-density and high-temperature packaging.

1.2. Recommended properties of encapsulation

1.2.1.Categories of encapsulation

Semiconductor encapsulation can be in the form of conformal coatings, underfills, molding compounds, and potting compounds [10, 11].

Conformal coating is a thin layer of polymer sprayed, spin-coated, or vapor-deposited onto circuit board. The two key functions of such coatings are environmental protection (e.g., against moisture, chemicals, contaminations, radiations, physical abuse, etc.) and electrical insulation [12]. Good adhesion, with the help of adhesion promoters, between the coating material and the substrates/components is crucial to realize these functions. Other requirements for the coating materials include strong chemical resistance, excellent electrical properties, low stress on components, etc. [12]. Chemically, low moisture adsorption is generally preferred because water vapor existing in most ambient environments could have a detrimental effect on reliability. Electrically, a high dielectric

strength is required to prevent premature breakdown. Mechanically, the coating should either have a coefficient of thermal expansion (CTE) matching those of the components or be soft and elastic in nature to avoid high internal stress.

Underfills and molding compounds are both rigid encapsulants. In addition to protection against chemical species and electrical stress, they can also enhance the reliability by reducing and redistributing thermo-mechanical stresses caused by mismatch of CTE [13-16]. When selecting these encapsulants, their CTE need to be as close to those of other components as possible. The typical CTE of underfills and molding compounds (below glass-transition temperature, T_g) range from ten to a few tens of ppm/K [17-19]. Regarding general chip-scale packaging for power electronics, the preferred CTE is 20 - 30 ppm/K for underfills [14, 20-22] and < 20 ppm/K for molding compounds [20].

Potting compounds are usually rubbery or gel-like encapsulants that electrically and chemically protect the circuit components without exerting too much stress on them [11, 23, 24]. In some cases, however, rigid materials (resins) are also used for potting. Glob tops, which serve for the same purpose, can also be either resins or rubbers. High dielectric strength and low moisture absorption are required to guarantee sufficient electrical insulation and chemical resistance. Rubbers and gels usually exert minor stress on chips, wires, and other components due to their low hardness and storage modulus as well as their excellent elasticity and resilience [11, 23, 24]. Since these characteristics greatly limit their mechanical protection against external forces [1], an outer case of metal or rigid plastic is usually applied for “soft” rubbers and gels. Glob tops are expected to provide some mechanical support in addition to electrical and chemical

protection. Their storage modulus is likely to be higher than that of potting compounds. Resins usually have high storage modulus, which can cause high thermo-mechanical stress when CTE-mismatch occurs between encapsulant and circuit components [4, 22]. Therefore, resin-based potting compounds and glob tops are preferred to have a CTE matching that of other circuit components.

1.2.2.Recommended properties of encapsulants

Appropriate encapsulants can ensure package reliability and increase production yield. The selection criteria are not definite, but should match the conditions of applications. For general applications, the recommended properties of the four types of encapsulants are summarized in TABLE 1-1.

TABLE 1-1
CATEGORIES AND RECOMMENDED PROPERTIES OF ENCAPSULANTS

	Properties	Conformal coating	Underfill	Molding compound	Potting compound and glob top
Electrical	E_{BD} (at working temperature)	≥ 20 kV/mm (500 V/mil)	> 10 kV/mm (250 V/mil)		
	Relative permittivity, ε_r (at working temperature)	< 5 [11]			
Physical	Moisture absorption	< 1% weight gain in 85°C/85RH [14, 16]			
	T_g	N/A	> Maximum application temperature [4, 20]		N/A
	Viscosity (at ~25°C)	N/A	< 20 Pa-sec at room temperature	Low at elevated temperature	< 50 Pa-sec at room temperature
	Pot life (at processing temperature)	Short (< 30 min)	8 - 24 hours [25]	N/A	8 - 24 hours [25]
Mechanical	CTE (at working temperature)	N/A	20 - 30 ppm/K [14, 20-23]	< 20 ppm/K [20]	N/A
	Elastic Modulus (at working temperature)	N/A	4 - 10 GPa		N/A

1.2.3.Requirement for high-temperature operation

Emergence of wide-bandgap devices results in a growing interest in high-density and high-temperature packaging. The encapsulants must also be able to operate at such temperature with sufficient reliability. Two aspects need to be satisfied to fulfill the reliability requirement. The recommended properties (listed in TABLE 1-1) should be retained throughout the entire temperature range of operation. Taking dielectric strength, which usually decreases with increasing temperature, as an example, it should not fall below the recommended value even at the maximum operation temperature. The materials must also not suffer from significant degradation or decomposition during operation, i.e., the material properties should be retained throughout the entire timeframe of operation.

For resin-based materials, including underfills, molding compounds, and some conformal coatings and potting compounds, the glass-transition temperature is an important parameter to consider during material selection. Both CTE and storage modulus (*E'*) of polymers are sensitive to temperature, especially within the glass-transition region, as shown in Fig. 1-2. CTE and *E'* change dramatically when temperature increases from below to above T_g, causing higher thermo-mechanical stresses (maybe hundreds times higher) within the transition region and impairing the long-term reliability [4]. The usage of these materials above their T_g is therefore not recommended [4, 22]. Gel- and rubber-based materials, including most potting compounds and some conformal coatings, are commonly made of silicones with a T_g no higher than -100°C. As long as the minimum operation temperature is above T_g, the properties of these materials (especially storage modulus and CTE) should not experience

significant change throughout the entire temperature range of operation.

High-temperature operation also tends to accelerate the degradation processes of polymers, including increase of crosslinking density and chemical decomposition. Considering the long-term reliability, the encapsulants are required to retain their properties over time even when subject to periodic or constant high-temperature exposure.

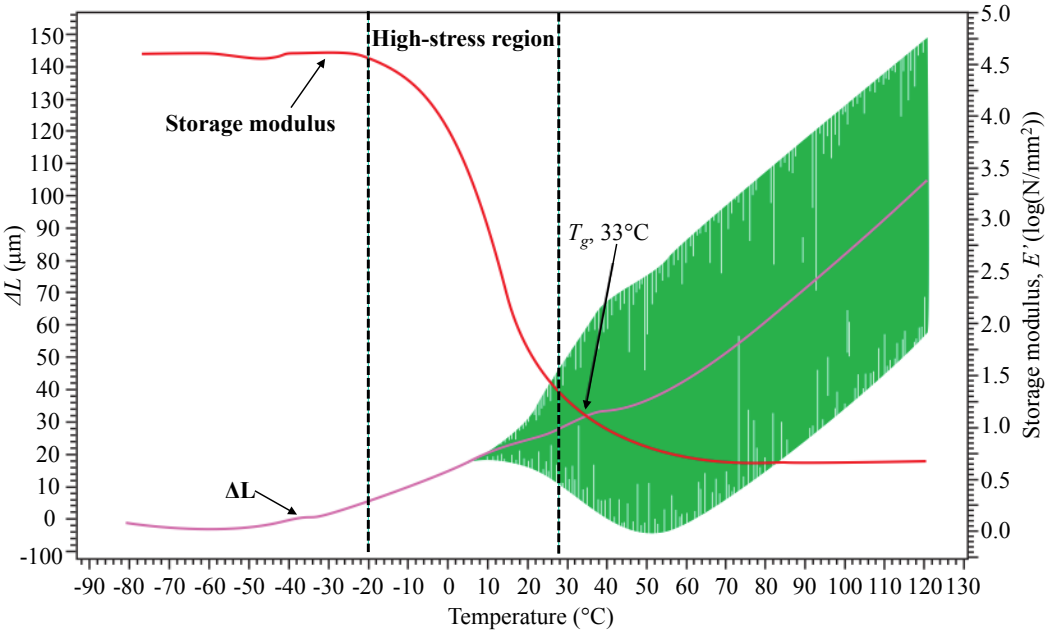

Fig. 1-2. Variation of storage modulus and coefficient of thermal expansion (CTE) of polymer with temperature.

1.3. Survey of commercial encapsulants

Commercial high-temperature encapsulants are surveyed in this session. Conformal coatings, underfills, molding compounds, and potting compounds are studied separately. The survey found that almost all encapsulants are able to operate at low temperature (≤ -65°C). Depending on the specific chemical composition and structure, the maximum operation temperature of these encapsulants varies. The survey focuses on crucial properties listed in technical datasheets, such as chemistry, range of operation

temperature, and dielectric strength. Commercial products with relatively high-temperature capability regarding their chemistry are highlighted in the survey results.

1.3.1.Conformal coatings

The typical ranges of dielectric strength and application temperature of commercial conformal coatings are plotted in Fig. 1-3, with several high-temperature products highlighted. Silicone, parylene HT, polyimide (PI), and benzocyclobutenes (BCB) have potential of high-temperature applications up to 350°C.

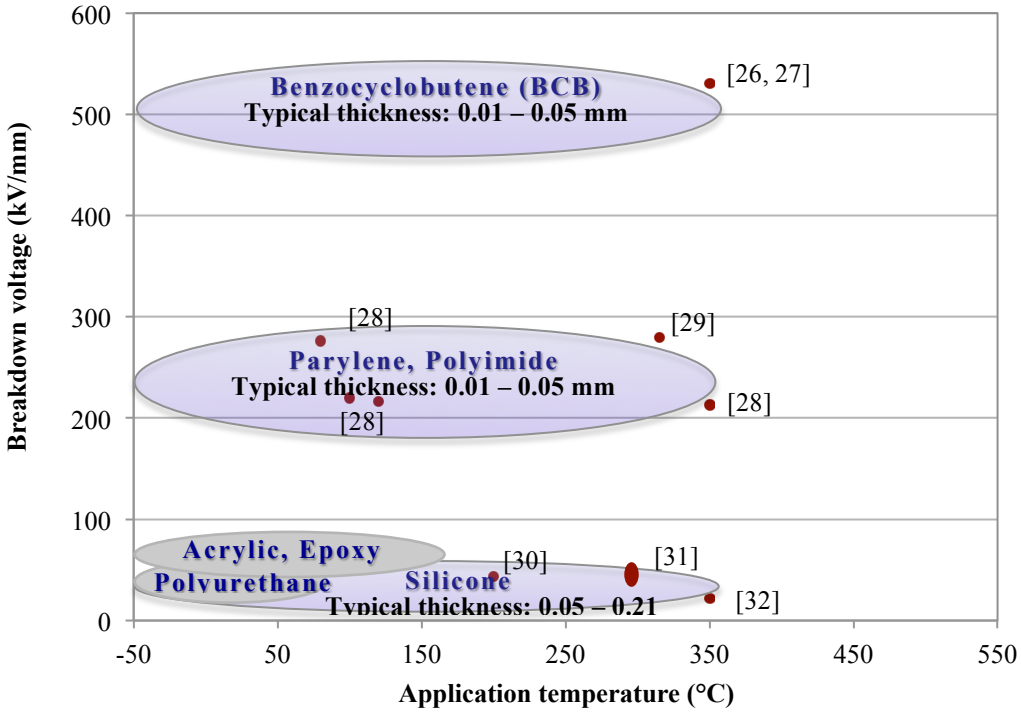

Fig. 1-3. Dielectric strength and maximum operation temperature of commercial conformal coatings.

Benzocyclobutene, parylene, and polyimide are usually applied in the thickness range of 10 - 50 μm, for which a dielectric strength of ≥ 200 kV/mm (5000 V/mil) is commonly observed. Silicone is usually applied in the thickness range of 50 - 210 μm. The typical dielectric strength for silicone-based conformal coatings is ≤ 40 kV/mm (1000 V/mil). Parylene needs to be synthesized and deposited via chemical vapor deposition (CVD)

[28] and can hardly fill into a package with complicated structure, such as a plate-bonded module. BCB and PI prior to cure may flow into gaps existing in electronic module if they have reasonable viscosity at processing temperature. These two types of materials were therefore selected for evaluation in Chapter 2.

1.3.2. Underfills and molding compounds

Fig. 1-4 plots the typical ranges of dielectric strength and application temperature of commercial underfills and molding compounds. Compared to bismaleimide (BMI), polyimide, and cyanate ester (CE), epoxy generally works at a lower temperature range due to the limitation of their glass-transition temperature, which is usually below 200°C [17, 33-36]. Since most high-temperature materials (TECOLITE, BMI, PI, etc.) are not designed for semiconductor packaging, information on their dielectric strength is rather limited. The several products marked on the figure are all electrically isolative, with their

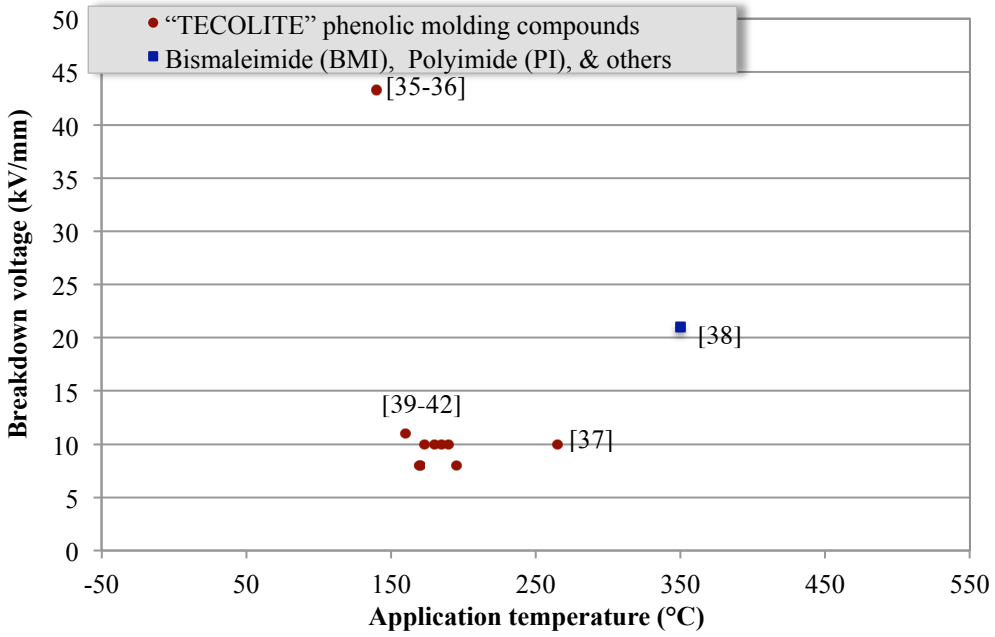

Fig. 1-4. Dielectric strength and maximum operation temperature of commercial underfills and molding compounds.

dielectric strength ranging from 10 to 43 kV/mm (250 to 1100 V/mil). Commercial BMI-, PI-, and CE-based molding compounds, which all have T_g above 250°C, are usually sold in prepreg form and require special processing techniques such as resin-transfer molding and injection molding to avoid voiding in the encapsulated module. These materials were not evaluated in Chapter 2 due to the difficulty of processing.

1.3.3.Potting compounds and glob tops

Dielectric strength and application temperature of commercial potting compounds and glob tops are plotted in Fig. 1-5. Epoxy usually has a T_g below 200°C, limiting their maximum operation temperature below that. Silicones are usually claimed for high-temperature operation (generally 300°C, and up to 350°C) [43-50]. The dielectric strength of these commercial materials usually falls into a narrow range of 12 - 28 kV/mm (300 - 700 V/mil) and may decrease 30% - 40% when temperature increases, as

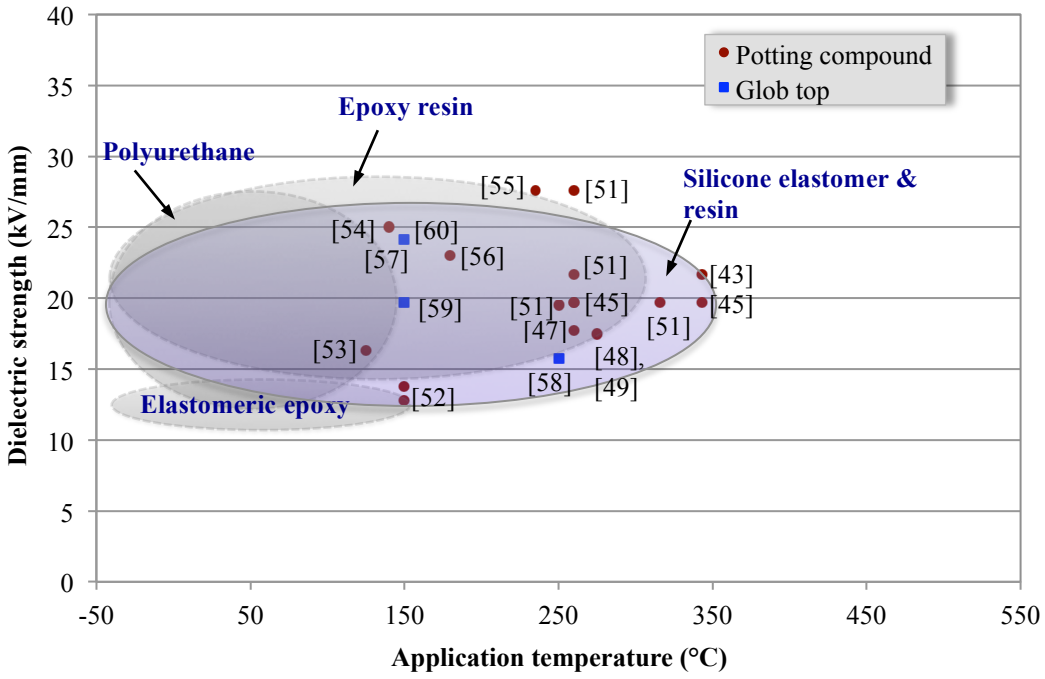

Fig. 1-5. Dielectric strength and maximum operation temperature of commercial glob tops and potting compounds.

shown in Fig. 1-6. These values are much lower compared to the ones exhibited by conformal coatings. This can be explained by the thickness difference between potting encapsulation and conformal coatings. Thin coatings usually contain smaller and fewer defects, which lead to higher dielectric strength than bulk materials [61]. Silicone based resins and rubbers that are claimed for high-temperature (at or above 300°C) operation were selected for evaluation in Chapter 2.

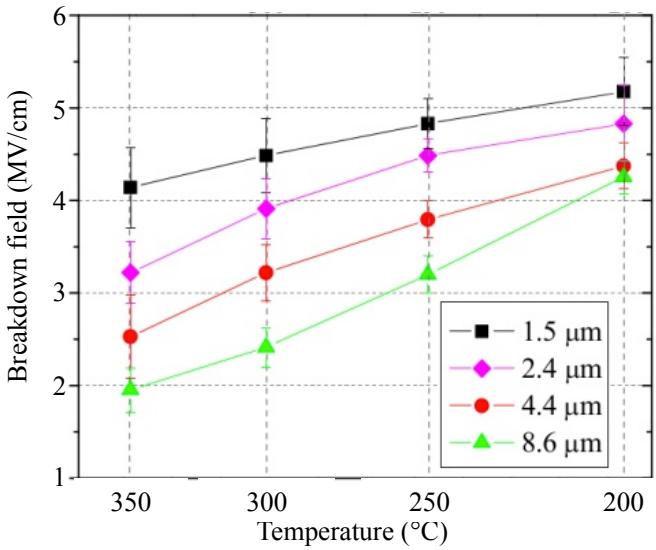

Fig. 1-6. Change of dielectric strength of polyimide with respect to temperature and thickness [62].

1.4. Selection of encapsulants

This work aims to look for high-temperature (≥ 250°C) encapsulants for the recently developed wide-bandgap power devices. Several packaging technologies may be used for high-temperature SiC devices, including conventional wire-bonded packages and the recently developed ribbon-bonded and plate-bonded ones. This work focuses on encapsulants that are suitable for all these packaging structures. The encapsulants are expected to maintain properties required by TABLE 1-1 throughout the entire application period. Using a material with uncertain thermal stability could risk the reliability of the

entire module. Since the reliability data (e.g., weight-loss percentage during temperature-sweep thermogravimetric (TGA) test or during isothermal soaking) is usually missing from their technical datasheets, commercial high-temperature materials need to be tested before being applied into a high-temperature module.

Since the thermo-mechanical stress experienced by circuit components is a product of the storage modulus of encapsulant and the strain from CTE-mismatch, two types of encapsulants are considered compatible with high-temperature (250°C) packaging. The first type is polymers with T_g higher than 250°C, for example, PI, BCB, etc. These materials work in their glassy state and exhibit small thermal expansion. The other type involves silicone-based rubbers and gels with T_g below -100°C. These materials work in rubbery state and exhibit small storage modulus (E'). The variation of E' from below to above T_g is exampled in Fig. 1-2. Based on the survey in Section 1.3, several commercial high-temperature encapsualnts were selected for further investigation. Their crucial properties are summarized in TABLE 1-2.

Epo-Tek 600 and Epo-Tek 390 (both manufactured by Epoxy Technology) are polyimide-based dielectrics used for electrical isolation and passivation (recommended

TABLE 1-2
PROPERTIES OF THE SEVEN ENCAPSULANTS SELECTED FOR EVALUATION

Material	T_g (°C)	CTE at 25°C (ppm/K)	Viscosity at 25°C (cP)	Application temperature (°C)	Dielectric strength (kV/mm)	Composition
A. Epo-Tek 600 [63]	260	10	160000	> 450	16.9	Polyimide
B. Epo-Tek 390 [64]	280	28	<1000	> 350	N/A	Polyimide
C. Cyclotene 3022 [26]	>350	42	260	≥ 350	530	Benzocyclobutene
D. CF-4721 [50]	N/A	N/A	125	≥ 300	19 - 30	Silicone resin
E. R-2188 [47]	<-55	N/A	12500	- 65 - 300	17.7	Silicone elastomer
F. EPM-2422 [43]	-120	490	3500	-65 - 300	21.7	Silicone elastomer
G. MasterSil 800 [46]	<-55	N/A	50000	-115 - 260	19.7	Silicone elastomer

for conformal coating of 10 - 50 μm but may be fabricated in thicker layer). Cyclotene 3022 (by Dow Chemical) is a benzocyclotene-based conformal coating for similar thickness but may also be fabricated in thicker layer. All these three materials are recommended for continuous operation at high temperature of 350°C or above. They have different dielectric strength but are all claimed for excellent electrical insulation (shown in Fig. 1-3). The high viscosity of Epo-Tek 600 (TABLE 1-2) is not considered hindrance to package filling because a material with even higher viscosity can be processed by techniques such as injection molding as long as the material satisfies the criteria (Chapter 2) to form void- and crack-free matrix in the module. CF-4721 is a silicone resin (by Nusil Technology) recommended for potting. R-2188, EPM-2422 (both by Nusil Technology) and MasterSil 800 (by Master Bond) are silicone elastomers recommended as potting compounds. Resins usually have a considerably larger storage modulus than rubbers (a few GPa compared to a few MPa), which leads to higher thermo-mechanical stress. The performance of CF-4721 can be compared with that of the three silicone rubbers to evaluate the suitability of resin- and rubber-/gel-based potting compounds for high-temperature power packaging.

Among the selected materials, silicone-based potting compounds (evaluated in Chapter 2) showed potential to work as high-temperature encapsulants but may not be sufficiently stable (dielectric strength falls below 10 kV/mm as silicone cracks, more than 70% degradation) if subject to prolonged heating at 250°C (within 500 hours), which could be the working condition of SiC power modules. Similar observation was reported by Locatelli *et al* [65], who evaluated two silicone encapsulants via dielectric characterization and isothermal weight-loss test. Isothermal weight-loss test performed at

250°C indicated that the silicone encapsulant degraded over time (~10% weight loss in 500 hours). Although the characteristic dielectric strength (obtained from Weibull distribution) of the silicone (freestanding film of approximately 0.8 mm thick) exhibited no significant change within 500 hours, the variation of shape parameter, which is proven to be more sensitive to material degradation (in Chapter 5), was not reported. The silicone evaluated by these authors seems to show a more stable dielectric performance than those reported in Chapter 2 because it experienced much less thermo-mechanical stress as a freestanding film. Encapsulants in real applications usually suffer from considerable thermo-mechanical stress due to CTE-mismatch between them and other circuit components.

1.5. Suggested methods to decelerate silicone decomposition

High-temperature encapsulants for packaging wide-bandgap devices are expected to have lower weight loss rate (change of weight percentage with respect to time, wt%/hour) and better crack resistance to maintain high dielectric strength (> 10 kV/mm) for longer time (e.g., > 500 hour, which is the time after which commercial high-temperature encapsulant exhibited severely degraded dielectric performance). The unstable performance of silicone (polysiloxane) at high temperature is caused by thermal degradation or decomposition, which is accelerated when the temperature increases. The degradation mechanisms of silicone and possible methods to decelerate the degradation process are explained in this section.

1.5.1.Decomposition mechanisms of polysiloxane

The highly flexible polysiloxane chains enable easy formation of local configurations that facilitate the inter- and intra-molecular reactions in the decomposition process [66],

which usually occurs via a variety of chemical processes, such as chain-scission, oxidation of hydrocarbon groups, etc. [67-69]. These chemical processes embrittle the material, cause higher stress in the package, and finally jeopardize the reliability of the assembly [70]. To understand the decomposition mechanisms of polysiloxane, the silicone structure is first reviewed.

Structure and characteristics of polysiloxane

The structural elements of polysiloxane include: (1) the siloxane bond (Si-O) as the main building block, (2) the exactly alternating arrangement of Si and O atoms within the entire molecule, and (3) the type and arrangement of organic substitutes attached to the main chain [66]. Fig. 1-7 shows the schematic of the most commonly used polysiloxane, polydimethylsiloxane (PDMS).

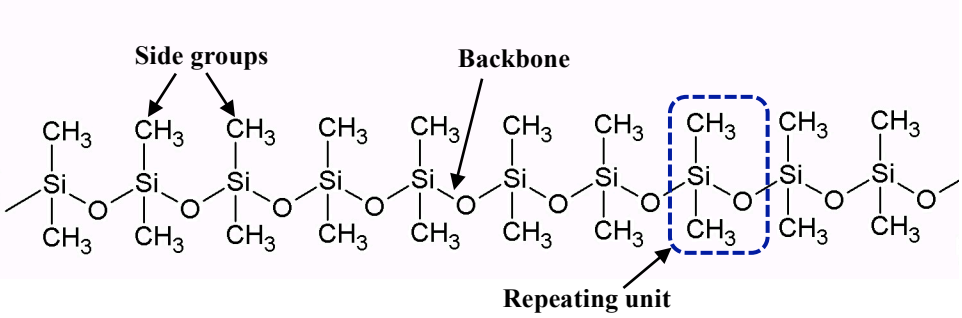

Fig. 1-7. Chemical structure of polydimethylsiloxane (PDMS).

The siloxane bond (Si-O) is a relatively long linkage with partial ionic and partial double-bond characters [66]. The ionic and double-bond characters result in the high bonding strength of Si-O bonds (dissociation energy = 465 kJ/mol [71], compared to 345 kJ/mol for C-C bonds) and hence their excellent performance in heat resistance. The length of the bond (usually 1.5 - 1.6 Å, compared to 1.3 - 1.4 Å for C-C single bonds) results in the unique flexibility even at low-temperature (≤ 40°C) [66].

Siloxane has the most flexible molecular chain known to polymer science [66]. The Si-O-Si bond is "soft" in nature: depending on the specific structure of polysiloxane, the bond angle ranges from as low as 104° up to almost 180°. Such "softness" enables considerable bending of polysiloxane chains at oxygen atoms. The O-Si-O bond is less flexible: depending again on the specific structure, the bond angle ranges from 102 to 112°. The relatively long Si-O bond provides increased spatial separation for neighboring substituents (side groups) and therefore releases molecular congestion. This effect is especially important for bulky substituents, such as methyl and phenyl. In PDMS, the rotation of methyl groups was found to occur at temperatures as low as -196°C [66].

Chemical decomposition

The decomposition of polysiloxanes is determined by their structural building blocks. Both bonding strength and chain flexibility are responsible for decomposition to occur. With a high dissociation energy of 465 kJ/mol, which is significantly higher than that of C-O bond (272 kJ/mol [72]) and C-C bond (345 kJ/mol), siloxane bond (Si-O) can withstand higher temperature without dissociation than many other organic bonds found in polymers and has a high thermal stability that is widely known to polymer science [66].

The flexibility of polysiloxane chains enables easy formation of local configurations that facilitate the inter- and intra-molecular reactions involved in the chemical decomposition process [66]. During reaction, Si-O bonds exchange with each other rather than directly break in the middle, scissoring the long polysiloxane backbone and forming cyclic products (exampled in Fig. 1-8), which are volatile due to the small molecular weight. Formation of cyclic products is favored by thermodynamics especially at high

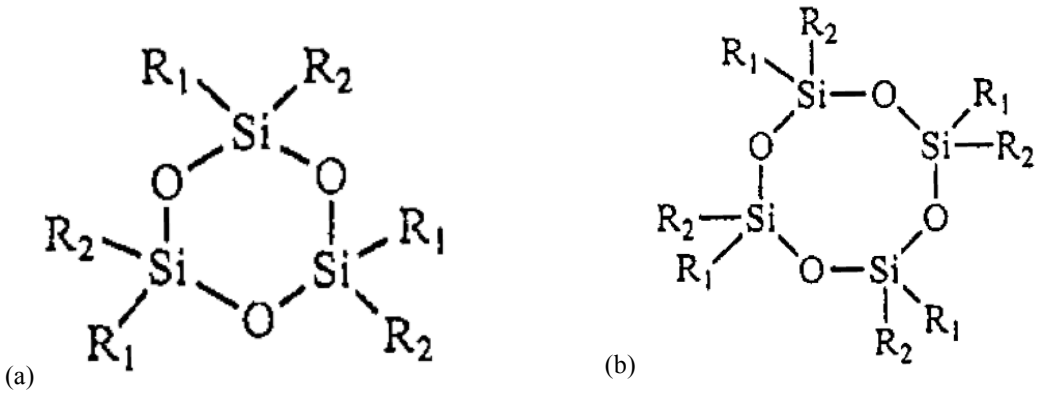

Fig. 1-8. Cyclic molecules generated during chemical decomposition: (a) with three Si-O units and (b) with four Si-O units.

temperature because they increase the entropy of the system. Considering its chain flexibility, the thermal stability of polysiloxane is considerably lower than what is predicted from the dissociation energy of siloxane bond. The chemical decomposition mechanisms of polysiloxane are widely documented [66-68]. As illustrated in Fig. 1-9, the decomposition occurs in multiple ways without involving chemicals in outer environment, i.e., the reaction occurs regardless of environment. Polysiloxane chains are sometimes manufactured with hydroxyl (–OH) terminals, which can catalyze the chain-scission (decomposition with the generation of cyclic products) process by bending back into the siloxane backbone and enabling bond exchange, as shown in Fig. 1-9 (a). Chain-scission can occur within a single polysiloxane chain, which folds to form a ring-like configuration prior to reaction (shown in Fig. 1-9 (b)). Favored by thermodynamics, bond exchange then completes the chain-scission process and produces a cyclic molecule. Chain scission can also occur between two polysiloxane chains, which are close enough to each other to enable bond exchange, as shown in Fig. 1-9 (c).

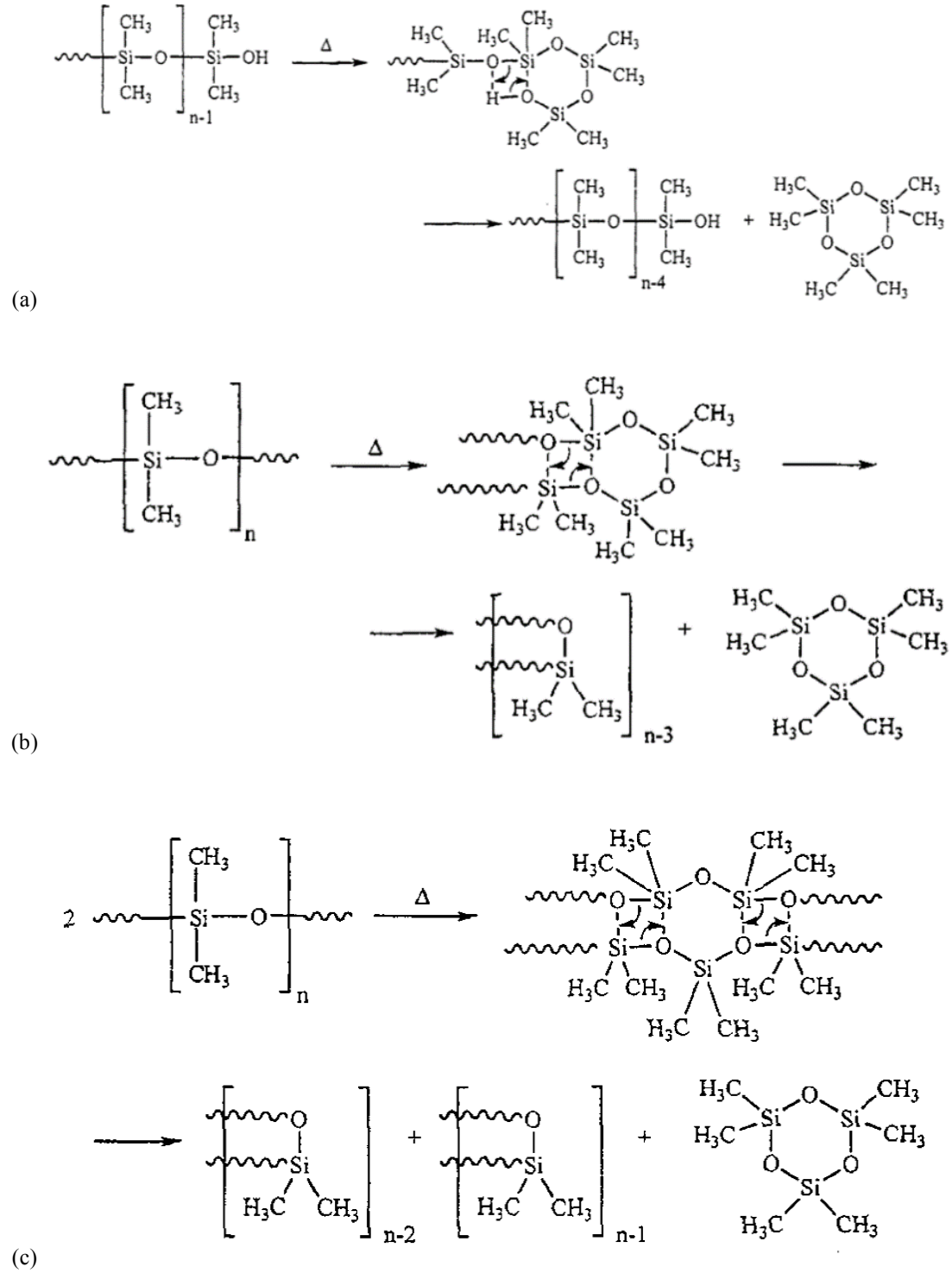

Fig. 1-9. Mechanisms of chemical decomposition of PDMS: (a) reaction initiated by –OHs at chain-ends, (b) reaction occurred in the middle of the chain, and (c) reaction occurred between two chains [66].

Thermo-oxidative degradation

In an oxygen-containing environment, thermo-oxidative degradation, which is accelerated by temperature, occurs in parallel with chemical decomposition. The oxidation mechanism of polysiloxane was reported by Camino *et al* [73]. CO_2 and H_2O are the degradation products of this reaction. Oxidation proceeds via a peroxidation process initiated by adventitious radical R•, such as "weak links" or impurity scission. Primary hydroperoxide is first generated during the process, as shown in Fig. 1-10. The hydroperoxide then undergoes further decomposition and produces CO_2 and H_2O, as shown in Fig. 1-11 [74]. The simplified reaction procedure is given in Fig. 1-12, which shows that thermo-oxidative degradation also leads to increased crosslinking density.

1.5.2.Effect of fillers on thermal stability

Thermal stability can be improved by adding fillers in many cases [75-90]. Fillers are suggested to interact with polymer matrix, reduce chain mobility, and decrease permeability of oxygen and degradation products [75,76, 80]. Adding fillers to polymer

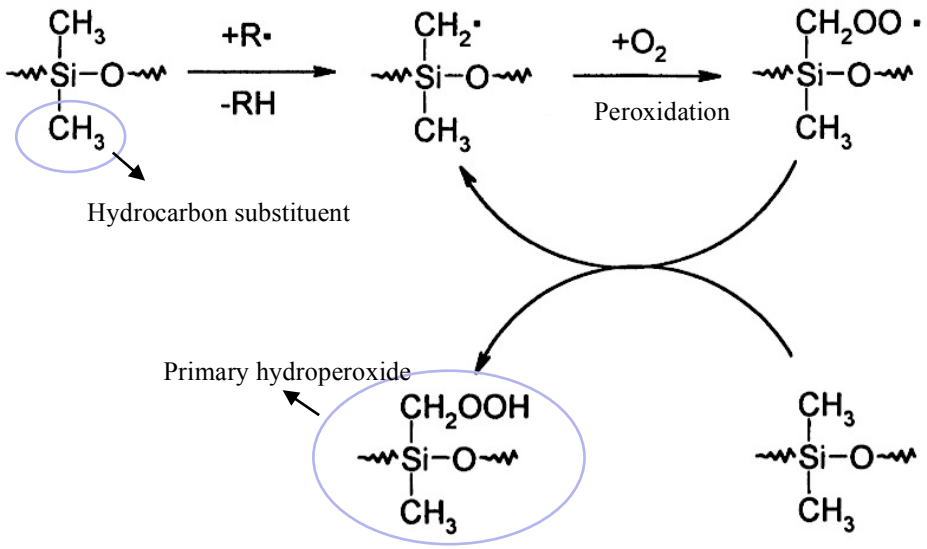

Fig. 1-10. Peroxidation of hydrocarbon substituent during thermo-oxidative degradation of PDMS [73].

matrix may also result in an increase of storage modulus (*E'*) and hardness, which is contradictory to the requirement (*E'* must be kept below a few MPa to prevent high stress on circuit components) mentioned in Section 1.2.2 [11, 23, 24]. According to (5) and (6) in [91], the change in modulus is linearly proportional to the fillers' volume percentage.

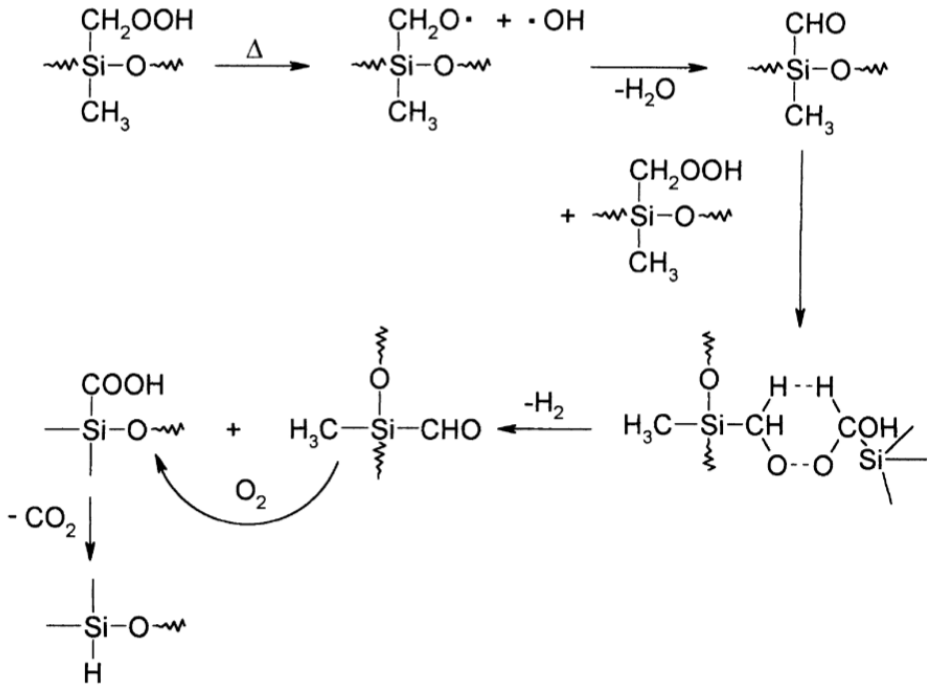

Fig. 1-11. Decomposition of hydroperoxide substituent PDMS [73, 74].

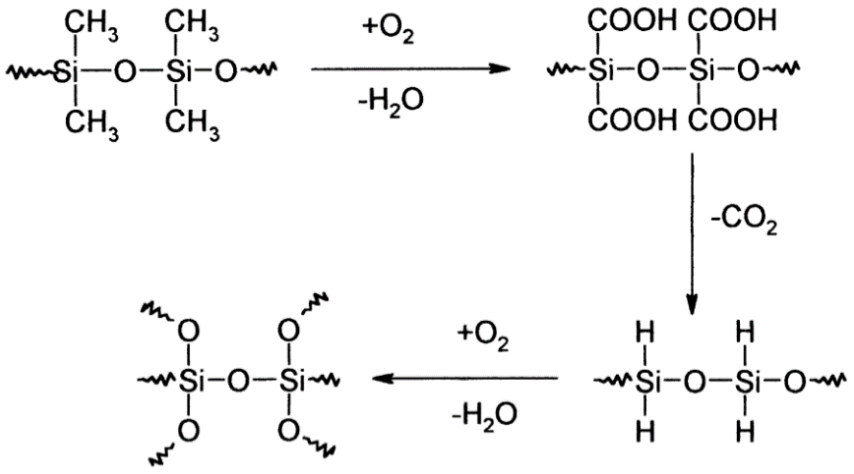

Fig. 1-12. Increase in crosslinking density caused by thermo-oxidative decomposition of PDMS [73].

Higher filler loading obviously results in higher modulus as well as higher hardness. Since the improvement of thermal stability mainly relies on the filler/matrix interaction, nanoscale fillers with high surface area per unit weight (or volume) are generally preferred over microscale ones [75].

The thermal stability of a polymer and its composites can be learned from TGA. The temperature at 5% weight loss is usually used as the indication of degradation onset [92-95]. Other criteria to determine degradation onset can be used as well, for example, the temperature at 1% weight loss. The effect of various fillers on the thermal stability of silicones was widely studied over the years [76-90, 92-97]. Among various fillers, silica (SiO_2) is the most widely used filler material in encapsulation industry [98]. The effect of silica fillers, either fused or in-situ precipitated, on thermal stability of polysiloxane has been studied by several research groups [77-79] with contradictory results. A fused silica (nanoscale)/silicone rubber system was studied by El-Hag *et al* [78], who reported that a slightly higher thermal stability was observed in the composite in an oxygen-containing (5%) atmosphere. A similar result was observed by Yang *et al* [79] for commercial nanoscale silica (25 nm), which contributed to thermal stability of silicone-based composites in an inert atmosphere. The effects of fumed and in-situ precipitated silica on thermal stability were compared by Sohoni *et al* [77], who reported that the thermal stability of silicone was improved by fumed silica in N_2 but was impaired by it in air and that in-situ precipitated silica led to higher thermal stability in either atmosphere. The results, summarized in TABLE 1-3, suggest that SiO_2 has potential to improve thermal stability of silicones. The variation in results may be caused by difference in surface conditions, such as chemistry, cleanliness, etc.

TABLE 1-3
EFFECT OF SiO_2 FILLERS ON ONSET TEMPERATURE OF SILICONE DEGRADATION

Reference	Material		Filler loading	Degradation onset
[78]	Silicone with nanoscale fume SiO_2 (12 nm)		0 wt%	415°C @ 5% weight loss
			5 wt%	477°C @ 5% weight loss
			10 wt%	477°C @ 5% weight loss
[79]	Polydimethylsiloxane (PDMS) with nanoscale SiO_2 (25 nm)		0 wt%	350°C @ deflection of weight loss curve
			25 wt%	404°C @ deflection of weight loss curve
[77]	PDMS with in-situ SiO_2		0 wt%	404°C (N_2), 371°C (air) @ 1% weight loss
			6.1 wt%	475°C (N_2), 381°C (air) @ 1% weight loss
	PDMS with commercial SiO_2	Fume (A130)	4.9 wt%	458°C (N_2), 372°C (air) @ 1% weight loss
		Fume (MOXSO)	4.9 wt%	418°C (N_2), 361°C (air) @ 1% weight loss

Improvement in thermal stability was also observed in silicone composites with other fillers, including Al_2O_3, BN (boron nitride), layered silicate (clay), [80-90, 96, 97]. Effects of Al_2O_3 fillers on thermal stability were reported in [80-83]. Significant increase in onset temperature of degradation was observed in [80-82], as summarized in TABLE 1-4. The improvement in thermal stability was also attributed to the restraint of chain mobility of polymer matrix. A minor effect of Al_2O_3 fillers on thermal stability of silicones was reported in [83] (shown in TABLE 1-4). The reason for the unsteady performance of fillers remains unclear. Suggested reasons, similar to those for silica fillers, include purity, dispersion, surface chemistry, etc. of fillers [75-77].

Layered silicate (clay)/silicone system is widely studied. The results are difficult to conclude due to the contradiction of results from various studies and the small difference in onset temperature reported by several groups (summarized in TABLE 1-5) [84-86, 96, 97]. A positive effect of layered silicate on thermal stability was reported by Garg *et al* [84]. Similar results were reported in [85, 86, 97] except that the authors observed a less stable system as filler loading went beyond certain value. A negative effect of layered

TABLE 1-4
EFFECT OF AL_2O_3 FILLERS ON ONSET TEMPERATURE OF SILICONE DEGRADATION.

Reference	Material	Filler loading	Degradation onset
[80]	Silicone rubber composites with microscale Al_2O_3 (3 - 20 μm)	0 wt%	425°C @ 5% weight loss
		44 wt%	525°C @ 5% weight loss
		55 wt%	540°C @ 5% weight loss
[81]	Silicone rubber with microscale Al_2O_3 (1 - 10 μm)	0 vol%	105°C @ 1% weight loss
		10 vol% (~30 wt%)	145°C @ 1% weight loss
[82]	Silicone resin with microscale Al_2O_3 (60 μm)	0 wt%	350°C @ 5% weight loss
		Not reported	540°C @ 5% weight loss
[83]	Silicone resin with nanoscale Al_2O_3 (40 - 47 nm)	0 wt%	359°C @ 3% weight loss
		1 wt%	364°C @ 3% weight loss
		3 wt%	355°C @ 3% weight loss
		5 wt%	350°C @ 3% weight loss
		7 wt%	356°C @ 3% weight loss

silicate on the thermal stability of silicone rubbers was reported by Kaneko *et al* [96]. The variation in results may be related to difference in degree of clay exfoliation. Since the improvement in thermal stability is possibly a result of restrained chain mobility, which mainly relies on the filler/matrix interaction, fully exfoliated clay, which has larger surface area to interact with polymer chains in matrix, is more likely to contribute to higher thermal stability.

1.5.3.Hypothesis of the deceleration mechanism

The literature survey suggests that incorporated fillers have potential to decelerate thermal decomposition of polysiloxanes, possibly by restraining the mobility of polymer chain via filler/matrix interaction. This argument is based on the hypothesis that physical or chemical bonds exist at the interface between polymer and filler surface. The interfacial bonds can alter the mobility of significant amount of polymer chains and therefore lead to reduction of the overall degradation rate.

TABLE 1-5
EFFECT OF EXFOLICATED CLAY FILLERS ON ONSET TEMPERATURE OF SILICONE DEGRADATION

Reference	Material	Filler loading	Degradation onset
[84]	Vinyl terminated PDMS with clay (Cloisite 30B)	0 wt%	430°C @ 10% weight loss
		1 wt%	510°C @ 10% weight loss
		3 wt%	512°C @ 10% weight loss
		5 wt%	510°C @ 10% weight loss
		10 wt%	507°C @ 10% weight loss
	Vinyl terminated PDMS with clay (Nanomer 1.30P)	1 wt%	480°C @ 10% weight loss
		3 wt%	500°C @ 10% weight loss
		5 wt%	485°C @ 10% weight loss
		10 wt%	500°C @ 10% weight loss
[85]	Silicone rubber with Fe-organo-montmorillonite	0 wt%	415°C @ 10% weight loss
		1 wt%	453°C @ 10% weight loss
		4 wt%	462°C @ 10% weight loss
		7 wt%	460°C @ 10% weight loss
[86]	Flame-retardant methyl vinyl silicone rubber (MVMQ) with montmorillonite	0 wt%	229.4°C @ 5% weight loss
		0.7 wt%	358.7°C @ 5% weight loss
		2.0 wt%	327.8°C @ 5% weight loss
		3.3 wt%	311.2°C @ 5% weight loss
		4.6 wt%	299.6°C @ 5% weight loss
[97]	Silicone rubber with organic montmorillonite	0 wt%	335.20°C, initial degradation
		5 wt%	347.89°C, initial degradation
		10 wt%	354.49°C, initial degradation
		20 wt%	292.75°C, initial degradation
[96]	PDMS rubber with natural montmorillonite	0 wt%	415°C @ 5% weight loss
		5 wt%	415°C @ 5% weight loss
		10 wt%	400°C @ 5% weight loss
		20 wt%	370°C @ 5% weight loss
		30 wt%	285°C @ 5% weight loss
	PDMS rubber with organic-modified montmorillonite	5 wt%	415°C @ 5% weight loss
		10 wt%	410°C @ 5% weight loss
		20 wt%	395°C @ 5% weight loss
		30 wt%	360°C @ 5% weight loss

Effect of chain mobility

As mentioned in Section 1.5.1, certain chain configurations (Fig. 1-9) facilitate the inter- and intra-molecular reactions of chemical decomposition. Since the formation of such configurations requires movement of polysiloxane chains such as bending, the chain mobility is a crucial factor affecting the degradation rate. If the chain motion is hindered by any means, formation of local configuration that facilitates decomposition within or between chains becomes more difficult. The chemical decomposition can therefore be decelerated.

Effect of fillers on the chain mobility

Fillers may reduce chain mobility if they absorb and anchor polysiloxane chains on their surface via interfacial bonding. The interfacial bond can be covalent bonds (chemical), hydrogen bonds (physical), or van der Waals force (physical). The possible mechanism for fillers to restrain the average mobility of polysiloxane chains is discussed in this session.

According to the model of Tsagaropoulos [99], each filler is surrounded by its own tightly and loosely bound layers, which contain chains with restrained mobility. Formation of interfacial bonds between filler surface and surrounding polymer chains is a prerequisite for the two layers to build up. With the existence of interfacial bonds, an adsorption layer (the tightly bound layer in the model of Tsagaropoulos) containing chain units nearest to the filler surface is built up, as shown in Fig. 1-13 [100]. Polymer chains in this layer are adsorbed on filler surface with either multiple (solid lines) or only a few (dashed lines) contacts [100]. Due to the multiple polymer-filler contacts, the mobility of polymer chains in the adsorption layer is strongly restricted. The thickness of this layer

depends on the type of filler and temperature and is estimated to be around 0.8 nm [100]. The existence of the adsorption layer was confirmed in [100, 101] by nuclear magnetic resonance (NMR). Sternstein *et al* [102] suggested that fillers have a far-field effect on the chain mobility, especially in polymers with high molecular weight. The far-field effect gives rise to a transition zone (shown in Fig. 1-13 [100]), in which polymer chains are crosslinked to or entangled with chain units in or close to the adsorption layer. The transition zone corresponds to the loosely bound layer in the model of Tsagaropoulos.

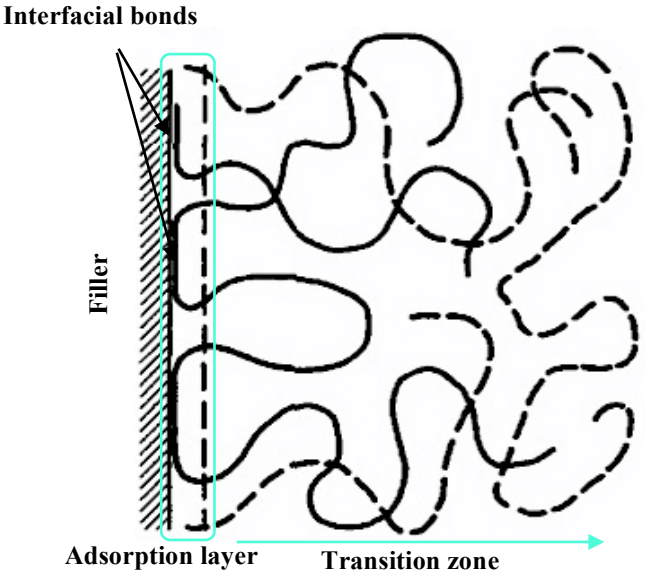

Fig. 1-13. Polymer chains adsorbed onto filler surface through interfacial bonding.

Fig. 1-14 shows the schematics of polymer-filler interaction according to the model of Tsagaropoulos [99, 103]. When filler loading is low, each filler particle is surrounded by its own tightly and loosely bound layers. No overlapping of loosely bound layer occurs due to the large inter-particle distance, as shown in Fig. 1-14 (a). As filler loading increases, inter-particle distance decreases accordingly. Since the thickness of tightly and loosely bound layers remains the same (before overlapping occurs), the amount of polymer chains with restrained mobility increases. At certain filler loading, inter-particle

distance becomes small enough for the neighboring loosely bound layers to overlap, as shown in Fig. 1-14 (b). When overlapping occurs, neighboring filler particles share their loosely bound layer and some chains are influenced by more than one particle. Such phenomenon is known as "bridging effect" or percolation [102], in which case the mobility of almost all chains is more or less affected by fillers. Further increase of filler loading obviously results in reduced thickness of loosely bound layer and more heavily restrained chains. With sufficient filler loading, it is possible that reduction in the average chain mobility is significant enough to decelerate the decomposition of polysiloxane.

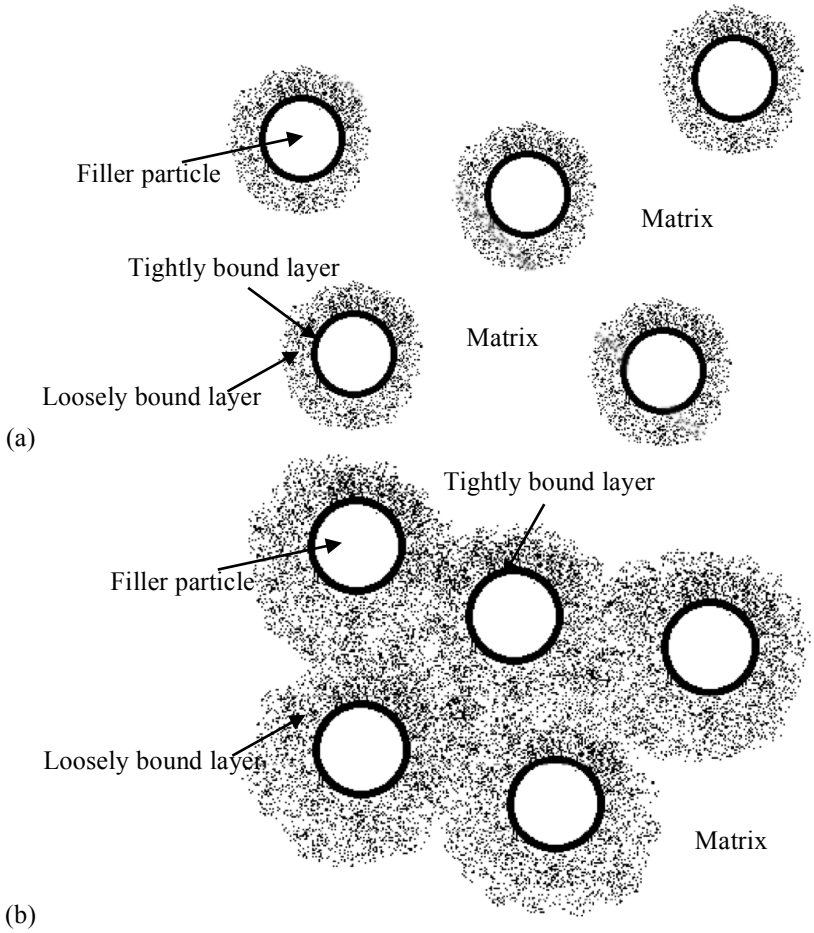

Fig. 1-14. Filler-matrix interaction described in the model of Tsagaropoulos: (a) at low filler loading and (b) at high filler loading [99].

1.6. Motivation and objectives

The interest in high-density and high-temperature packaging is now challenging conventional encapsulants, which are designed mainly for applications below 175°C. With a purpose of evaluating the suitability of commercial high-temperature encapsulants for packaging wide-bandgap power devices, some of these materials were obtained and experiment can provide information on long-term stability of commercial high-temperature encapsulants. The evaluation found that the obtained high-temperature materials degraded and cracked quickly when they were aged isothermally at 250°C. Due to the initiation and development of cracks, dielectric strength of these materials dropped significantly to only five kV/mm, which is approximately equal to that of the air. The observed changes in physical properties may be closely related to the degradation of chemical structures. The poor thermal stability revealed in the study should be considered inadequate for continuous operation at 250°C. The experiment also raises the question of how to improve thermal stability of encapsulants and to enable them to operate at higher temperature.

Fillers have potential to decelerate thermal decomposition of polymeric materials, possibly by restraining the mobility of polymer chains via chemical or physical adsorption [77-90]. Since the exact mechanism of how fillers improve thermal stability has not been fully understood, this study aims to address the effects of nano-scaled Al_2O_3 fillers on the thermal stability of silicone-based encapsulant. Since the chemical decomposition of silicone can usually be reflected by change of weight, the long-term stability of unfilled and Al_2O_3-filled silicones can be compared by soaking the materials isothermally. A material with higher thermal stability should exhibit lower rate of

chemical decomposition (weight-loss rate: wt%/hour). The impact of the interaction between Al_2O_3 fillers and silicone chains is also investigated to understand how to improve thermal stability and to fabricate high-temperature encapsulants in future.

Dielectric strength is another important parameter to consider in real applications. Since a material qualified for high-temperature operation should maintain a high dielectric strength (listed in TABLE 1-1) over time, this study also monitors the change in dielectric strength of unfilled and Al_2O_3-filled silicones with respect to time of isothermal soak. Change of dielectric strength is sensitive to the microstructure evolution during degradation. Results of dielectric characterization supplement the information on thermal stability provided by weight-loss measurement.

1.7. Summary of organization

Following this chapter, Chapter 2 evaluates seven commercial high-temperature encapsulants for their processability for planar module (the packaging structure that requires the highest processability) and their dielectric properties (dielectric strength and relative permittivity) with respect to temperature (25 - 250°C) and time (for isothermal soak at 250°C). Processability test aims to identify materials that are suitable for encapsulating power electronic modules in this study. The temperature dependence of dielectric properties is characterized from 25 to 250°C. The time dependence of dielectric properties is investigated by monitoring their variation during isothermal soaking at 250°C. A material with higher thermal stability is expected to maintain its dielectric properties for longer time during thermal soaking (aging).

To improve thermal stability of commercial silicone encapsulant, Chapter 3 describes the material selection and procedure for sample preparation. Nano-scaled Al_2O_3 fillers

and silicone elastomer were used to make Al_2O_3/silicone composites with various compositions. As-prepared materials are characterized for their viscosity and microstructure in this chapter and are ready for measurements of thermal stability, which are presented in Chapters 4 and 5.

Chapter 4 compares the thermal stability of unfilled and Al_2O_3-filled silicones by performing weight-loss experiments, which include TGA in linear temperature-sweep mode and isothermal soak test at 250°C. The effect of Al_2O_3 fillers on thermal stability is discussed by investigating the molecular interaction at Al_2O_3/silicone interface. Formation of interfacial bonds is expected to restrain the mobility of polymer chains and decelerate the degradation process. Since hydrogen bonds are known to form between hydroxyls (-OHs) on Al_2O_3 surface and silicone chain, the effect of these bonds on thermal stability is discussed in this chapter.

Chapter 5 compares the thermal stability of unfilled and Al_2O_3-filled silicones by monitoring the change of their dielectric strength with respect to time of isothermal soak (aging). Dielectric failure closely relates to the defects existed in material matrix. Degradation of silicone can cause the initiation and growth of defects (cracks and voids), which make the material more vulnerable to electric stress due to impaired integrity. To better explain the difference in dielectric behavior of unfilled and Al_2O_3-filled silicones, evolution of their microstructure (initiation and growth of defects) is monitored and discussed. The results can also reflect the difference in thermal stability of unfilled and Al_2O_3-filled silicones.

Chapter 6 summarizes the main conclusions of this dissertation and proposes potential future work.

Chapter 2. Evaluation of Commercial Encapsulants

2.1. Introduction

Conventional microelectronic and power electronic packages based on Si devices usually work below 150°C. The reliability of conventional encapsulants [25, 104], solders [105], and substrates [106] is found inadequate in extended temperature range (above 200°C). The emergence of wide-bandgap devices, which potentially operate above a junction temperature of 250°C, results in growing research interest in high-density and high-temperature packaging [107-109].

Since the wider application temperature range challenges conventional encapsulants, which are designed mainly for applications below 175°C, identifying encapsulants for high-temperature application is necessary. With a targeted temperature extreme of 250°C, commercial encapsulants are evaluated in this chapter for their processability as well as their temperature- and time-dependence dielectric properties (dielectric strength and permittivity). Processability test aims to identify materials that are suitable for encapsulating power electronic modules in this study. Dielectric characterization reveals how dielectric strength and permittivity change with respect to temperature from 25 to 250°C. Thermal stability examines the change of dielectric properties during isothermal soaking at 250°C. The results of this evaluation lead to a problem statement questioning

the thermal stability (at 250°C) of commercial silicone-based encapsulants. Efforts to improve their thermal stability are therefore described in the following chapters of this dissertation.

2.2. Evaluation of encapsulants

2.2.1.Processability

Conventional wire-bonded packages and the recently developed ribbon-bonded and plate-bonded ones can be used to package SiC power devices. The structure of all these types of package could include crevices of a few tens of micrometers, across which a high voltage drop (1.2 kV or higher) may exist. The encapsulants are responsible to prevent any partial discharge of air in those regions. This requires encapsulants to form no or only negligible cracks or voids within the entire package and thus to have good processability to guarantee the uniformity and integrity of themselves and to achieve the capability of electrical insulation (> 10 kV/mm) required by high-voltage power devices.

Since plate-bonded package requires the best processability of encapsulants among the three packaging structures, the processability of each selected material as encapsulant for this package was mainly investigated. Materials found un-processable for planar packages may be used for other types of packages if they satisfy the requirement specified in TABLE 1-1 and result in packages with acceptable insulation capability.

Processability tests were designed to evaluate the flowability and curability of selected encapsulants. Flowability reveals the shape of flow front and the as-flowed texture of each material. Encapsulants that cannot entirely fill the tester within reasonable time (e.g., ≤ 15 min) were considered un-processable, because such material should also experience difficulty of filling an electronic package (regardless of package type). Curability

indicates the degree of volume shrinkage and the change in material texture during the curing process. For a variety of crosslinked polymers, the curing process is similar: viscosity gradually increases as the chemical reaction goes on, featuring an increase in the average length of oligomers and in the degree of crosslinking density between them. As a three-dimensional network is formed upon the completion of curing, the cured material is hardened and no longer flowable. The texture formed after curing was considered as the material's curability, which is a significant parameter for the selection of an appropriate encapsulant. Electrical breakdown occurs through the "weakest link" existing in the material matrix and is thus sensitive to defects such as voids and cracks. Partial discharge of air can occur at an electric field (< 10 kV/mm) much lower than the breakdown strength of polymer. Since electrical insulation is a required property for power module, a dielectric breakdown test was therefore used to confirm the importance of good processability on its insulation capability. In the breakdown test, the dielectric strength of the encapsulated sample, which was designed to simulate the planar package by attaching the four corners of silicon chip to direct bonded copper (DBC) substrate, was measured. DBC substrate is commonly used for power electronics, which is fabricated through a high-temperature process to achieve an intimate bond between copper and the ceramic in an inert atmosphere [110]. The copper foils and the ceramic substrate are heated to a temperature of about 1070°C (slightly below the melting point of Cu) in nitrogen. The copper oxide forms a eutectic melt that wets at this temperature and produces a strong bond between copper and ceramic when cooled.

The dielectric strength measured via this method was the dielectric behavior of the test sample encapsulated with certain type of material, rather than that of the material itself. If

a crack and/or void (sized a few micrometers or larger) exists in the encapsulant, partial discharge of air can occur in such defect at an electric field lower than 10 kV/mm, causing breakdown to occur at a low electric field (usually 5 - 10 kV/mm) through the linkage of defects (weakest pathway) even though the dielectric strength of the crack- and void-free material is much higher (e.g., 20 kV/mm). By comparing the dielectric strength of the test sample and that of the material encapsulating the sample, the relationship between the processability of a material and the overall dielectric strength of the package encapsulated with that material can be recognized.

Flowability

In the materials flow test, a glass chip measured 6 mm × 6 mm was used. The glass piece was chosen because of the transparency of glass and the similarity of materials' wetting behavior (surface tension: 890 and 1000 mN/m for silver and glass, respectively, compared to 24 and 40 mN/m for silicone and polyimide) on glass and metal surfaces. The transparency of the glass chip allowed direct observation of the material's flowing behavior throughout the processability test.

The glass chip was attached to silver-plated DBC substrate with double-sided Kapton® tapes (approximately 100 μm in thickness, close to the usual thickness of solder in a package) to simulate that a semiconductor chip is soldered on the substrate, as shown in Fig. 2-1. The metallization on DBC surface was achieved by nickel electro-plating on cleaned DBC surface, immediately followed by silver electro-plating on the nickel surface. DBC substrate was cleaned with DI water prior to plating. The substrate was then connected to the electrode and immersed in plating solution (composition documented in [111]), as shown in Fig. 2-2. The plating parameters were 10 A/cm^2 and

10 min for Ni and 20 A/cm^2 and 15 min for Ag. The designed structure created a gap that was thin, long, and deep (0.1 mm × 6 mm × 6 mm) and was comparable to that may exist in a plate-bonded module. This sample structure greatly challenged the flow property of the material under test. Once a material was confirmed to be able to flow from one side of the chip to the other, it could be confidently considered as passing the materials flowability test (for all packaging types).

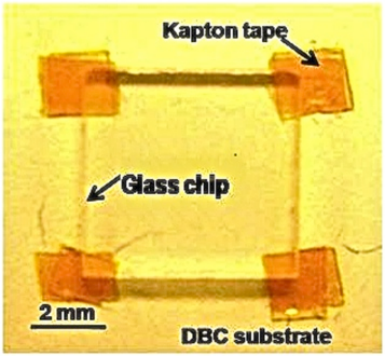

Fig. 2-1. Processability tester: 6 mm × 6 mm glass chip mounted on silver-plated DBC substrate with double-sided Kapton® tape of 0.1 mm.

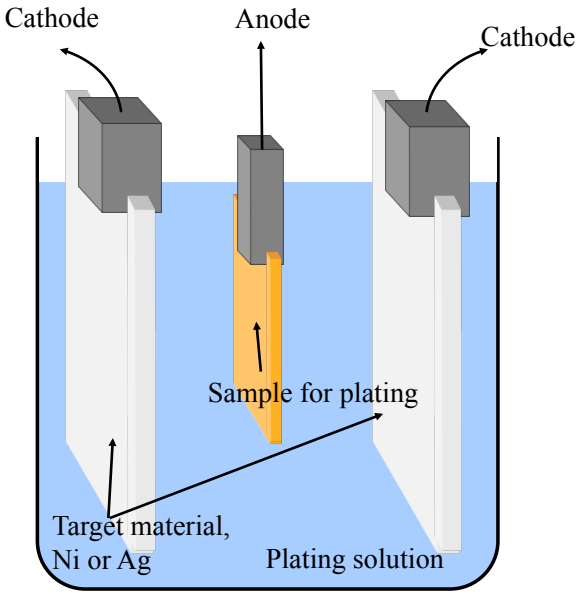

Fig. 2-2. Schematic setup for electro-plating.

Upon the construction of the above test structure, flowability of each material can be studied by dropping 0.05 to 0.1 ml of material on one side of the glass chip and observing the corresponding material behavior. Vacuuming can help fill the gap quickly and completely for viscous materials [112]. Solvent(s) can usually help tailor the viscosity of un-cured material but is proven in the later experiments to cause voids underneath the chips after the curing process. Tailoring viscosity by adding solvents is therefore beyond the consideration of this study.

The shape of the flow front of a material determines whether or not this material can lead to voids when the material is applied into the planar gap between chip and substrate. According to Goodelle *et al* [113], there are two types of flow-front shapes - flat and wedge (shown in Fig. 2-3), that will not lead to voids.

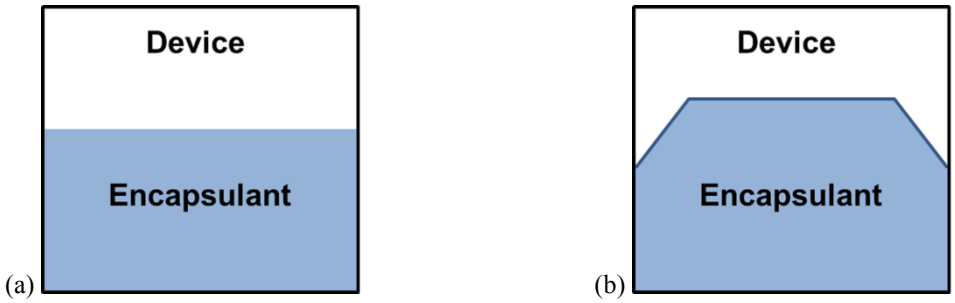

Fig. 2-3. Examples of desirable front shape of encapsulant: (a) flat and (b) wedge shape.

The chip filling time indicates the filling rate of a material. The filling time was counted in seconds as the material was flowing from one side of the 6 mm × 6 mm glass chip to the other. A desirable encapsulant should thoroughly fill up any small gap in the test structure and result in a void-free texture. If a material does not fill the gaps between substrate and chip, or results in voids after filling, that material should be considered unsuitable for encapsulating purpose. All required properties are summarized in TABLE 2-1.

TABLE 2-1
REQUIRED PROPERIES TO PASS PROCESSABILITY TEST

Tested property	Requirement
Flow-front shape	Wedge or flat
Filling time	< 15 min
Cured texture	Void- and crack-free
Breakdown strength of encapsulated tester	Close to breakdown strength tested with standard method (documented in datasheet)

The flow-front shapes of six materials (Epo-Tek 600, Epo-Tek 390, Cyclotene 3022, CF-4721, EPM-2422, and EPM-2482) are shown in Fig. 2-4. Each material was dropped on the side of a single tester. All pictures were taken within one second of the material being dropped at the edge of the glass chip. The flow of Epo-Tek 600 from one side to the other of the chip took too long (> 1day) due to its high viscosity (160000 cP). All other materials showed desirable flow-front shapes. The as-flowed textures of encapsulants are shown in Fig. 2-5. Although Epo-Tek 390 (Epoxy Technology Inc.) had

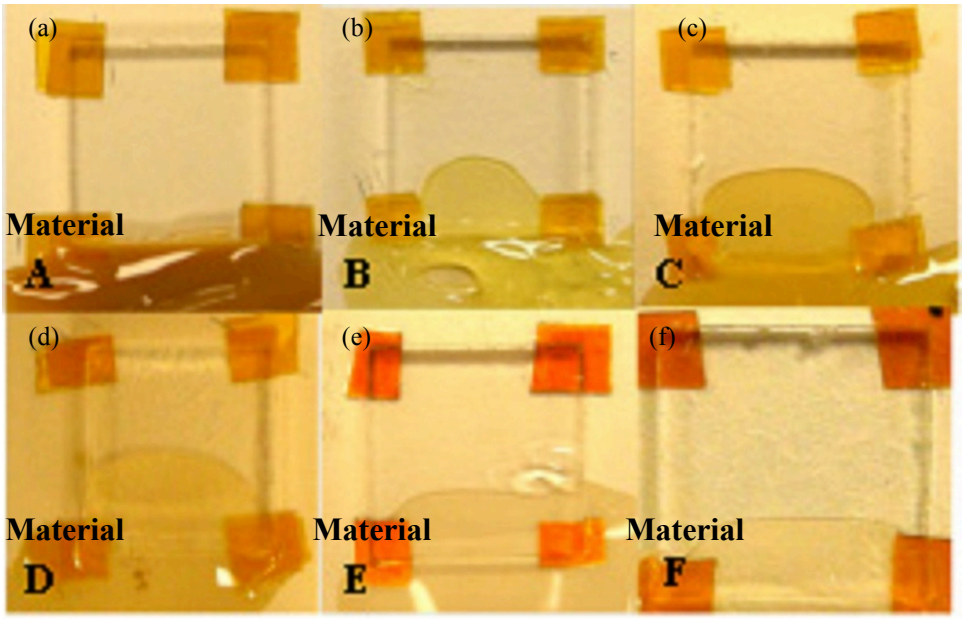

Fig. 2-4. Flow front of potential encapsulants: (a) Epo-Tek 600 (material A), (b) Epo-Tek 390 (material B), (c) BCB (material C), (d) CF-4721 (material D), (e) R-2188 (material E), and (f) EPM-2422 (material F). Size of glass chip: 6 mm × 6 mm. Pictures were taken within one second of the material being dropped at the edge of chip.

a good flow-front shape, it dried too soon and shrinked too much to fill itself into any gap and was therefore considered not passing the flowability test. All the rest materials passed this test because they formed no void under the glass chip.

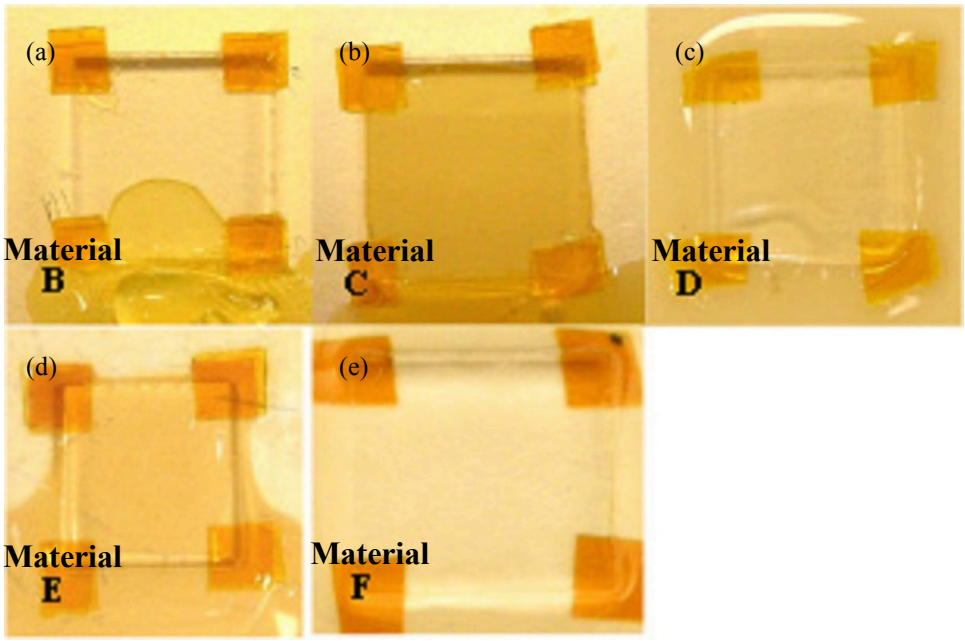

Fig. 2-5. Textures of materials after the completion of flowing process: (a) Epo-Tek 390 (material B), (b) BCB (material C), (c) CF-4721 (material D), (d) R-2188 (material E), and (e) EPM-2422 (material F). Size of glass chip: 6 mm × 6 mm.

To compare each material's flowability, the chip-filling time (average of three independent measurement of each material) is given in TABLE 2-2. The filling time may vary by a few seconds, depending on the position and the amount of the material dropped on the flowing side of the chip. The flowing process of encapsulant under chip can be described by the widely studied flow process of underfill in ball-grid array (BGA) [112, 113]. After the chip is assembled to substrate, dispensed underfill is drawn into the small gap between chip and substrate by capillary force - viscous flow. Viscous flow is defined as a fluid movement in which all particles of the fluid flow in a straight line parallel to the axis of a containing pipe or channel with little or no mixing or turbidity. The viscous flow

between chip and substrate was modeled by Schwiebert *et al* [112], with the filling time given by

$$t = \frac{3\eta L^2}{h\gamma \cos\theta} \quad , \qquad (2\text{-}1)$$

where t is the time to complete viscous flow, η is the absolute viscosity of the material, L is the gap length, h is the gap distance, γ is the surface tension of the liquid-vapor interface, and θ is the wetting angle that the encapsulant makes with the plane. Polymer melts usually form a contact angle of < 80° with high-energy surfaces (metal, ceramic, glass, etc.) [114]. Commercial encapsulants are designed to wet these surfaces well (at a lower contact angle) so as to achieve good adhesion. Assuming that the contact angle between encapsulant and substrate is 60°, the chip-filling time calculated from (2-1) is also given in TABLE 2-2. The reason why the calculated values for CF-4721, R-2188, and EPM-2422 was much larger than the experimental ones was possibly that the actual contact angle between silicone and substrate is much smaller than 60°. The actual contact angle between silicone and silver surface was estimated to be less than 30° by comparing the difference in measured and calculated filling times of CF-4721, R-2188, and EPM-2422.

TABLE 2-2
CHIP FILLING TIME OF MATERIALS (AT ROOM TEMPERATURE OF ~25°C)

Material	Chip-filling time (sec) measured in experiment, gap size: 0.1 mm × 6 mm × 6 mm)	Chip filling time (sec) calculated from (2-1), gap size: 0.1 mm × 6 mm × 6 mm), assumed θ: 60°
A. Epo-Tek 600	Not filling	8640 (144 minutes)
B. Epo-Tek 390	Not filling	N/A (dries too fast to measure viscosity)
C. BCB	10 - 20	~18
D. CF-4721	2 - 3	10
E. R-2188	40 - 60 in air / 10 - 15 in vacuum	1125
F. EPM-2422	10 - 20	315

MasterSil 800 (Master Bond Inc.) can start to cure from the surface within seconds at room temperature when in contact with O_2. The regular flowability test, which was performed in air, was not suitable for MasterSil 800 because curing significantly increased the viscosity of the material and thus impeded the free flowing motion. An alternative method to process this material was injection molding, which forced the material into the designed cavity in the absence of O_2.

To simulate the process of injection molding, another test structure was designed, as shown in Fig. 2-6. This tester was built by attaching a silicon chip on top of a glass substrate with double-sided tape, as shown in Fig. 2-6 (a). The tape simulated the solder joint in a real module. The glass substrate was used due to its transparency and similarity of wetting behavior to that of metal surfaces. Between the edges of chip and substrate, a thin gap was created (around 0.1 mm thick and 0.5 mm wide), which was supposed to be filled by encapsulant, as shown in Fig. 2-6 (b). Injection molding process was simulated by pushing the material into the thin gap with a sharp-tip syringe (gauge size: 25, outer diameter: 0.51 mm, inner diameter: 0.26 mm). As the syringe went around the chip, the

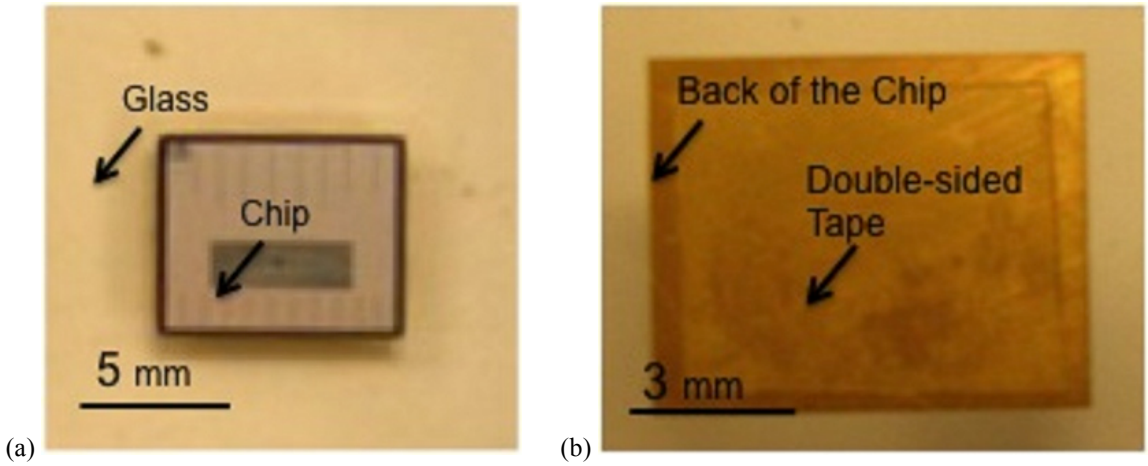

Fig. 2-6. Processability tester for MasterSil 800: (a) top view and (b) bottom view.

material was pushed into the thin gap at the edges. The flowability and the curability could then be examined.

The resulted texture of MasterSil 800 is shown in Fig. 2-7. MasterSil 800 filled the gap underneath the chip; the later curing process caused no crack or void that was observable by optical microscope in the material. This result revealed that MasterSil 800 is an elastic and low-outgassing material and is expected to form a crack-free and void-free texture in the power module by injection molding. Although this material was not injected into the sample shown in Fig. 2-1 in this study due to the processing limitation in the current facility, it could be considered, according to the previously drawn conclusion, processable once the proper processing technique was used. Injection molding was also not applied to Epo-Tek 600 and Epo-Tek 390 because they were found in separate experiment to have volume shrinkage of at least 40% during curing.

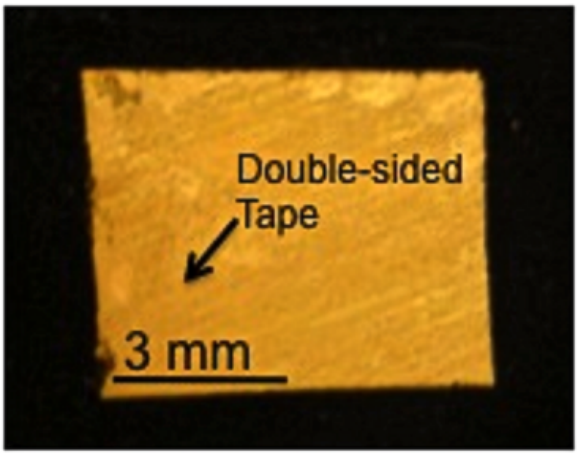

Fig. 2-7. Processability tester injected with MasterSil 800.

Curability

Materials that had passed the flowability tests were cured according to curing profiles as soon as they had flowed through the gaps. The curing profiles, shown in Fig. 2-8, are provided by the manufacturers and may be modified slightly in order to achieve optimal

results. Examining the texture of the material after curing helps decide whether that material is a potential encapsulant. A good encapsulant should not crack or form any void after curing.

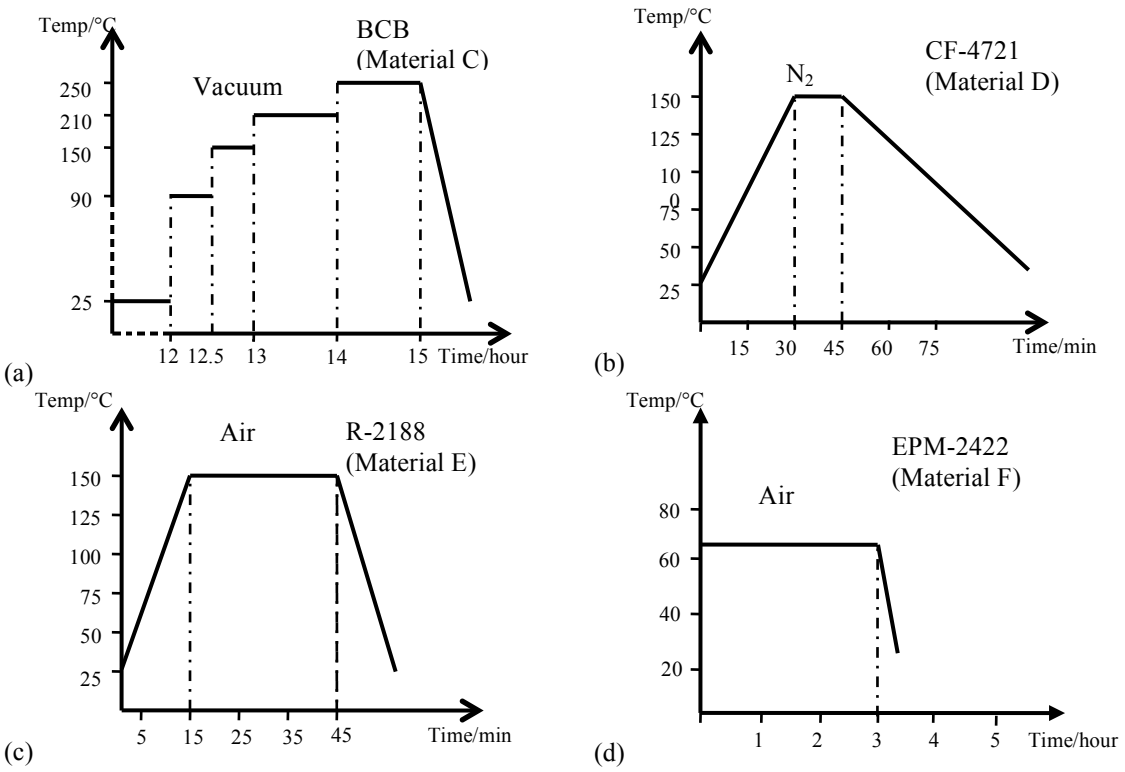

Fig. 2-8. Curing profiles of (a) BCB (material C), (b) CF-4721 (material D), (c) R-2188 (material E), and (d) EPM-2422 (material F).

The curing results for Cyclotene 3022 (Dow Chemical), CF-4721 (Nusil Technology), R-2188 (Nusil Technology), and EPM-2422 (Nusil Technology) are shown in Fig. 2-9. Cyclotene 3022 resulted in voids underneath the die after curing, whereas CF-4721 resulted in cracks. Voids in Cyclotene 3022 resulted from the outgassing of solvents during the curing process. Cracks in CF-4721 were the result of the combination of high T_g and high modulus (below T_g) of the material. Similar cracking behavior of underfills was documented in literature, indicating that the combination of high T_g and high modulus could result in high residual stress in underfill when cooled down after curing

and thus cause cracking in the material [115]. Neither void nor crack is acceptable because they can impair the package insulation by reducing the breakdown voltage. R-2188 and EPM-2422 passed the curability test by forming void-free and crack-free texture after curing.

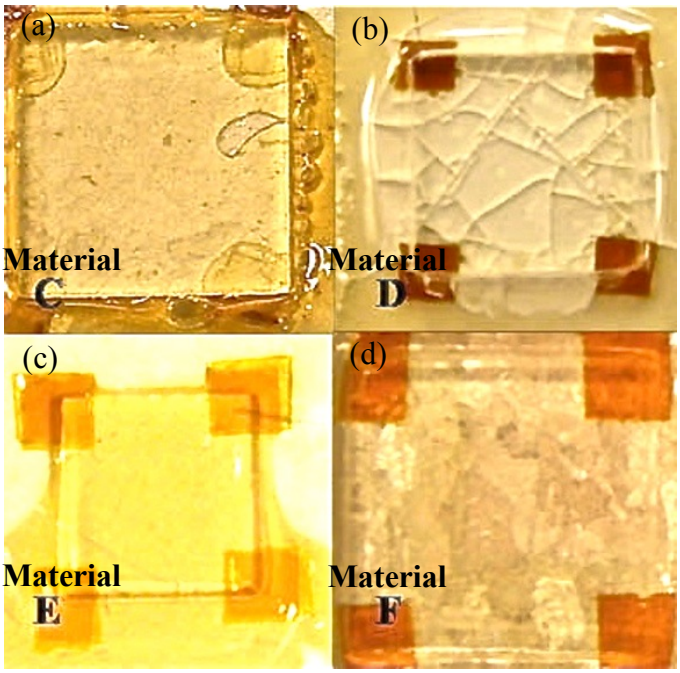

Fig. 2-9. As-cured textures of materials: (a) BCB (material C), (b) CF-4721 (material D), (c) R-2188 (material E), and (d) EPM-2422 (material F). Size of glass chip: 6 mm × 6 mm.

Slowly drying materials with low viscosity were able to fill in small gaps existing in a planar package through viscous flow. According to (2-1), the filling time is proportional to viscosity and square of the gap length and is inversely proportional to the thickness of the gap, the surface tension, and the wetting angle. Setting a desired filling time to be < 15 min and assuming a surface tension of 20 mN/m and a wetting angle of 60°, the viscosity of encapsulant calculated from (2-1) should be lower than 18750 cP to ensure that a gap with 0.1 mm in thickness and 4 mm in length can be fully covered by the material under 1 atm. Soft and elastic materials free of volatiles were also required to

form void-free and crack-free textures after curing. When both points are satisfied, the material can be considered processable.

In terms of injection molding process, the filling time is mainly determined by the injection pressure [116], as shown in (2-2), which describes the pressure drop from the entrance to the exit of a cavity as a function of viscosity. Assuming an injection pressure of 4 atm (injection-molding machine can achieve an injection pressure of up to 150 atm), materials with much higher viscosity (> 5000000 cP) can fill the gap described in Fig. 2-6 within a short time.

$$\Delta p = \frac{12\eta L^2}{h^2 t} \ , \qquad (2\text{-}2)$$

where, Δp is the pressure drop from the entrance to the exit of the cavity, η is the absolute viscosity of the material, L is the gap length, h is the gap distance, and t is time to complete viscous flow.

Breakdown Test of Encapsulated Samples

Test samples with a more complicated structure were designed to simulate real electronic packages and to evaluate the relationship between processability of encapsulant and package insulation. In a plate-bonded package, thin gaps measured a few tens of micrometers usually exist between chips and substrate. The thickness of these gaps equals to that of solder joint, while the voltage across them may be more than 1000 V. Properly processed encapsulants should fill into these gaps and withstand the voltage drop. The structure shown in Fig. 2-10 was designed and assembled as the sample for breakdown test, which helped confirm the result of processability test, assuming that the dielectric strength of a processable encapsulant can be retained when it is applied into any

module.

Fig. 2-10 (a) shows the cross-section of test sample. Voltage was applied between the isolated copper island and the back of the silver-coated silicon chip during the test. Fig. 2-10 (b) shows the top view of the patterned DBC substrate with solder preforms and spacers in place. Four tests could be performed under the same chip with the designed sample. The solder preforms placed on the corners were used to attach the chip to the substrate and to provide gaps for encapsulant flow. The Kapton® spacers, which are as thick as the solder preforms (0.1 mm), were used to prevent chip tilting. Fig. 2-10 (c) shows an as-built sample for the breakdown test. The cross-section from the cut line exhibits the structure shown in Fig. 2-10 (a).

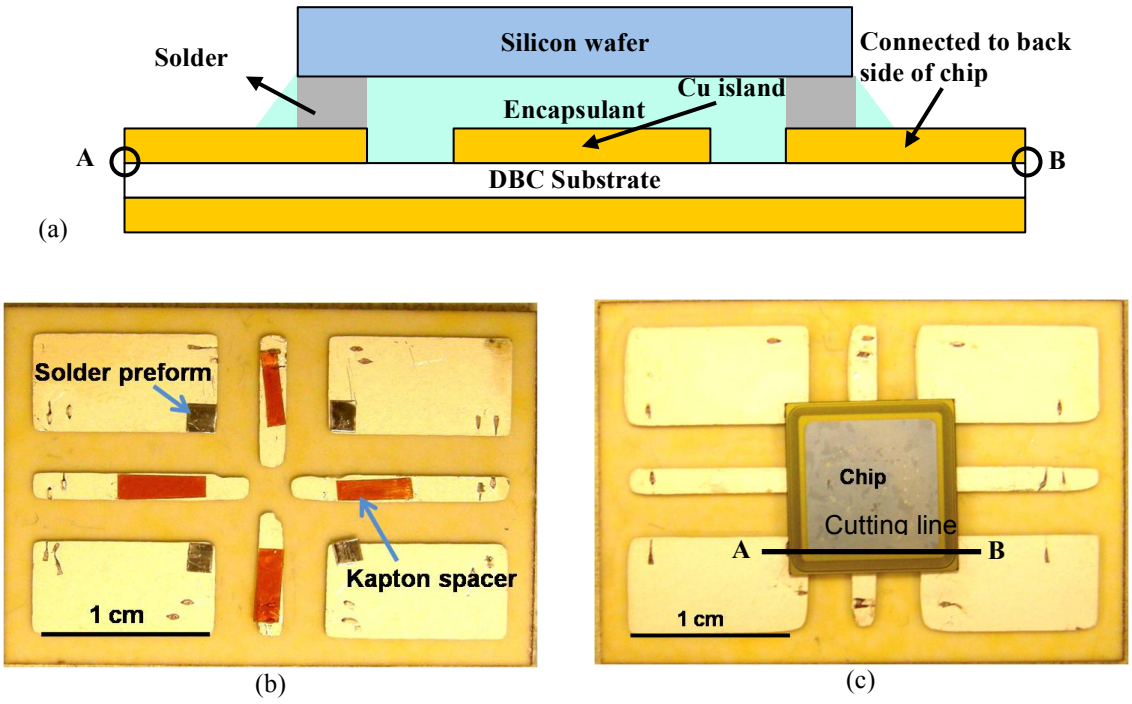

Fig. 2-10. Design of the sample for breakdown test: (a) sample cross-section, (b) solder and spacer on patterned Ag-coated DBC substrate, and (c) assembled sample. Thickness of Kapton® spacer was approximately 0.1 mm.

When encapsulating the sample, each material was dropped on only one side of the chip and was let flow freely to the other side. The curing process used the same profiles shown in Fig. 2-8. Dielectric strength of encapsulated samples (after curing) was measured at room temperature by Hipot megaohmmeter, whose cathode and anode were connected the isolated copper island and the back of the silver-coated silicon chip, respectively. The threshold current was set to around 1 mA. The voltage was ramped up linearly (approximately 200 V/s) during test until breakdown was detected by Hipot. The maximum voltage prior to breakdown at room temperature (~25°C) was recorded as the breakdown voltage, V_{BD}, The dielectric strength, E_{BD}, was calculated by dividing V_{BD} by the distance between silicone and copper, t, as expressed by

$$E_{BD} = \frac{V_{BD}}{t}. \qquad (2\text{-}3)$$

The breakdown test of encapsulated samples helps confirm the result of processability test. A processable encapsulant is assumed to retain its dielectric strength when it is applied into a module. The results of breakdown test and the relationship between processability of encapsulant and dielectric strength of encapsulated sample are shown in TABLE 2-3. Cyclotene 3022 and CF-4721, which exhibited poor processability, resulted in low breakdown strength (E_{BD}) of the samples, whereas processable materials, R-2188 and EPM-2422, led to high E_{BD} of the samples. The dielectric strength of the samples encapsulated by materials with high processability was comparable to that listed in the material datasheets. The results proved that good processability was necessary to retain the dielectric strength of the material as it was applied into the electronic package.

TABLE 2-3
RELATIONSHIP OF PROCESSABILITY AND DIELECTRIC STRENGTH OF SAMPLES ENCAPSULATED WITH MATERIALS C-F

Material	Processability	Dielectric strength of test vehicle at ~25°C (kV/mm)	Dielectric strength in datasheet at ~25°C (kV/mm)
C. BCB	Poor	6 - 8	530
D. CF-4721	Poor	8 - 10	19 - 30
E. R-2188	Good	~20.9	17.7
F. EPM-2422	Good	~20.0	21.7

2.2.2.Temperature dependence of dielectric performance

Based on the results of processability tests (Section 2.2.1), materials that led to crack-free and void-free textures were considered processable. These materials were further evaluated for their dielectric performance, including dielectric strength and relative permittivity, with respect to temperature up to 250°C. Test coupons were fabricated with the three processable silicone elastomers, Nusil R-2188, EPM-2422, and MasterSil 800. Fig. 2-11 illustrates the preparation procedure.

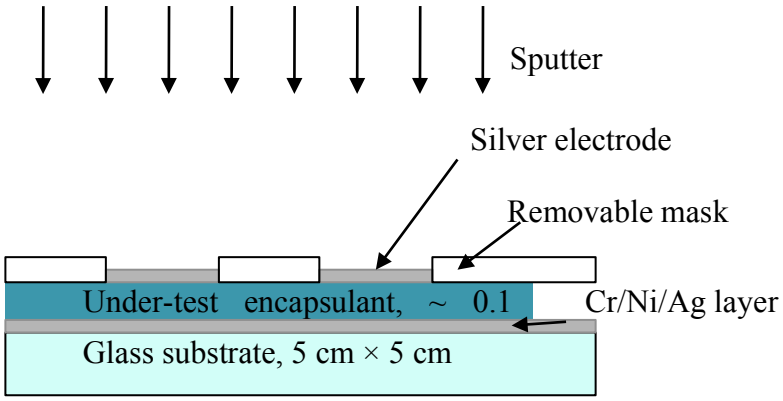

Fig. 2-11. Preparation of dielectric test coupon.

Silver was chosen to be the electrode material. The encapsulant was stencil-printed onto the Cr/Ni/Ag-metalized (total thickness of metallization: approximately 2 μm) glass substrate and cured according to the curing profile shown in Fig. 2-8. The thickness of

the stencil-printed material was controlled by Kapton® spacers to approximately 0.1 mm. Five silver electrodes with diameter of 1 cm and thickness of approximately 10 μm were then sputtered onto the as-cured polymer by a custom-designed PVD (physical vapor deposition) machine (Angstrom Engineering, Inc.). A ceramic mask (attached to sample surface and removed after sputtering) was used to achieve electrical isolation between the silver electrodes. Five individual tests under the same condition could be conducted with one coupon. The as-prepared sample is shown in Fig. 2-12.

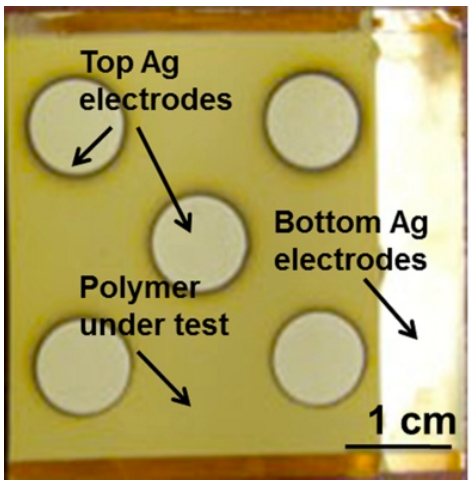

Fig. 2-12. Top view of dielectric test coupon.

The sampling temperatures for dielectric characterization were 25, 100, 150, 200, and 250°C. The temperature was controlled within ±10°C (measured by thermocouples mounted on polymer film and in the chamber) by a vacuum chamber (Cascade Technical Sciences, Inc, Model: TVO-2). The permittivity can be obtained by measuring the capacitance, C, of the material between the top and bottom electrodes at 1 kHz and 1 MHz with an impedance analyzer (Agilent 4294A). The oscillation level was set to 0.5 V. The relative permittivity, ε_r, was calculated by

$$\varepsilon_r = \frac{1}{\varepsilon_0} \cdot C \cdot \frac{t}{A} \quad , \qquad (2\text{-}4)$$

where, ε_0 is the permittivity of vacuum, t is the thickness of sample, and A is the area of top electrode (diameter of 1 cm, as shown in Fig. 2-12). The dielectric strength was measured by Hipot megaohmmeter, whose cathode and anode were slightly pressed (force < 0.1 N) onto the top and bottom electrodes, respectively, to achieve electrical conduction without severely deforming the polymer film, as shown in Fig. 2-13. The contact resistance was less than 50 Ω. The threshold current was set to around 1 mA. The voltage was ramped up linearly at a rate of approximately 200 V/s during test until breakdown was detected by Hipot. The dielectric strength was calculated by (2-3).

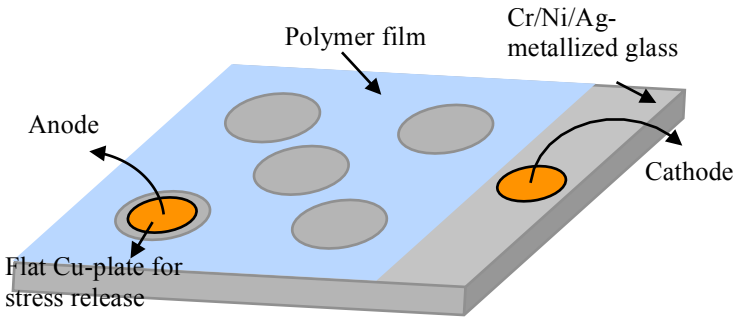

Fig. 2-13. Schematic of test setup for measurement of dielectric strength.

The temperature dependence of dielectric strength and relative permittivity is shown in Figs. 2-14 and 2-15, respectively. Dielectric strength and relative permittivity of all three materials decreased as temperature increased. Among the three materials, EPM-2422 exhibited the highest dielectric strength, whereas MasterSil 800 exhibited the lowest. Within the temperature range of 25 - 250°C, the degradation percentage of their dielectric strength was comparable. The dielectric strength of R-2188 dropped by approximately 40%, that of EPM-2422 dropped by approximately 39%, and that of mastersil 800 droped by 53%. Fig. 2-15 shows that the relative permittivity of R-2188, EPM-2422, and MasterSil 800 dropped by 24%, 42%, and 33%, respectively. A similar

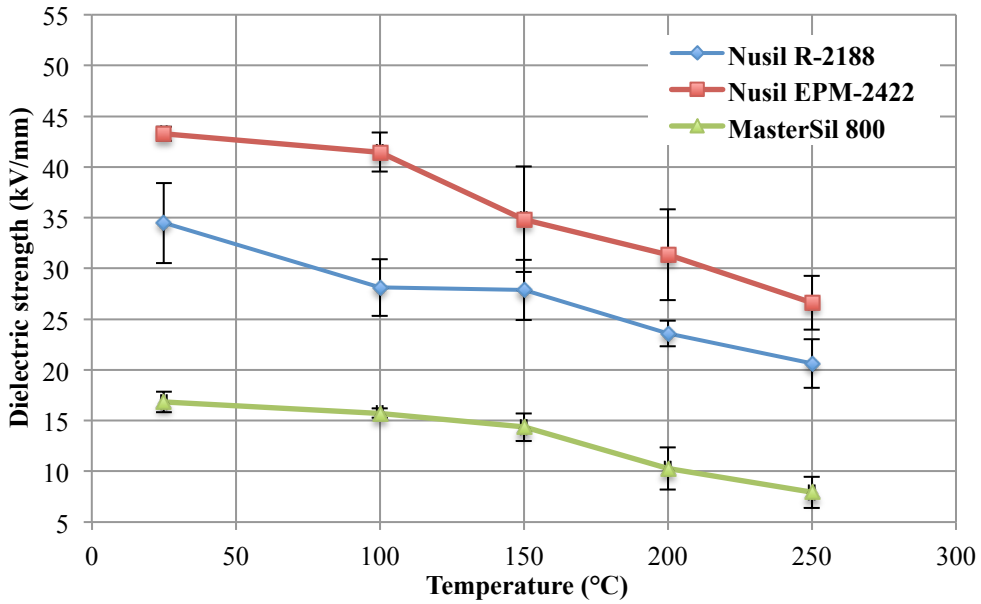

Fig. 2-14. Temperature dependence of dielectric strength of EPM-2422, R-2188, and MasterSil 800.

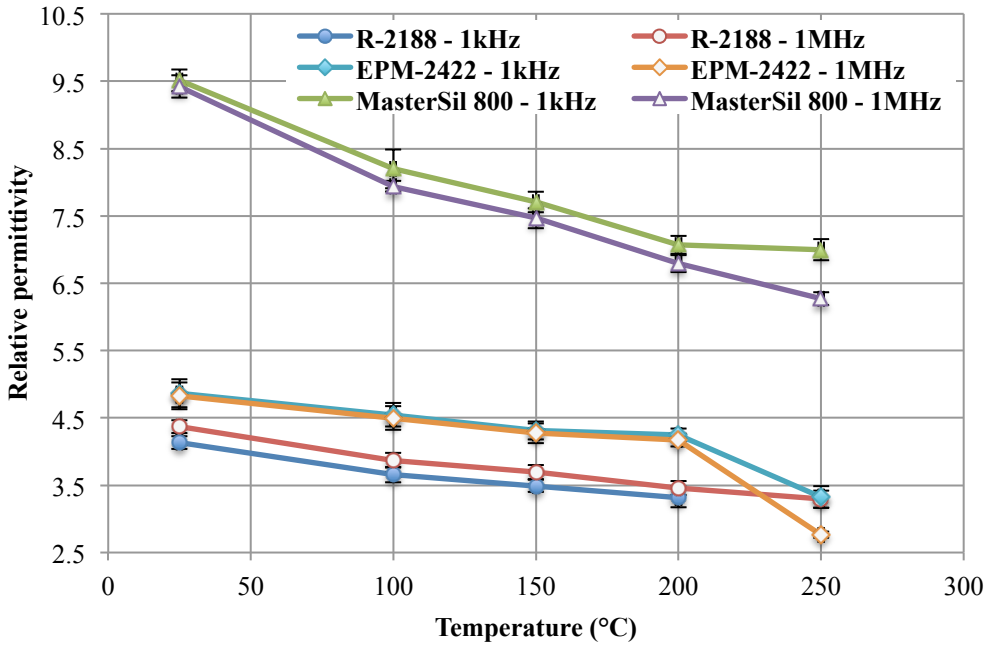

Fig. 2-15. Temperature dependence of relative permittivity of R-2188, EPM-2422, and MasterSil 800.

drop of approximately 25% was reported in [117], in which the permittivity of a silicone gel was measured from -150 to 300°C. R-2188 and EPM-2422 showed similar permittivity, whereas MasterSil 800 showed a permittivity nearly doubled that of the other two materials. Permittivity of a material is determined by many factors including the composition, polarity, etc. The high permittivity of MasterSil 800 may relate to the high polarity (e.g., hydroxyl groups) of the formula. According to TABLE 1-1, the relative permittivity of MasterSil 800 exceeds the recommended value.

The degradation of dielectric strength was possibly due to the impact of temperature on material density. At room temperature or above, silicone elastomers (rubbers) usually have a CTE ranging from 100 to 500 ppm/K, as documented in [43, 117]. The attractive force between chains of rubbery polymers is van der Waals force, which is relatively weak when compared with covalent and ionic bonds. The weak bonding between the chains results in an obvious thermal expansion effect and large CTE values. Thermal expansion leads to loosened network structure and increased free volume (usually in nanoscale) in the polymer matrix. Manufacture defects, such as voids ranging from a few to several tens of micrometers, are inevitably created in polymer matrix during processing. Both free volume and manufacture defect are filled with air and expand as temperature increases, causing decrease of critical field for partial discharge of air. According to Paschen's law, critical field of air partial-discharge decreases as defect size increases. With a defect of >10 μm, the critical field is below 5 kV/mm. Since partial discharge is the most possible breakdown mechanism occurred in bulk polymer (tens of micrometers or thicker) at room temperature or above, the thermal expansion behavior leads to the negative temperature dependence of breakdown strength of materials under

test. Decrease of permittivity with respect to temperature can also be explained by the thermal expansion of material structure and manufacture defects. Permittivity represents the material's capability to store charges. Such capability of air is usually 2 - 5 times lower than that of polymer. When temperature increases and defect size expands, the polymer's capability to store charges is expected to degrade, leading to the negative temperature coefficient of permittivity.

2.2.3.Change in dielectric performance during temperature aging

High-temperature encapsulants need to work at a temperature of 250°C or higher. When polymeric encapsulants are subject to prolonged heating, certain amount of degradation usually occurs. The dielectric properties may vary with respect to time of thermal aging.

To determine the variation of dielectric properties with respect to time of thermal aging, materials that had passed the processability test were soaked isothermally at 250°C for up to 28 days, with the sampling points as three, seven, 14, and 28 days. Samples structured as shown in Fig. 2-12 were used for aging. Five tests (on one test coupon) were performed for each condition. After being assembled, the samples were soaked in an Isotemp Programmable Muffle Furnace (Fisher Scientific). The soaking temperature was set to 250°C. Two thermocouples hung inside the furnace to monitor the temperature close to ceiling and floor indicated that the temperature variation in the furnace was within ± 5°C.

The soaking process hardened the materials, resulting in visible cracks in R-2188 and EPM-2422, as shown in Fig. 2-16. Cracks in R-2188 started to appear after 28 days of aging, whereas those in EPM-2422 appeared in as soon as three days. No crack was

observed in MasterSil 800 throughout the entire aging period. Considering that the samples assembled in Section 2.2.2 for characterization of the temperature dependence of dielectric properties showed no cracking or random failure in R-2188 and EPM-2422, the hardening and cracking phenomena of these two materials should result from thermal aging. The polymer film in the test coupon (cross-sectional view shown in Fig. 2-11) was subject to elastic stress caused by CTE mismatch between the polymer film and the glass substrate when the coupon was cooled down to room temperature from 250°C. Such stress increased with increasing elastic/storage modulus of the polymer. When silicone was continuously exposed to high temperature (e.g., 250°C), degradation occurred via a series of chemical reaction, including chain scission, formation of volatile products, oxidation of hydrocarbon groups, etc. [67-69]. Shortening of the chain led to an increase in crosslink density and therefore a higher storage modulus (hardening), which then resulted in higher stresses caused by the CTE mismatch. Silicone flexibility was also impaired as the long chains were shortened, worsening the elasticity and the crack resistance. The silicone film in the coupon suffered from both increasing elastic stress and decreasing crack resistance as aging continues. Cracking occurred when the film was no longer strong enough to maintain its integrity. No crack was observed (by optical microscope) in MasterSil 800 possibly because it is formulated with organic or inorganic fillers, which are widely known to reinforce the material by resisting the development of cracks. Microscale cracks measured a few micrometers or smaller may still initiate and develop within the material matrix as degradation continued and as stress built up. Fillers were able to deflect these cracks and prevent them from quickly propagating into macroscale ones without any interference.

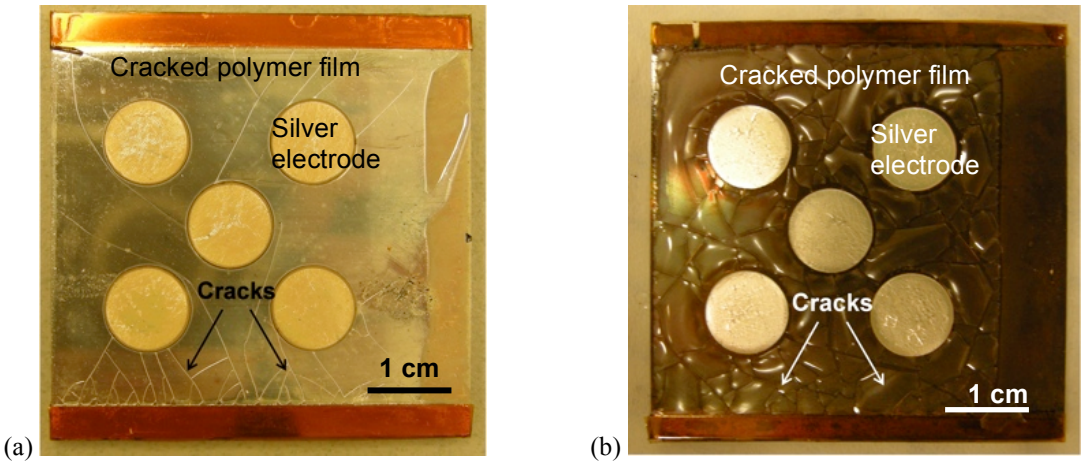

Fig. 2-16. Cracks in aged samples: (a) R-2188 after 28-day aging and (b) EPM-2422 after 14-day aging.

Changes in dielectric strength and relative permittivity with respect to time of thermal aging are shown in Figs. 2-17 and 2-18, respectively. The dielectric strength of R-2188 remained stable within 14 days of aging at 250°C and then dropped by approximately 60%. The dielectric strength of EPM-2422 exhibited the most significantly drop (~77%) within three days and kept dropping slowly as aging proceeds. Although no crack was observed in MasterSil 800, the dielectric strength of this material dropped by 67% within three days of aging.

Cracking observed in the aging process was responsible for the sudden drop of dielectric strength. When cracks appeared and approached the top electrode, the measured dielectric strength decreased significantly because partial discharge of air in those cracks occurred at a much lower electric field. This can explain the sudden drop of dielectric strength of R-2188 and EPM-2422. Although no crack was observed in MasterSil 800 under optical microscope, the dielectric strength could be significantly impaired by microscale cracks (< a few tens of micrometers) that initiated and propagated during the aging process.

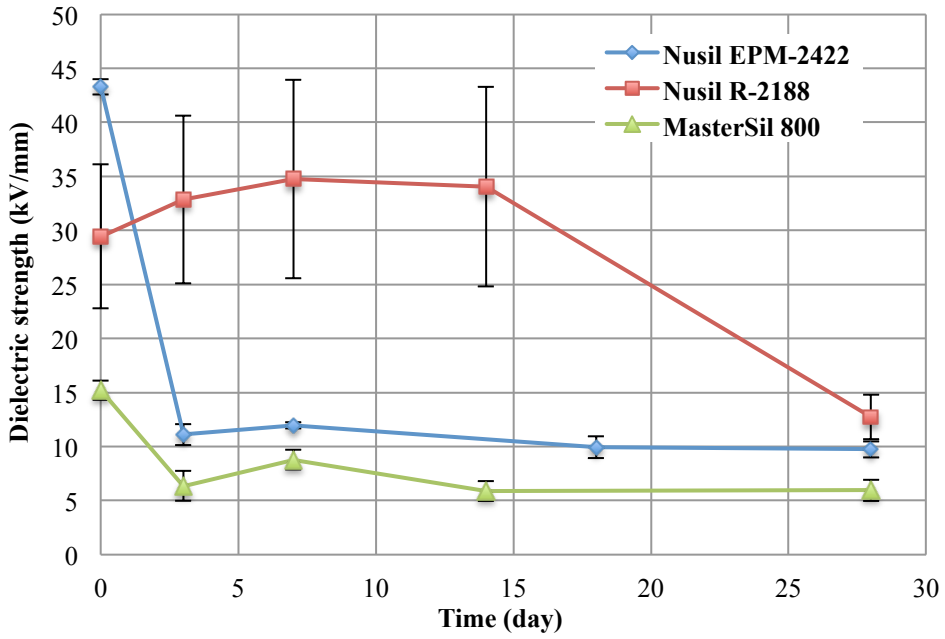

Fig. 2-17. Dielectric strength of EPM-2422, R-2188, and MasterSil 800 with respect to aging (250°C) time.

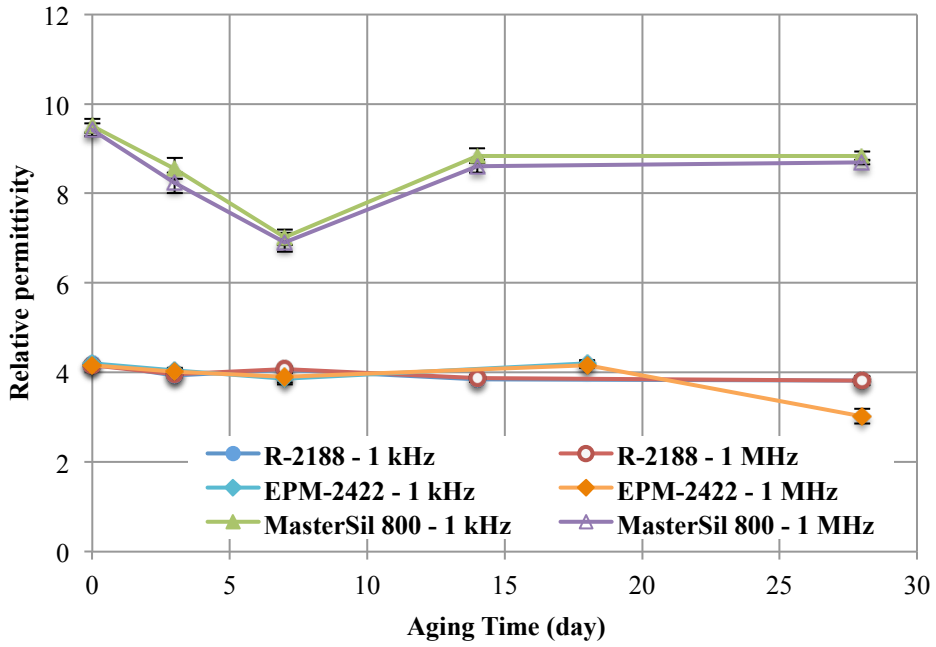

Fig. 2-18. Relative permittivity of EPM-2422, R-2188, and MasterSil 800 with respect to aging (250°C) time.

Relative permittivity of R-2188, EPM-2422, and MasterSil 800 appeared to slowly drop with respect to time of thermal aging. Experimental data for R-2188 and EPM-2422 almost overlapped. The relative permittivity of R-2188 dropped slightly by 9% and that of EPM-2422 dropped by 29% in 28 days of aging. The relative permittivity of MasterSil 800 exhibited a variation of 26%, with the lowest value observed after 7 days. The permittivity of these polymers was less sensitive than their dielectric strength to thermal aging and cracks developed in material matrix. This is because the "weakest path" through the material determines dielectric strength, whereas the average of permittivity of all types of dielectric existing in the material determines its capability to store charges. Since polymer usually has a permittivity only 2 - 5 times higher than air, the change of permittivity due to the existence of cracks is not obvious.

2.3. Summary and problem statement

2.3.1.Summary of results

Seven high-temperature encapsulants were evaluated in this chapter for packaging wide-bandgap devices. In the processability test, Epo-Tek 390 failed in the flow test because it dried too fast (in seconds) to flow freely. Epo-Tek 600, Cyclotene 3022, and CF-4721 failed the curability test: due to outgassing, Epo-Tek 600 and Cyclotene 3022 induced approximately 40% and 10% of shrinkage, respectively; CF-4721 cracked after curing due to its brittle nature below the high T_g. R-2188, EPM-2422, and MasterSil 800 passed the processability tests by exhibiting low outgassing and forming soft and elastic matrices.

Dielectric properties of the three processable materials were characterized within the temperature range of 25 - 250°C. The dielectric strength of R-2188 dropped from around

34.5 kV/mm to 20.6 kV/mm, representing 40% of degradation. The relative permittivity of R-2188 at 1 KHz and 1 MHz within the same temperature range exhibited roughly 30% degradation. EPM-2422 degraded 39% in dielectric strength from 43.4 to 26.6 kV/mm and 42% in relative permittivity. MasterSil 800 degraded 53% in dielectric strength from 16.9 to 7.9 kV/mm and 33% in relative permittivity.

In the thermal aging test, samples of R-2188 cracked after being aged at 250°C for 28 days, resulting in a dramatic drop in dielectric strength from 33 to 13 kV/mm. EPM-2422 cracked within three days of aging at 250ºC, causing the dielectric strength to drop significantly from 43.3 to 9.7 kV/mm. MasterSil 800 exhibited no crack after 28 days of aging, yet its dielectric strength still dropped from 15 to 5 kV/mm. The dramatic drop in dielectric strength is possibly a result of matrix cracking or changes in material composition and microstructure, as will be explained in Section 5.5.1. The permittivity of R-2188, EPM-2422, and MasterSil 800 was more stable with respect to aging time. The relative permittivity of R-2188 dropped by only 7% from 4.3 to 3.8; that of EPM-2422 dropped by 29%; and that of MasterSil 800 dropped by 26%.

2.3.2.Problem statement

Seven commercial high-temperature encapsulants were evaluated for their capability of packaging wide-bandgap devices. Among the seven materials of various chemistry, only silicone elastomers could survive the processability test, which was designed to select materials for chip-scale packaging. Although the three silicone elastomers evaluated in this work all performed satisfactorily when exposed temporarily to a 250°C-environment, their thermal stability was found insufficient for long-term operation at such temperature.

The interest of high-temperature (250°C) packaging for wide-bandgap devices is calling for research on improving thermal stability of silicone-based encapsulants. This can be realized by either changing the material chemistry or by making appropriate modification to the existing material. The latter approach is proposed in the rest of this study because silicone elastomer is proven in experiments for their good processability and satisfactory properties (during temporary high-temperature application) for high-temperature packaging. Inorganic fillers are hypothesized to improve the thermal stability of silicone elastomers by restraining the mobility of polysiloxane chains. The effect of Al_2O_3 fillers on silicone stability will be investigated in the following chapters of this dissertation.

Chapter 3. Experimental Plan and Sample Preparation

3.1. Introduction

Silicone elastomers are widely used for semiconductor encapsulation due to their excellent electrical and chemical resistance and high thermal stability. The evaluation of commercial high-temperature encapsulants in Chapter 2 proved that silicone exhibited good processability and dielectric performance during temporary exposure to high-temperature (up to 250°C) but suffered from quick degradation during long-term exposure to such temperature. The degradation resulted in increased modulus and tendency to crack, both of which limited the high-temperature capability of silicone. Increased modulus leads to increasing thermo-mechanical stresses experienced by encapsulant itself and other circuit components. Cracks (impaired integrity) in encapsulant significantly reduce the material's electrical resistance, for example, dielectric strength measured in Chapter 2 decreased from more than 20 to only ~5 kV/mm (recommended values listed in TABLE 1-1) due to the existence of cracks.

The commercialization of SiC power devices, which can work continuously at up to 250°C, requires packaging materials that can stably work in the same temperature range. The minimum requirement for thermal stability of an encapsulant is not general but should be determined by the specific application expectation, such as survival of certain

number (may be several hundred to a few thousand) of temperature-storage hours (thermal soaking) or thermal cycles. The thermal stability of commercial high-temperature silicones needs to be improved because these materials could significantly degrade within only days (results presented in Chapter 2). Whether the improvement is sufficient for a particular application is again determined by its specific expectation. Literature survey performed in Chapter 1 suggested that silicone stability could be improved by adding fillers, which form interfacial bonds to polymer matrix and restrain chain mobility. Among various fillers, Al_2O_3 was selected due to its relatively high thermal conductivity (20 - 30 W/m-K [118]) and moderate price.

This chapter describes the procedure to prepare Al_2O_3/silicone composites. Uniform dispersion of fillers is crucial for a composite system to prevent the concentration of mechanical stresses and electric field. Since the uncured silicone may be rather viscous to prevent filler dispersion, a careful selection of solvent that is both miscible with and removable from silicone is necessary to enable easy fabrication and to achieve satisfactory sample quality. As-prepared Al_2O_3/silicone composites are then characterized by rheometer, scanning electron microscopy (SEM), and energy-dispersive X-ray spectroscopy (EDS).

3.2. Starting materials

3.2.1.Fillers

According to literature survey (Chapter 1), various fillers, including silica, alumina, exfoliated clay, etc., have potential to improve the thermal stability of silicone. Since high thermal conductivity of encapsulant that guarantees the ease of heat transfer is generally preferred by power applications due to the reduced risk of device overheating

during high-temperature use, alumina (Al_2O_3) was chosen as the filler material in this study because of its high thermal conductivity (~30 W/m-K [118] for Al_2O_3, compared to ~0.2 W/m-K for most polymers). A thin alumina layer may exist or be created on surface of aluminum nitride (AlN) [119, 120], which has even higher thermal conductivity (~320 W/m-K [118]). By choosing Al_2O_3 as filler material, this research is helpful for future development of thermally conductive potting compounds. Two Al_2O_3 fillers, Al_2O_3 fiber (Part No. 43912 by Alfa Aesar, γ phase) and Al_2O_3 particle (Part No. 44932 by Alfa Aesar, α phase), were used as filler in this study.

As-received Al_2O_3 fillers were characterized by scanning electron microscopy (SEM) to confirm their dimensions and to check for possible agglomeration. One layer of conductive tape was placed on the sample holder during sample preparation. Al_2O_3 fillers were then sprinkled on the tape and slightly pressed with a clean glass slide until they stuck to the tape. Excess fillers were removed to avoid contaminating the SEM. The experiment was performed with a LEO (Zeiss) 1550 field-emission SEM. An accelerating voltage of 5 kV was used. In-lens detector that mainly collects backscattered electrons was used. A few nanometers of gold was sputter-coated on top of the fillers prior to SEM characterization to create an electrically conductive surface.

SEM images of Al_2O_3 fillers are shown in Figs. 3-1 and 3-2. Al_2O_3 fibers (shown in Fig. 3-1) appeared as irregular-shaped micro-rods. The measured dimensions are compared with those listed in datasheet in TABLE 3-1. Since the observed dimension was significantly larger than that claimed by the manufacturer possibly due to entanglement and agglomeration, sonication was performed during sample preparation. The agglomerated fibers with dimensions larger than 100 nm are referred to as “rods” in

following sections. Al_2O_3 particles (shown in Fig. 3-2) appeared in spherical shape with dimensions comparable to that listed in datasheet. Sonication was also performed during sample preparation to eliminate possible agglomeration and to keep the preparation procedure comparable to that designed for Al_2O_3 rods (to avoid the effect of uncontrolled parameter).

TABLE 3-1
DIMENSIONS OF Al_2O_3 FILLERS (MEASURED AND PROVIDED BY DATASHEET)

	Al_2O_3 fiber (Part No. 43912)	Al_2O_3 particle (Part No. 44932)
Dimension listed on datasheet	Diameter: 2 nm Length: 100 nm	Average diameter: 50 nm
Measured dimension	Diameter: ~500 nm Length: ~2 μm	Diameter: 30 – 100 nm

3.2.2.Silicone matrix

EPM-2422 (Nusil Technology), which is one of the three silicone elastomers evaluated in Chapter 2, was selected as the polymer matrix. It is a two-part (Mixing ratio: part A/part B = 10/1 by weight) silicone elastomer curable with platinum catalyst. This material exhibits no degradation onset (temperature corresponding to the first sudden slope change of TGA curve in linear temperature-sweep mode) below 300°C in TGA test but showed unstable dielectric performance during 250°C aging in Section 2.4.3. The effect of the two Al_2O_3 fillers on the thermal stability of EPM-2422 is investigated in this study. Effect of fillers can be learned by comparing the performance of composites with different filler loading. Three filler loadings 10, 15, and 30 wt% were selected for each filler. A weight percentage of 30 wt% converts to a volume percentage of approximately 10 vol%. Commercial potting compounds may possess fillers but should have low filler loading (usually < 20 vol%) to limit the storage modulus of the material and the thermo-mechanical stress it may exert onto circuit components.

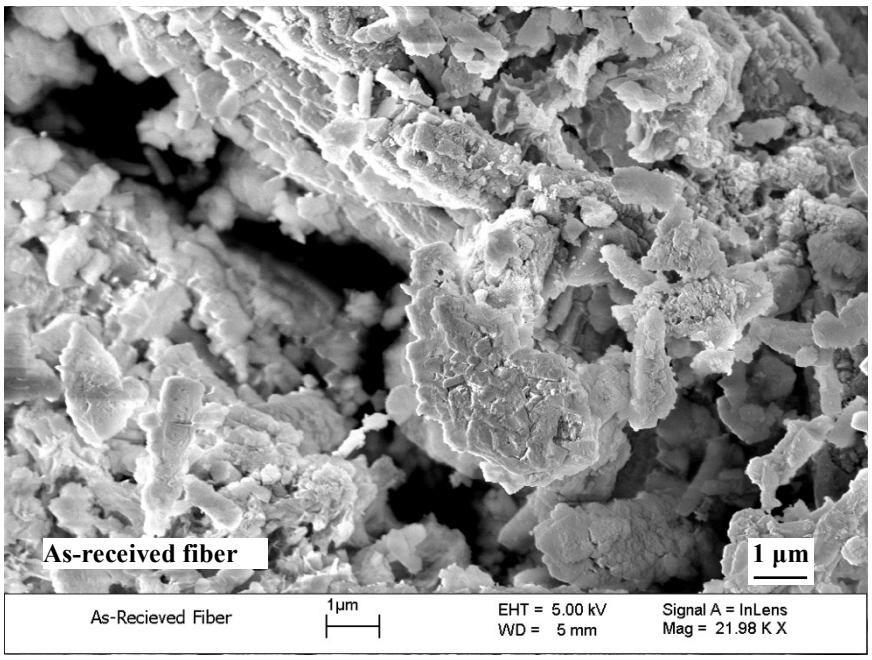

Fig. 3-1. SEM image of as-received Al_2O_3 fibers (Part No. 43912).

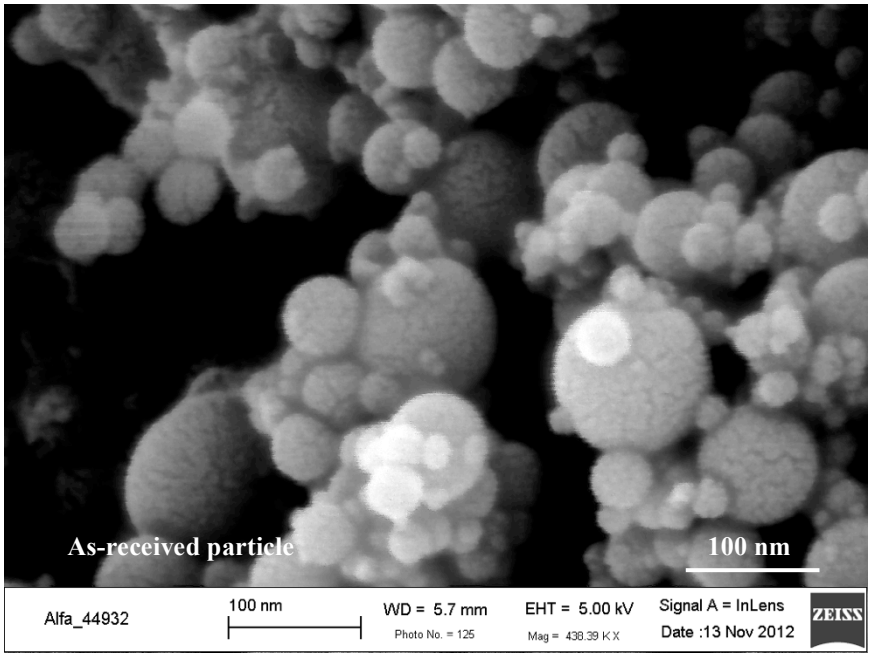

Fig. 3-2. SEM image of as-received Al_2O_3 particles (Part No. 44932).

Fourier transform infrared spectroscopy (FTIR) was used to characterize the chemical structure of EPM-2422 before and after cure. Parts A (long polysiloxane chains) and B (crosslinking agent) were characterized separately before cure. Approximately 1 ml of un-cured material (Part A or B) was evenly spread on the sample stage (perpendicular to the direction of IR beam) for each measurement. The cured silicone was directly placed under the IR beam during measurement. The test of each material was repeated twice, with consistent results observed. FTIR result can provide supplemental information on the chemical structure of silicone, such as that of substituent groups, which is missing from both technical and material safety datasheets (MSDS). The result helps understand the exact structure of silicone and confirm that the degradation process follows the mechanisms specified in Section 1.5.1.

The FTIR result is shown in Fig. 3-3. The spectrum of part A, represented by the dotted line, shows strong absorbance peaks of siloxane backbone (Si-O-Si) in the frequency range of 1130 - 1000 cm^{-1} and of methyl groups attached to Si ($Si-CH_3$) in frequency ranges of 1275 - 1245 cm^{-1} and 865 - 750 cm^{-1} [121]. Two weak absorbance peaks appeared at approximately 1410 and 1010 cm^{-1}, indicating the existence of $-CH=CH_2$ substituent (vinyl functional group) on siloxane backbone. Vinyl groups appeared only in small quantity because they served as crosslinking sites in the silicone elastomer. As suggested in [122], an elastomer with molecular weight on the order of 1×10^5 g/mol is typically crosslinked (randomly) after every $5 - 10 \times 10^3$ g/mol along the chain, producing 10 - 20 crosslinks per molecule. The FTIR result suggested that part A consists mainly of polydimethylsiloxane (PDMS), with occasional vinyl groups replacing the methyl groups. The chemical structure of part A is shown in Fig. 3-4, with the values

of x and y undefined. Although these values cannot be obtained from FTIR characterization, x is known to be significantly larger than y [122]. The structure shown in Fig. 3-4 may repeat itself for 10 times or more in a single chain of part A.

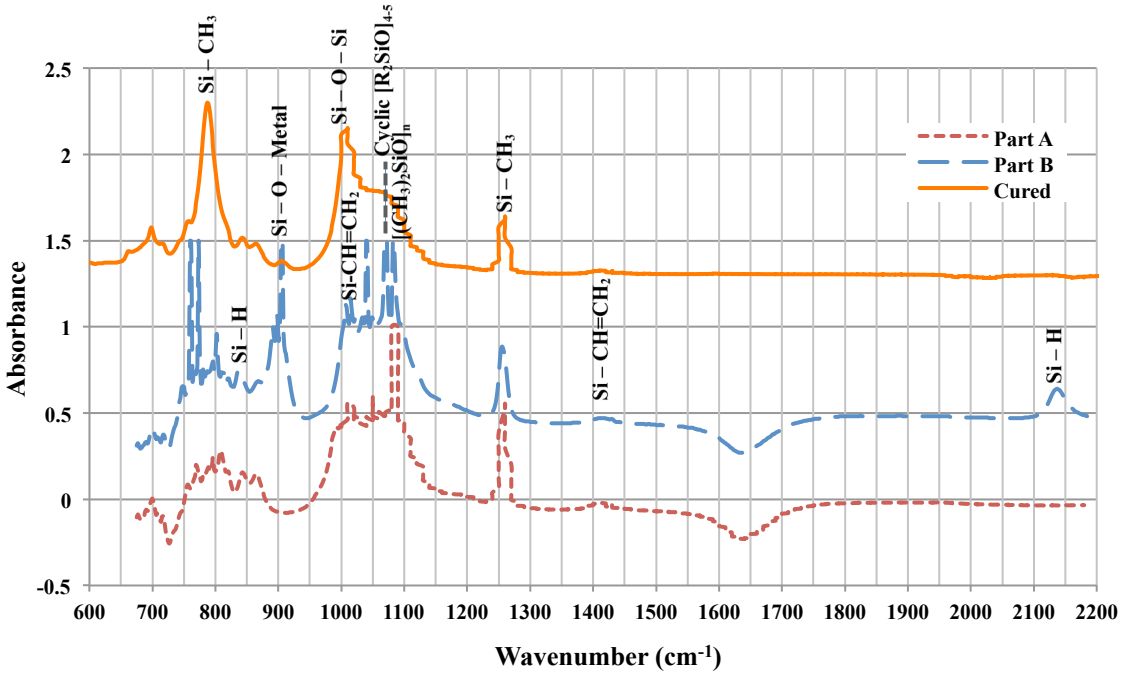

Fig. 3-3. FTIR results of uncured and cured silicone (EPM-2422).

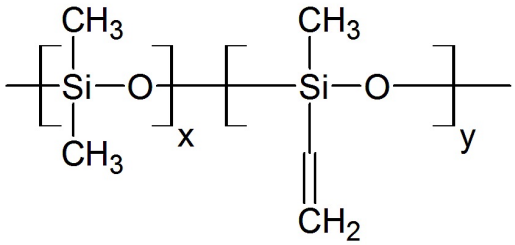

Fig. 3-4. Chemical structure of part A, x >> y. The sketched structure may repeat itself for 10 times or more in a single chain.

The FTIR spectrum of part B, represented by the dashed line, shows strong absorbance peaks of siloxane backbone (Si-O-Si) and methyl substituent attached to it (Si-CH_3), as well as weak peaks of Si-CH=CH_2 as crosslinking sites. A strong peak at 2140 cm^{-1} and a weak peak at 840 cm^{-1}, both corresponding to Si-H substituent (hydride functional group)

that can react with vinyl group, are shown in the spectrum of part B. The spectrum also shows an absorbance peak of cyclic siloxane tetramers or pentamers ($[(CH_3)_2SiO]_{4\text{-}5}$) in the frequency range of 1090 - 1075 cm^{-1} [121] and a peak of Si-O-metal (probably corresponds to the platinum catalyst) in the range of 1000 - 900 cm^{-1} [121, 123]. According to the MSDS of EPM-2422, part B consists of at least two components - dimethyl-methylhydrogen siloxane and cyclic vinylmethyl-dimethylsiloxane [124]. The approximate chemical structure of part B was speculated based on the FTIR results (shown in Fig. 3-5). The FTIR spectrum of cured silicone, represented by the solid line, shows mainly strong peaks of crosslinked siloxane backbone (1130 - 1000 cm^{-1}) and methyl substituent (1275 - 1245 cm^{-1} and 865 - 750 cm^{-1}), indicating that the cured silicone is simply crosslinked PDMS.

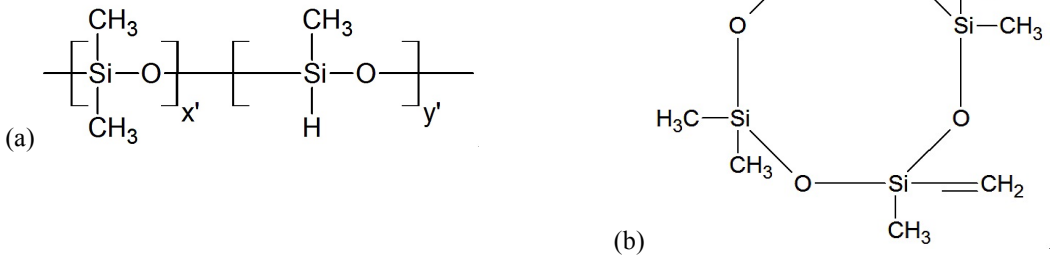

Fig. 3-5. Chemical structure of the two components in part B: (a) dimethyl-methylhydrogen siloxane and (b) cyclic vinylmethyl-dimethylsiloxane.

Hydride and vinyl functional groups react with the existence of platinum catalyst when the silicone cures as described in Fig. 3-6. Since no small molecule such as H_2O is generated during this addition reaction, volume shrinkage is rather limited. For potting compounds, low shrinkage is preferred because it limits stresses caused by volume change. Based on information from both MSDS and FTIR results, the overall structure of the cured EPM-2422 may be described by Fig. 3-7.

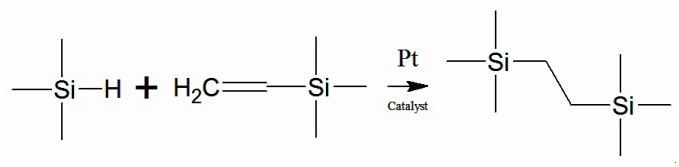

Fig. 3-6. Crosslinking mechanism of platinum-catalyzed silicone

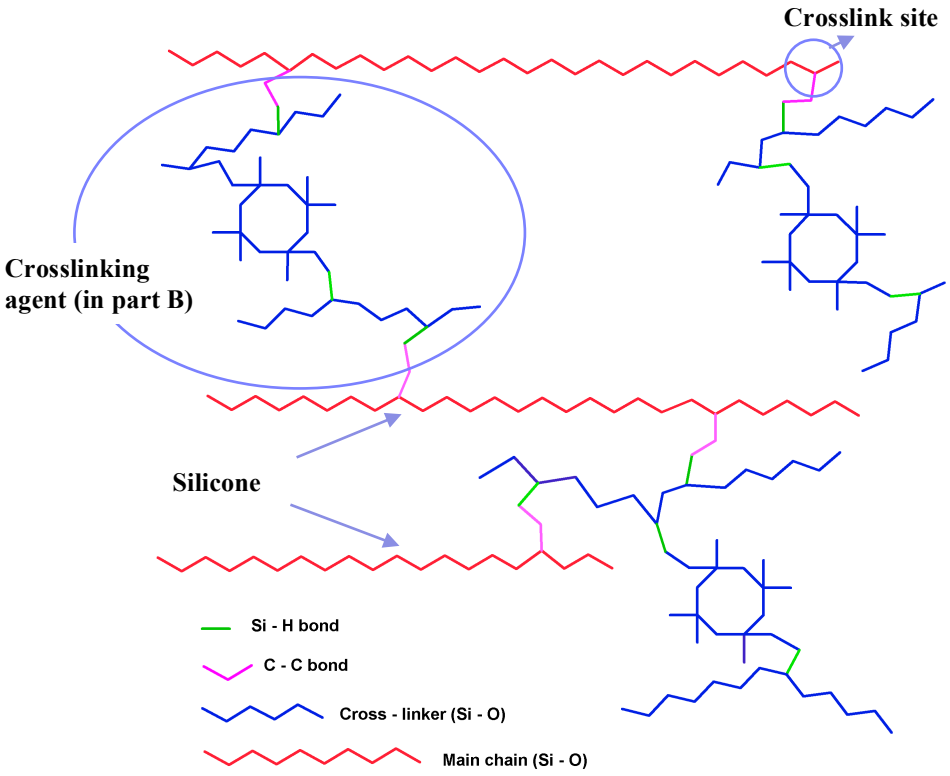

Fig. 3-7. Approximate structure of cured silicone.

3.2.3.Solvent

Since uncured EPM-2422 has a relatively high viscosity of 3600 cP [43], which may cause difficulty to filler dispersion, the silicone needed to be diluted during sample preparation. A proper solvent should meet several requirements: the solvent should not react with silicone during sample preparation and should be miscible with silicone matrix and easily separated from it without causing degradation.

Mesitylene (98%, Alfa Aesar), whose chemical structure is shown in Fig. 3-8, was selected as the solvent for viscosity modification in this study. This material is miscible

with silicone EPM-2422 in any mixing ratio. With a boiling point of 165°C, it can be evaporated at that temperature without severely degrading the silicone matrix. No sign of chemical reaction between silicone and mesitylene was observed during sample preparation.

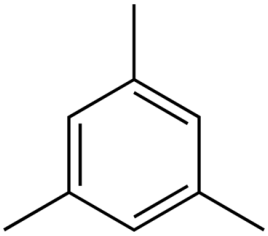

Fig. 3-8. Chemical structure of mesitylene.

3.3. Sample preparation

Silicone (EPM-2422) and Al_2O_3 fillers were first weighed separately according to the specific mixing ratio. Approximately 10 g (volume of ~10 ml) of silicone was used in each experiment. To achieve better filler dispersion, weighed Al_2O_3 fillers were mixed with mesitylene (approximately the same volume as the silicone in use) in a beaker by sonication at a frequency of 20 kHz (VirTis VirSonic 475 cell disruptor). The sonication was carried out in an ice-water bath (setup shown in Fig. 3-9), with the power alternated between on and off for 30 seconds and five minutes, respectively. The 30-second on-time was not long enough to overheat the mixture and to cause degradation or oxidation of silicone and mesitylene. The 5-minute rest-time was sufficient for the mixture to cool down for another cycle of sonication. The total power-on-time was about two minutes. The mixture of mesitylene and filler was then transferred into part A of EPM-2422, which consists of uncured polydimethylsiloxane chains. Extra mesitylene (usually about 2 ml) was used to guarantee that all Al_2O_3 fillers were transferred. The mixture of

silicone, Al_2O_3 fillers, and mesitylene was then subject to sonication in ice-water bath, with the same power-alternation profile mentioned above. The total power-on time was about 10 minutes. After sonication, the mixture was heated up to approximately 175°C (surface temperature of hot plate) by a hot plate in a vented hood to remove mesitylene. A stir-bar was dropped into the beaker (stir rate set to about 300 rpm) to speed up the evaporation process, which took about four hours. The mixture of EPM-2422 part A and Al_2O_3 fillers was cooled down to room temperature before part B was added into it according to the mixing ratio specified by the manufacturer (part A: part B = 10:1 by weight). The mixture of EPM-2422 parts A and B and Al_2O_3 fillers was mixed and then deaerated in a vacuum chamber. When no bubble measured larger than 10 μm was seen on the surface (air bubbles float on silicone surface due to their light weight), the mixture was cured in vacuum at 65°C for four hours. The complete process flow for sample preparation is shown in Fig. 3-10.

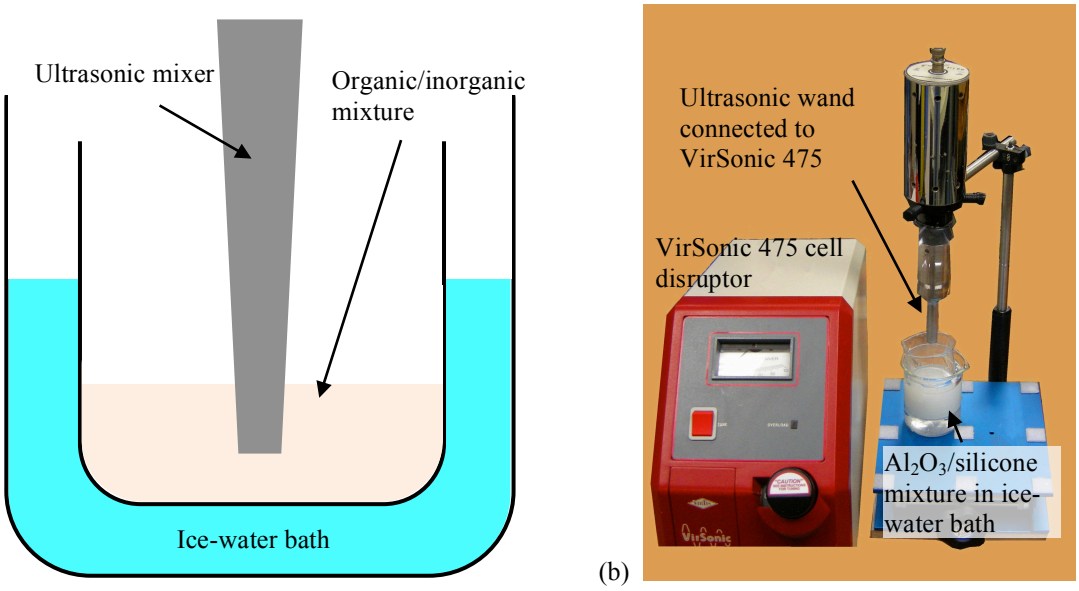

Fig. 3-9. (A) Schematic and (b) experimental setup for sonication in ice-water bath to disperse Al_2O_3 fillers in silicone, with the help of mesitylene as solvent.

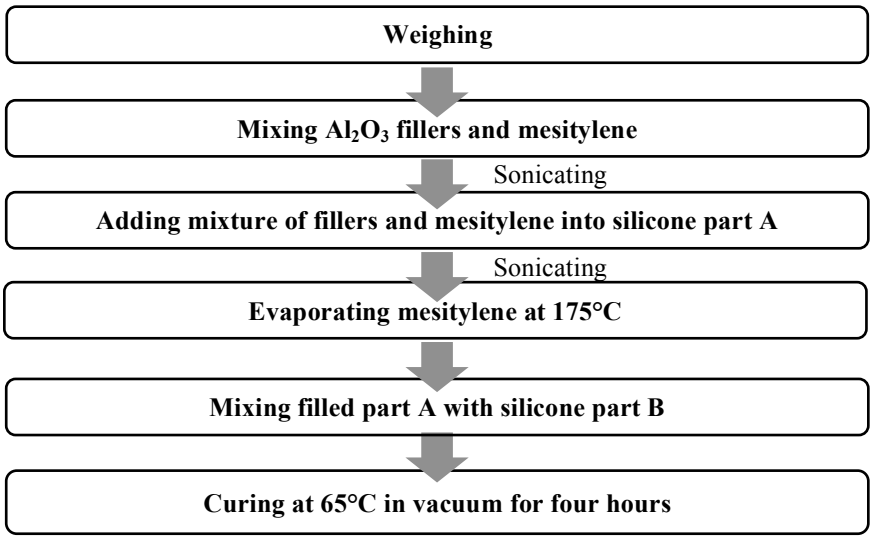

Fig. 3-10. Procedure of sample preparation.

3.4. Characterization of as-prepared Al_2O_3/silicone composites

The composites filled with Al_2O_3 rods at selected filler loading were characterized for microstructure to illustrate the efficiency of sonication. The viscosity of un-cured composites filled with Al_2O_3 rods was measured to confirm the processability of the material. The composites made with Al_2O_3 particles (Part No. 44932 by Alfa Aesar) were not characterized here because they were found in later experiments (specified in Section 4.3) to have no potential to improve thermal stability and were excluded from this study.

3.4.1.Rheology of uncured Al_2O_3/silicone composites

Nano-fillers can increase the viscosity of encapsulants due to their large surface area (e.g., 500 m2/g), which cause significant interfacial resistance with the polymer matrix [125-127]. Section 2.2.1 determined that a viscosity higher than 18750 cP (18.75 Pa-s) might risk the ease of processing (potting without the need of injection molding) of an encapsulant, the viscosity of Al_2O_3/silicone composites is measured in this section to confirm their processability.

The viscosity of uncured composites filled with different loading of Al_2O_3 rods was

measured by a Discovery hybrid rheometer (TA Instruments) with parallel-plate geometry (diameter of 8 mm) at room temperature (approximately 25°C). At least three samples of each composition were measured. The measurement error of each composition was less than ±2%. Within the shear-rate range of 1 - 250 1/s, the measured viscosity is plotted in Fig. 3-11.

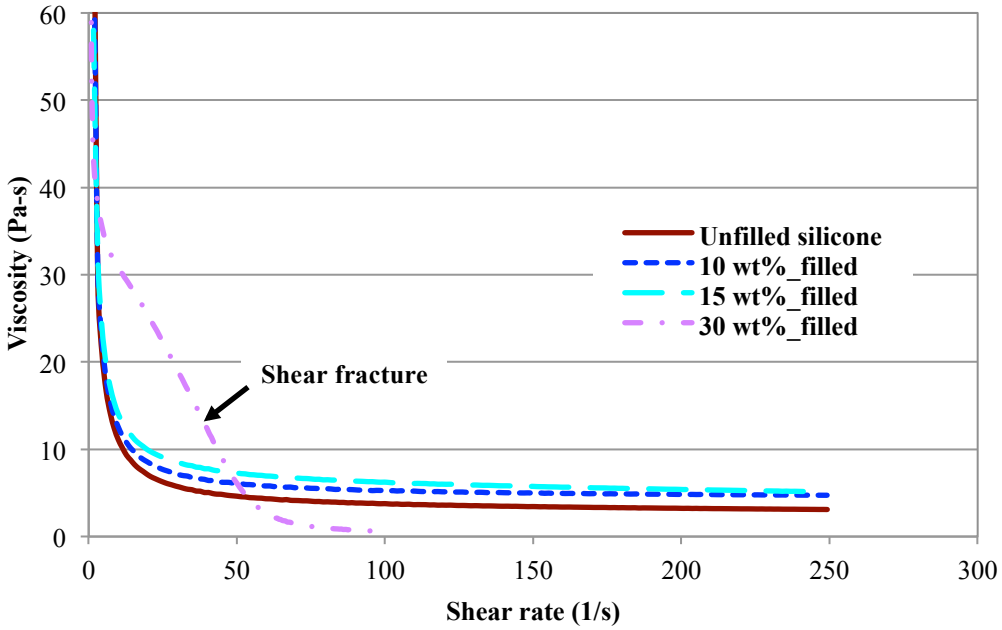

Fig. 3-11. Measured viscosity (at ~25°C) of unfilled and Al_2O_3 (rod)-filled silicones with respect to shear rate.

At shear rate below 50 1/s, unfilled silicone (represented by the solid line) exhibited the lowest viscosity, which increased with increasing filler loading. The composite filled with 30 wt% of rods (represented by the dash-dot line) exhibited a significantly higher viscosity than others. This is in agreement with the common observation in nanocomposite rheology that flocculated or agglomerated fillers result in a higher viscosity than well-dispersed ones [128]. According to the model of Tsagaropoulos, the loosely bound layers around the filler surface (as explained in Section 1.5.3) possibly interact with each other (known as percolation) at high filler loading, causing significant

resistance between fillers and therefore increasing the viscosity at low shear rate. All materials exhibited shear-thinning behavior, featured by a decreasing viscosity with increasing shear rate. Shear thinning of unfilled silicone is caused by the reduced number of chain entanglements as the chains orient along the lines of flow [122]. Al_2O_3-filled silicone exhibited a more significant shear-thinning characteristic, possibly due to the release of liquid from flocculated particle structures that were broken at high shear rates [129]. The 30-wt%-filled silicone exhibited the most significant shear-thinning effect possibly due to its strong filler-matrix and filler-filler interaction [129]. This material gradually fractured from the middle (known as shear fracture, as shown in Fig. 3-12) as shear rate increased, causing the viscosity to approach zero. Shear fracture is widely believed to result from mechanical instability within the fluid (polymer or suspension) and to cause measurement artifact as the fracture reduces the shearing cross-section of the fluid [130, 131]. The measurement for this composite had to stop early because viscosity reaches zero beyond 100 1/s due to complete material fracture. The 30-wt%-filled silicone was also tested for its flowing capability via the processability test described in Section 2.2.1. The uncured material filled into the gap measured 0.1 mm × 6 mm × 6 mm in approximately 2 min. Although the 30-wt%-filled silicone has a considerable higher viscosity than the unfilled one, the quick gap-filling behavior resulted from the good wetting of silicone on silver surface (discussed in Section 2.2.1).

3.4.2.Scanning electron microscopy (SEM)

Fig. 3-13 shows the image of as-prepared composite filled with 30 wt% of Al_2O_3 rods. Compared to the transparency of unfilled material shown in Fig. 2-5, the composite became opaque as fillers were added into the matrix. Unfilled and Al_2O_3-filled silicones

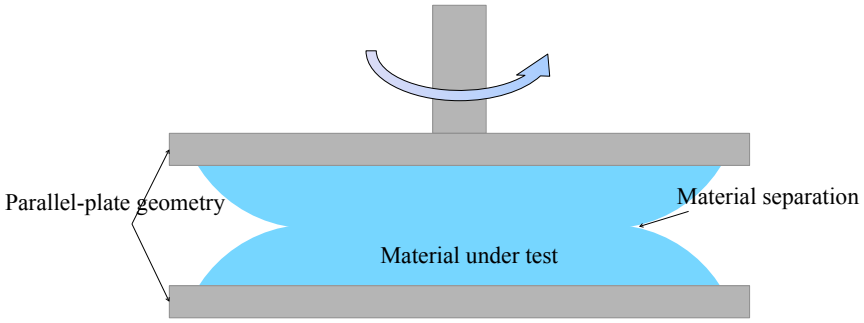

Fig. 3-12. Shear fracture during viscosity measurement at high shear rate (> 50 1/s).

were characterized by SEM. For each composition, two samples were sliced from the bulk with a razor blade, which gave a surface flat enough for SEM characterization. The experiment was performed with a LEO (Zeiss) 1550 field-emission SEM. An accelerating voltage of 5 kV was used to avoid overheating or degrading the polymer film [132]. The top surface of polymer was gently cleaned with ethanol and sputter-coated with gold (a few nanometers in thickness) before SEM observation. Since each SEM image covered only a very tiny area on sample surface, multiple spots were examined on each sample. The results were consistent at all spots of each composition.

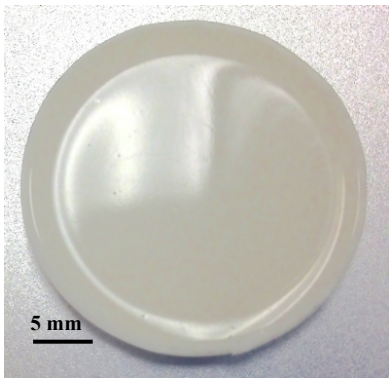

Fig. 3-13. A representative image of as-prepared sample (filled with 30 wt% of Al_2O_3 rods).

The SEM image of unfilled silicone (Fig. 3-14) shows a smooth surface in absence of fillers. Parallel marks were a result of the razor blade. The SEM images at low- and high-magnification of Al_2O_3/silicone composite filled with 10 wt% of Al_2O_3 rods are shown in

Fig. 3-15 (a) and (b), respectively. The low-magnification view (Fig. 3-15 (a)) indicates that a filler loading of 10 wt% caused an increase in surface roughness over that of pure silicone. Sub-microscale rods were well dispersed in the matrix, with occasional aggregates of 2 - 5 μm observed. Since each sample was randomly cross-sectioned, the uniformity in the third dimension can be speculated. The parallel marks with rods along them resulted from cutting. The high-magnification view is given by Fig. 3-15 (b), which shows that Al_2O_3 rods had an average dimension of 200 - 300 nm after sonication.

The SEM images of Al_2O_3/silicone composite filled with 30 wt% of Al_2O_3 rods are shown in Fig. 3-16 (a) and (b) of low- and high-magnification, respectively. The large-scale view shown in Fig. 3-16 (a) indicates that a filler loading of 30 wt% significantly increased surface roughness. Al_2O_3 rods were well dispersed in the matrix with acceptable uniformity. The high-magnification view is given by Fig. 3-16 (b), which shows that the average rod dimension was 200 - 300 nm. There were more large-

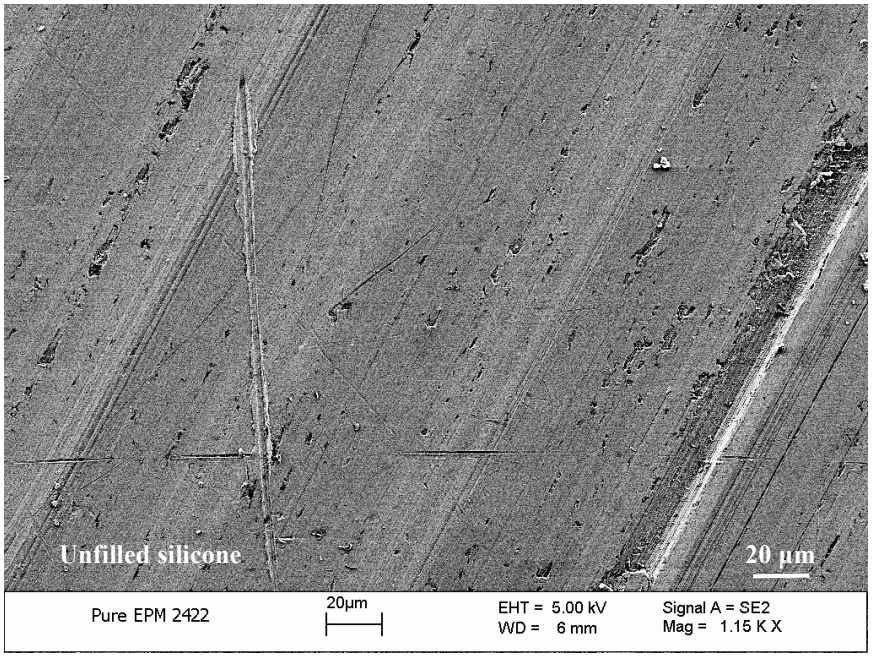

Fig. 3-14. SEM image of unfilled silicone (EPM-2422).

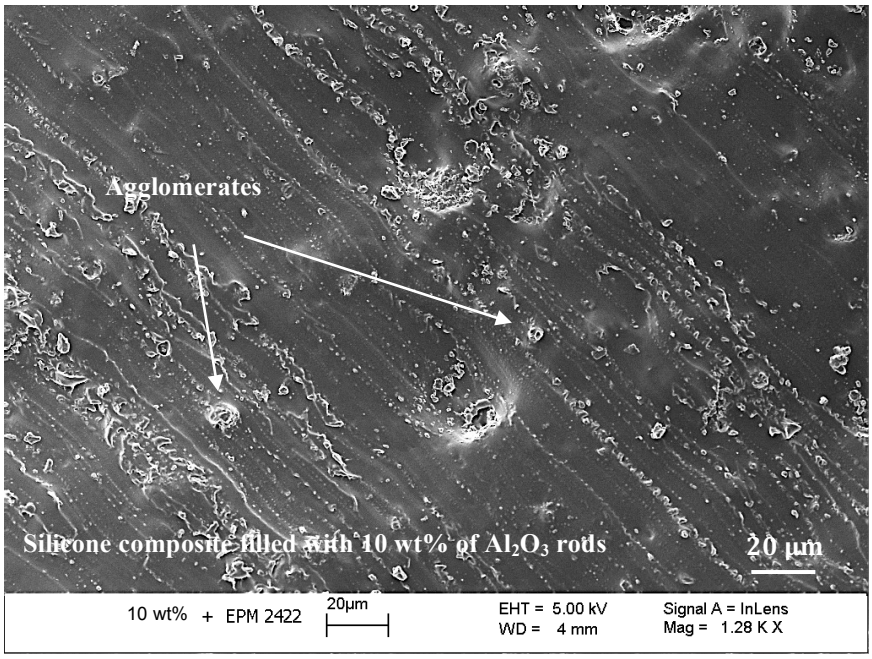

(a)

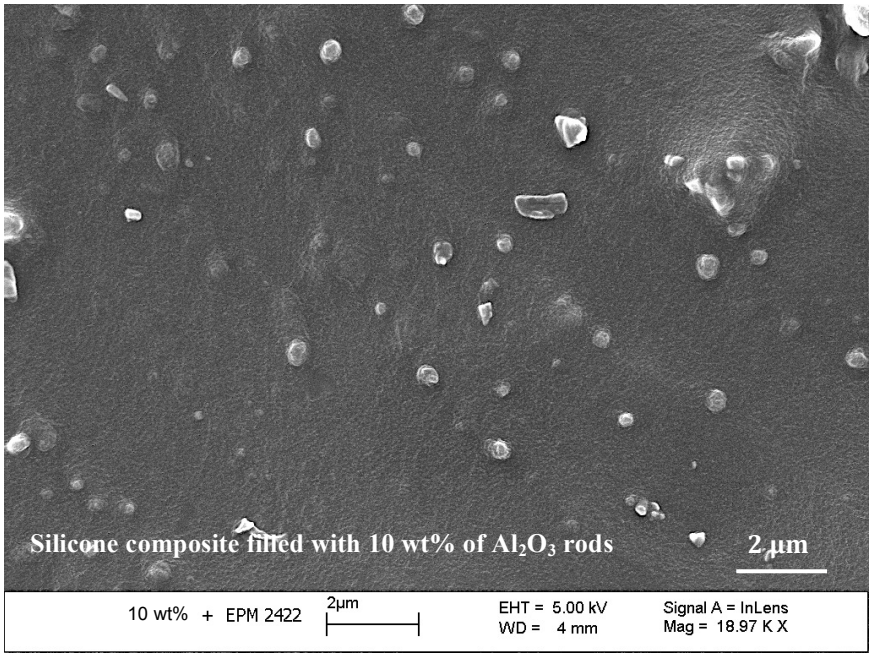

(b)

Fig. 3-15. SEM images of silicone (EPM-2422) composite filled with 10 wt% of Al_2O_3 rods: (a) 1.28 k × magnification and (b) 18.97 k × magnification.

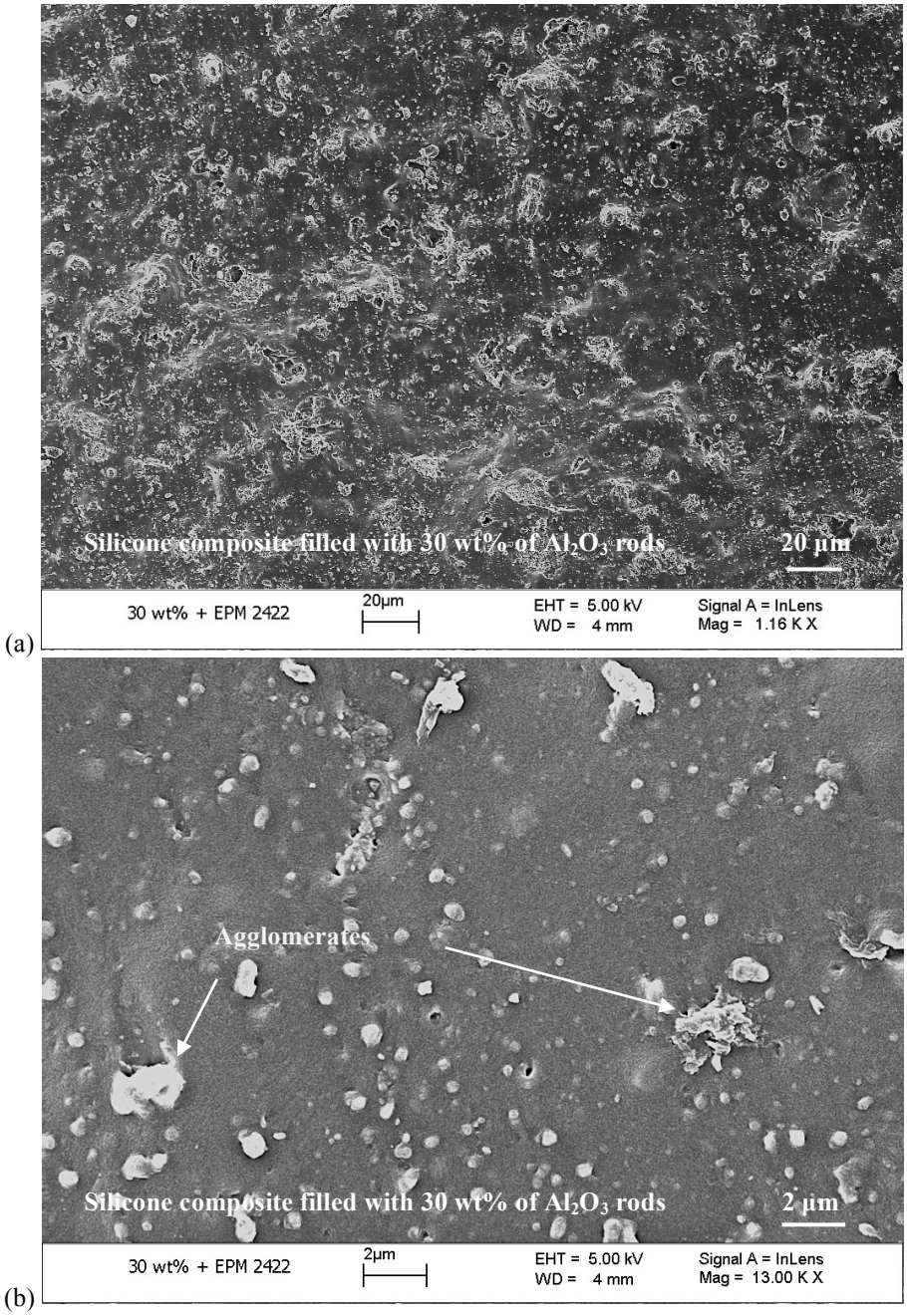

Fig. 3-16. SEM images of silicone (EPM-2422) composite filled with 30 wt% of Al_2O_3 rods: (a) 1.18 k × magnification and (b) 13.00 k × magnification.

dimension aggregates (2 - 5 μm) due to the high filler loading. The cross-section of composite filled with 15 wt% of Al_2O_3 rods was not examined by SEM but the microstructure can be speculated. The Al_2O_3 rods in this material was expected to have an average dimension of 200 - 300 nm and a slighter tendency of agglomeration than the in 30-wt%-filled one.

3.4.3.Energy-dispersive X-ray spectroscopy (EDS)

SEM images of Al_2O_3-filled silicone composites (shown in Section 3.4.2) indicated that most Al_2O_3 fibers entangled or agglomerated into rods (200 - 300 nm) with dimension much larger than that claimed by the manufacturer (2 nm in diameter, 100 nm in length) but smaller than the as-received dimension (0.5 - 2 μm), suggesting that sonication effectively broke down the large aggregates into smaller ones. There is a possibility that Al_2O_3 fibers of much smaller dimension also exist in the matrix but cannot be distinguished by SEM. EDS was then used to investigate this possibility.

Energy-dispersive X-ray spectroscopy was used to analyze the silicone matrix, where no particle was observed by SEM, as marked in Fig. 3-17 (a). The EDS spectrum (shown in Fig. 3-17 (b)) gives a strong peak of silicon, corresponding to the silicone matrix. The oxygen peak corresponded to both silicone matrix and organic contamination on sample surface. The carbon peak came also from the organic contamination. The EDS spectrum shows no aluminum peak in the scanned area, suggesting that aluminum in any form was not found in this region and Al_2O_3 fibers that are too small to be resolved by SEM did not exist in the silicone matrix. The EDS result was repeatable in multiple regions (silicone matrix where no Al_2O_3 cluster was seen by SEM) of all samples. All Al_2O_3 fibers formed rods in dimension of 200 - 300 nm or larger and could be identified by SEM.

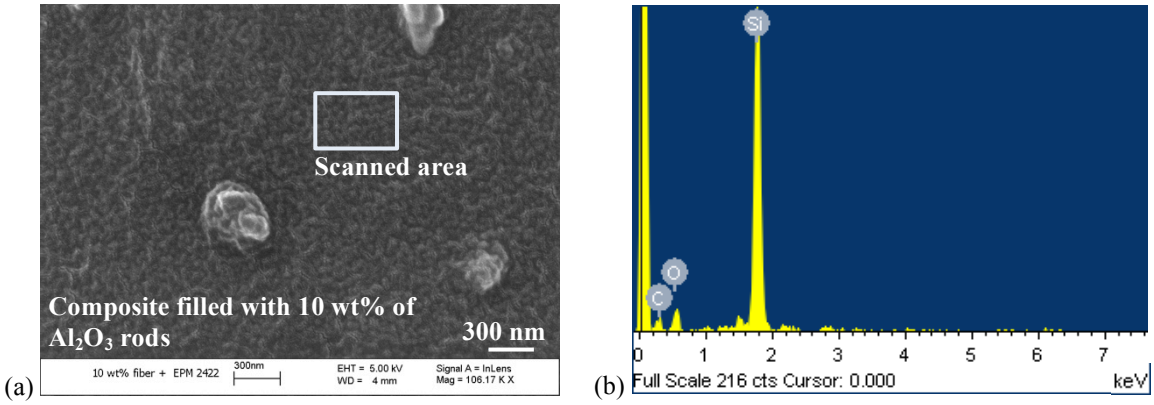

Fig. 3-17. EDS characterization of Al_2O_3 filled silicone: (a) scanned area and (b) resulted spectrum.

3.5. Summary

Experiments were designed to investigate the effect of Al_2O_3 fillers on thermal stability of silicone elastomer. Al_2O_3 fiber (Part No. 43912 by Alfa Aesar), Al_2O_3 particle (Part No. 44932 by Alfa Aesar), and EPM-2422 silicone elastomer (Nusil Technology) were selected as starting materials. Mesitylene was used as solvent to dilute EPM-2422 for better filler dispersion.

Prior to sample preparation, silicone and Al_2O_3 fillers were characterized by FTIR and SEM, respectively. FTIR revealed that the chemical structure of EPM-2422 is crosslinked PDMS, confirming that its degradation process followed the mechanisms mentioned in Section 3.3. SEM showed that Al_2O_3 fibers clustered into irregular-shaped rods of approximately 2 μm × 0.5 μm, whereas Al_2O_3 particles appeared in spherical shape ranging from 30 to 100 nm. Since SEM revealed the tendency of filler aggregation, sonication was performed during sample preparation to break down large clusters.

The procedure of sample preparation was described in this chapter. Unfilled silicone that experienced the same preparation procedure except that no filler was added was used as control. Al_2O_3/silicone composites were fabricated with various filler loadings: 10, 15,

and 30 wt%. As-prepared samples filled with Al_2O_3 rods (Part No. 43912 by Alfa Aesar) were characterized by SEM and EDS. The results showed that Al_2O_3 rods that were formed due to fiber aggregation were uniformly dispersed in silicone matrix, with an average size of 200 - 300 nm. Larger agglomerates measured 2 - 5 μm occurred more often in the sample with high filler loading (30 wt%). As-prepared samples were ready for weight-loss measurement, which directly indicates the thermal stability of these materials. The experiments, results, and discussions are detailed in next chapter.

Chapter 4. Weight Loss of Al_2O_3/Silicone Composites

4.1. Introduction

The importance of improving thermal stability of silicone was discussed in previous chapters. The literature survey performed in Chapter 1 suggested that the thermal stability of silicone could be improved by adding fillers, which possibly interact with the polymer matrix and restrain chain mobility. One type of filler/matrix interaction is due to the hydrogen bonds formed between hydroxyl groups on filler surface and oxygen atoms in polysiloxane backbone [133-135]. The existence and concentration of hydrogen bonds depend on those of the surface hydroxyls. This study investigated the effect of Al_2O_3 fillers and that of surface hydroxyls on the thermal stability of a silicone elastomer, which is a commercial high-temperature (300°C continuous operation as claimed by manufacturer [43]) potting compound but showed inadequate thermal stability as evaluated in Chapter 2.

The Al_2O_3/silicone composites with various filler loadings were prepared and characterized in Chapter 3. In this chapter, the effect of Al_2O_3 fillers on thermal stability is studied by weight-loss experiments, including TGA in linear temperature-sweep mode and isothermal soak test at 250°C. A material with higher thermal stability should exhibit a higher temperature for degradation onset in TGA and higher residual weight in

isothermal soak test. To study the effect of hydrogen bonds on thermal stability, the concentration of surface hydroxyls was altered by high-temperature dehydration in an inert atmosphere. The thermal stability of Al_2O_3/silicone composites with dehydrated fillers was compared with that of composites with as-received ones via weight-loss experiments.

4.2. Thermogravimetric analysis (TGA)

Thermogravimetric analysis is widely used to analyze the thermal stability of polymers and their composites. A linear temperature-sweep profile is usually used for quick test results. Pure and Al_2O_3-filled silicones were subjected to TGA tests with a similar profile in this study. A typical TGA result of linear temperature-sweep is shown in Fig. 4-1. The curve usually exhibits a sudden slope increase when temperature increases beyond certain point. The temperature corresponding to this sudden slope change is defined as onset temperature of material degradation. To simplify the determination of onset temperature and to reduce the error of results, the onset

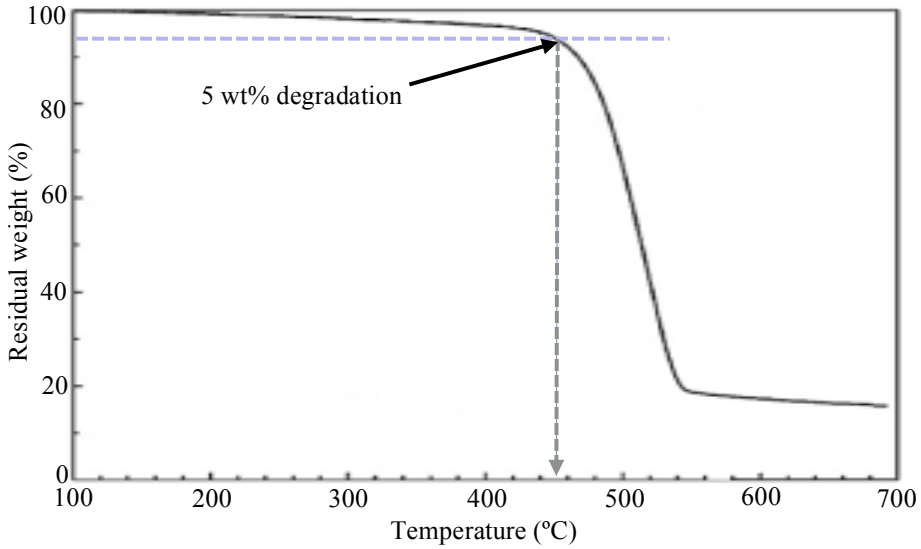

Fig. 4-1. Example result of TGA in linear temperature-sweep mode.

temperature of degradation is usually defined as the temperature corresponding to certain percentage of weight loss, for example, the temperature at 5% weight loss was used in this study. The onset temperature of degradation is an indication of material's thermal stability because a higher onset temperature means that more thermal energy is required to decompose the material. Thermal stability of different materials can be compared by their onset temperature obtained with the same TGA profile.

4.2.1.Test condition

This section describes the test condition for TGA test. The tests were performed by a NETZSCH simultaneous thermal analyzer (STA) 449 Jupiter (Fig. 4-2). Compressed air (80% N_2 and 20% O_2) was used in the TGA tests because electronic encapsulants are usually exposed to air during operation. A sample of approximately 20 mg was placed in the crucible prior to each test. Because silicone-based elastomers are expected to have their onset temperature of degradation below 500°C, the temperature range used in this test was 35 - 500°C. Since the thermal conductivity of Al_2O_3 (20 - 30 W/m-K) is two orders of magnitude higher than that of unfilled silicone (~0.2 W/m-K [45]), Al_2O_3-filled silicones are highly possible to be more thermally conductive than the unfilled one. During TGA test, the silicone was heated up from the bottom of sample crucible (made of aluminum). A thermocouple mounted close to the crucible bottom provides the temperature read on test results. The heat transfer from heater to under-test silicone took certain amount of time, which depends on the thermal conductivity of the silicone. The lower the thermal conductivity, the longer the time. Due to the difference in thermal conductivity, the temperature experienced by the unfilled silicone was expected to be lower than that experienced by the composite during a temperature-sweep test, especially

when a high ramp rate (e.g., ≥ 5°C/min) was applied. To reduce the error caused by variation in thermal conductivity of silicones with different filler loadings, a slow ramp rate of 1°C/min was used in all tests. The test of each composition was repeated twice with consistent results obtained.

Fig. 4-2. Simultaneous thermal analyzer NETZSCH STA 449 Jupiter.

4.2.2.Results and discussion

The TGA results of silicones unfilled and filled with Al_2O_3 rods are shown in Fig. 4-3. The residual weight of all samples was stable at low temperature (< 300°C) but suddenly decreased as the temperature exceeded a certain value. The temperature corresponding to 5% weight loss was used as the indication of onset degradation for this study. The temperature of degradation onset, as summarized in TABLE 4-1, increased with increasing filler content, indicating that incorporation of Al_2O_3 rods, especially at high loading (e.g., 30 wt%), was effective in improving the thermal stability of silicone elastomer.

The improvement in thermal stability can be attributed to restrained chain mobility caused by filler surface [75, 76]. According to the model of Tsagaropoulos [99], each

filler is surrounded by its own tightly and loosely bound layers, both of which have restrained chain mobility. The interfacial layers are speculated in [136] to have different chain conformation from that in the polymer matrix. The interface might therefore behave differently from the matrix during thermal decomposition.

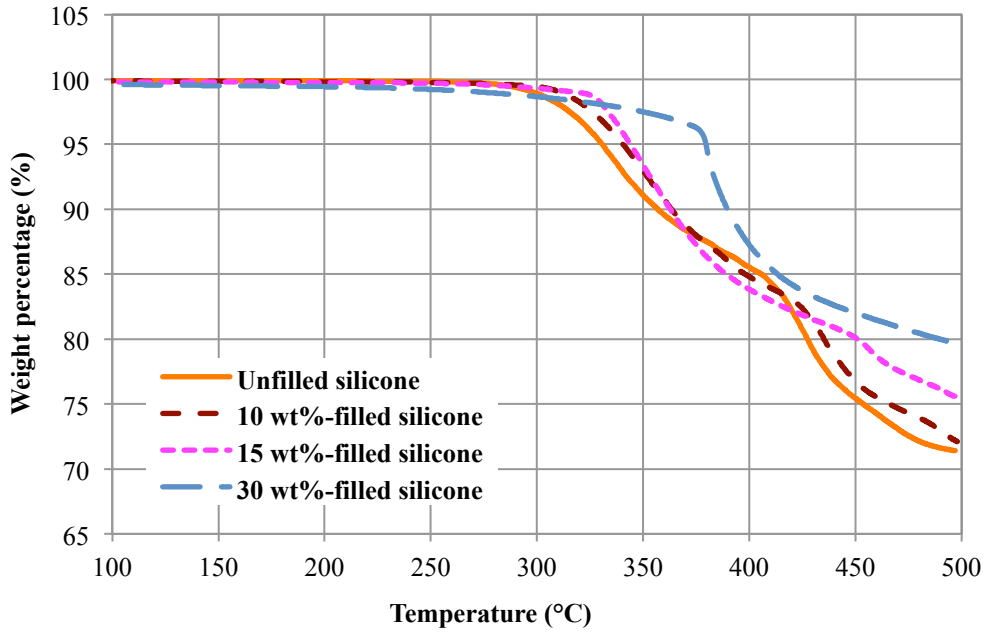

Fig. 4-3. TGA results of unfilled and Al_2O_3 (rod)-filled silicones (EPM-2422).

TABLE 4-1
TEMPERATURE OF DEGRADATION ONSET OF UNFILLED AND AL_2O_3-FILLED SILICONES

Filler loading (wt%)	Onset temperature (°C)
0	330
10	340
15	343
30	379

The TGA residues may serve as an indirect evidence for the existence of interfacial layer. The residues of samples prepared with different combinations of Al_2O_3 rods, mesitylene (solvent), and polymer matrix were examined after TGA tests, with the

images shown in TABLE 4-2. The residue of pure silicone appeared as white powder. When mesitylene was added into and later removed from pure silicone during sample preparation, the resulting sample also changed into white powder after TGA test. When mesitylene was used to coat Al_2O_3 rods before TGA test, the residue appeared as white powder indistinguishable from the as-received rods. Such phenomena suggested that mesitylene did not affect the performance of either the silicone matrix or the Al_2O_3 rods during TGA test. When Al_2O_3 rods were mixed into silicone matrix with and without mesitylene, the residues in both cases appeared in the original shape (i.e., the shape that the sample was cut into to fit the TGA crucible before test) with a brownish color. The results clearly show that neither pure silicone nor Al_2O_3 rod exhibited a color change during TGA test but the composite made from the two materials did. The color change

TABLE 4-2
SAMPLE RESIDUES AFTER THERMOGRAVIMETRIC ANALYSIS

Polymer matrix	Rods	Mesitylene	Residue
Yes	No	No	
Yes	No	Yes	
No	Yes	Yes	
Yes	Yes	No	
Yes	Yes	Yes	

was possibly due to local carbonization, which occurred within the Al_2O_3/silicone interfacial layers because they have chain conformations different from those of the matrix.

4.3. Isothermal weight loss

Thermogravimetric analysis with a linear temperature-sweep profile detects the temperature of degradation onset, at which the material being tested starts to quickly decompose. When applied as encapsulants for electronic packaging, potting compounds are more likely to suffer from slow/long-term decomposition at and below the maximum operation temperature, which is much lower than their onset temperature detected by TGA. To observe the decomposition process occurring at a specific temperature, an isothermal soak test was carried out. Unfilled and Al_2O_3-filled silicones were subject to isothermal soak, during which their residual weight was monitored as an indication of their decomposition status.

4.3.1.Test condition

The isothermal soak test was performed in a Delta Design 9023 environmental chamber at 250°C, which is the maximum operation temperature of current SiC devices. The temperature was ramped up from room temperature to 250°C in 20 minutes and maintained there throughout the test. The temperature variation during isothermal soaking was within ±0.5°C. The initial weight of each sample was about 3 - 4 g. At least three samples of each composition were soaked in air for at least 2000 hours. Every 24 hours, all samples were weighed outside the furnace at room temperature (~25°C).

4.3.2.Results and discussion

The average of residual weight percentage of each composition is plotted against

aging time in Figs. 4-4 and 4-5. The variation in results among samples of the same composition is reflected in Fig. 4-6, which shows the initial weight-loss rate of each composition.

The green solid line in Fig. 4-4 represents the residual weight percentage of unfilled silicone (EPM-2422, modified with mesitylene according to the procedure given in Fig. 4-9), which, serving as the benchmark in this experiment, drops below 90% within 700 hours. The blue dotted line, which shows a slightly lower weight-loss rate than the green solid line at the initial stage (i.e., within the first 350 hours), represents the residual weight percentage of Al_2O_3/silicone composite filled with 10 wt% of Al_2O_3 rods. The maroon dashed line, which represents the composite filled with 15 wt% of Al_2O_3 rods, exhibits an even lower weight-loss rate within the first 1000 hours, indicating a higher thermal stability of this composition. The orange dash-dotted line, which represents the composite filled with 30 wt% of Al_2O_3 rods, exhibits the lowest weight-loss rate throughout the isothermal soak test, indicating the highest thermal stability among all materials.

Al_2O_3 particles seemed to speed up the weight-loss (decomposition) rate. The purple long-dash-dotted line, which represents the Al_2O_3/silicone composite with a particle loading of 10 wt%, exhibits the most severe weight-loss among all materials. The grey long-dashed line, which represents the Al_2O_3/silicone composite with a particle loading of 30 wt%, exhibits a similar behavior.

The calculated weight percentage shown in Fig. 4-4 is based on the total sample weight, i.e., the sum of the weight of polymer matrix and that of Al_2O_3 fillers, which are thermally stable at 250°C and should not exhibit any significant weight loss during the

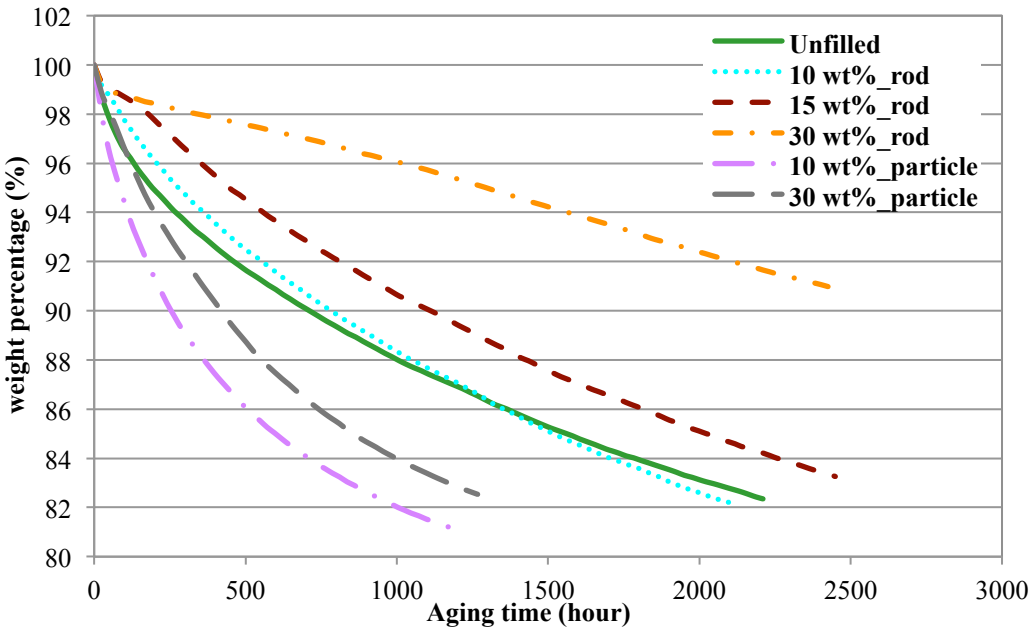

Fig. 4-4. Change of weight of unfilled and Al_2O_3-filled silicones during isothermal (250°C) aging.

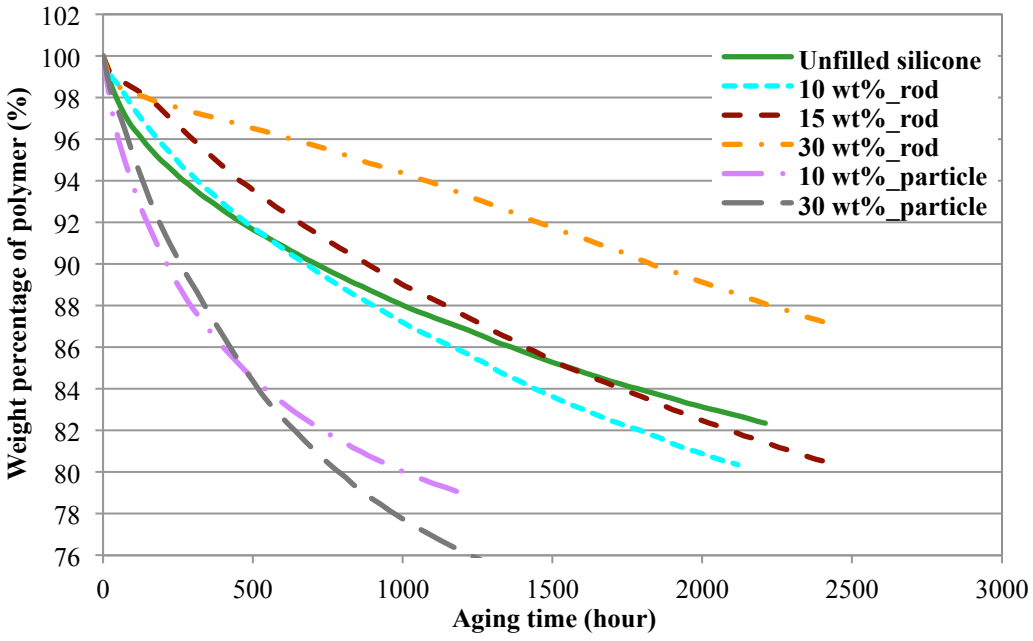

Fig. 4-5. Change of weight in polymer matrix of unfilled and Al_2O_3-filled silicones during isothermal (250°C) aging.

test. To fairly compare the weight-loss behavior of composites with different filler loadings, the residual weight needs to be calculated based on the weight of polymer matrix only. The calculated results are shown in Fig. 4-5.

The green solid line is the same as that in Fig. 4-4 because it represents unfilled silicone containing no Al_2O_3 filler. This line, showing that 10% of weight was lost in approximately 700 hours, again served as the benchmark for the experiment. The blue dotted line, which shows that 10% of polymer weight was lost in approximately 650 hours, represents the residual weight percentage of the polymer matrix in Al_2O_3/silicone composite filled with 10 wt% of rods. The maroon dashed line, which shows that 10% of polymer weight was lost in approximately 860 hours, represents the residual weight percentage of the polymer matrix in Al_2O_3/silicone composite filled with 15 wt% of rods. These results suggested that a 15 wt% loading of Al_2O_3 rods effectively improved the thermal stability of silicone matrix. A 30 wt% loading of Al_2O_3 rods had a more pronounced effect on the thermal stability of silicone matrix, as shown by the orange dash-dotted line. The sample lost 10% of its polymer weight in approximately 1800 hours. Throughout the entire experiment, Al_2O_3/silicone composite filled with 30 wt% of Al_2O_3 rods had the highest residual weight percentage of the polymer matrix among all samples and was thus the most thermally stable material prepared in this study.

Al_2O_3 particles decreased the thermal stability of silicone matrix, as shown by the purple long-dash-dotted and the grey long-dashed lines, which represent Al_2O_3/silicone composites with particle loadings of 10 wt% and 30 wt%, respectively. The residual weight percentage of polymer matrix in the Al_2O_3/silicone composites with particle loadings of 10-wt% and 30-wt% quickly dropped below 90% in 210 and 260 hours,

respectively. One possible reason for the different impact of Al_2O_3 rods and particles on thermal stability is their phase difference: Al_2O_3 rods are in γ phase, whereas the particles are in α phase.

The weight-loss rates of Al_2O_3/silicone composites were calculated based on the results of isothermal soak test. The initial weight-loss rate was defined as the slope of the isothermal weight-loss curve at the aging time of 24 hours. The selection of 24 hours was based on the assumption that any residual solvent that may exist in sample can be removed within the first 24 hours of isothermal soak at 250°C. The initial rates of isothermal weight loss of composites filled with various loadings of Al_2O_3 rods are shown in Fig. 4-6. The error bars represent the variation in measurements obtained from different samples of same composition. The blue diamonds represent the initial weight-loss rate calculated based on the total weight of composites, whereas the red squares

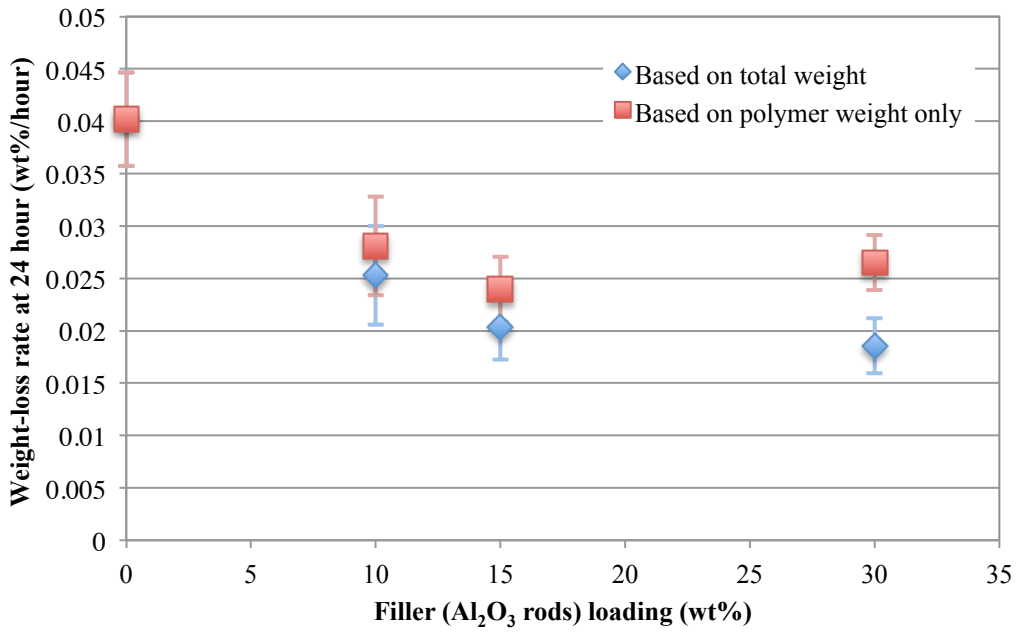

Fig. 4-6. Initial rate of weight loss (in 250°C isothermal aging) of unfilled and Al_2O_3-filled silicones.

represent that based on only the weight of polymer matrix. As filler loading increased, the initial weight-loss rate decreased monotonically except for that of the composite with a filler loading of 30 wt% calculated based on only the polymer weight. Compared to the 15-wt%-filled composite, a slightly higher rate was observed in the 30-wt%-filled one possibly because mesitylene was more difficult to remove due to the higher filler loading, which led to a higher viscosity before and a denser structure after cure. The 30-wt%-filled composite still had the highest thermal stability because both Figs. 4-4 and 4-5 show that it exhibited the lowest weight-loss rate (slope) among all samples after 24 hours of isothermal soak.

Results of isothermal soak test revealed that Al_2O_3 rods improved the thermal stability of silicone, whereas the particles decreased it. Since Al_2O_3 particles showed no potential to achieve a more thermally stable silicone encapsulant, it was excluded from further investigation at this point. The effect of Al_2O_3 rods on thermal stability is discussed in the rest of the chapter.

The improved thermal stability could be a result of restrained chain mobility. As suggested by the model of Tsagaropoulos in Section 1.5.3, tightly and loosely bound layers that exhibit different chain organization and low mobility are built up around filler surface due to the existence of interfacial bonds, which can be either physical (e.g., van der Waals force and hydrogen bond) or chemical (e.g., covalent bonds) in nature. Hydrogen instead of covalent bond was assumed to exist at the polymer-filler interface in this study because no silane coupler was used to modify the surface of Al_2O_3 rods [133-135]. Chain mobility can be restrained if hydrogen bond is strong enough to impact sufficient amount of silicone chains. The effect of interfacial hydrogen bond is

investigated in the rest of this chapter.

4.4. Hydrogen bonds between Al_2O_3 rods and silicone

Hydrogen bonds may form between Al_2O_3 surface and polysiloxane backbone. Existence of hydroxyl groups on Al_2O_3 surface is a prerequisite for interfacial hydrogen bond to form. This section describes the chemistry of Al_2O_3 surface and the formation of hydrogen bonds between Al_2O_3 rods and silicone backbone.

4.4.1.The surface of Al_2O_3

Formation of interfacial bonds requires specific chemical groups on both filler surface and polysiloxane chain. Al_2O_3 surface is covered by significant amount of hydroxyl (–OH) groups [137-141], as illustrated in Fig. 4-7. The formation of hydroxyl coverage is possibly a result of water dissociation on oxide surface, assuming that surface oxygen can link to a hydrogen atom in water molecule and form a hydroxyl group, which is bound to the metal atom that was originally bound to the surface oxygen [138]. Two types of hydroxyl groups exist on Al_2O_3 surface, i.e., isolated –OH and hydrogen-bonded –OH, as sketched in Fig. 4-7 [137].

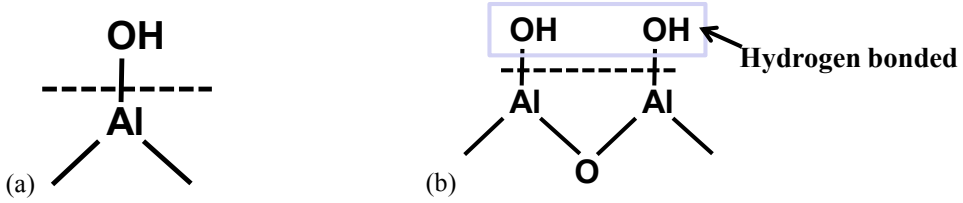

Fig. 4-7. Hydroxyl groups on Al_2O_3 surface: (a) isolated –OH and (b) hydrogen-bonded –OHs.

4.4.2.Hydrogen bonds at Al_2O_3/silicone interface

Hydrogen bonds can form between hydroxyl group on oxide surface and PDMS chain [133-135], as illustrated in Fig. 4-8 (a) and (b). A hydroxyl group on Al_2O_3 surface can form hydrogen bond with either another hydroxyl group as the terminal of silicone chain

(Fig. 4-8 (a)) or with an oxygen atom on the backbone (Fig. 4-8 (b)). The polymer chain can be immobilized in either case. The schematic of Al_2O_3/silicone interface is shown in Fig. 4-9.

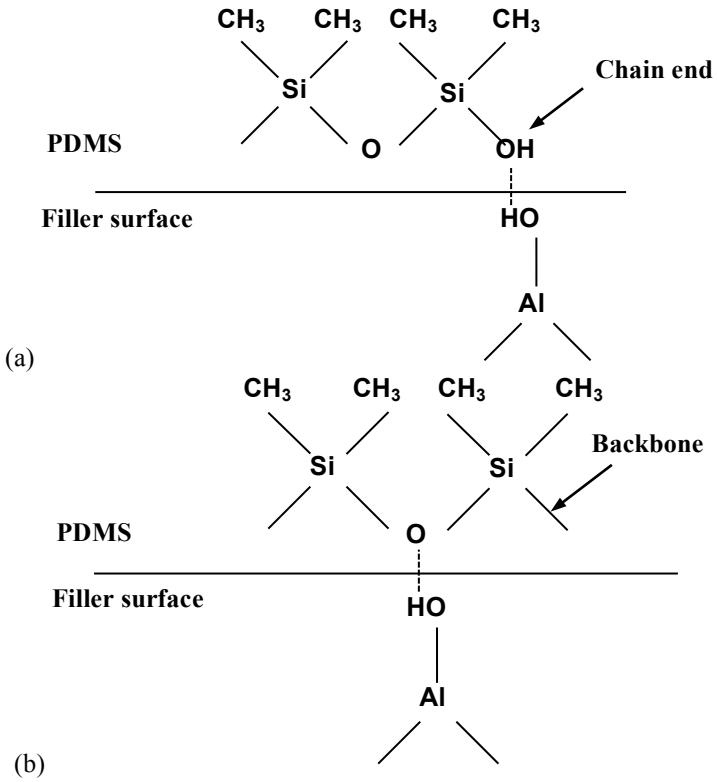

Fig. 4-8. Hydrogen bonds between Al_2O_3 surface and silicone chain: (a) between two –OHs, one on Al_2O_3 surface and one at the end of silicone chain and (b) between –OH on Al_2O_3 surface and Si-O backbone.

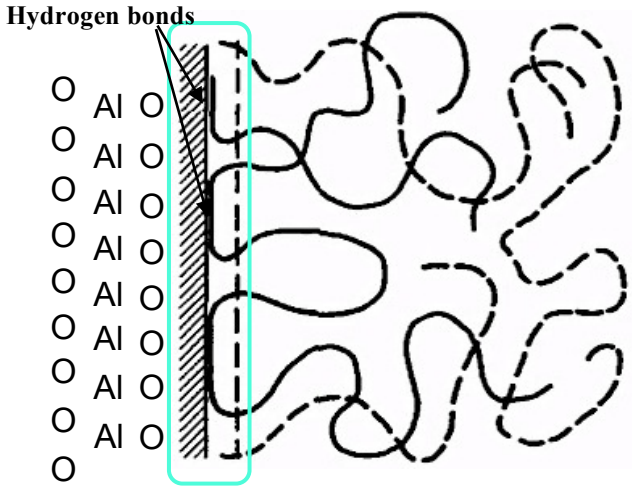

Fig. 4-9. Schematic of the Al_2O_3-silicone interface.

4.5. Effect of hydrogen bond on thermal stability

Improved thermal stability observed in silicones filled with Al_2O_3 rods may be explained by restrained chain mobility caused by interfacial hydrogen bonds. According to the model of Tsagaropoulos [99], a tightly bound layer containing chain segments hydrogen-bonded to Al_2O_3 surface is created. Assuming that hydrogen bond has a profound impact on chain mobility, an interface with higher concentration of hydrogen bonds should adsorb and immobilize more chain segments. The chain mobility of the loosely bound layer, which arises due to the far-field effect of interfacial bond, should also be affected by the concentration of hydrogen bonds. With more chain segments adsorbed onto filler surface, chains in the loosely bound layer are more strongly restricted. According to this assumption, the concentration of hydrogen bonds determines the average chain mobility of the Al_2O_3/silicone composite.

Since hydrogen bonds form between hydroxyl group on Al_2O_3 surface and PDMS chain, the existence and concentration of hydrogen bonds depends on those of surface hydroxyls. The concentration of surface hydroxyls is expected to be proportional to filler loading. The fact that thermal stability of silicone improves with increasing filler loading seems to indicate the positive effect of interfacial hydrogen bond. To further prove such effect, Al_2O_3 rods were treated for reduced hydroxyl concentration. If hydrogen bonds have a positive effect on thermal stability, reduction of its concentration should worsen the stability and cause higher weight-loss rate. Silicones filled with 10 wt% of Al_2O_3 rods with different surface condition (different concentration of hydroxyl groups/hydrogen bonds) were compared in the experiment.

4.5.1.Removal of hydroxyl groups on Al_2O_3 surface

To investigate the effect of hydrogen bond on thermal stability of silicone, high-temperature dehydration was performed to (partially) remove hydroxyl groups on Al_2O_3 surface [137, 139]. As suggested in [137], when Al_2O_3 was soaked at elevated temperature, surface –OHs react with one another to form H_2O molecules, which can be quickly removed if the reaction is performed in high vacuum (< 10^{-5} mmHg). As shown in Fig. 5 of [139], surface –OHs that are hydrogen-bonded to each other can be removed below 500°C and isolated –OHs can be removed at a higher temperature of 750 - 900°C. The dehydration in this study was performed at 500 or 900°C in N_2 instead of vacuum for five hours each. The experiment was performed in a tube furnace (Lindberg, Model: Blue M) with a temperature-ramp rate of 10°C/min and a constant gas flow of approximately 0.1 L/min. The setup is shown in Fig. 4-10. Al_2O_3 rods (approximately 1 g) were placed in a combustion boat, which was inserted into the center of the tube furnace during experiment.

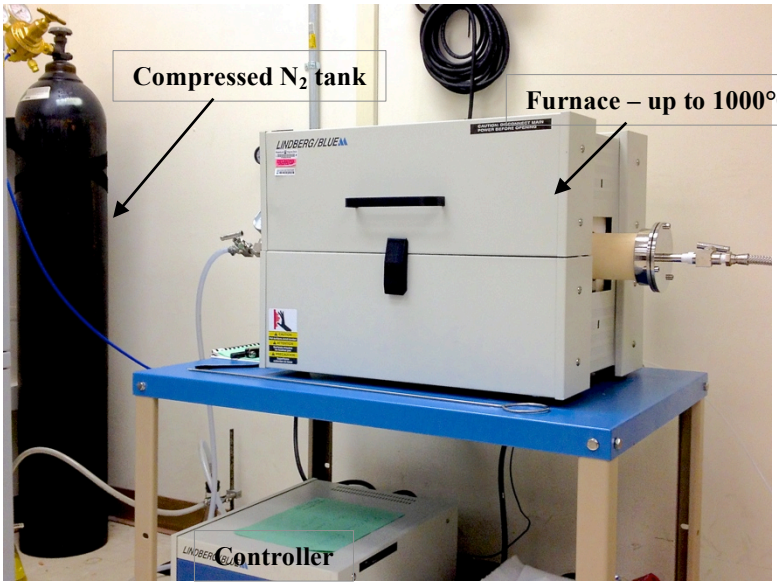

Fig. 4-10. Tube furnace connected to compressed N_2 tank for high-temperature dehydration of Al_2O_3.

4.5.2.Characterization of Al_2O_3 surface with X-ray photoelectron spectroscopy (XPS)

High-temperature dehydrated and as-received Al_2O_3 rods were characterized by XPS to quantify the hydroxyl content on their surface. Prior to XPS analysis, Al_2O_3 rods (dehydrated or as-received, approximately 100 mg) were sprinkled on double-sided tape (1 cm × 1 cm) mounted on the sample stage, as shown in Fig. 4-11. A survey (low-resolution) scan with a step size of 1.0 eV throughout the entire energy range confirmed the composition of the test sample. High-resolution scan with a step size of 0.1 eV in narrow energy ranges where C 1s and O 1s peaks were located generated data that were used for quantification of surface hydroxyl.

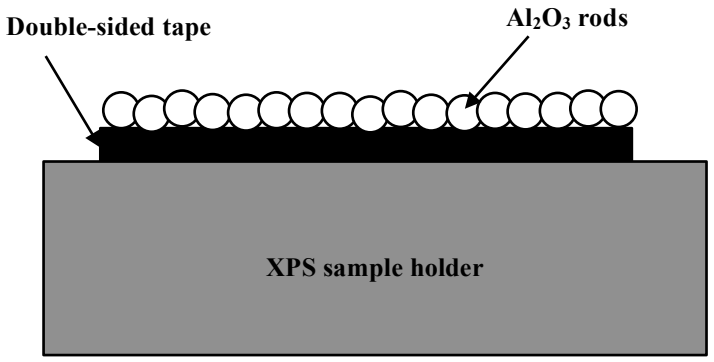

Fig. 4-11. Sample preparation for XPS.

The survey spectra that represent as-received and dehydrated rods are given in Fig. 4-12, with C-C/C-H component of the C 1s peaks shifted to 248.8 eV for charging correction. Survey results revealed that all three types of rods appeared to be pure Al_2O_3, with no impurity peak and a tiny contamination peak (C 1s) observed. The O 1s peaks of high-resolution, as shown in Fig. 4-13, were corrected for charging by shifting the C-C/C-H component of C 1s peak to 248.8 eV. Dehydration at 500 and 900°C caused a shift of O 1s peak to lower binding energy, which was possibly the result of changed hydroxyl fraction.

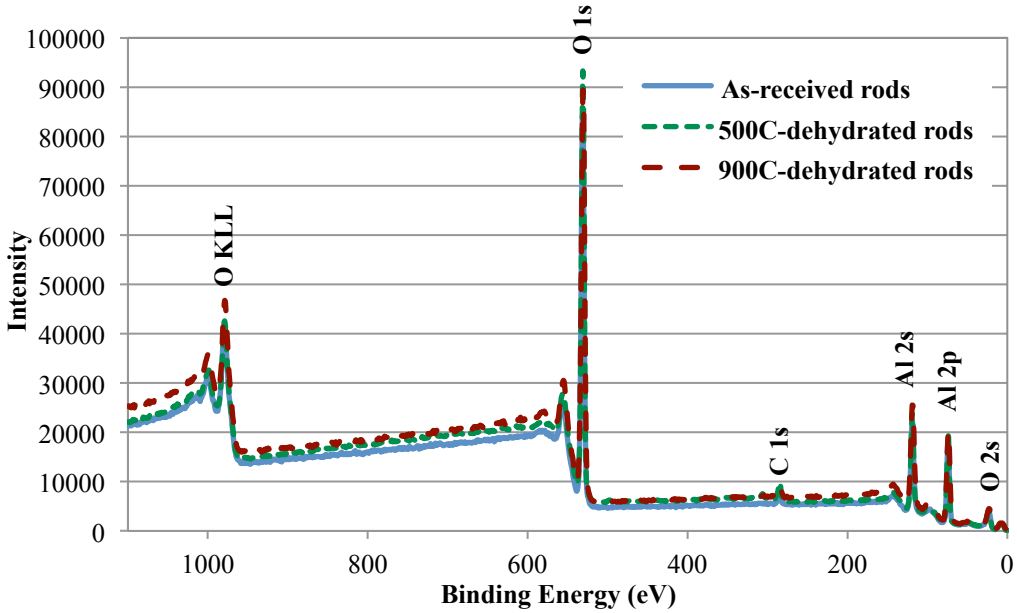

Fig. 4-12. Spectrum of XPS survey on as-received and dehydrated Al_2O_3 rods.

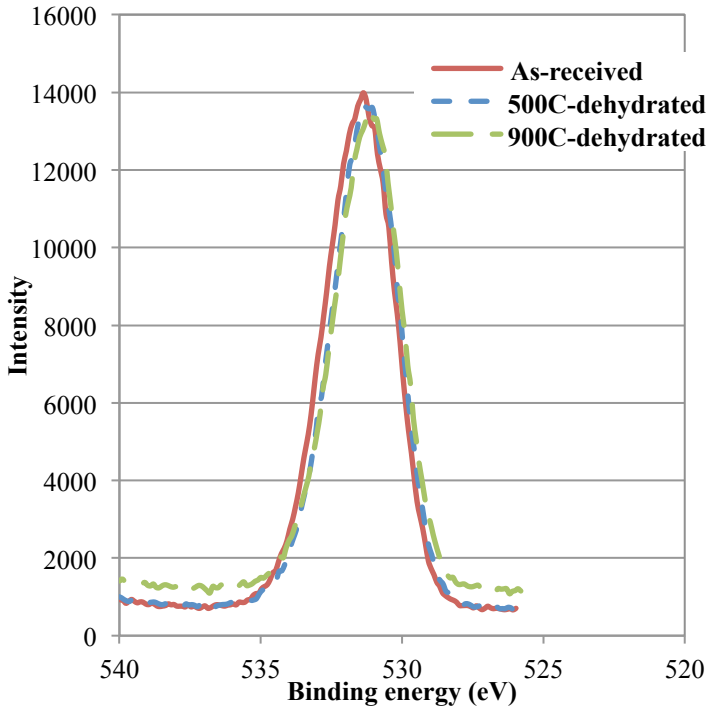

Fig. 4-13. Representative high-resolution O 1s peaks from XPS characterization on as-received and dehydrated Al_2O_3 rods.

Curve-fitting was performed according to the peak location of O^{2-}, OH^-, and chemisorbed-H_2O components reported in literature [142-146]. Binding energy of OH^- is approximately 1.4 - 1.8 eV higher than that of O^{2-} but around 1.3 eV lower than that of chemisorbed-H_2O. The results of as-received and dehydrated Al_2O_3 rods are shown in Figs. 4-14, 4-15, and 4-16. Peak location of each component was kept the same for all types of rods, as listed in TABLE 4-3. Each set of data (as shown in a single row in TABLE 4-3) obtained for dehydrated Al_2O_3 was averaged from multiple spots on one sample. Each set of data for as-received Al_2O_3 was obtained from a single spot because this sample is assumed to be highly uniform. Student's t-test (2-tail, unequal variance) proved that the hydroxyl content on the three types of Al_2O_3 surface was statistically different from each other at a confidence level of 99%. Hydroxyl fraction dropped

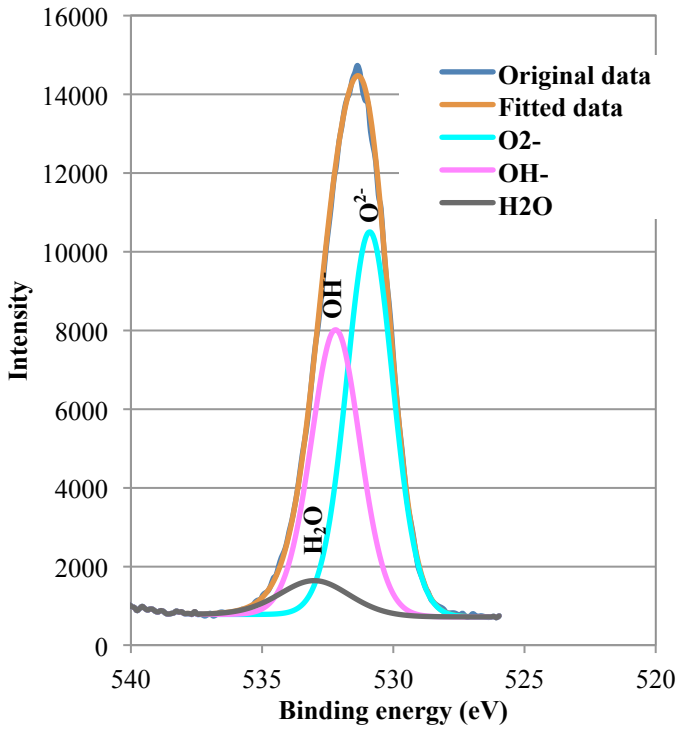

Fig. 4-14. Curve-fitting of a representative O 1s peak of as-received Al_2O_3 rods.

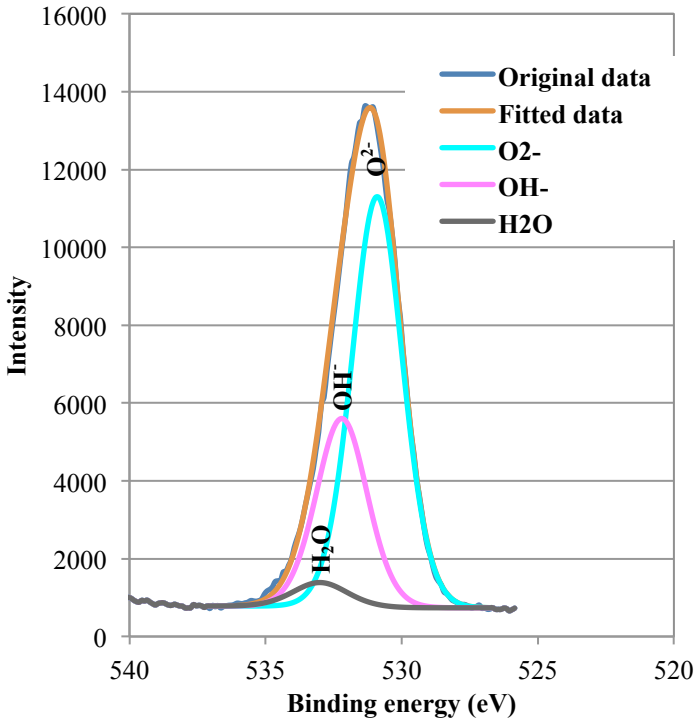

Fig. 4-15. Curve-fitting of a representative O 1s peak of 500°C-dehydrated rods.

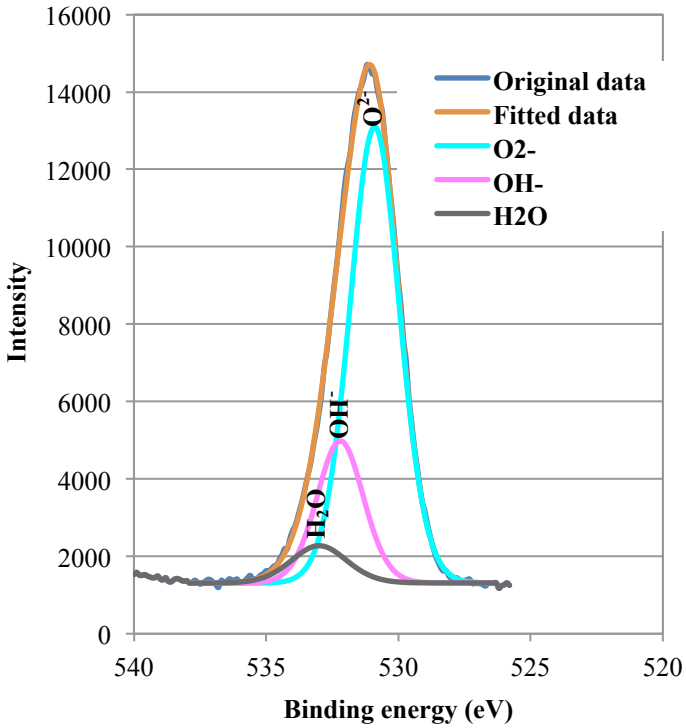

Fig. 4-16. Curve-fitting of a representative O 1s peak of 900°C-dehydrated rods.

significantly after dehydration, suggesting that high-temperature dehydration in inert atmosphere can partially remove hydroxyls on the surface of Al_2O_3 rods.

TABLE 4-3
CURVE-FITTING RESULTS OF O 1S PEAKS OF
AS-RECEIVED AND DEHYDRATED AL_2O_3 RODS

	O2- 530.9 eV	OH- 532.3 eV	H_2O 533.0 eV
As-received	53.32% 55.20% 52.40% 55.93%	39.89% 41.26% 40.69% 39.76%	6.79% 3.54% 6.90% 4.31%
500°C dehydrated	63.83% 66.31% 65.83% 62.68%	30.26% 29.92% 30.06% 30.48%	5.90% 3.77% 4.11% 5.84%
900°C dehydrated	72.24% 73.25% 72.74% 71.04%	20.75% 20.14% 21.17% 21.92%	7.02% 6.61% 6.09% 7.05%

4.5.3.Characterization of Al_2O_3 surface with FTIR

As-received and dehydrated Al_2O_3 rods were also analyzed by FTIR to verify the content of surface hydroxyls. The experiment was performed on a Varian 670-IR in ATR (attenuated total reflectance) mode. ATR is a technique that allows direct analysis of samples in all forms (e.g., solids, liquids, powders, slurries, etc.) and overcomes the drawback of tedious sample preparation for traditional IR spectrometer [147, 148]. During measurement, the infrared beam enters the ATR crystal, which has refractive index considerably higher than that of the sample, at a specific angle (typically 45°) and is totally reflected at the ATR/sample interface [147]. An evanescent wave, which decays exponentially within the sample versus the distance away from interface, is formed due to the wave-like property of infrared beam. The penetration depth (into sample surface) of the evanescent wave is usually 0.5 - 3 μm, depending on the wavelength of the incident light. In frequency ranges that the sample absorbs energy, the evanescent wave is

attenuated or altered. The attenuated evanescent wave carries the structural information of the sample because each chemical group only absorbs photons (energy) of specific frequency(ies). The attenuated energy of each evanescent wave is passed back to IR beam, which exits the other side of the ATR crystal after several reflections. The system then generates a spectrum with the information carried by the IR beam [148]. Fig. 4-17 illustrates the mechanism of ATR technique [148].

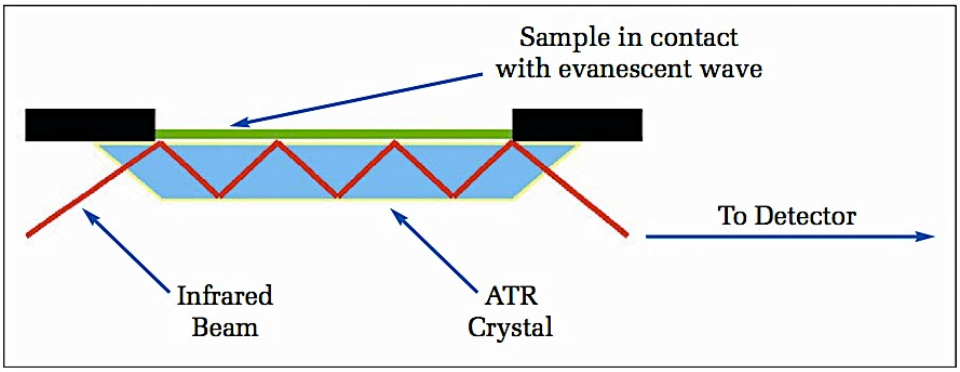

Fig. 4-17. Schematic of attenuated total reflectance (ATR) mode of FTIR measurement [148].

Fig. 4-18 shows the sample loaded to FTIR for measurement in ATR mode. Excessive powder (approximately 100 mg) was loaded to guarantee good contact between the sample and ATR crystal. The results (after ATR correction) obtained from as-received and dehydrated Al_2O_3 rods are given in Fig. 4-19, which shows the absorbance in the frequency range of 3800 - 3300 cm^{-1}, where multiple peaks corresponding to hydroxyl groups were observed [137, 139]. As-received Al_2O_3 rods exhibited the highest absorbance, which decreased with increasing dehydration temperature. The FTIR results indicated that high-temperature dehydration in inert atmosphere reduced the hydroxyl content on Al_2O_3 surface. The higher the temperature, the more efficient the dehydration, in agreement with results reported in [137, 139].

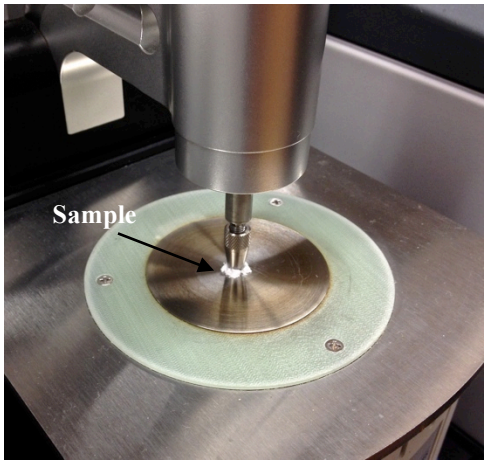

Fig. 4-18. FTIR measurement in ATR mode on a Varian 670-IR.

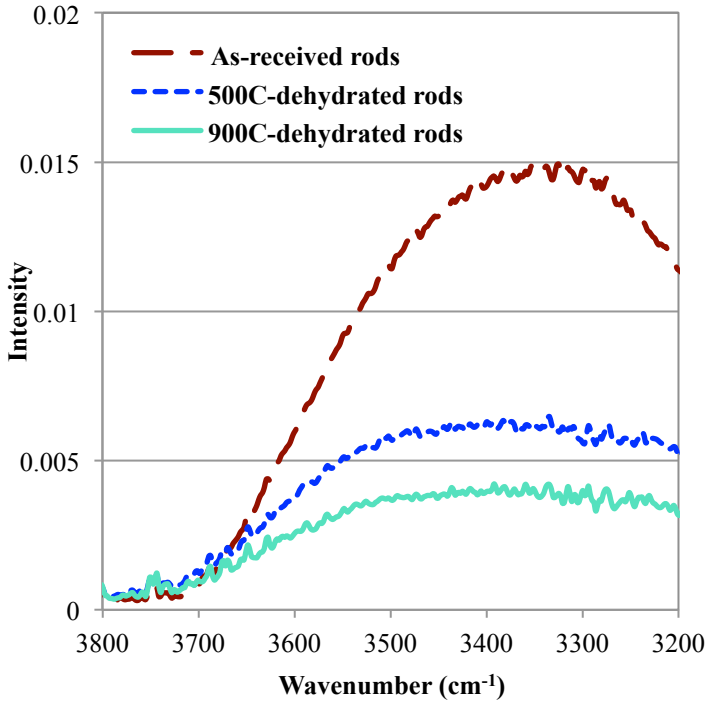

Fig. 4-19. FTIR results of as-received, 500°C-dehydrated, and 900°C-dehydrated rods.

4.5.4.Isothermal weight loss of composites with dehydrated rods

Dehydrated rods were used to make Al_2O_3/silicone composite with a filler loading of 10 wt% by following the preparation procedure described in Fig. 3-10. Weight loss of composites made from Al_2O_3 rods that were differently dehydrated (500 or 900°C) was

monitored in isothermal soak test performed in air at 250°C. The test condition was the same as described in Section 4.3.1. At least three samples of the same composition were tested. The average residual weight percentage is plotted in Fig. 4-20. The variation in measurements obtained from the same type of sample is again represented by the error bars of calculated initial weight-loss rates given in Fig. 4-21.

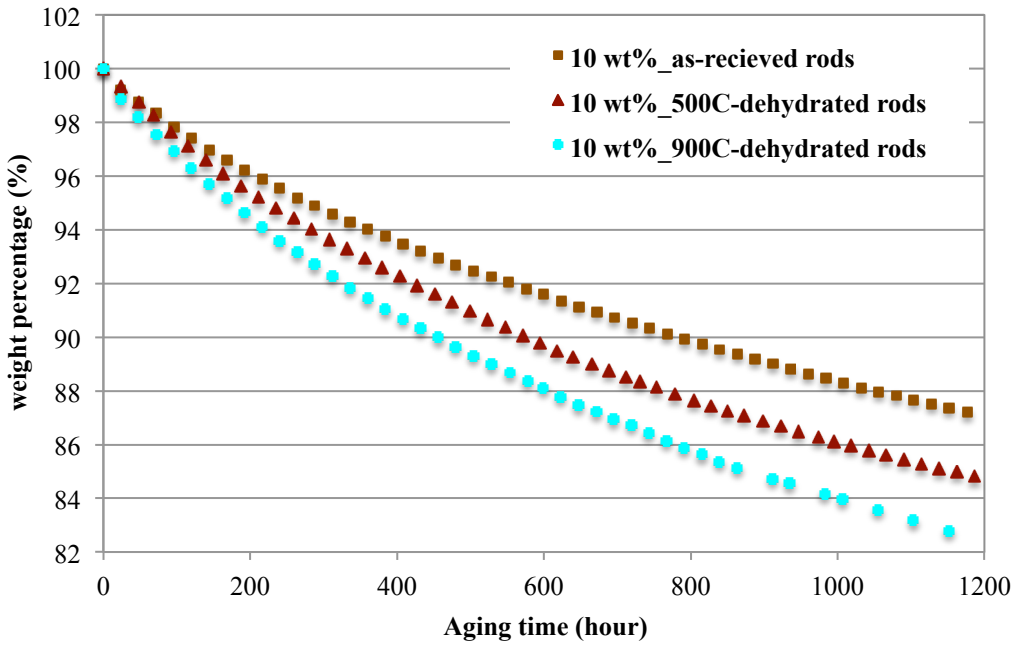

Fig. 4-20. Residual weight of silicones filled with 10 wt% of as-received and dehydrated Al_2O_3 rods during isothermal (250°C) aging.

The composite made from as-received Al_2O_3 rods, as represented by the squares, exhibited the highest thermal stability. The composite made from rods dehydrated at 500°C for 5 hours, as represented by the triangles, indicated slightly lower thermal stability. The lowest thermal stability was observed in the composite made from rods dehydrated at 900°C for 5 hours, as represented by the circles. The results suggested that thermal stability decreased with increasing dehydration temperature and decreasing hydroxyl content. The initial weight-loss rates of composites filled with 10 wt% of Al_2O_3

rods having undergone different treatments are plotted in Fig. 4-21. With increasing dehydration temperature, the initial weight-loss rate increased from approximately 0.025 to 0.036 wt%/hour, reflecting a decrease in thermal stability. When calculated based on only the weight of polymer matrix, as explained in Section 4.3.2, the weight-loss rate of the composite filled with 10 wt% of 900°C-dehydrated rods was comparable with that of the pure silicone.

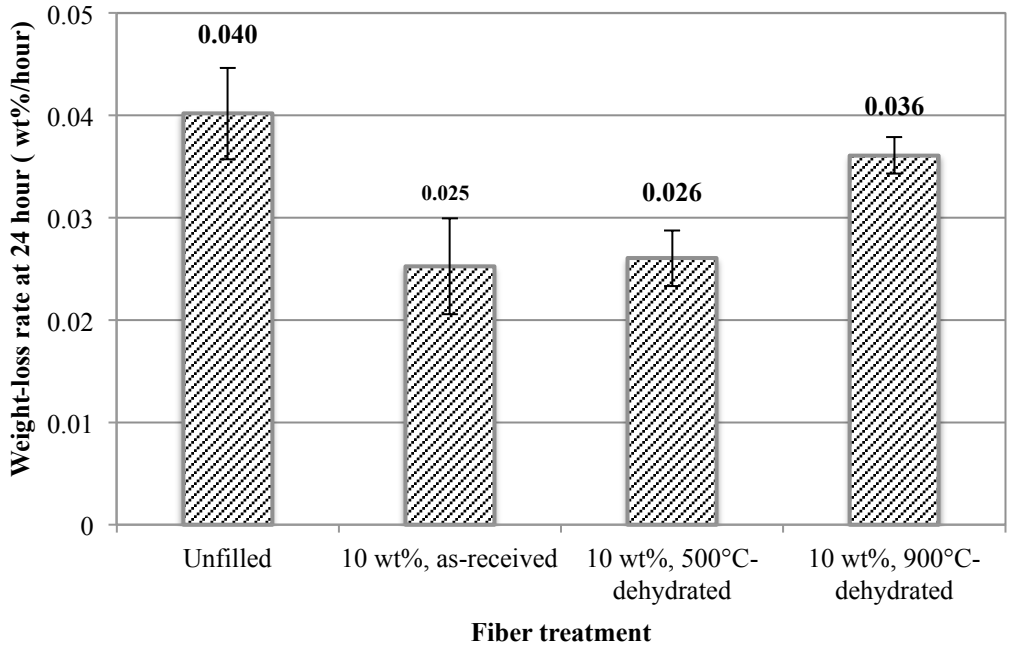

Fig. 4-21. The initial rates of weight loss (at 24 hour) of 10-wt%-filled silicones subject to isothermal (250°C) soak.

Reduced thermal stability can be explained by the restored chain mobility, which was a result of the removal of hydroxyl groups on Al_2O_3 surface. Hydrogen bonds formed between surface –OHs and silicone matrix restrained chain mobility and therefore hindered the decomposition of silicone backbone. When surface –OHs were (partially) removed, the total number of hydrogen bonds at the interface decreased, thus restoring chain mobility.

4.6. Summary

The weight-loss behavior of pure silicone and its Al_2O_3-filled composites with different filler contents was analyzed by both TGA and isothermal soak tests. Both tests revealed that Al_2O_3 rods obtained from Alfa Aesar (Part No. 43912) could improve the thermal stability of silicone elastomer (EPM-2422 by Nusil Technology). TGA results indicated that the temperature of onset degradation increased from 330 to 379°C with the addition of 30 wt% of rods. In the isothermal soak test performed at 250°C in air, pure silicone lost 10% of polymer weight in 700 hours, whereas the composite filled with 30 wt% of Al_2O_3 rods (Part No. 43912 by Alfa Aesar) lost the same amount of weight in 1800 hours. The improved thermal stability was attributed to the hydrogen bonds formed at the Al_2O_3/silicone interface, which restrained the chain mobility of silicone matrix and hindered the formation of decomposition products. Al_2O_3 particles (Part No. 44932 by Alfa Aesar) appeared to impair thermal stability of the same silicone elastomer, possibly due to reasons like phase difference (α phase, compared to γ phase for Al_2O_3 rods), surface impurity, surface charges, etc.

To verify the effect of hydrogen bonds on thermal stability, experiments were designed to examine whether the weight-loss rate could be restored when interfacial bonds were (partially) removed. Removal of interfacial hydrogen bonds was achieved by reducing the hydroxyl content on Al_2O_3 surface via high-temperature dehydration in N_2. XPS and FTIR results confirmed the reduction of hydroxyl content. Isothermal soak test performed at 250°C in air showed that the 10-wt%-filled silicone composites made from dehydrated rods exhibited a lower thermal stability than that made from as-received ones, with the initial weight-loss rate increased from ~0.025 wt%/hour (with as-received rods)

to ~0.036 wt%/hour (with rods dehydrated at 900°C). The restored weight-loss rate resulted from the loss of interfacial bonds and weakening of interfacial restriction, both of which directly impacted the tightly bound layer by reducing the amount of adsorption sites. The loosely bound layer was also impacted because it was formed by the far-field effect of interfacial bonds. Decreasing number of interfacial bonds increased the chain mobility of both layers, and thus increased the initial weight-loss rate and reduced the thermal stability.

Effect of Al_2O_3 rods on thermal stability is summarized as follows:

1. Hydroxyl groups on Al_2O_3 surface formed hydrogen bonds with oxygen atoms in silicone backbone or with hydroxyl groups at chain terminals.
2. Interfacial hydrogen bonds restrained chain mobility by producing tightly and loosely bound layers containing chain segments with restricted motion.
3. Reduced mobility impaired the flexibility of silicone backbone, causing difficulty to the formation of certain local chain configurations that facilitate the decomposition process and thus hindering the generation of volatile decomposition products.
4. With the formation of decomposition products being hindered, the weight-loss rate was reduced and the weight-loss process was decelerated, leading to an improved thermal stability.

Chapter 5. Dielectric Performance of Al_2O_3/Silicone Composites

5.1. Introduction

The importance of improving thermal stability of silicone was discussed in previous chapters. Weight-loss experiments in Chapter 4 proved that Al_2O_3 rods (Part No. 43912 by Alfa Aesar) could effectively improve the thermal stability of silicone elastomer (EMP-2422 by Nusil Technology). The weight-loss experiments quantitatively measured the weight of volatile products generated during degradation but could hardly provide any information on the evolution of material microstructure. Silicone tended to crack when continuously aged at high temperature in Chapter 2, indicating that microstructural change occurred together with thermal degradation. Dielectric strength was very sensitive to silicone microstructure because partial discharge of air may occur in microscale cracks at a very low electric field (< 10 kV/mm).

The effect of Al_2O_3 rods on thermal stability of silicone is investigated in this chapter by monitoring the change in dielectric strength during thermal aging. Further aging can adversely affect dielectric strength when degradation is sufficiently significant to weaken and crack the material. Since the development of defects and cracks is slower in a material with higher thermal stability, change in dielectric strength is used as an indication of silicone degradation. The dielectric strength of unfilled silicone and

Al_2O_3/silicone composites with various filler loadings are compared before and after thermal aging at 250°C in air. A more thermally stable material is expected to experience slower degradation and maintain its original dielectric strength for a longer time.

5.2. Sample preparation

Silicones unfilled and filled with Al_2O_3 rods were prepared according to the procedure described in Fig. 3-10. The coupon for dielectric characterization was similar to the one showed in Fig. 2-12. A flat glass substrate (5 cm × 5 cm) was sputter-coated with a Cr/Ni/Ag tri-layer (thickness for Cr, Ni, and Ag: 200, 300, and 500 nm) by physical vapor deposition (PVD). This metallized substrate served as the bottom electrode. Uncured Al_2O_3/silicone composite (immediately used after preparation to prevent viscosity increase) was spin-coated on top of the metallized glass substrate, with the thickness controlled to approximately 120 micrometers. The composite was then cured in air at 65°C for four hours. Five silver electrodes were painted on the cured composite film by using a silver paste (NanoTach X, NBE Technology). The coupon was then placed on a hot plate at 250°C for 10 minutes to sinter the silver electrodes. Figs. 5-1 and 5-2 show the top and cross-sectional views of the test coupon for dielectric characterization, respectively.

5.3. Test conditions

5.3.1. Characterization of dielectric strength

The dielectric strength of the composite film was measured at room temperature (approximately 25°C) by Hipot megaohmmeter, whose cathode and anode were connected to the top and bottom electrodes of the test coupon, respectively. A flat and polished copper plate was used to release possible stress-concentration that may be

caused by the Hipot electrode, as shown in Fig. 2-13. The contact resistance measured by multimeter between top electrode and copper plate was less than 50 Ω. The test was performed with ac voltage, which was ramped up at a constant rate (~200 V/s) until breakdown was detected by Hipot. At least 10 samples were measured for each composition and aging condition.

5.3.2.Thermal aging

To investigate the effect of Al_2O_3 rods on thermal stability of silicone, test coupons made of unfilled silicone and Al_2O_3/silicone composites with filler loadings of 10, 15, and 30 wt% were subject to thermal aging in an environmental chamber (Model 9023,

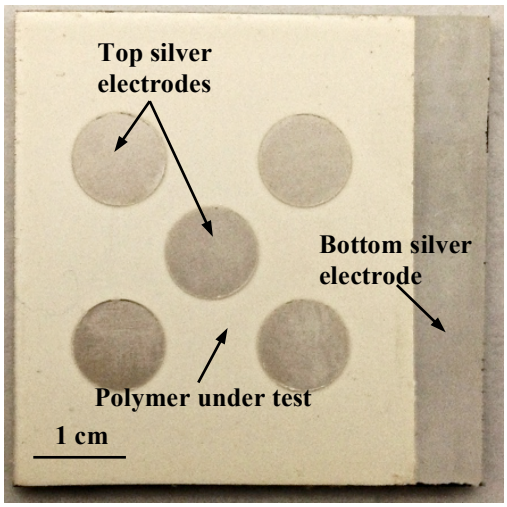

Fig. 5-1. Top view of test coupon for dielectric characterization.

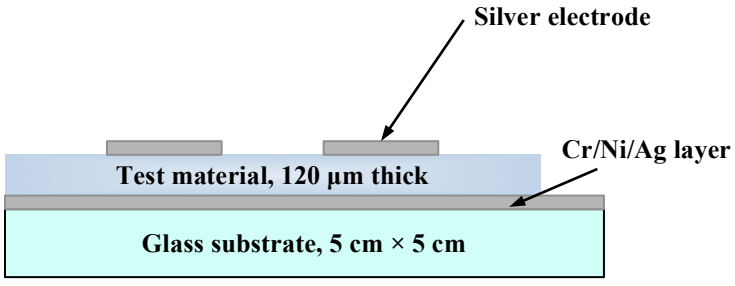

Fig. 5-2. Cross-sectional view of test coupon.

Delta Design) at 250°C - the maximum operation temperature of current SiC devices. At the beginning of aging, the temperature was ramped up from room temperature to 250°C in 20 minutes and maintained there throughout the test. The temperature variation during aging was kept within ±0.5°C. At least two coupons (enabling 10 measurements) were removed from the furnace at each sampling point and their dielectric strength was soon measured after the coupon was cooled down to room temperature. The sampling points used in this study were 80, 160, 240, 320, 400, and 480 hours.

5.3.3.Scanning electron microscopy (SEM)

To explain the relationship between silicone degradation and the low dielectric strength, aged coupons made of unfilled silicone and its composite filled with 15 wt% of Al_2O_3 rods were examined by SEM after dielectric measurements. The experiment was performed with a LEO (Zeiss) 1550 field-emission SEM. An accelerating voltage of 5 kV was used to avoid overheating or degrading the polymer film. In-lens detector that mainly collects backscattered electrons was used. The top surface of test coupon was gently cleaned with ethanol and sputter-coated with gold (a few nanometers in thickness) before SEM observation. During the experiment, the top electrodes and the polymer film adjacent to them were carefully examined to find signs of defect development that were responsible for dielectric failure. SEM images of polymer film containing no crack and microscale cracks are exampled in Fig. 5-3 (a) and (b), respectively.

5.4. Dielectric characterization of Al_2O_3/silicone composites

5.4.1.Dielectric strength of as-prepared Al_2O_3/silicone composites

The test results of dielectric breakdown of polymers are often analyzed with a statistical method. The Weibull distribution is widely accepted for such data analysis

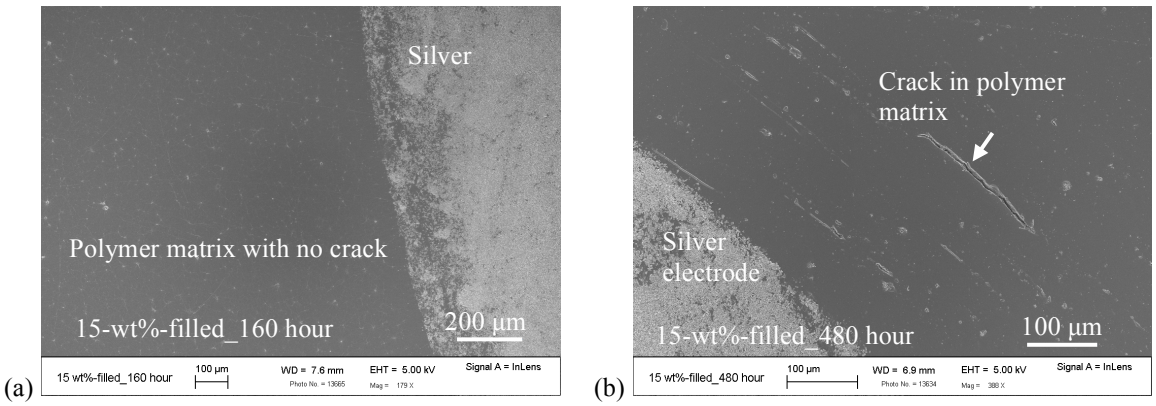

Fig. 5-3. SEM images of polymer film surrounding top electrode: (a) no crack observed and (b) microcracks observed.

because dielectric failure of an entire system depends on that of the weakest point [149-151]. The probability of failure, P, at a given electric field follows the mathematical expression of

$$P = 1 - \exp\left[-\left(\frac{E}{E_0}\right)^{\beta}\right], \qquad (5\text{-}1)$$

where E is the applied field and E_0 and β are the Weibull parameters. The characteristic dielectric strength E_0 represents the electric field at which the failure probability is 63.2%. The shape parameter β measures the spread of the data. The higher the β, the narrower the distribution. The calculation of the two parameters as well as their confidence interval of 90% was based on the methods given in [152, 153]. A dielectric measurement similar to the one used in this study was performed by Locatelli *et al* [65] on a silica-filled silicone elastomer. The author tried to analyze the data by using Weibull distribution but did not fully interpret the results by considering only the Weibull parameter (E_0), which is less sensitive to aging.

The Weibull plot of the breakdown data obtained from as-prepared unfilled silicone

(which was prepared according to the procedure described in Section 3.3 except that no Al_2O_3 rod was added) is shown in Fig. 5-4. The characteristic dielectric strength and shape parameter of this sample are listed in TABLE 5-1. E_0 of the unfilled silicone (~ 20 kV/mm) fell in the typical range of dielectric strength of silicone [45, 47]. The narrow distribution observed on the Weibull plot yielded a $\beta > 15$.

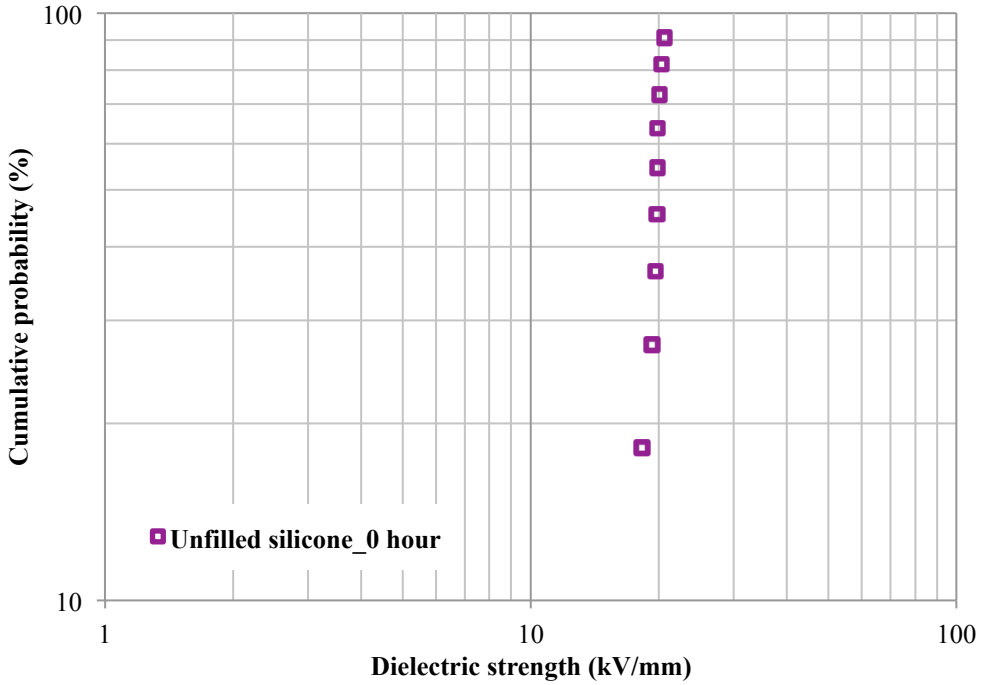

Fig. 5-4. Weibull plot of measured dielectric strength of as-prepared unfilled silicone.

The Weibull plots of the breakdown data from as-prepared Al_2O_3/silicone composites with filler loadings of 10, 15, and 30 wt% are shown in Fig. 5-5. The two Weibull parameters for these samples are also listed in TABLE 5-1. Considering the mathematical expression of Weibull distribution (expressed by (5-1)), the shape parameter becomes increasingly sensitive to the variation of E/E_0 as β increases and as E/E_0 falls in a narrower range. For example, the three Weibull plots shown in Fig. 5-5 all exhibit a narrow distribution within ±1.5 kV/mm but the β calculated from them have a large fluctuation from 22.55 to 41.60, together with large confidence (90%) intervals.

Increasing sample population is possible to narrow down the confidence intervals of β. The characteristic dielectric strength of all three composites was comparable to that of the unfilled silicone. The data obtained from the three composites also showed a narrow distribution on the Weibull plot, with $\beta > 15$. The results therefore indicated that the Al_2O_3 rods had no adverse impact on the insulation capability of the silicone encapsulant.

TABLE 5-1
CHARACTERISTIC DIELECTRIC STRENGTH AND SHAPE PARAMETER OF AS-PREPARED UNFILLED AND AL_2O_3-FILLED SILICONES

As-prepared (Unaged)*	0 wt%	10 wt%	15 wt%	30 wt%
E_0 (kV/mm)	20.13	22.30	20.27	20.67
β	33.82	41.26	22.55	41.60

* No crack observed in any of the samples.

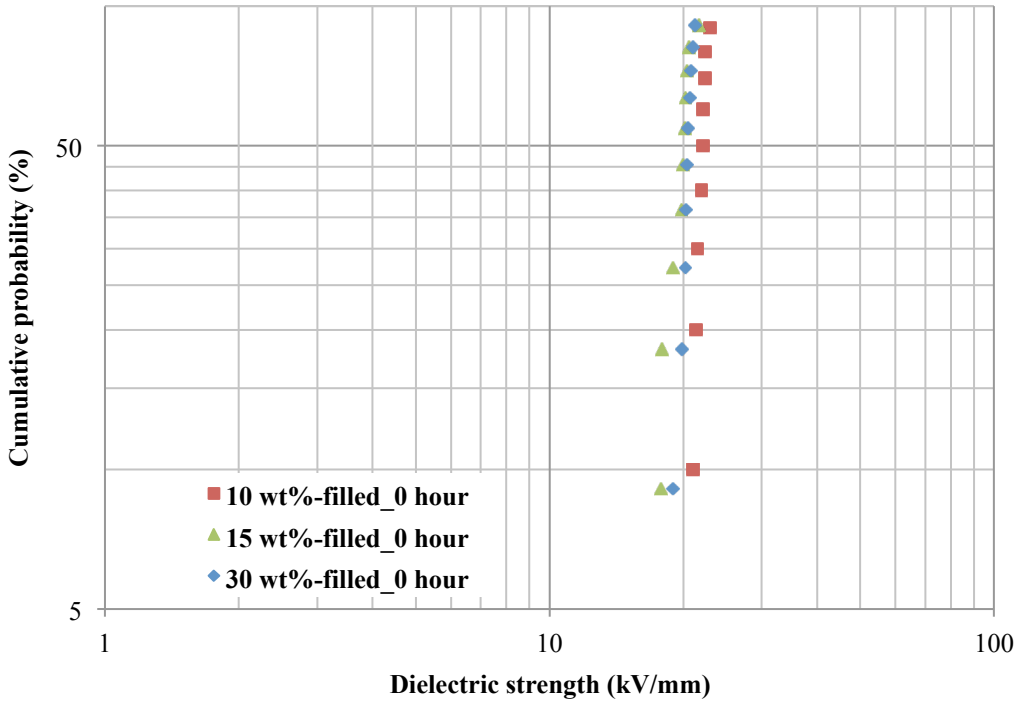

Fig. 5-5. Weibull plots of measured dielectric strength of as-prepared Al_2O_3/silicone composites.

5.4.2.Effect of thermal aging on dielectric strength of unfilled silicone

Test coupons built with unfilled silicone were aged isothermally at 250°C in air for at least 480 hours. The silicone film showed no change in physical appearance under optical microscope within 200 hours of aging. The Weibull plots of unfilled silicone aged for up to 480 hours are shown in Figs. 5-6 and 5-7. The dielectric data for the unfilled silicone aged for 80 hours exhibited good consistency, with a large β value of 23.14. E_0 of the unfilled silicone aged for 80 hours was calculated to be 20.82 kV/mm, which was comparable to that of the as-prepared one. As aging continued to 160 and 200 hours, dielectric failure below 15 kV/mm was detected. Such early failure could be explained by the formation of microscale cracks and voids as a result of silicone degradation. The microstructure of aged samples were examined to prove the existence of such defects, as will be shown in Section 5.5. Both cracks and voids are considered as cavities in the matrix and are filled with air, which has much lower dielectric strength than the polymer matrix. When a cavity is large enough, the electric field in the cavity can reach the dielectric strength of air before breakdown occurs in the polymer matrix. Partial discharge may occur in the cavity and damage the polymer matrix, leading to electrical breakdown of the entire film.

Dielectric failure below 15 kV/mm occurred more frequently as aging continued to 240 hours. A few visible macroscale cracks appeared in the polymer matrix, as shown in Fig. 5-8. A similar phenomenon was observed in coupons aged for 320 hours as well. The cracks identified in such samples were found to propagate through the entire thickness of the polymer film, as illustrated in Fig. 5-9. When voltage is applied between top and bottom electrodes, electric field exist in the polymer film directly under the top electrode

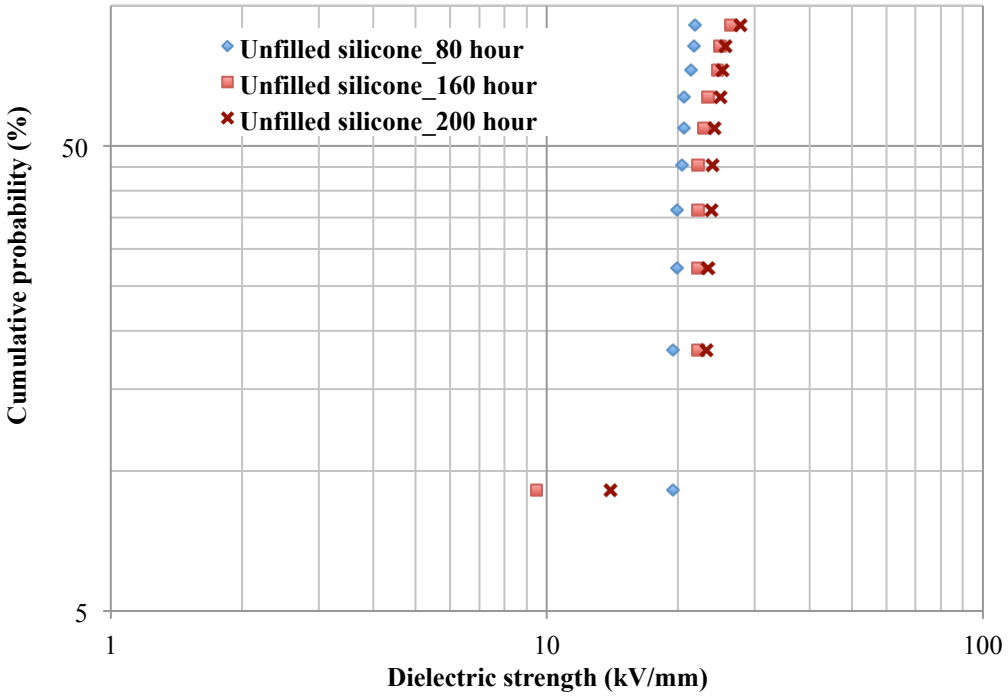

Fig. 5-6. Weibull plots of measured dielectric strength of unfilled silicone aged at 250°C for 80, 160, and 200 hours.

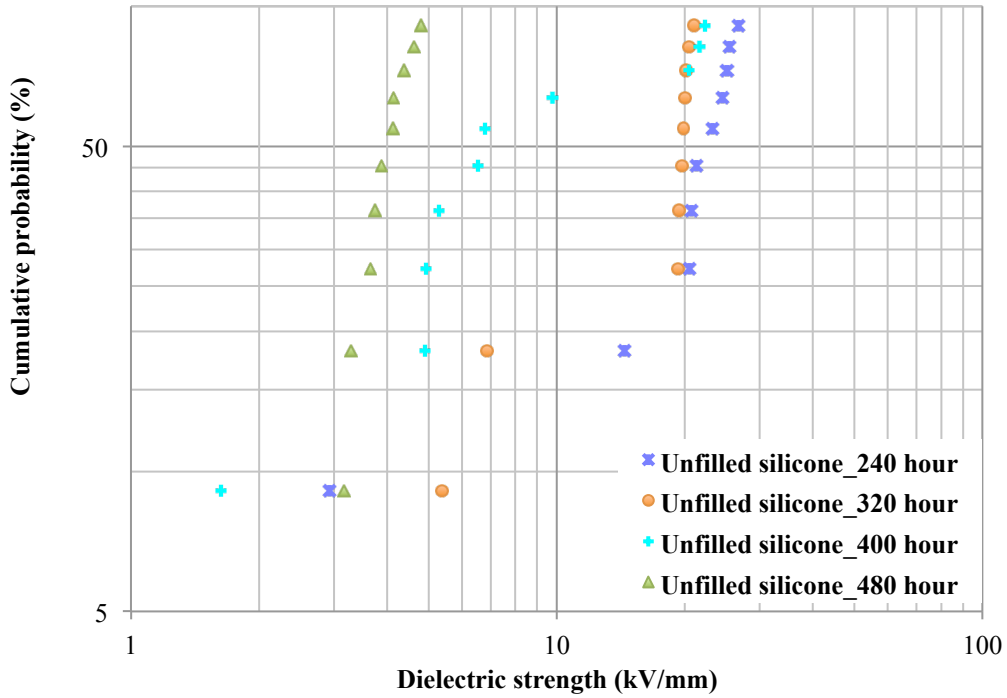

Fig. 5-7. Weibull plots of measured dielectric strength of unfilled silicone aged at 250°C for 240, 320, 400, and 480 hours.

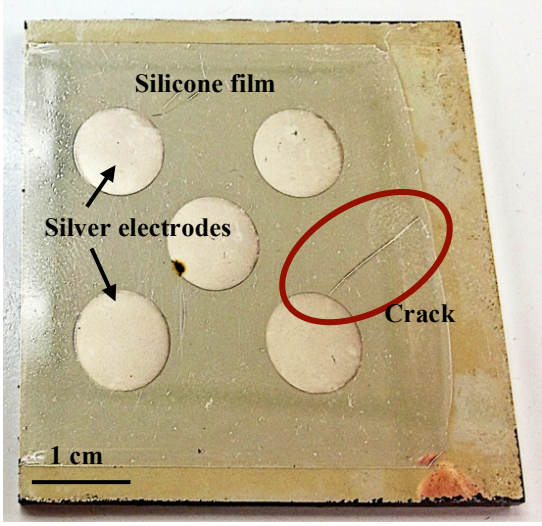

Fig. 5-8. Test coupon after 240 hours of aging with cracks appearing in polymer film.

as well as in the film surrounding it (known as fringing electric field). The intensity of the fringing field decreases as the distance away from the top electrode increases. If the polymer film contains a crack as shown in Fig. 5-9, air in the crack is exposed to the fringing electric field. Although the fringing field is lower than that directly under the top electrode, dielectric breakdown may still occur in the crack if it is sufficiently close to the top electrode (e.g., < 0.5 mm) because air has a much lower dielectric strength than the polymer film (~3 kV/mm compared to ~20 kV/mm). Fig. 5-10 proves that dielectric failure can occur in defects existing in the area surrounding a top electrode by showing a burned site that is about 200 μm away from it. Since cracks may occur at different distance away from a top electrode and the dielectric strength of a sample is calculated by directly dividing the measured voltage by the film thickness, the results obtained after 160 - 400 hours show large spread on the Weibull plots shown in Fig. 5-7. The area where a top electrode was not impacted by cracks maintained a high dielectric strength of approximately 20 kV/mm, which was comparable to the result obtained from the as-prepared silicone. Since only a small fraction of data points (~20%) was impacted by

cracks in the silicone film, the characteristic dielectric strength was still higher than 20 kV/mm. The shape parameter was significantly reduced to below five because cracks adjacent to top electrodes caused a wide distribution of data points and thus significantly reduced the shape parameter.

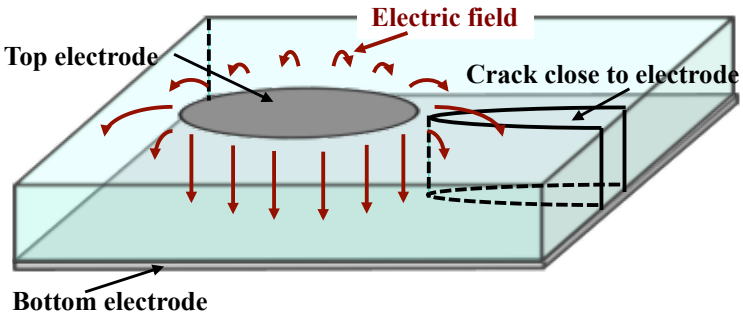

Fig. 5-9. Schematic of distribution of electric field under and around a top electrode with a crack in the surrounding polymer film.

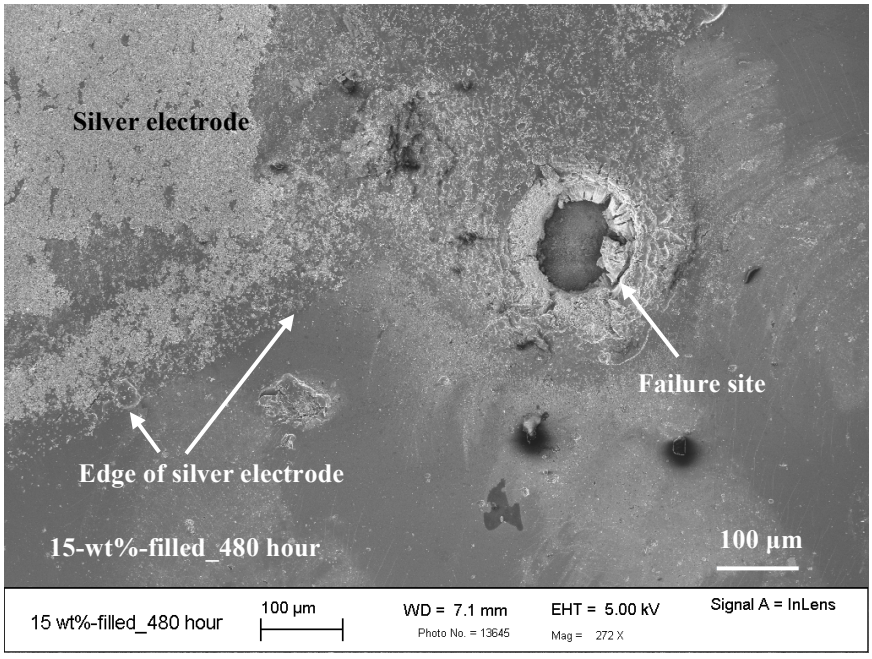

Fig. 5-10. Dielectric failure site close to a top electrode.

As aging continued to 400 hours, cracks were more frequently found in the silicone film and started to form a network (as shown in Fig. 5-11), resulting in a significant

decrease of dielectric strength in most of the measurements, as plotted in Fig. 5-7. Since 70% of the data exhibited dielectric strength below 10 kV/mm, the characteristic dielectric strength, which represents the value corresponding to a failure probability of 63.2%, was reduced dramatically to 10.60 kV/mm. A wide distribution of data points was observed in the meantime, resulting in a very small β of 1.18.

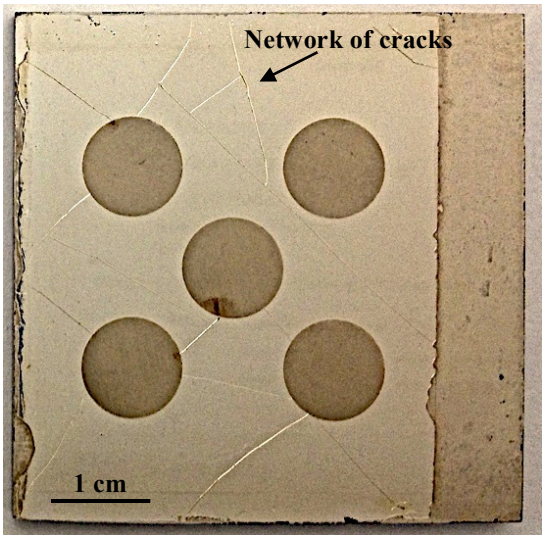

Fig. 5-11. Test coupon with unfilled silicone after 400 hours of aging.

After 480 hours of aging, all top electrodes were severely impacted by cracks, resulting in a dielectric strength lower than five kV/mm in each measurement, as shown in the Weibull plot given in Fig. 5-7. The characteristic dielectric strength was further reduced to 4.11 kV/mm, whereas the shape parameter was restored to 7.73 due to the consistency in failure mechanism.

The variations of the two Weibull parameters of unfilled silicone with aging time are plotted in Fig. 5-12. The error bars represent the 90% confidence interval. The E_0 remained above 20 kV/mm for 240 hours when the integrity of most of the silicone film remained intact, but dramatically decreased after 320 hours when a large fraction ($\geq$ 63.2%) of the data points were impacted by cracks. When all data points fell below five

kV/mm after 480 hours of aging, E_0 reached the minimum of 4.11 kV/mm, which was comparable to the dielectric strength of air at that thickness. The slight increase in E_0 after 80 - 240 hours of aging may be caused by several reasons including possible densification of polymer structure, the slight change in thickness (< 10%), and the artifact caused by the reduction of R^2 (goodness of fit) during calculation. The shape parameter was more sensitive to the degradation of the silicone film. Even before cracks could be observed by optical microscope (after 160 hours of aging), β fell to below five due to the occasional dielectric failure below 15 kV/mm. β remained low (less than five) until all measurements were impacted by cracking and all data points fell below five kV/mm after 480 hours.

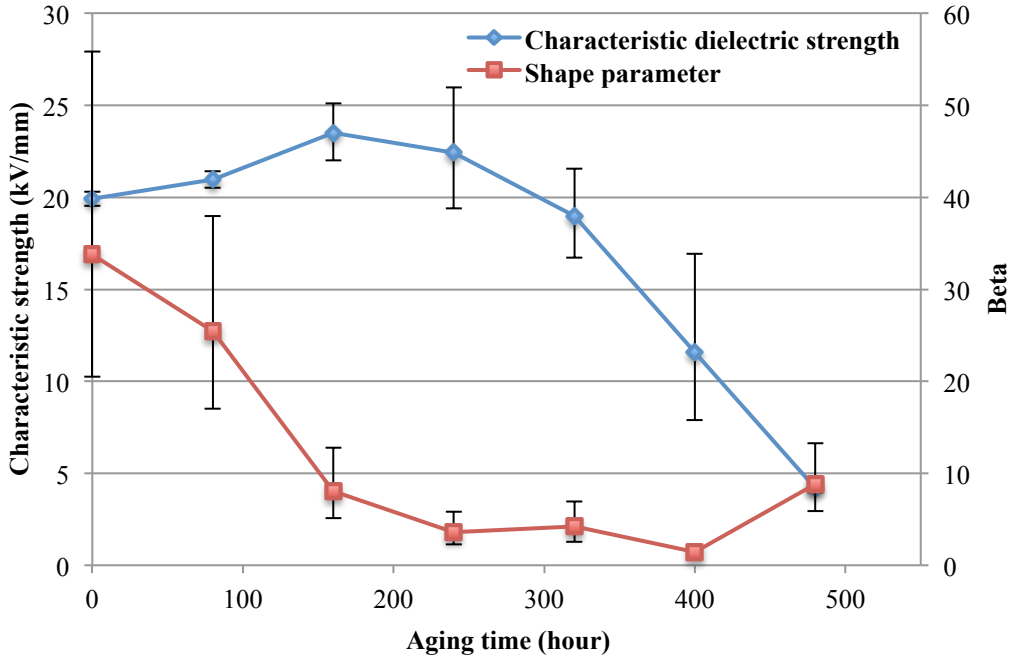

Fig. 5-12. Variations in Weibull parameters of unfilled silicone with time of thermal aging.

5.4.3.Effect of thermal aging on dielectric strength of Al_2O_3/silicone composites

Al_2O_3/silicone composites with filler (Al_2O_3 rods) loadings of 10, 15, and 30 wt% were also used to fabricate dielectric test coupons, which were then subject to thermal

aging at 250°C before dielectric measurements. None of the coupons made of a composite exhibited noticeable change in physical appearance under optical microscope throughout the entire aging period. The Weibull plots of the measured dielectric strength of composite filled with 10 wt% of Al_2O_3 rods are shown in Fig. 5-13. For this composite, as for the unfilled silicone, dielectric failure below 15 kV/mm began after 160 hours of aging, causing the reduction of shape parameter. The dielectric strength measured after 320 hours of aging on the 10-wt%-filled composite was found to be an exception: no dielectric failure below 15 kV/mm was detected in the test, causing a large β value. The occurrence of dielectric failure relies on the existence and development of defects, which is random and is rare at the beginning stage of degradation. Therefore, a much larger sample population may help to reduce the error in β calculation.

The Weibull plots of dielectric strength measured on the 15-wt%-filled composite are

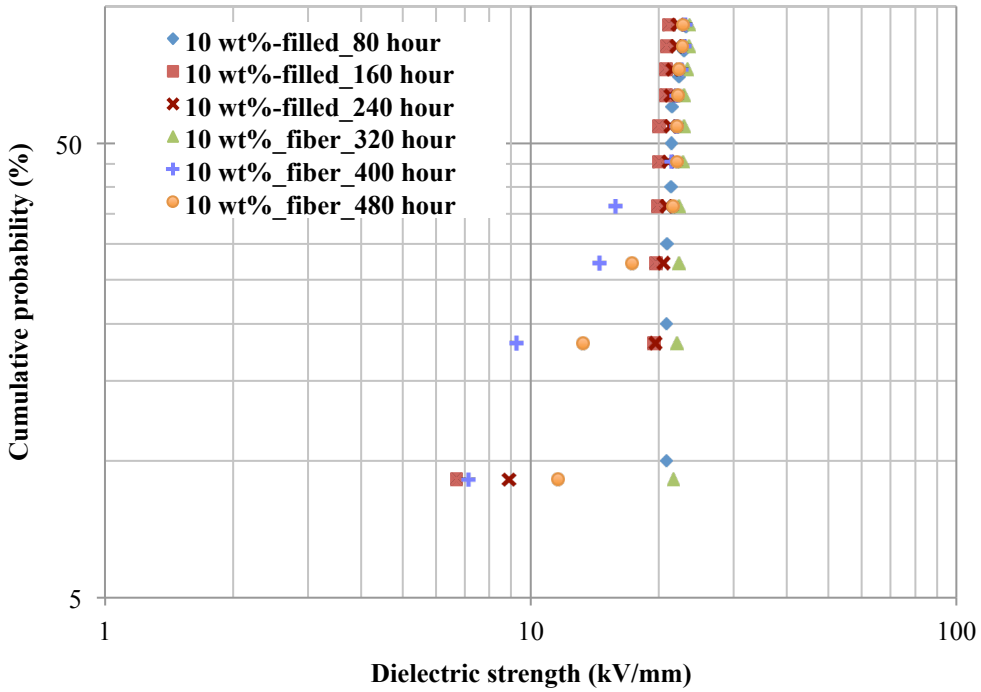

Fig. 5-13. Weibull plots of measured dielectric strength of 10-wt%-filled silicone aged at 250°C for 80, 160, and 240 hours.

shown in Fig. 5-14. For up to 320 hours of aging, dielectric failure rarely occurred below 15 kV/mm, with only one exception observed at 80 hours. Such unusual behavior (failure at ~10 kV/mm) of the composite film aged for 80 hours could be explained by occasional manufacture defects created during sample preparation (e.g., spin-coating, curing, etc.). The data points started to exhibit a slightly wider spread on the Weibull plot after 320 hours of aging, possibly indicating that the integrity of polymer film had been impaired. Dielectric failure was more likely to occur below the typical value of 20 kV/mm after longer aging time, resulting in an even wider spread of data points on Weibull plot and a smaller shape parameter.

The Weibull plots of dielectric strength measured on the 30-wt%-filled composite are shown in Fig. 5-15. Dielectric failure rarely occurred below 15 kV/mm for up to 400 hours of aging, with only one exception observed at 160 hour. This unusual behavior

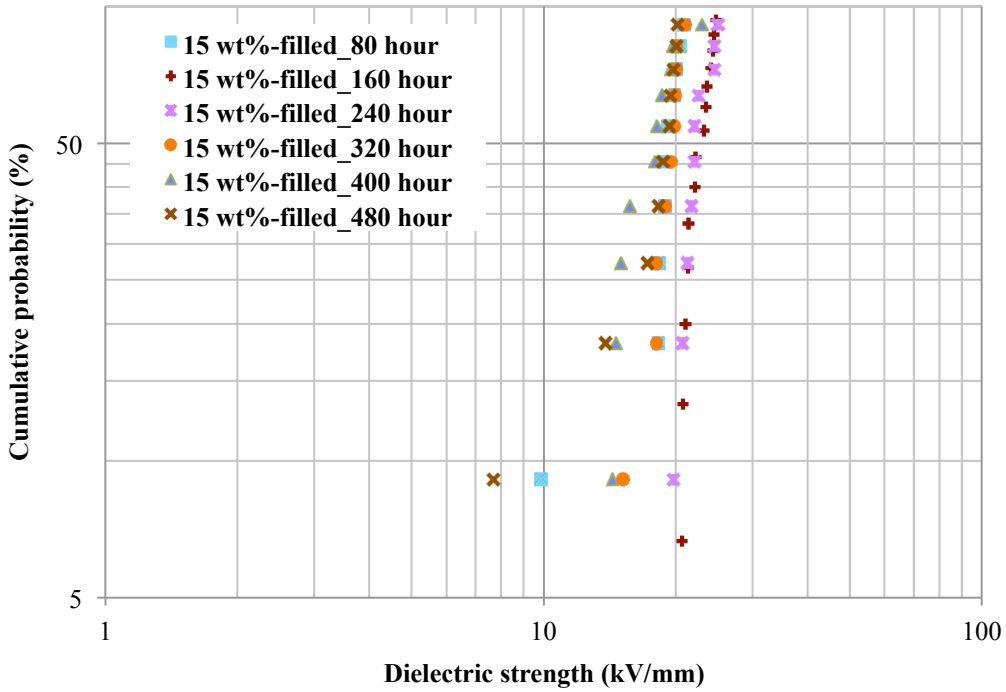

Fig. 5-14. Weibull plots of measured dielectric strength of 15-wt%-filled silicone aged at 250°C for up to 480 hours.

could also be explained by defects introduced into the composite during sample preparation. At 320 hours, a large β value with a wide confidence interval was observed and was again due to the randomness of defect existence and development. After 480 and 560 hours of aging, dielectric failure below 15 kV/mm were detected because of the degradation of film integrity, which widened the distribution of data points and reduced β.

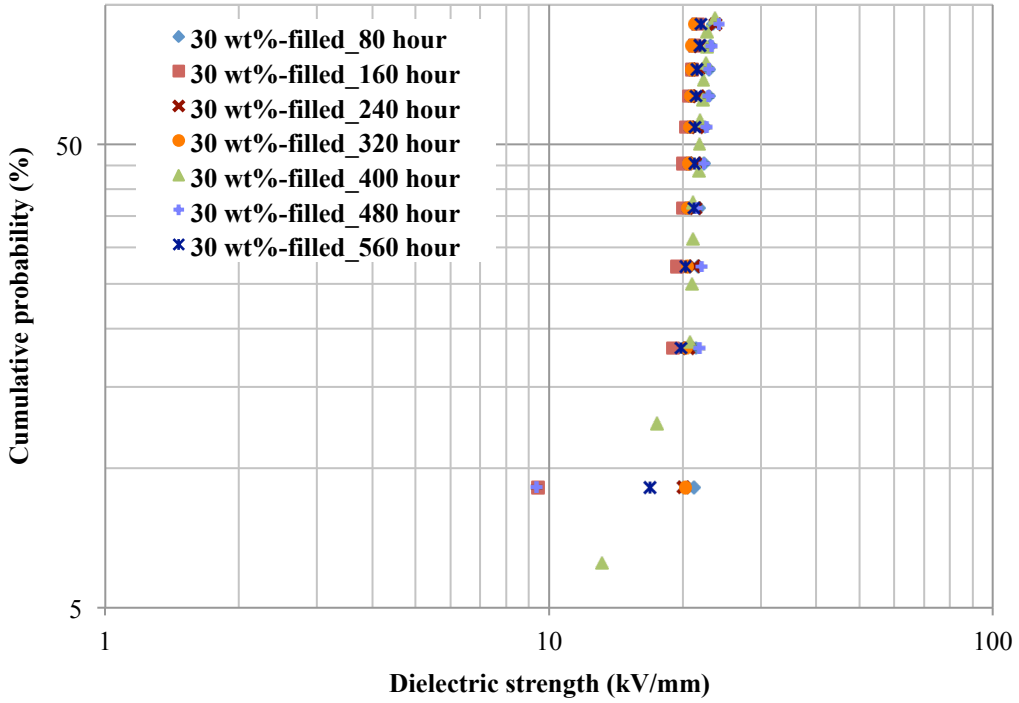

Fig. 5-15. Weibull plots of measured dielectric strength of 30-wt%-filled silicone aged at 250°C for up to 560 hours.

Figs. 5-16 and 5-17 show plots of characteristic dielectric strength and shape parameter, respectively, against aging time for unfilled and filled silicones. The error bars represent the 90% confidence interval. E_0 of the unfilled silicone exhibited a dramatic decrease after 320 hours, which was caused by the formation of a network of macroscale cracks developed in the silicone film during aging. E_0 of the Al_2O_3/silicone composites with filler loadings of 10, 15, and 30 wt% remained at approximately 20 kV/mm throughout the entire aging period. The confidence interval of each data point, as

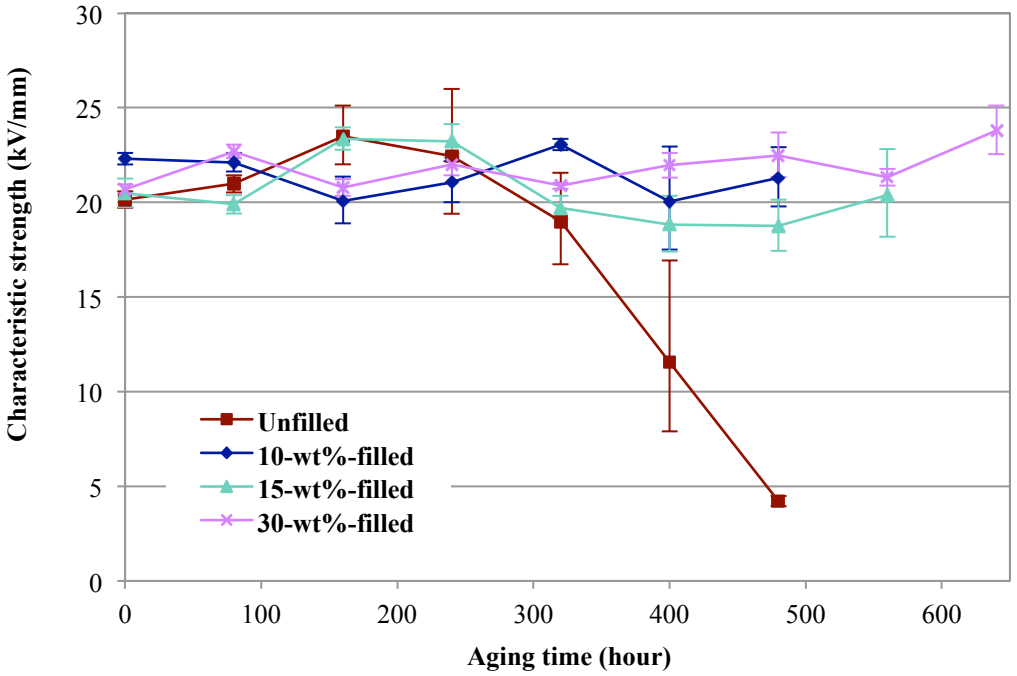

Fig. 5-16. Variations in characteristic dielectric strength of unfilled and Al_2O_3-filled silicones with aging time.

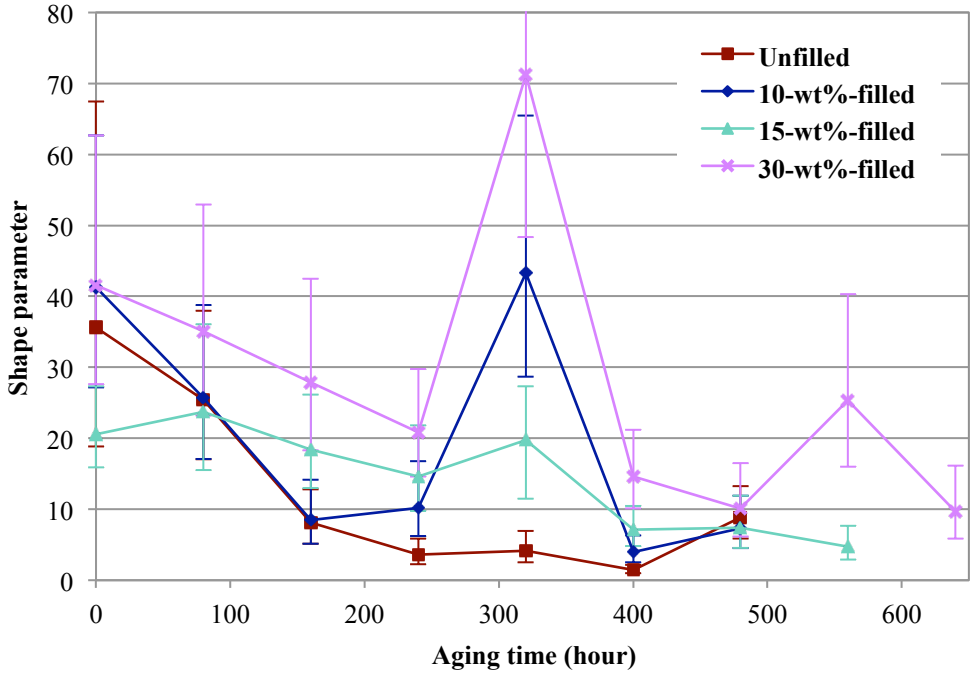

Fig. 5-17. Variations in shape parameter of unfilled and Al_2O_3-filled silicones with aging time.

expressed by the error bars, became larger after longer aging time, indicating that the integrity of the composite films had been gradually impaired. These results suggested that Al_2O_3 rods could effectively improve the thermal stability of silicone. The variation of E_0 of Al_2O_3/silicone composites with respect to aging time was in agreement with the results reported by Locatelli *et al* [65], in which the authors measured the breakdown behavior of a silica-filled silicone elastomer. The β of unfilled and 10-wt%-filled silicone exhibited a dramatic decrease after 160 hours due to the development of cracks and defects caused by quick degradation during thermal aging. The β of the Al_2O_3/silicone composite with a filler loading of 15 wt% exhibited a gradual decrease with aging time and remained above five for 400 hours, indicating an improved thermal stability over that of the unfilled and 10-wt%-filled silicones. The β of the Al_2O_3/silicone composite with a filler loading of 30 wt% remained the highest of all materials studied. The increase of β (of aged samples) with increasing filler loading also indicated that the thermal stability of silicone was improved by the addition of Al_2O_3 rods and that the 30-wt%-filled composite had the highest thermal stability.

5.5. Microstructure evolution of unfilled silicone and Al_2O_3/silicone composites

The polymer film in the coupon (cross-sectional view shown in Fig. 5-2) was subject to elastic stresses caused by CTE mismatch between the polymer film and the glass substrate when the coupon was cooled down to room temperature after the long-term annealing in furnace at 250°C. The stress increased with increasing elastic/storage modulus of the polymer. When exposed to high temperature such as 250°C, the silicone suffered from severe degradation, involving scission of the polysiloxane chain and generation of volatile species [67-69]. Shortening of the chain led to an increase in

crosslink density and therefore a higher storage modulus, which then resulted in higher stresses caused by the CTE mismatch.

Flexibility of silicone was impaired by the degradation process, in which the long polysiloxane chains were shortened, embrittling the polymer matrix. The silicone film in the coupon suffered from both higher elastic stress and matrix embrittlement as aging continued. When the film was no longer strong enough to maintain its integrity, cracking occurred. Thermal aging at 250°C was also expected to introduce voids, which can assist in crack initiation and propagation. Both crack and void damaged the film integrity and caused dielectric failure to occur at a lower electric field. These defects in the aged silicone matrix were examined by SEM.

5.5.1.Microstructure of unfilled silicone

Test coupons made with unfilled silicone and its composites filled with Al_2O_3 rods were examined by SEM after dielectric measurements. The results were expected to help explain the effect of thermal aging on the degradation of silicone matrix and dielectric strength observed even before macroscale cracks appeared in the aged film. The SEM images of the as-prepared unfilled silicone, serving as the benchmark for comparison, are shown in Fig. 5-18. The as-prepared silicone exhibited a flat surface in the absence of noticeable defects (e.g., cracks and voids). A few particles were found on the silicone film and were believed to be debris from top silver electrodes during the cleaning process prior to SEM examination.

The SEM images of the unfilled silicone aged for 80 and 200 hours are shown in Figs. 5-19 and 5-20, respectively. No change in physical appearance was seen after 80 hours. The silicone film maintained its integrity and showed no noticeable crack or void,

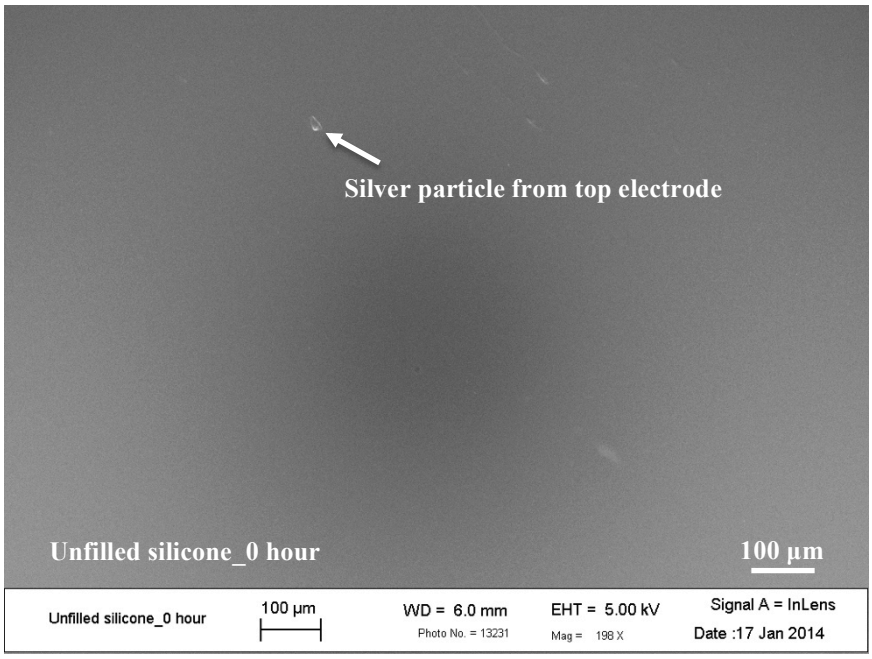

(a)

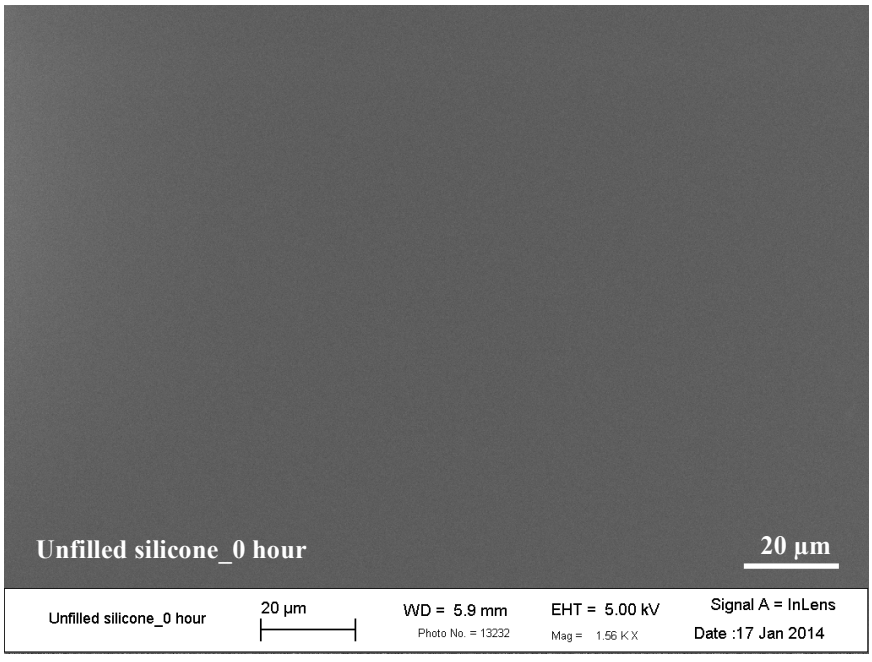

(b)

Fig. 5-18. SEM images of as-prepared unfilled silicone under magnification of (a) 198 × and (b) 1.56 k ×.

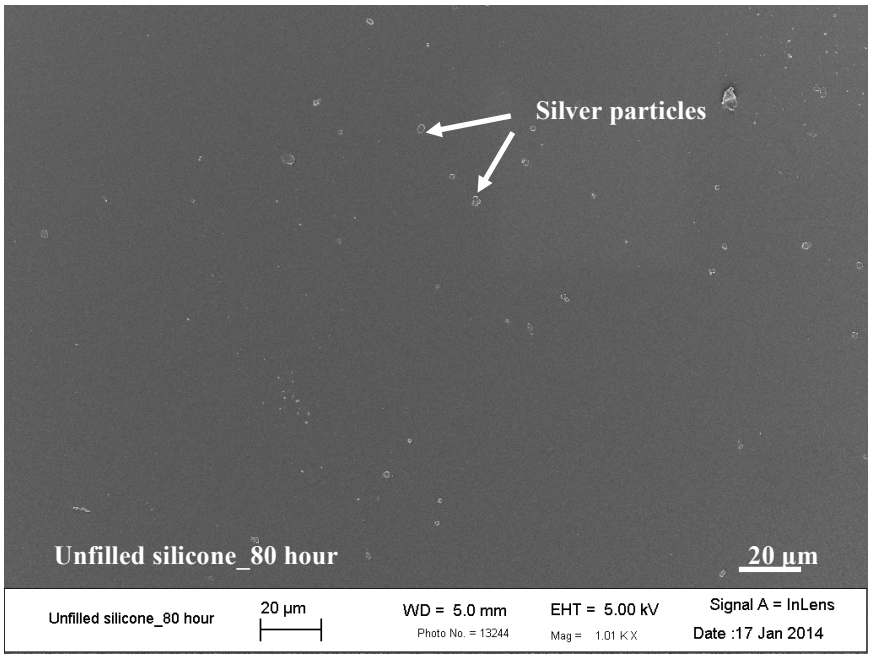

Fig. 5-19. SEM image of unfilled silicone aged at 250°C for 80 hours.

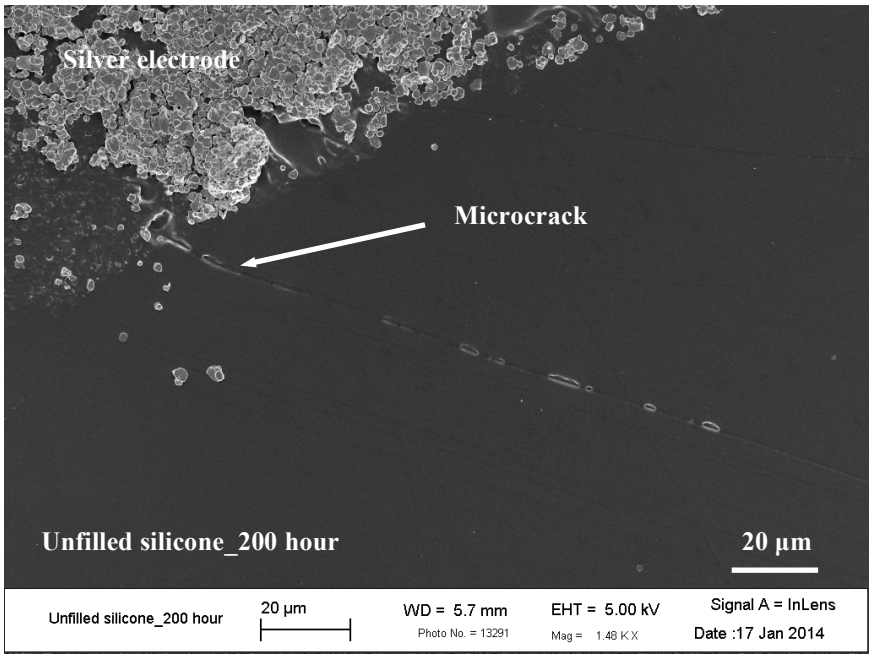

Fig. 5-20. SEM image of unfilled silicone aged at 250°C for 200 hours.

explaining the high dielectric strength (~20 kV/mm) of the film aged for 80 hours. Microscale cracks appeared in polymer matrix after 200 hours of aging, as indicated by the arrow in Fig. 5-20. Such cracks were too small to be seen under optical microscope but could still have a significant impact on the insulation capability of the silicone film. If a microcrack appears adjacent to a top electrode, dielectric failure measured from that electrode may occur at a lower electric field due to the reduction of creepage distance or partial discharge in the cracked region.

The SEM images of the unfilled silicone aged for 320 hours are shown in Fig. 5-21 (a) and (b). Macroscale cracks measured a few tens of micrometers in width (exampled in Fig. 5-21 (a)) were also visible under optical microscope. Such cracks usually stopped propagating when approaching a top electrode, where the stress caused by CTE mismatch could be slightly released by the ductile silver film (electrode). This phenomenon provides an idea that controlling and limiting the thermo-mechanical stresses within the package can possibly improve the reliability of polymeric encapsulants and other circuit components. The Al_2O_3-filled silicones prepared in this study exhibit slower increase in storage modulus (detailed in Appendix I) as they are subject to continuous aging at 250°C, suggesting that they can better control stresses during high-temperature application. Other methods to limit thermo-mechanical stresses such as designing a CTE-matching layer (similar to the top silver electrode used in this study) between two surfaces with large difference in CTE may help improve reliability as well but is beyond the scope of this study. The retarded crack propagation in polymer film underneath the top electrodes may also result from slower degradation in those regions because the silver layer can possibly block the diffusion pathway of the volatile degradation products.

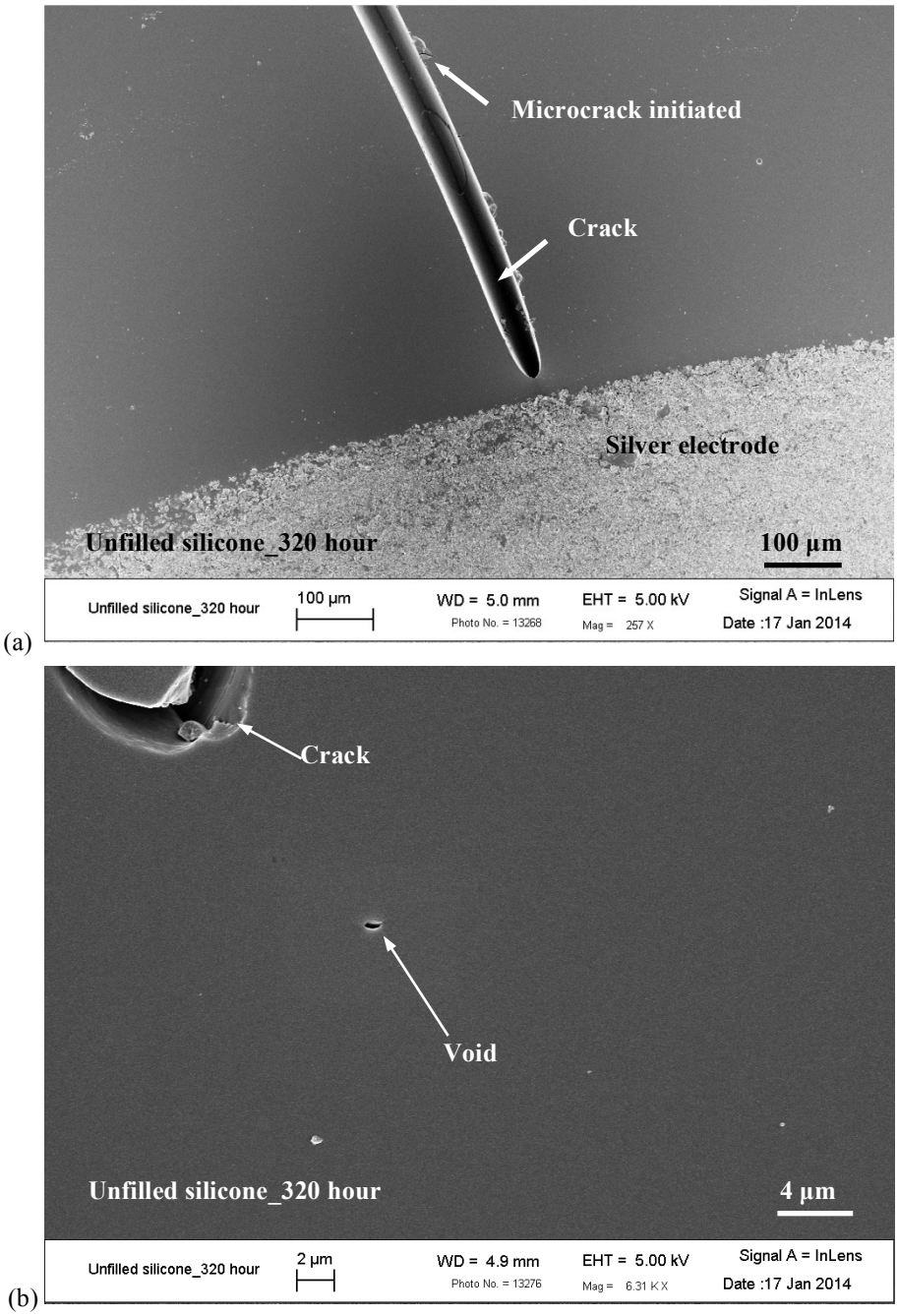

Fig. 5-21. SEM images of unfilled silicone aged at 250°C for 320 hours under magnification of (a) 257 × and (b) 6.31 k ×.

SEM also confirmed that microscale cracks tended to initiate from a large one, forming a network of cracks in silicone films aged for even longer times. Voids measuring approximately one micrometer was also identified in the silicone matrix after 320 hours (Fig. 5-21 (b)). Although such voids were unlikely to cause partial discharge due to its small size that guarantees a very high dielectric strength of air according to Paschen's law [154, 155], they can assist in crack initiation and propagation, as exampled in Fig. 5-22 (a), which shows the micrograph of the unfilled silicone after 400 hours of aging.

The SEM images of the unfilled silicone aged for 400 hours are shown in Fig. 5-22 (a), (b), and (c). Cracks propagated directly into a top electrode after 400 hours (Fig. 5-22 (b)), an indication that the polymer had become more brittle with further aging. Microscale cracks also initiated under a top electrode and crack the silver film, as shown in Fig. 5-22 (c). Voids of a few micrometers assisting in crack initiation and propagation (Fig. 5-22 (a)) were identified from the silicone film. The SEM images clearly demonstrated that the degradation of silicone caused the development of cracks and voids in the matrix, both of which were responsible for dielectric failure at low electric field (5 - 10 kV/mm).

5.5.2.Microstructure of Al_2O_3/silicone composite

The microstructure evolution in the aged composite filled with a 15 wt% of Al_2O_3 rods was also examined by SEM. The composite film exhibited no defect after 80 hours of aging, as shown in Fig. 5-23. The surface of the composite, with wrinkle-like structures around Al_2O_3 rods measuring two to five micrometers, was obviously rougher than that of the unfilled silicone (Fig. 5-20 (a)) after the same aging time. The wrinkle-like

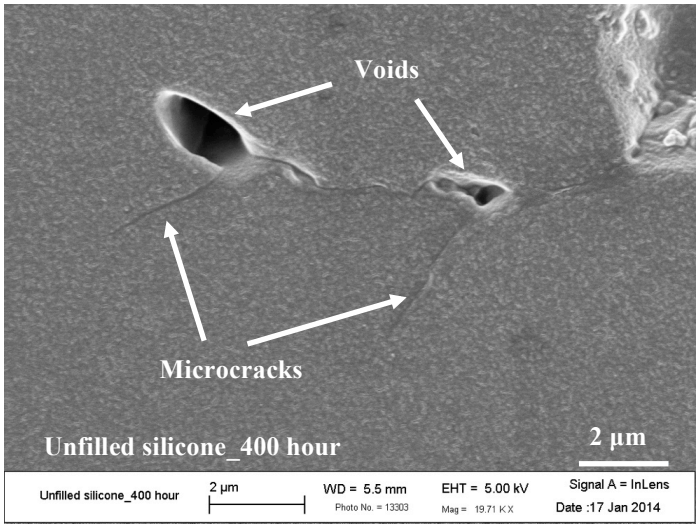

(a)

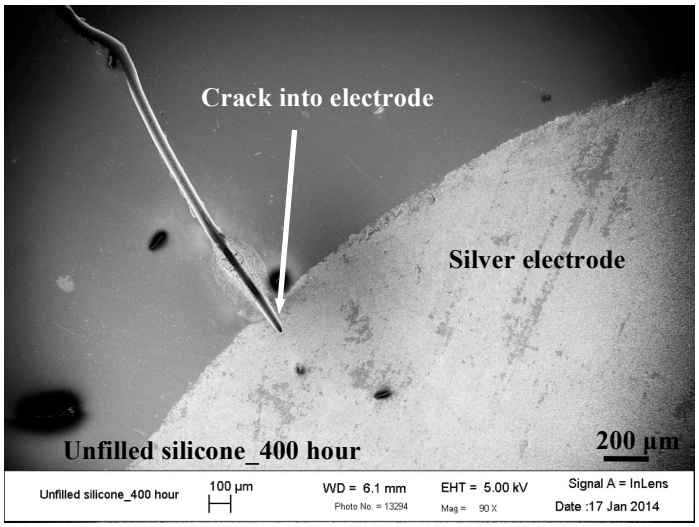

(b)

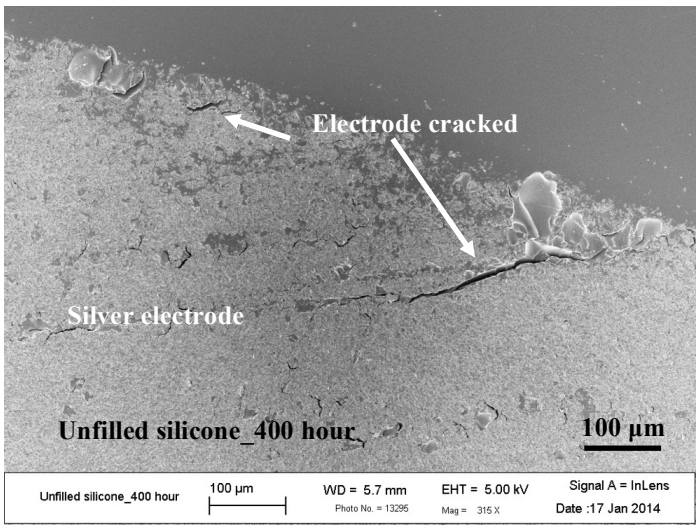

(c)

Fig. 5-22. SEM images of unfilled silicone aged at 250°C for 400 hours: (a) microcracks initiating from voids, (b) crack propagating into top electrode, and (c) microcracks in top electrode.

structure was observed on all composite surfaces and was probably formed during the curing process: when the silicone tended to slightly shrink, the chain movement was anchored by the surface of large agglomerates, causing non-uniform shrinkage of the composite film.

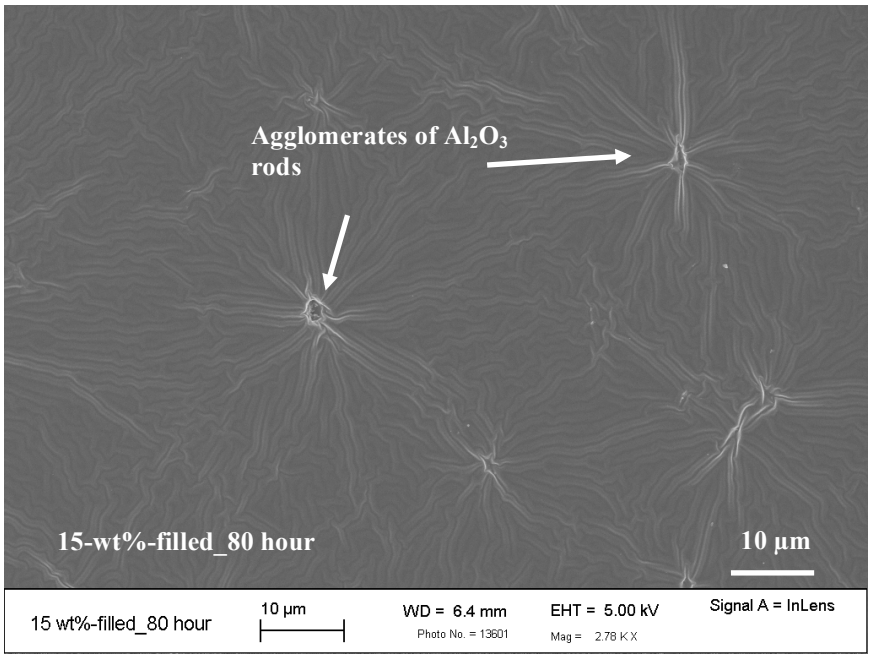

Fig. 5-23. SEM image of Al_2O_3 (rod)/silicone composite with a filler loading of 15 wt% aged at 250°C for 80 hours.

The composite film still maintained its integrity after 240 hours of aging (Fig. 5-24 (a)), explaining the absence of dielectric failure below 20 kV/mm (Fig. 5-14). The slower degradation of the composite than that of the unfilled silicone was attributed to the filler-matrix interaction, which restrained chain mobility and decelerated the chain-scission process, as confirmed in Chapter 4. Possible initiation of microscale cracks was observed in the composite with a filler loading of 15 wt% after 240 hours of aging, as shown in Fig. 5-24 (b). The initiation site was near the Al_2O_3/silicone interface, where the stress condition may be different from that in the matrix far from the interface. The microscale cracks observed at this stage had no significant effect on dielectric strength, as

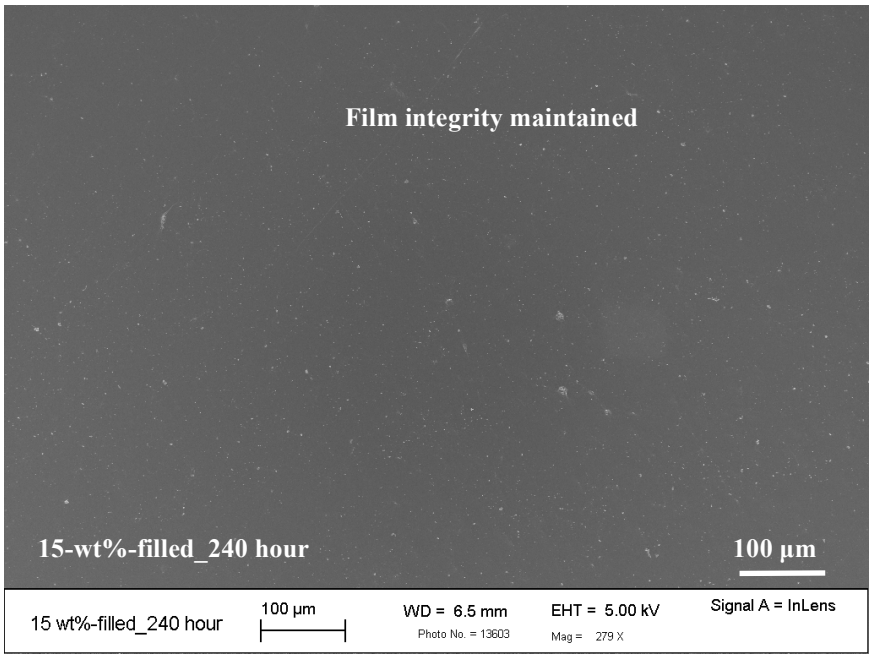

(a)

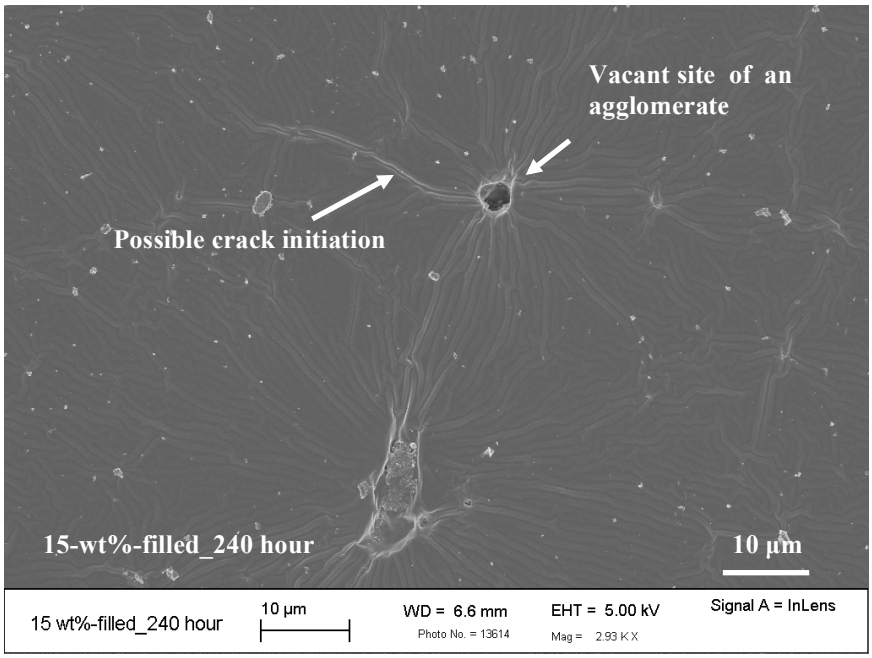

(b)

Fig. 5-24. SEM images of Al_2O_3 (rod)/silicone composite with a filler loading of 15 wt% aged at 250°C for 240 hours: (a) integrity of composite film maintained and (b) crack initiation around Al_2O_3 fillers.

demonstrated by the test results presented in Section 5.4.2. Although the sign of crack initiation suggested the ongoing degradation in the polymer matrix, such initiation occurred after a much longer aging time in the composite than in the unfilled silicone, an indication that the thermal stability was enhanced by Al_2O_3 rods.

Cracks that initiated from the filler-matrix interface were observed after 320 hours of aging, as shown in Fig. 5-25 (a), which also shows the tendency of two microcracks connecting with each other, indicating their growth and propagation within the polymer matrix. Microcracks similar to those seen in unfilled silicone aged for 200 hours were observed in the composite after 480 hours of aging, as shown in Fig. 5-25 (b). The corresponding dielectric results presented in Section 5.4.3 showed that dielectric failure could occur at an electric field much lower than 20 kV/mm, proving that even microcracks (in both unfilled and Al_2O_3-filled silicones) that are not visible to the eyes or under optical microscope could significantly affect the dielectric behavior. The microcracks were a result of silicone degradation caused by long-term thermal aging, which shortened the flexible polysiloxane chains and introduced voids in the matrix. The defects (cracks and voids) took longer time to develop in the composite, which exhibited slower degradation and higher thermal stability than the unfilled silicone in Chapter 4. The degradation of dielectric strength, as represented by the decrease of both E_0 and β obtained from Weibull distribution, with aging time was also slower in the composite than in the unfilled silicone.

5.6. Summary

The dielectric strength of silicone filled with various loadings of Al_2O_3 rods, including 0, 10, 15, and 30 wt%, were compared before and after thermal aging at 250°C in air. The

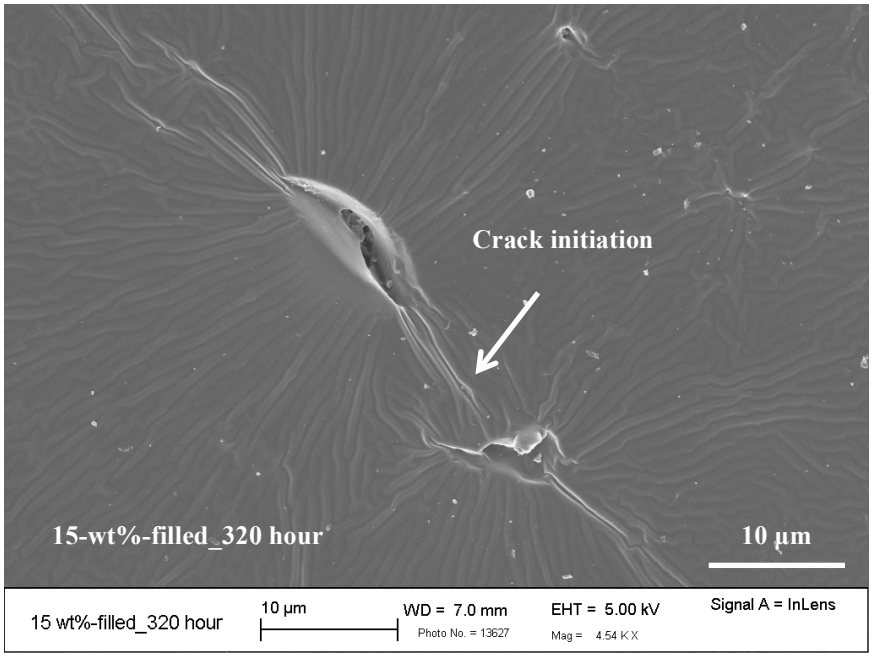

(a)

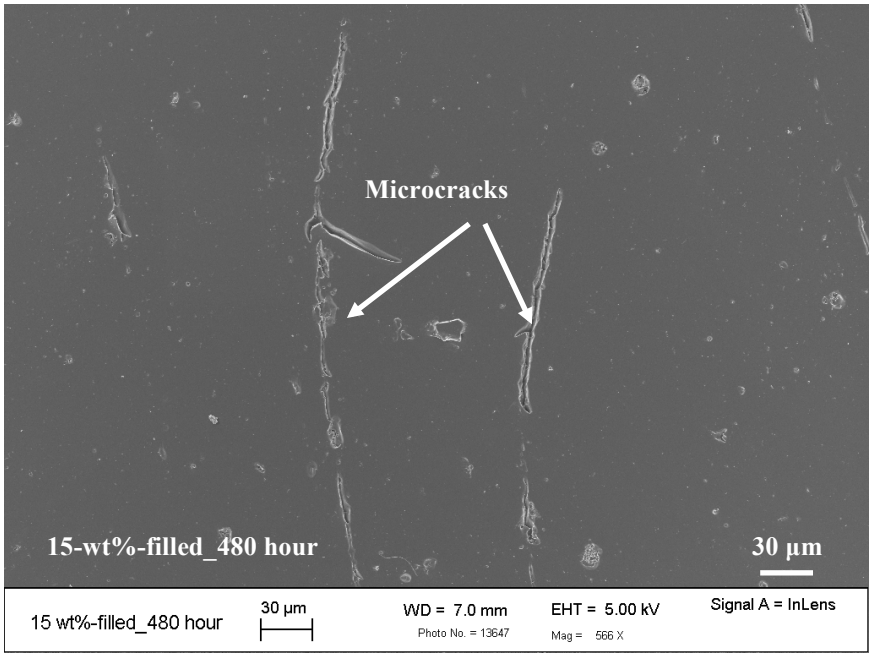

(b)

Fig. 5-25. SEM images of Al_2O_3 (rod)/silicone composite with a filler loading of 15 wt% aged for (a) 320 hours and (b) 480 hours.

results of the dielectric measurements were analyzed by using Weibull distribution. The two Weibull parameters obtained in the statistical analysis were used to compare the dielectric behavior of unfilled silicone and the composites. The dielectric strength prior to thermal aging was first compared. The characteristic dielectric strength (E_0) of the unfilled silicone was measured to be 20.13 kV/mm, whereas that of the Al_2O_3/silicone composites with filler loadings of 10, 15, and 30 wt% were 22.31, 20.08, and 20.61 kV/mm, respectively. The measured shape parameter (β) was above 15 for the four materials. This narrow distribution on the Weibull plot indicated the consistency of dielectric failure observed in all samples prior to aging. Such results clearly demonstrated that the Al_2O_3 rods added into the silicone matrix had no detrimental effect on the dielectric strength.

The thermal stability of the unfilled silicone and its composites was represented by the degradation in their dielectric performance with respect to the time of thermal aging performed at 250°C in air. Microcracks were seen in unfilled silicone by SEM after 200 hours of aging and macrocracks appeared after 320 hours. Microcracks that were comparable to those observed in unfilled silicone after 200 hours appeared in the Al_2O_3/silicone composite after a much longer time (480 hours). No macrocrack was found in the composite throughout the entire aging period. E_0 of unfilled silicone decreased dramatically after 320 hours of aging, meaning that most of the measurements were impacted by macro- or microscale cracks developed in the silicone film as a result of thermal degradation. E_0 of the Al_2O_3/silicone composite showed no significant change throughout the entire 560 hours of aging. β was more sensitive to silicone degradation because even a small portion of the dielectric failure detected at low electric fields due to

the presence of cracks could cause a wide distribution. β of the unfilled silicone decreased significantly to approximately one after 160 hours of aging, whereas that of the Al_2O_3/silicone composite filled with 15 wt% of Al_2O_3 rods decreased gradually to a similar value after 480 hours and that of the composite filled with 30 wt% of Al_2O_3 rods remained the highest among the values of the four materials throughout the entire aging time. The change of both Weibull parameters with aging time indicated that unfilled silicone had the lowest thermal stability, which increased monotonically with increasing loading of Al_2O_3 rods.

Chapter 6. Conclusions and Future Work

6.1. Conclusions

This study first investigated the thermal stability of commercial silicone elastomers, which were intended for encapsulating wide-bandgap devices that can operate at high temperature up to 250°C. Commercial silicones were found insufficiently stable when subject to long-term aging at 250°C, suggesting the importance of improving silicone stability. Since literature survey suggested that thermal stability of polymer may be improved by adding fillers, the effect of Al_2O_3 fillers on silicone stability was investigated in this study. Thermal stability of unfilled and Al_2O_3-filled silicones was compared via weight-loss measurements and dielectric characterization. The positive effect of Al_2O_3 rods on thermal stability was discussed. Main conclusions of this dissertation are summarized here.

6.1.1. Thermal stability of commercial silicone encapsulants

Seven commercial high-temperature encapsulants of various chemistry were evaluated for their capability of packaging wide-bandgap devices. Only silicone elastomers (used as potting compounds) survived the processability test, which was used to select suitable materials for chip-scale packaging. Two of the silicone elastomers, R-2188 and EPM-2422 (both made by Nusil Technology), exhibited excellent dielectric properties

(dielectric strength > 20 kV/mm) within the temperature range of 25 - 250°C. Another silicone elastomer, MasterSil 800 (Master Bond, Inc.), exhibited slightly lower dielectric strength (> 7 kV/mm) within the same temperature range.

All three silicones were found to degrade fast during the thermal aging test, in which all materials were soaked at 250ºC in air. EPM-2422 cracked after three days of aging, which significantly decreased its dielectric strength from 43.3 to only 9.7 kV/mm. R-2188 cracked after 28 days of aging, resulting in a dramatic drop of its dielectric strength from 33 to 13 kV/mm. MasterSil 800 exhibited no observable crack under optical microscope throughout the entire aging period (28 days) but its dielectric strength also dropped from 15 to only 5 kV/mm. The dramatic drop of dielectric strength was due to the change of material microstructure, i.e., initiation and development of cracks. Dielectric strength was sensitive to microstructure because partial discharge of air may occur in cracks at a low electric field. The material was considered failed when its dielectric strength dropped below the required value (10 kV/mm). The short lifetime observed in thermal aging test indicated that the thermal stability of the three commercial silicones was insufficient for packaging wide-bandgap devices, which are expected to operate continuously at or above 250°C.

6.1.2.Effect of Al_2O_3 filler on thermal stability of silicone elastomer

According to the demand for high-temperature and high-density packaging for wide-bandgap devices, the thermal stability of commercial silicone elastomer needs to be improved. The effect of Al_2O_3 filler on thermal stability was studied by weight-loss measurement and dielectric characterization. The weight-loss performance of unfilled and Al_2O_3 filled-silicones was measured by both TGA and isothermal soak tests. Both tests

revealed that Al_2O_3 rods obtained from Alfa Aesar (Part No. 43912) was able to improve thermal stability of silicone elastomer (EPM-2422 by Nusil Technology). TGA results indicated that the temperature of degradation onset increased from 330 to 379°C with a filler loading of 30 wt%. In isothermal soak test performed at 250°C in air, unfilled silicone lost 10% of polymer weight in 700 hours, whereas it took approximately 1800 hours for the composite filled with 30 wt% of Al_2O_3 rods to lose the same amount of polymer weight. Al_2O_3 particle (Part No. 44932 by Alfa Aesar) appeared to impair the thermal stability of the same silicone elastomer, possibly due to reasons like phase, impurity, surface charges, etc.

While weight-loss experiments directly measure the weight of degradation products, the dielectric characterization provides information on microstructural change within the silicone matrix. The dielectric strength of Al_2O_3 (rods)/silicone composites with various filler loadings, including 0, 10, 15, and 30 wt%, were compared before and after thermal aging at 250°C in air. The results of the dielectric measurements were analyzed by using Weibull distribution. The two Weibull parameters (characteristic dielectric strength E_0 and shape parameter β) obtained in the statistical analysis were used to compare the dielectric behavior of unfilled and Al_2O_3-filled silicones. The thermal stability of a material is indicated by the degradation of its dielectric performance with respect to the time of thermal aging. The test result clearly demonstrated that the thermal stability of silicone was improved by Al_2O_3 rods. E_0 of the unfilled silicone decreased dramatically after 320 hours of aging, whereas that of the composites showed no significant change throughout the entire 560 hours of aging. β was more sensitive to silicone degradation because even a small portion of the dielectric failure detected at low electric field due to

the presence of cracks could cause a wide distribution. β of the unfilled silicone decreased significantly to approximately one after 160 hours of aging, whereas that of the Al_2O_3/silicone composite took much longer time to decrease to a similar value. Microstructure examination by SEM revealed that cracks developed quickly (microcracks appeared in 200 hours and macrocracks appeared in 320 hours) in unfilled silicone. Microcracks comparable to those observed in unfilled silicone after 200 hours appeared in Al_2O_3/silicone composite after a much longer time (480 hours). No macrocrack was found in any composite throughout the entire aging period. The slower development of cracks in the composite also indicated improved thermal stability.

Improvement in thermal stability may be explained in a way that interfacial hydrogen bonds, which were formed between the hydroxyl (-OH) groups on Al_2O_3 surface and the silicone backbone, restrained the chain mobility of polymer matrix and hindered the formation of decomposition products. The model of Tsagaropoulos describes the possible relationship between interfacial bond and chain mobility. Each filler is surrounded by a tightly bound layer, which contains chain segments adsorbed onto filler surface at multiple sites. The adsorption is caused by physical or chemical bonding between filler surface and polymer matrix. The chain mobility of this layer is highly restrained due to multiple interfacial contacts. Surrounding the tightly bound layer, there is a loosely bound layer formed due to the far-field effect of interfacial bonds. Mobility of polymer chains in both bound layers was restrained according to the model of Tsagaropoulos. With sufficient filler loading, the two bound layers may efficiently reduce the average chain mobility of silicone and lead to increased thermal stability.

6.1.3.Effect of interfacial hydrogen bond on thermal stability

Since hydrogen bonds that were assumed to exist at Al_2O_3/silicone interface may be responsible for restraint of chain mobility and improvement of thermal stability, the effect of interfacial hydrogen bond on thermal stability of silicone was verified in this study by comparing the weight-loss behavior of Al_2O_3 (rod)/silicone composites (10-wt%-filled) with various concentration of interfacial hydrogen bond. The variation of hydrogen-bond concentration was achieved by reducing hydroxyl content on Al_2O_3 surface via high-temperature dehydration in N_2.

Results of XPS and FTIR demonstrated that hydroxyl content on Al_2O_3 surface was successfully reduced by high-temperature dehydration. Isothermal soak test performed at 250°C in air discovered that Al_2O_3/silicone composites made from dehydrated rods exhibited a lower thermal stability than that made from as-received ones, with the initial weight-loss rate increased from ~0.025 (with as-received rods) to ~0.036 wt%/hour (with 900°C-dehydrated rods). The restored weight-loss rate resulted from the loss of interfacial bond and weakening of interfacial restriction, both of which directly impacted the tightly bound layer by significantly reducing the amount of adsorption sites or interfacial bonds. The loosely bound layer was also impacted because it was formed due to the far-field effect of the interfacial bonds. Chain mobility in both layers increased with reducing number of interfacial bonds, causing a higher initial weight-loss rate and therefore a lower thermal stability.

6.1.4.Mechanism of thermal-stability improvement

Al_2O_3 rods improved the thermal stability of silicone via the following mechanisms:

1. Hydroxyl groups on Al_2O_3 surface formed hydrogen bond with oxygen atoms in

silicone backbone or with hydroxyl groups at chain terminals.

2. Interfacial hydrogen bonds restrained chain mobility by producing tightly and loosely bound layers containing chain segments with restricted motion.
3. Reduced mobility impaired the flexibility of silicone backbone, causing difficulty to the formation of certain local chain configurations that facilitate the decomposition process and thus hindering the generation of volatile decomposition products.
4. With the formation of decomposition products being hindered, the weight-loss rate was reduced and the weight-loss process was decelerated, leading to an improved thermal stability.

6.2. Future work

6.2.1.Dielectric characterization

Dielectric characterization in this study found that the top electrode painted on polymer film may have varied the stress condition and retarded the degradation process, preventing cracks to initiate and propagate near and underneath the top electrode. One possible way to solve this problem is to paint the electrode after aging is completed. This section discusses the advantages and disadvantages of this approach.

Painting electrodes after aging may help achieve higher uniformity of stress distribution and material degradation in polymer film and reduces the possibility of artifact caused by the stop of crack propagation near top electrodes but may cause another artifact of electrical short between top and bottom electrodes because the silver painted or sputtered on polymer film as top electrodes can be easily deposited on sidewalls of the vertical crack during processing. This action may also cause extra damage to the aged

samples because polymer film becomes increasingly brittle as degradation continues.

6.2.2.Other high-temperature candidates for encapsulation

Silicone-based encapsulant is a promising candidate for high-temperature power electronic packaging because of its high thermal stability, excellent dielectric strength and chemical resistance, etc. Other types of materials may also serve for the same purpose, for example, polymers such as cyanate ester (CE), bismaleimide (BMI), and polyimide (PI) that can withstand at least 300°C. These materials usually exhibit a T_g higher than 250°C, which is the maximum operation temperature of commercial SiC power devices. The neat (unfilled) polymer usually exhibits a large CTE of at least 40 ppm/K below T_g. Commercial molding compounds (commonly fabricated as polymer matrix filled with certain type(s) of fillers) made of these high-temperature formula also exhibit CTE larger than the required value for semiconductor packaging, as shown in Fig. 6-1, which compares the operation temperature and CTE of high-temperature (CE-, PI-,

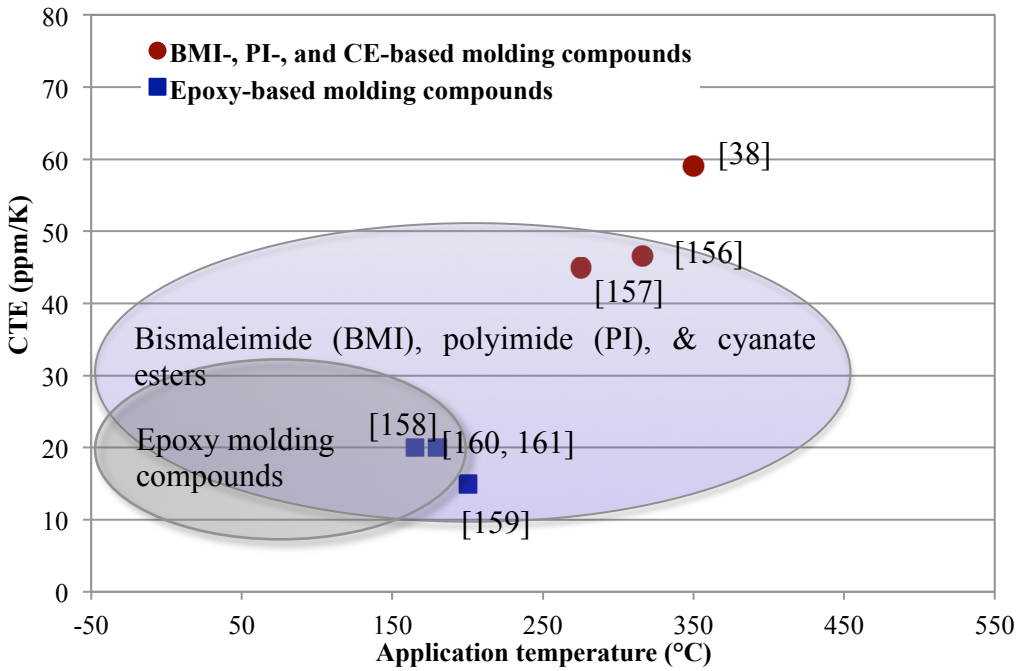

Fig. 6-1. Coefficient of thermal expansion and maximum operation temperature of commercial underfills and molding compounds.

and BMI-based) and conventional (epoxy-based) molding compounds. Since high CTE can cause large thermo-mechanical stresses especially at high temperature, it needs to be reduced to match that of other circuit components when designing a high-temperature encapsulant with these materials. Among the aforementioned high-temperature polymers, polyimides are known for their water susceptibility. Future research on modifying polyimide for increased hydrophobicity would be worthwhile.

Glass-based materials are the second option for high-temperature encapsulation because they can easily survive 400°C. Glass encapsulation provided high reliability for microelectronic packages against thermal cycling in temperature range of 25 - 250°C [162]. It may also be capable to encapsulate high-temperature power modules because of its high thermal stability and low CTE. Glasses are known to have high modulus, which could cause large thermo-mechanical stresses if CTE-mismatch exists between encapsulation and circuit components. Tailoring of CTE to match that of other circuit components is therefore important for this type of encapsulant.

Ceramic-based materials are the third option for high-temperature encapsulation because of their excellent thermal stability against at least 1000°C. Commercial products designed for potting are currently available on the market [163, 164] and are used for encapsulating power SiC module by Grummel *et al* [165]. One drawback of these commercial encapsulants is they usually have a low dielectric strength of no higher than 10 kV/mm, possibly due to the porous structure of ceramics. Porous ceramic is also known for water susceptibility, which can significantly impact the reliability of electronic packages. Future research can be carried out to increase the density of ceramic encapsulants and to improve the dielectric performance and chemical resistance.

Appendix A – Mechanical Performance of Al_2O_3/Silicone Composites

During the thermal degradation process of polysiloxane, the long chains are shortened when volatile molecules are produced. Shortening of the chain leads to increased crosslinking density and higher storage modulus. A material with higher thermal stability should exhibit slower change in *E'*. The mechanical performance of the unfilled silicone and the composite filled with 15 wt% of Al_2O_3 rods was compared before and after isothermal aging (250°C in air) by a dynamic mechanical analyzer (DMA).

1. Dynamic mechanical analysis (DMA)

Unfilled and Al_2O_3-filled silicones were prepared according to the procedure described in Fig. 3-10. The un-cured silicone (or the composite) was casted in films of approximately 0.6 mm thick and then deaerated in vacuum. After cure, the silicone film was cut into strips measured approximately 6.5 mm × 40 mm. The samples were then aged isothermally at 250°C in air. The aging condition was the same as described in Section 4.3.1. Dynamic measurements were performed after 60, 120, 180, and 240 hours. Storage modulus of unfilled silicone and Al_2O_3/silicone composite were measured by DMA (TA Instruments, Model Q800). The silicone (or composite) film was carefully mounted between the movable and the fixed clamps of DMA without being distorted or stressed, as illustrated in Fig. A-1. The measurement was performed from -130 to 250°C

with a ramp rate of 2°C/min in N_2.

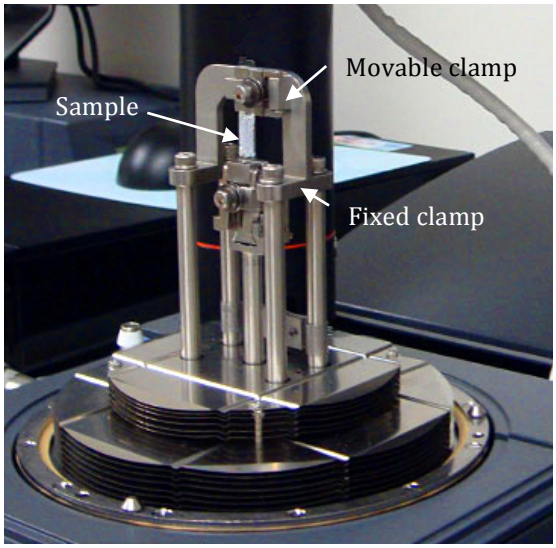

Fig. A-1. Sample mounted on DMA Q800.

2. Mechanical properties of unfilled silicone

The storage modulus of unfilled silicone after aging is plotted in Fig. A-2 against temperature. As-cured silicone (aged for zero hour) exhibited the lowest modulus and at above 150°C experienced a post-cure process, which is an irreversible chemical reaction that leads to additional crosslinking density. The same post-cure effect was observed in as-cured Al_2O_3/silicone composite (Fig. A-3). *E'* above T_g increased significantly (from approximately one to 10 MPa at 25°C) as aging time increased, indicating an increased crosslinking density resulting from the ongoing degradation process.

3. Mechanical properties of Al_2O_3/silicone composite

Storage modulus of aged Al_2O_3/silicone composite filled with 15 wt% of Al_2O_3 rods is shown in Fig. A-3. Prior to aging, the composite exhibited a storage modulus of approximately one MPa, which was comparable to that of the unfilled silicone. The modulus of the composite also increased with increasing time of thermal aging (from

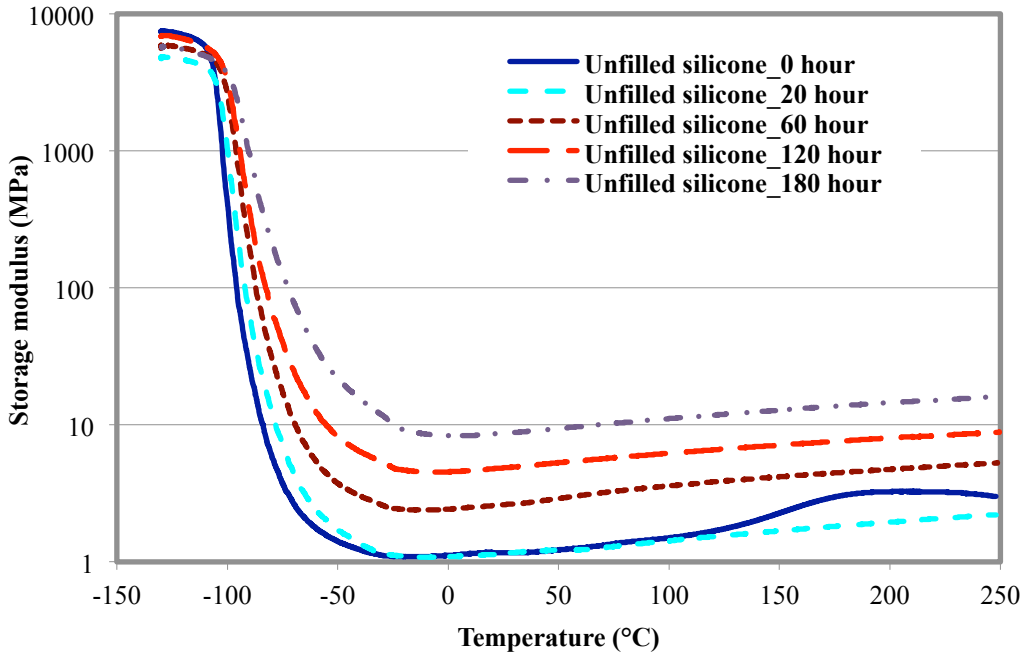

Fig. A-2. Storage modulus of unfilled silicone aged at 250°C for up to 180 hours.

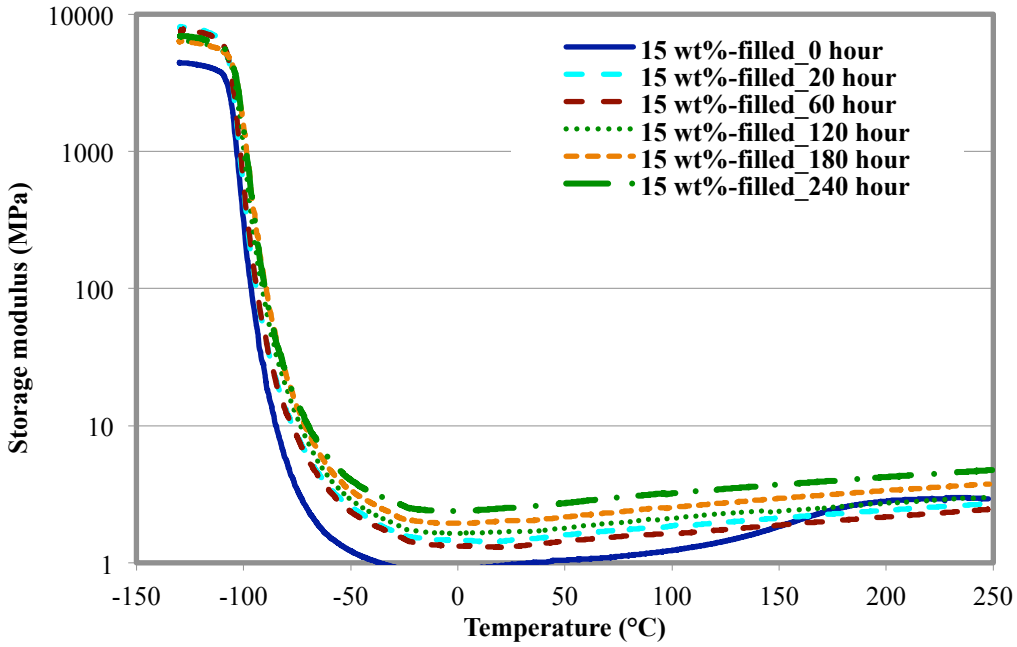

Fig. A-3. Storage modulus of Al_2O_3 (rod)/silicone composite with a filler loading of 15 wt% aged at 250°C for up to 240 hours.

approximately one to five MPa at 25°C in 240 hours) but at a much lower rate than that observed for unfilled silicone, indicating that the crosslinking density of the composite grew slower. This phenomenon proved that the Al_2O_3/silicone composite had a higher thermal stability than the unfilled silicone.

4. Summary

Change of dynamic mechanical property of unfilled and 15-wt%-filled silicones with respect to time of thermal aging was measured by DMA from -130 to 250°C. Both materials exhibited a storage modulus of approximately one MPa prior to aging, indicating that the addition of Al_2O_3 rods (15 wt%) did not significantly increase the storage modulus. During thermal aging performed at 250°C in air, storage modulus of both materials increased with respect to time. The storage modulus of unfilled silicone increased to approximately 10 MPa in 180 hours, whereas that of the composite increased to approximately 5 MPa in 240 hours. The increase of storage modulus directly related to the increase of crosslinking density occurred during thermal degradation process. The slower increase of modulus observed in the composite indicated a slower increase of cross-linking density in it and an improvement of thermal stability achieved by adding Al_2O_3 rods.

Appendix B – Effect of Encapsulant on High-Temperature Reliability of Direct Bonded Copper (DBC) Substrates

1. Introduction

Direct bonded copper substrates are widely used as interconnect and support board for packaging power semiconductor chips [110, 166]. Although DBC substrates provide excellent performances in electrical isolation and thermal management, their reliability is being questioned for high temperature applications, in which they are subject to large temperature swings, i.e. over 250°C.

Direct bonded copper substrates were found to fail within several tens to a few hundreds of cycles, depending on the sample structure and cycling conditions [167, 168]. A possible way to improve the DBC reliability is to seal the copper-ceramic edge with encapsulation materials [169]. Possible explanations are: (1) sealing material is able to release the stress concentration at the edge of Cu/Al_2O_3 joint and slow down the crack initiation and propagation processes; and (2) sealing material may prevent the delivery of corrosion species from the environment to the edge of Cu/Al_2O_3 joint and slow down stress-corrosion cracking of the joint.

This work compared the lifetime improvement by different sealing materials. Parylene

HT and Nusil R-2188 were used to seal the DBC edges. DBC substrates with no coating were used as control. The substrates were subject to thermal cycling from -55 to 200°C. To accurately capture the onset of DBC failure, cracks within the substrate were monitored by SEM. The substrates were considered failed as soon as the crack in the ceramic layer became parallel to the substrate surface [168]. The reliability of unsealed, parylene-sealed, and Nusil-sealed DBC substrates were compared in the experiment. The effect of different sealing materials on the reliability was discussed.

2. Experiments

In this study, the temperature range for cycling was chosen to be -55 - 200°C. The temperature profile is shown in Fig. B-1. There is a temperature dwell of 13 min at both -55 and 200°C. The ramping rate between the two temperatures is approximately 20°C/min. This temperature profile was achieved by using the Tenney environmental chamber (Tenney Junior), with a hot plate inserted into it, as shown in Fig. B-2. All samples were placed on the hot plate during the experiment. The temperature of each sample (±5°C variation) was measured by a thermocouple mounted on its surface. The

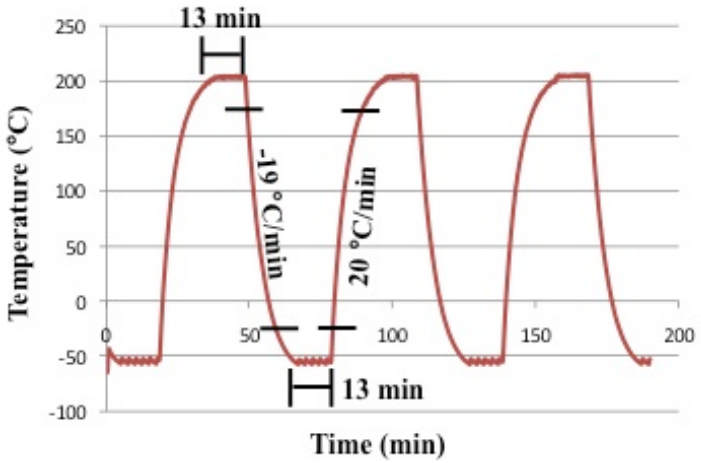

Fig. B-1. Temperature profile used in the cycling experiment [6].

environmental chamber was set to a constant temperature of -65°C. The current flowing into the hot plate was carefully controlled to obtain both ramping and steady states in the profile.

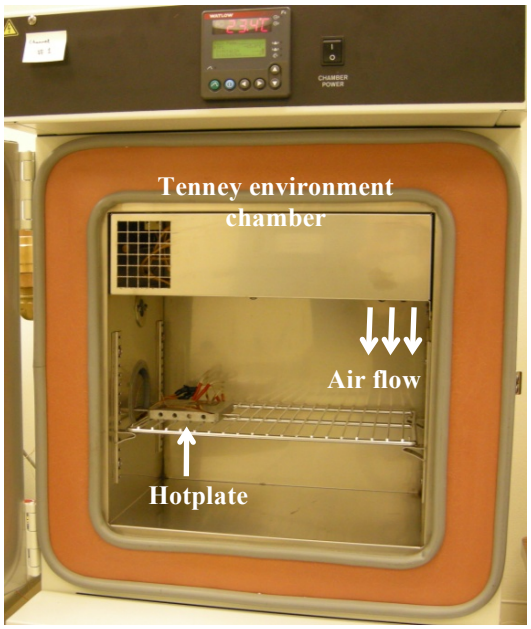

Fig. B-2. Setup of thermal cycling experiment.

The samples used in the cycling experiment were DBC substrates (manufactured by Curamik, Cu thickness: 8 mil, Al_2O_3 thickness: 25 mil) measured 40.5 mm × 27.5 mm. Through wet chemical etching by $FeCl_3$ solution, the Cu on the topside was patterned, whereas the backside was left unpatterned, as shown in Fig. B-3 (a) and (b), respectively. The step-edges were developed by chemical etching as well, with the thickness of the step-edge controlled to be four mils, which was half of the thickness of the original Cu foil. After etching, the samples were plated with silver through electro-less plating plus electro plating to prevent any possible oxidation caused by the edge-sealing materials. As-patterned DBC was cleaned with deionized (DI) water and dried before immersed into electro-less plating solution (manufactured by Alfa Aesar, part #: 44068), which was

heated up to 85 - 90°C in water-bath. The electro-less plating lasted approximately 15 min. The sample was then cleaned with DI water and connected to the electrode for electro-plating. The sample was immersed in silver-plating solution (composition documented in [111]) during plating, which lasted for 10 min. The plating current was set to 20 A/cm^2. The setup for electro-plating is shown in Fig. 2-2.

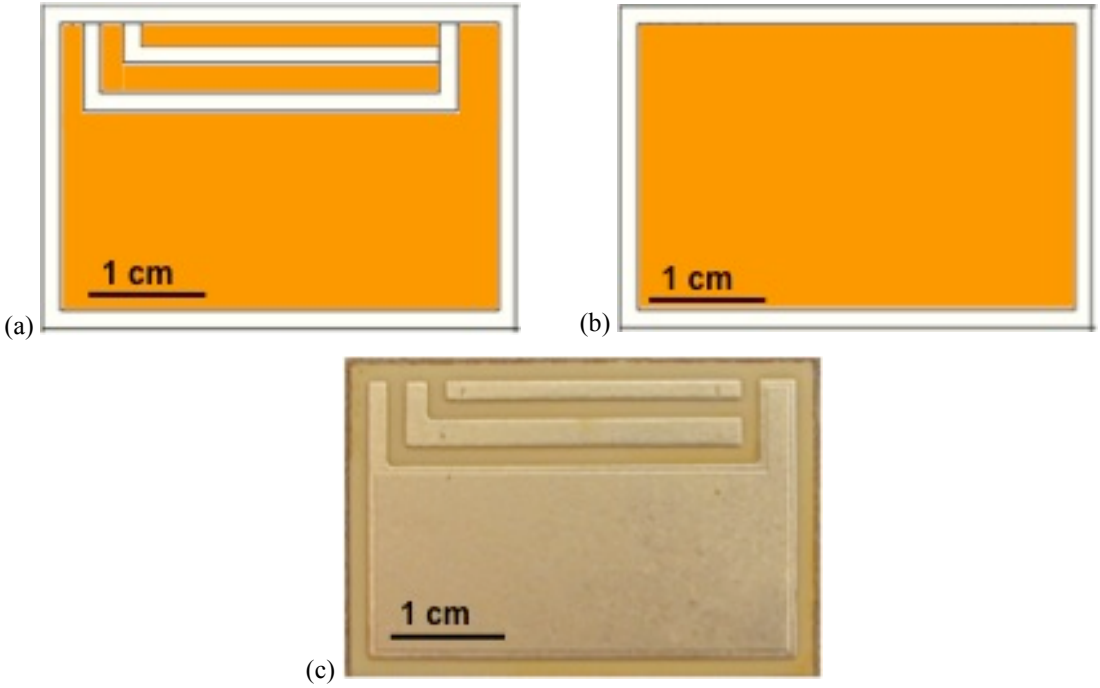

Fig. B-3. Sample designed for thermal cycling: (a) topside, (b) backside, and (c) after silver plating.

Silver-plated DBC substrates without sealed edges were used as control. The two types of seal-edged samples were achieved with Parylene HT and Nusil R-2188, respectively. Parylene was deposited on the entire DBC surface through chemical vapor deposition (CVD). The thickness was controlled to be ~10 μm. Edge-sealing with Nusil was achieved with Asymtek fluid dispenser C-720. Approximately 200 μm (minimum thickness that can be achieved with the dispenser) of material was dispensed and cured at the edges of Cu/Al_2O_3 joint (both top and bottom sides). Optical microscope and

scanning electron microscope (SEM) were used to examine the interfaces between Cu and Al_2O_3 in seal-edged samples and in the control.

3. Results and discussion

3.1. Optical microscopy

The samples were examined by optical microscope before cross-sectioning. In the control group, detachment of Cu from Al_2O_3 was captured in samples having undergone 100 cycles, as shown in Fig. B-4. Cracking occurred from the edges of Cu/Al_2O_3 joints and gradually propagated into the center. Failure in both parylene- and Nusil-sealed samples was not resolved by optical microscope even after 400 cycles from -55 to 200°C, as exampled in Fig. B-5.

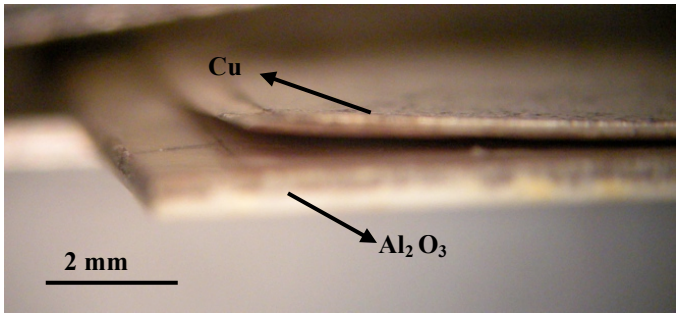

Fig. B-4. Optical microscope image of control DBC having undergone 100 cycles (-55 - 200°C).

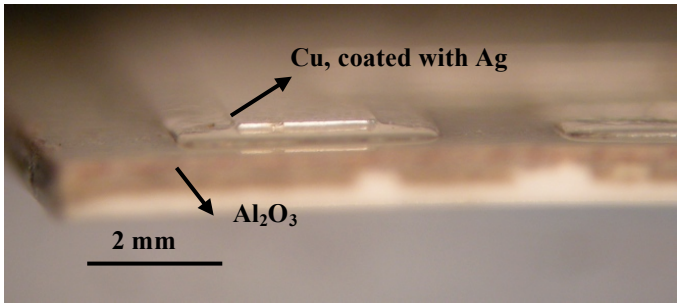

Fig. B-5. Optical microscope image of parylene-sealed DBC having undergone 400 cycles (-55 - 200°C).

3.2. Scanning electron microscopy (SEM)

To better reveal the crack initiation and propagation at Cu/Al_2O_3 interfaces, especially in seal-edged samples, SEM was used to examine the cross-sections of DBC substrates. Experimental results showed that the failure of DBC occurred most probably from the corners of Cu/Al_2O_3 joints. This phenomenon can be explained by the stress distribution during cycling process. Since the thermo-mechanical stresses induced by CTE mismatch gradually increase from the center to the edge of Cu/Al_2O_3 joints, the four corners of DBC substrates are subject to the highest stress and should therefore fail first.

Based on the aforementioned results and analysis, exposing the Cu/Al_2O_3 joints at the four corners when cross-sectioning cycled DBC substrates is necessary. Cross-sectioning was performed along the two diagonals, as illustrated in Fig. B-6. When preparing the SEM samples, cycled DBC substrates were mounted in the molding epoxy and then cross-sectioned along their two diagonals. The exposed surfaces were polished with SiC sand papers, in the order of grits 240, 320, 400, 600, 800, and 1200. Then the surfaces were further polished with diamond suspensions, in the order of 1, 0.3, and 0.05 μm. A gold film of a few nanometers thick was sputtered on each sample's surface prior to SEM examination to achieve electrical conduction. Cu/Al_2O_3 joints in control, parylene-sealed,

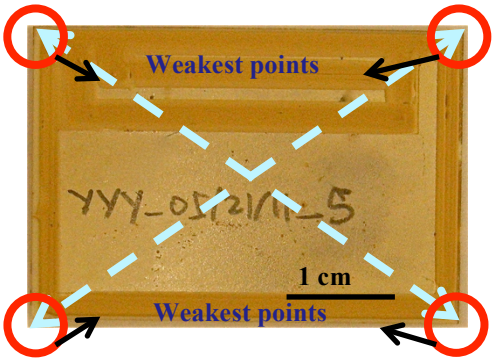

Fig. B-6. Cross-sectioning lines (dashed) used in SEM sample preparation.

and Nusil-sealed samples were examined by SEM. Both in-lens and backscatter detectors with an accelerating voltage of 5 kV were used. Results of each group at selected sampling point were based on three samples (six cross-sections).

The SEM results revealed that cracks at Cu/Al_2O_3 interface initiated between 50 cycles and 75 cycles. No crack was found at Cu/Al_2O_3 interfaces after 50 cycles, whereas cracks of approximately 100 μm were detected in substrates after 75 cycles, as shown in Fig. B-7 (a) and (b). Since the corners of Cu/Al_2O_3 joints were subject to the highest thermo-mechanical stresses, crack possibly initiated there and gradually propagated into the center through the interface. Based on the observations by both optical microscope (presented in section 3.1) and SEM, the lifetime of DBC substrates with respect to the current cycling condition was about 100 cycles.

In parylene-sealed samples, Cu/Al_2O_3 interface did not crack even after 200 cycles, as shown in Fig. B-8 (a) and (b). Fig. B-8 (a) shows the interfacial cross-section of parylene-sealed substrates after 100 cycles from -55 to 200°C. No crack was detected at the Cu/Al_2O_3 interfaces in any sample. After 200 cycles, as shown in Fig. B-8 (b), no crack was found at the Cu/Al_2O_3 interface either. The thermal reliability of DBC substrates was obviously improved by the thin polymer coating, which was pointed out to release the stress concentration at the tip of Cu/Al_2O_3 interface [169]. Parylene detached from the DBC surface after 200 cycles possibly because the adhesion of parylene to DBC surfaces was impaired by the CTE mismatch between polymer and substrate. Such detachment led to the loss of mechanical support from the parylene coating and then resulted in a rapid failure of the substrates.

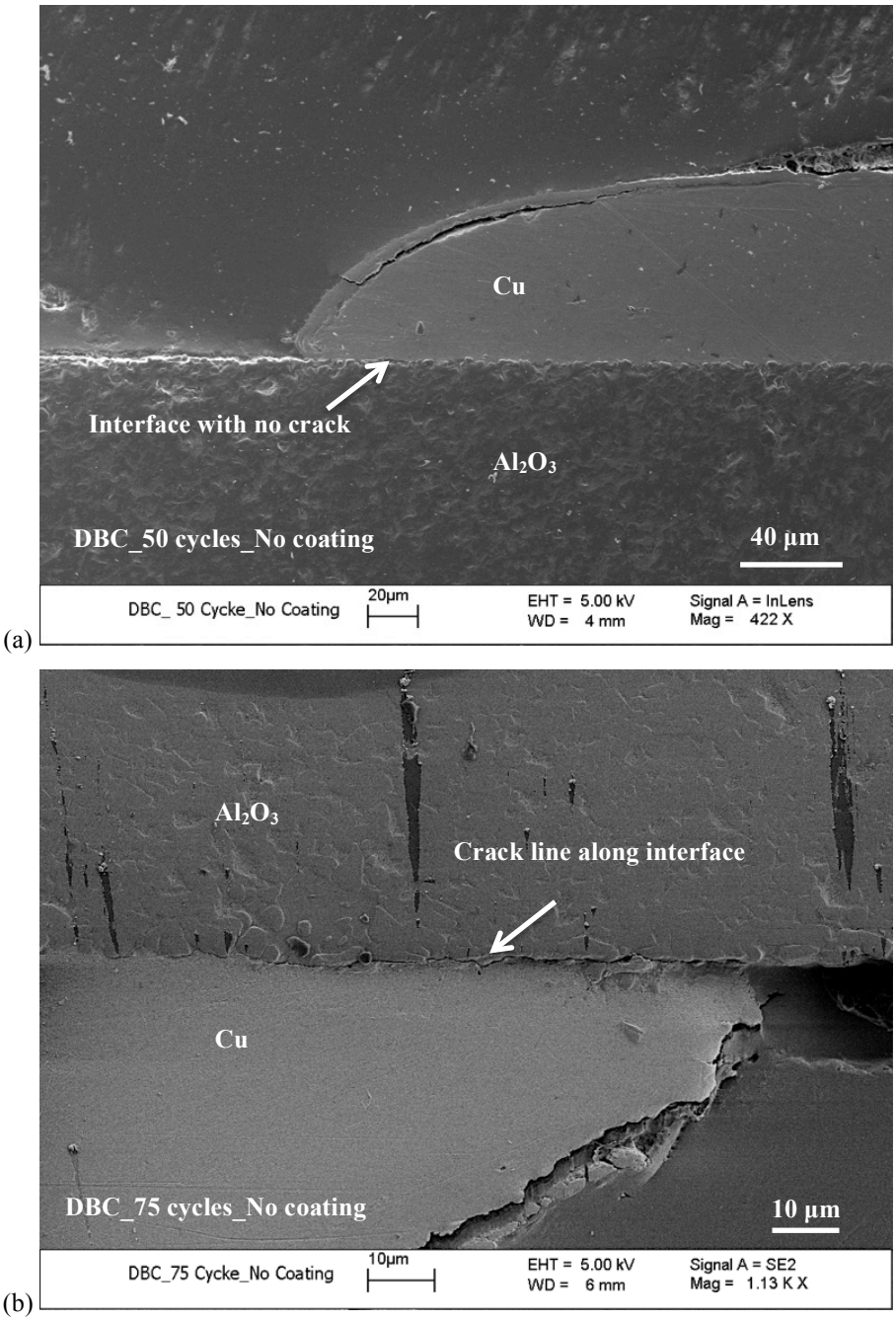

Fig. B-7. SEM images of cross-section of unsealed DBC after: (a) 50 and (b) 75 thermal cycles (-55 - 200°C).

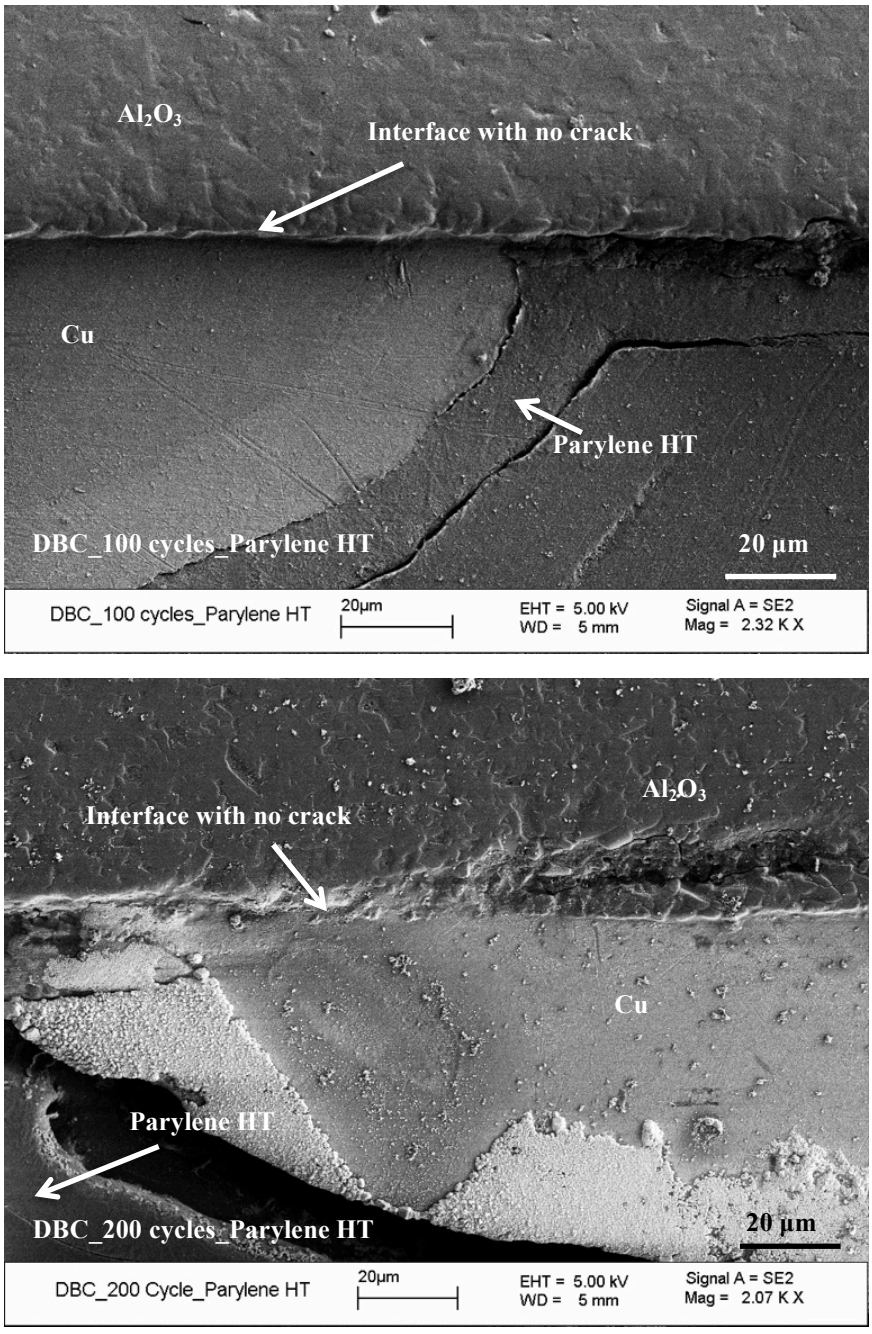

Fig. B-8. SEM images of cross-section of parylene-sealed DBC after: (a) 100 and (b) 200 thermal cycles (-55 - 200°C).

The SEM image of parylene-sealed samples after 300 cycles is shown in Fig. B-9. Parylene also detached from DBC surface. A crack initiated at the tip of Cu/Al_2O_3 joint and deflected into Al_2O_3 after propagating 50 μm along the interface. The failure of parylene-sealed DBC occurred before 300 cycles, which was 100 cycles after the detachment of parylene from DBC surfaces.

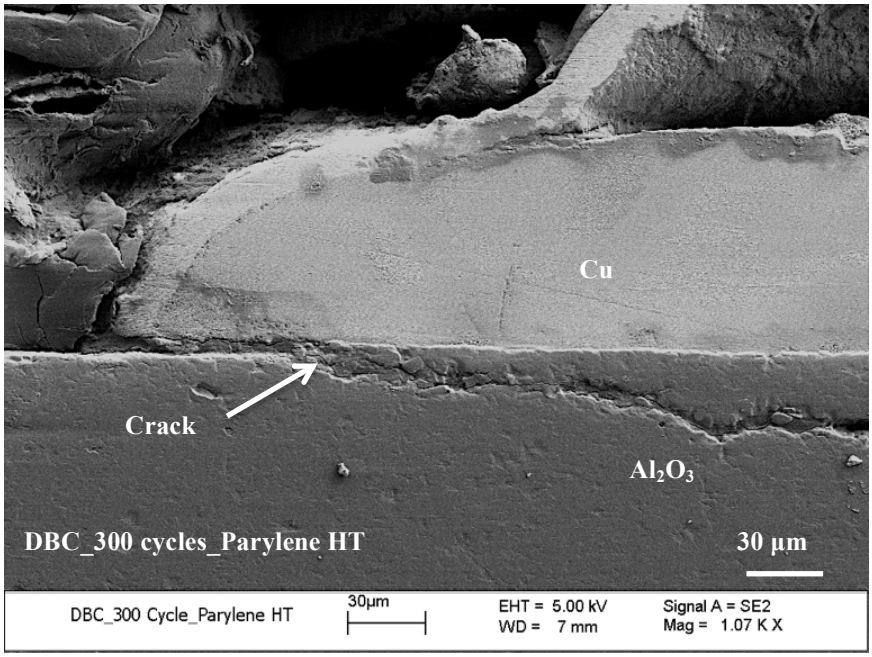

Fig. B-9. SEM image of cross-section of parylene-sealed DBC after 300 thermal cycles (-55 - 200°C).

Another group of samples under investigation is the DBC substrates sealed with Nusil. The SEM image of the cross-section of Nusil-sealed DBC substrates after 300 cycles is shown in Fig. B-10, which reveals the mechanical integrity at the tip of Cu/Al_2O_3 joint. No sign of crack initiation was found at Cu/Al_2O_3 interface. No detachment between Nusil and DBC surface was shown either. Such results indicated that Nusil-sealed DBC substrates had successfully survived 300 cycles from -55 to 200°C. Fig. B-11 shows the cross-section of Nusil-sealed DBC substrates after 900 cycles. A crack at Cu/Al_2O_3 interface of approximately 60 μm was clearly shown, indicating the degradation of DBC

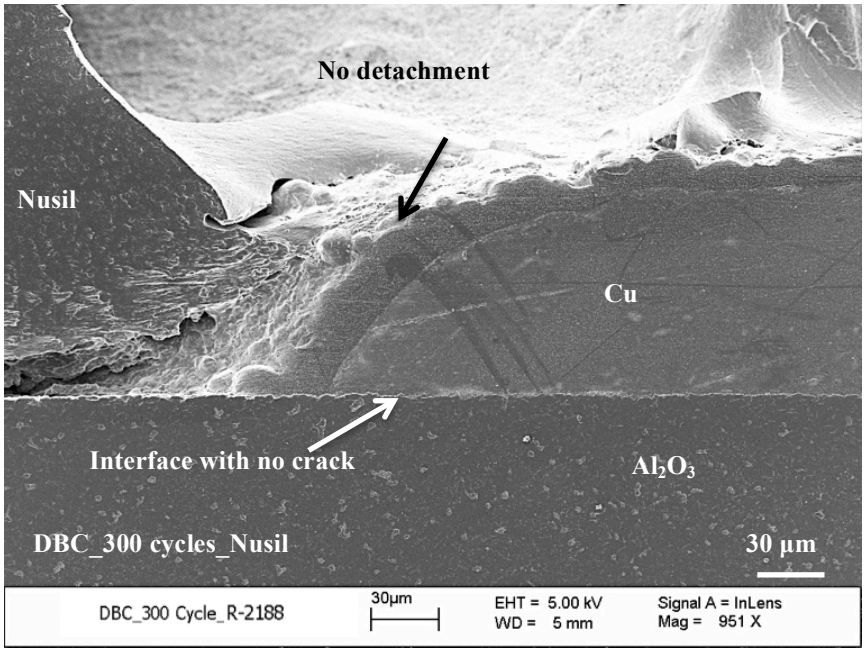

Fig. B-10. SEM image of cross-section of Nusil-sealed DBC after 300 thermal cycles (-55 - 200°C).

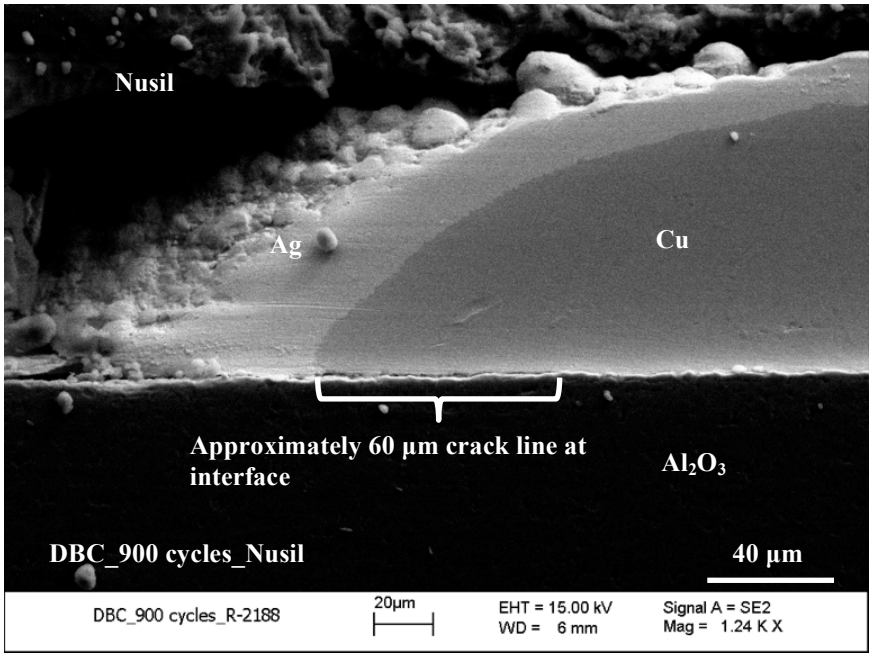

Fig. B-11. SEM image of cross-section of Nusil-sealed DBC after 900 thermal cycles (-55 - 200°C).

substrates. The crack at Cu/Al_2O_3 interface deflected into the ceramic after 1200 cycles (shown in Fig. B-12), indicating that the substrate was about to fail. The lifetime of Nusil-sealed DBC substrate was therefore approximately 1200 cycles with respect to the current cycling condition.

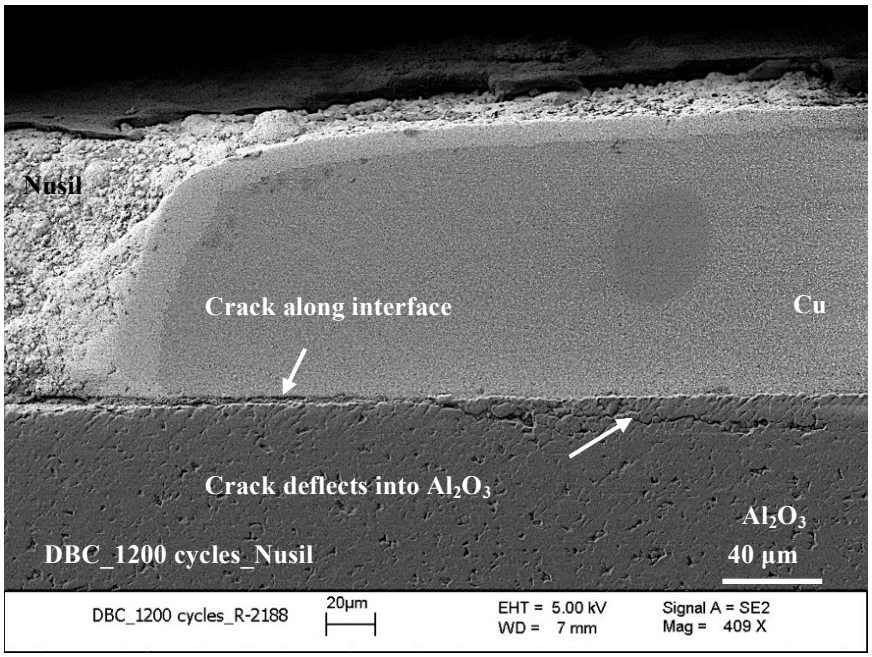

Fig. B-12. SEM image of cross-section of Nusil-sealed DBC after 1200 thermal cycles (-55 - 200°C).

The results proved that Nusil R-2188 was a better edge-sealing material compared to parylene HT under the cycling condition of -55 - 200°C. In 100 cycles after the detachment of parylene from DBC surfaces, rapid failure in the substrates occurred. No detachment was found between Nusil and DBC surfaces even after 1200 cycles possibly because silicone elastomer released the thermo-mechanical stresses through elastic deformation and therefore prevented itself from detaching from DBC surface.

4. Conclusion

The reliability of direct bonded copper (DBC) substrates with respect to thermal cycling from -55 to 200°C was investigated. In order to improve the reliability, parylene

HT and Nusil R-2188 were used to seal DBC edges. Optical microscope and SEM were used to examine cycled DBC substrates with and without sealing materials.

Optical microscope showed that unsealed DBC substrates failed within 100 cycles, whereas no failure was detected in both parylene- and Nusil-sealed samples within 300 cycles. SEM was demonstrated to be a better technique to detect failure in seal-edged DBC substrates. Cross-sections of DBC substrates with and without sealed edges were examined by SEM. Failure of unsealed DBCs was observed after 100 cycles, with interfacial crack at Cu/Al_2O_3 joint appeared between 50 and 75 cycles. When sealed with parylene HT, failure was delayed until 300 cycles, which was 100 cycles after the detachment of parylene from DBC surface. When sealed with Nusil R-2188, the lifetime was further improved to 1200 cycles. The results are summarized in TABLE B-1.

TABLE B-1
DBC LIFETIME WITH RESPECT TO THERMAL CYCLING (-55 - 200°C)

Coating material	Number of cycles prior to failure observation	Failure position
None	100 cycles	Cu/Al_2O_3 joint and Al_2O_3 matrix
Parylene HT	200 - 300 cycles	< 200 cycles: Parylene HT/DBC
		200 - 300 cycles: Cu/Al_2O_3 joint and Al_2O_3 matrix
Nusil R-2188	1200 cycles	900 cycles: Cu/Al_2O_3 interface
		1200 cycles: Cu/Al_2O_3 interface and Al_2O_3

Appendix C – Measured Data for Dielectric Characterization

TABLE C-1
DATA OF DIELECTRIC CHARACTERIZATION OF UNFILLED AND AL_2O_3 (ROD)-FILLED SILICONE AGED AT 250°C (PRESENTED IN CHAPTER 6, UP TO 480 HOURS)

	Breakdown voltage (V)	Dielectric strength (kV/mm)	Thickness before aging (μm)	Thickness after aging (μm)
Unfilled silicone, 0 hour	2350	18.2	129.4	
	2550	18.3	139.7	
	2600	19.3	135.0	
	2500	19.6	127.4	
	2600	19.8	131.2	
	2600	19.8	131.4	
	2900	19.8	146.2	
	2800	20.0	139.8	
	2800	20.3	138.0	
	2750	20.6	133.4	
Unfilled silicone, 80 hours	2900	19.4	149.4	149.2
	2900	19.4	149.6	149.2
	2900	19.9	145.9	145.8
	2900	19.9	146.0	145.6
	2750	20.4	135.5	135.0
	2700	20.6	132.0	130.8
	3000	20.7	145.4	145.0
	2650	21.5	123.9	123.4
	2850	21.8	131.1	131.0
	2650	21.9	121.4	121.0
Unfilled silicone, 160 hours	1000	9.5	107.2	105.8
	2450	22.2	113.7	110.4
	2450	22.2	111.8	110.2
	2500	22.2	113.7	112.4
	2500	22.2	113.2	112.4
	2500	23.0	110.8	108.8
	2550	23.4	111.2	108.8
	2750	24.6	113.4	111.8
	2750	25.0	113.3	110.0
	2800	26.4	109.2	106.0
Unfilled silicone, 240 hours	340	2.9	118.9	116
	1720	14.5	125.3	119
	2450	20.5	123.2	119.4
	2400	20.8	122.5	115.4
	2500	21.4	122.8	117
	2700	23.2	119.3	116.2
	2700	24.5	118.3	110.2

	2800	25.1	117.3	111.4
	2600	25.5	109.3	102
	2700	26.7	107.2	101
Unfilled silicone, 320 hours	700	5.4	130.3	129.8
	800	6.9	124.3	116.5
	2250	19.3	121.3	116.4
	2300	19.4	125.9	118.6
	2500	19.7	133.2	127.0
	2300	19.9	124.5	115.8
	2600	20.0	135.2	130.0
	2550	20.1	128.9	126.6
	2700	20.5	136.3	131.9
	2450	21.0	122.5	116.4
Unfilled silicone, 400 hours	200	1.6	125.6	123.0
	560	4.9	124.3	114.2
	580	4.9	125.3	117.4
	620	5.3	127.8	117.0
	750	6.5	124.0	114.6
	760	6.8	120.3	112.0
	1200	9.8	128.4	123.0
	2400	20.5	127.3	117.0
	2500	21.6	123.9	115.6
	2550	22.4	122.1	114.0
Unfilled silicone, 480 hours	400	3.2	135.3	126.4
	420	3.3	134.0	128.0
	440	3.7	125.8	120.3
	470	3.7	133.6	125.6
	490	3.9	132.2	126.4
	500	4.1	126.0	121.2
	480	4.1	126.4	116.0
	580	4.4	143.2	132.7
	530	4.6	123.8	114.5
	570	4.8	126.8	118.8
10-wt%-filled, 0 hour	2560	21.0	121.8	
	2590	21.4	121.0	
	2690	21.6	124.8	
	2680	21.9	122.2	
	2760	22.1	124.8	
	2700	22.2	121.8	
	2700	22.4	120.8	
	2690	22.6	118.8	
	2820	23.0	122.6	
10-wt%-filled, 80 hours	1600	13.5	118.9	118.2
	2420	20.8	116.8	116.2
	2590	20.9	124.5	124.2
	2510	20.9	121.1	120.0
	2600	21.4	121.9	121.6
	2680	21.4	125.3	125.0
	2520	21.5	117.5	116.5
	2600	22.3	116.9	116.8
	2800	22.9	122.4	122.2
	2720	23.2	117.3	117.4
10-wt%-filled, 160 hours	800	6.7	121.8	119.6
	2400	19.4	124.6	123.4
	2430	19.7	124.1	123.2
	2400	19.8	122.5	121.0
	2420	20.0	122.4	121.2
	2450	20.0	122.8	122.4
	2450	20.8	120.3	118.0
	2520	20.8	122.7	121.2

	2500	20.9	120.4	119.8
	2520	21.1	120.5	119.4
10-wt%-filled, 240 hours	900	8.9	106.4	101.2
	2390	19.6	122.7	121.8
	2420	20.6	120.5	117.6
	2450	20.8	119.8	117.6
	2520	21.1	123.1	119.6
	2580	21.3	123.6	121.2
	2500	21.3	120.3	117.2
	2480	21.6	118.3	114.8
	2620	22.0	122.3	119.0
	2480	22.2	115.3	111.8
10-wt%-filled, 320 hours	2620	21.6	125.9	121.2
	2700	22.1	127.5	122.0
	2700	22.3	126.8	121.0
	2720	22.3	126.2	121.8
	2820	22.8	127.9	123.6
	2800	22.9	129.4	122.2
	2790	23.0	125.3	121.4
	2750	23.3	124.3	117.8
	2830	23.5	126.2	120.4
	2850	23.6	125.9	120.6
10-wt%-filled, 400 hours	850	7.1	126.8	119.4
	1100	9.3	125.4	118.8
	1720	14.5	125.2	118.8
	1910	15.8	127.3	120.8
	2580	21.4	128.4	120.6
	2600	22.0	126.1	118.4
	2590	22.1	123.7	117.4
	2700	22.6	127.6	119.6
	2700	23.0	126.3	117.4
	2800	23.1	127.2	121.4
10-wt%-filled, 480 hours	1350	11.6	124.3	116.3
	1600	13.3	129.4	120.4
	2000	17.3	127.1	115.6
	2650	21.6	132.7	123.0
	2700	22.1	127.2	122.4
	2650	22.1	125.3	119.8
	2650	22.2	128.3	120.5
	2700	22.2	127.5	121.4
	2650	22.7	126.4	116.6
	2700	22.8	127.5	118.2
15-wt%-filled, 0 hour	2300	17.8	129.0	
	2300	17.9	128.2	
	2650	19.0	139.6	
	2750	19.8	138.8	
	2700	20.0	135.2	
	2800	20.1	139.0	
	2800	20.2	138.6	
	2750	20.4	134.8	
	2750	20.6	133.4	
	2800	21.6	129.4	
15-wt%-filled, 80 hours	1260	9.9	127.3	127.7
	2550	18.3	138.7	139.4
	2400	18.4	130.9	130.6
	2600	18.9	138.2	137.7
	2600	18.9	137.5	137.4
	2650	19.3	137.7	137.6
	2550	19.9	128.9	128.1
	2570	20.1	127.3	127.9

	2630	20.5	129.6	128.2
	2700	20.9	129.5	129.1
15-wt%-filled, 160 hours	2500	20.7	122.7	120.8
	2400	20.8	115.7	115.4
	2400	21.1	115.9	114.0
	2500	21.4	118.0	117.1
	2400	21.4	115.2	112.0
	2550	22.1	115.7	115.3
	2570	22.2	116.2	115.7
	2500	23.2	110.4	107.7
	2580	23.4	114.0	110.1
	2660	23.6	114.6	112.5
	2850	24.1	119.6	118.2
	2850	24.3	117.8	117.2
	2800	24.5	120.7	114.4
	2900	24.8	118.6	117.0
15-wt%-filled, 240 hours	2400	19.8	125.8	121.1
	2550	20.7	126.2	123.0
	2600	21.3	124.7	122.0
	2550	21.8	120.5	117.0
	2600	22.0	120.4	118.0
	2500	22.1	116.8	113.2
	2650	22.5	121.3	117.5
	2700	24.6	117.3	109.8
	2700	24.6	114.2	109.8
	2760	25.0	115.3	110.4
15-wt%-filled, 320 hours	1730	15.2	115.7	113.8
	2050	18.1	116.7	113.4
	2050	18.1	118.3	113.4
	2080	18.9	115.2	109.9
	2200	19.5	118.4	112.6
	2250	19.9	118.5	113.3
	2250	20.0	116.2	112.6
	2320	20.1	120.1	115.6
	2300	20.1	118.3	114.3
	2350	21.0	118.2	111.9
15-wt%-filled, 400 hours	1650	14.4	120.8	114.8
	1770	14.6	124.3	121.2
	1700	15.1	117.8	112.9
	1800	15.7	119.5	114.5
	2100	18.0	125.9	116.7
	1980	18.1	112.8	109.1
	2100	18.6	118.8	112.9
	2350	19.5	128.9	120.2
	2310	19.7	123.7	117.3
	2650	22.9	120.4	115.5
15-wt%-filled, 480 hours	940	7.7	126.3	122.3
	1630	13.8	122.9	118.0
	2000	17.2	123.3	116.0
	2150	18.3	124.6	117.5
	2100	18.7	123.2	112.1
	2220	19.4	123.7	114.6
	2250	19.5	124.7	115.3
	2300	19.8	124.7	116.0
	2300	20.1	123.2	114.4
	2200	20.2	120.7	109.1
30-wt%-filled, 0 hour	2350	19.0	123.9	
	2400	19.9	120.7	
	2450	20.2	121.3	
	2400	20.3	118.5	

	2400	20.3	118.0	
	2350	20.5	114.8	
	2350	20.7	113.7	
	2300	20.8	110.4	
	2400	21.0	114.1	
	2400	21.3	112.8	
30-wt%-filled, 80 hours	2580	21.2	122.7	121.8
	2600	21.5	121.3	121.1
	2620	21.6	121.0	121.1
	2600	21.8	119.5	119.2
	2600	22.4	116.8	116.3
	2700	22.4	120.9	120.5
	2700	22.9	117.9	117.7
	2600	23.0	113.7	113.2
	2650	23.1	114.8	114.7
	2650	23.4	113.2	113.1
30-wt%-filled, 160 hours	1150	9.5	121.8	121.7
	2350	19.1	122.4	123.3
	2350	19.4	120.8	120.9
	2450	20.0	123.4	122.5
	2350	20.0	119.2	117.5
	2450	20.4	123.1	120.2
	2450	20.7	120.6	118.4
	2450	20.9	120.1	117.0
	2450	21.3	118.5	115.3
	2500	21.7	120.3	115.1
30-wt%-filled, 240 hours	2450	20.1	121.6	122.0
	2500	20.6	122.4	121.6
	2530	21.3	120.5	119.0
	2450	21.4	120.5	114.6
	2550	21.4	122.6	119.0
	2520	21.6	120.4	116.7
	2550	21.7	121.5	117.5
	2600	21.7	123.7	119.7
	2610	21.9	120.4	119.4
	2800	23.7	121.8	117.9
30-wt%-filled, 320 hours	2400	20.3	124.2	118.2
	2300	20.4	120.9	113.0
	2500	20.5	125.3	122.1
	2350	20.5	117.8	114.7
	2430	20.7	123.9	117.3
	2450	20.8	123.6	118.0
	2500	20.9	124.2	119.4
	2450	20.9	120.5	117.0
	2370	21.0	120.5	112.9
	2500	21.3	117.9	117.4
30-wt%-filled, 400 hours	1550	13.2	122.4	117.6
	1900	17.5	113.2	108.7
	2380	20.8	116.3	114.4
	2300	20.9	116.3	109.8
	2300	21.1	117.2	108.9
	2380	21.1	117.1	112.6
	2570	21.8	118.3	118.1
	2590	21.8	125.6	118.6
	2500	21.9	118.3	114.1
	2400	22.2	116.0	108.2
	2450	22.2	118.2	110.1
	2650	22.5	120.7	117.6
	2600	22.7	117.3	114.7
	2480	22.7	114.3	109.1

30-wt%-filled, 480 hours	1050	9.4	114.8	112.0
	2380	21.5	116.8	110.6
	2470	21.8	120.8	113.3
	2450	22.1	117.4	111.1
	2500	22.3	120.3	112.0
	2400	22.6	111.3	106.1
	2440	22.9	114.3	106.6
	2380	22.9	112.9	103.8
	2480	23.2	110.3	106.8
	2530	24.1	112.7	105.0

References

[1] C.P. Wong, "Thermal-Mechanical Enhanced High-Performance Silicone Gels and Elastomeric Encapsulants in Microelectronic Packaging," *IEEE Trans. Components, Packaging, and Manufacturing Technology Part A*, vol. 18, no. 2, pp. 270-273, Jun. 1995.

[2] C.P. Wong, "Application of Polymer in Encapsulation of Electronic Parts," *Advances in Polymer Science*, vol. 84, pp 63-83, 1988.

[3] A.M. Jorgensen, K.B. Mogensen, W. Rong, P. Telleman, and J.P. Kutter, "Bio/Chemical Microsystem Designed for Wafer Scale Testing," *Proc. of SPIE 4407, MEMS Design, Fabrication, Characterization, and Packaging Conference*, pp. 164-171, Apr. 30, 2001, doi:10.1117/12.425298.

[4] P. McCluskey, "Reliability Concerns in High Temperature Electronic Systems," *Proc. of High-Temperature Electronic Materials, Devices and Sensors Conference*, San Diego, CA, Feb. 22-27, 1998.

[5] P.G. Neudeck, "Silicon Carbide Technology," in *The VLSI Handbook*, 2nd ed., W. Chen ed. FL: CRC Press, 2006, Ch. 5, pp. 5-1 - 34.

[6] Z. Chen, PhD Dissertation, "Electrical Integration of SiC Power Devices for High-Power-Density Applications," 2013.

[7] A. Elasser and T.P. Chow, "Silicon Carbide Benefits and Advantages for Power Electronics Circuits and Systems," *Proc. of the IEEE*, vol. 90, no. 6, pp. 969-986, Jun. 2002.

[8] "Normally - OFF Silicon Carbide Super Junction Transistor - 2N7635-GA" [online]. Available: http://www.genesicsemi.com/images/hit_sic/sjt/2N7635-GA.pdf, accessed on Oct. 3, 2014.

[9] "Normally - OFF Silicon Carbide Super Junction Transistor - 2N7640-GA" [online]. Available: http://www.genesicsemi.com/images/hit_sic/sjt/2N7640-GA.pdf, accessed on Oct. 3, 2014.

[10] W.W. Sheng and R.P. Colino, *Power Electronic Modules: Design and Manufacture*, FL: CRC Press, 2005, Ch. 3, pp. 11-101.

[11] J.H. Lupinski and R.S. Moore, "Polymeric Materials for Electronics Packaging and Interconnection," in *Polymeric Materials for Electronics Packaging and Interconnection*, vol. 407, J. Lupinski, *et al*. ed. Washington, DC: American Chemical Society, Sept. 1989, pp. 1-24.

[12] J.J. Licari, Coating Materials for Electronic Applications - Polymers, Processes, Reliability, Testing, NY: William Andrew Publishing/Noyes, 2003, Ch. 1, pp. 1-63.

[13] K. Gilleo. The Chemistry & Physics of Underfill [Online]. Available: http://www.et-trends.com/files/NepWest98_Chem-UF.pdf, accessed on Oct. 3, 2014.

[14] A. Genovese, F. Fontana, M. Cesana, S. Miliani, and E. Pirovano, "Solder Extrusions and Underfill Delaminations: A Remarkable Flip Chip Qualification

Experience," *The International Journal of Microcircuits and Electronic Packaging*, vol. 25, no. 1, pp. 53-60, 2001.

[15] L.P. Rector, S. Gong, T.R. Miles, and K. Gaffney, "Transfer Molding Encapsulation of Flip Chip Array Packages," *The International Journal of Microcircuits and Electronic Packaging*, vol. 23, no. 4, pp. 400-406, 2000.

[16] X.J. Fan, T.Y. Tee, C.Q. Cui, and G.Q. Zhang, "Underfill Selection against Moisture in Flip Chip BGA Packages," in *Moisture Sensitivity of Plastic Packages of IC Devices, Micro- and Opto-Electronic Materials, Structures, and Systems*, 1st ed. NY: Springer, 2010, Ch. 17, pp. 435-460.

[17] "UF 1220 - Technical Data Sheet" [online]. Available: http://www.united adhesives.com/datasheets/UF1220-Datasheet.pdf, accessed on Oct. 3, 2014.

[18] "Thermoset ME-531 Underfill Encapsulant - Technical Data Sheet" [online]. Available: http://www.lord.com/?action=download&document_id=306&output =download, accessed on Oct. 3, 2014.

[19] "Loctite UF3810 - Technical Data Sheet" [online]. Available: http://hybris. cms.henkel.com/medias/sys_master/8802969878558.pdf, accessed on Oct. 3, 2014.

[20] T. Braun, K.F. Becker, M. Koch, V. Bader, R. Aschenbrenner, and H. Reichl, "Flip Chip Molding - Recent Progress in Flip Chip Encapsulation," *Proc. of the International Symposium on Advanced Packaging Materials*, Stone Mountain, GA, Mar. 3-6, 2002, pp. 151-159.

[21] M.C. Paquet, M. Gaynes, E. Duchesne, D. Questad, L. Belanger, and J. Sylvestre, "Underfill Selection Strategy for Pb-Free, Low-K and Fine Pitch Organic Flip

Chip Applications," *Proc. of the Electronic Components and Technology Conference (ECTC)*, San Diego, CA, May 30 - Jun. 2, 2006, pp. 1595-1603.

[22] I.J. Rasiah, "Selecting an Underfill for Flip Chip Packaging," *Asian Electronics Engineer*, pp. 354-358, May 1999.

[23] J.H. Davis, D.W. Rees, and I.H. Riley, "Silicone Encapsulating and Potting Materials," *Proc. of the Institution of Electrical Engineers - Part B: Electronic and Communication Engineering*, vol. 109, no. 21, pp. 266-270, 1962.

[24] C.P. Wong, J.M. Segelken, and J.W. Balde, "Understanding the Use of Silicone Gels for Nonhermetic Plastic Packaging," *IEEE Trans. Components, Hybrids, and Manufacturing Technology*, vol. 12, no. 4, pp. 421-425, Dec. 1989.

[25] Y. Yao, Z. Chen, G. Lu, D. Boroyevich, and K.D.T. Ngo, "Characterization of Encapsulants for High-Voltage High-Temperature Power Electronic Packaging," *IEEE Trans. Components, Packaging, and Manufacturing Technology*, vol. 2, no. 4, pp. 539-547, Apr. 2012.

[26] "Cyclotene* 3000 Series - Processing Procedures for CYCLOTENE 3000 Series Dry Etch Resins" [online]. Available: http://www.dow.com/cyclotene/docs/cyclotene_3000_dry_etch.pdf, accessed on Oct. 3, 2014.

[27] "Cyclotene* 4000 Series - Processing Procedures for CYCLOTENE 4000 Series Resins - DS3000 Immersion Develop Process" [online]. Available: http://www.dow.com/webapps/lit/litorder.asp?filepath=cyclotene/pdfs/noreg/888-00008.pdf&pdf=true, accessed on Oct. 3, 2014.

[28] "Parylene Properties" [online]. Available: http://scscoatings.com/corporate/library.aspx, accessed on Oct. 3, 2014, accessed on Oct. 3, 2014.

[29] "P84® Polyimide Solution - Technical Information" [online], Available: http://hppolymer.com/pdfs/P84-%20Polyimide%20Solution1.pdf, accessed on Oct. 3, 2014

[30] "SR Silicone Conformal Coating 2102 - Technical Data Sheet" [online]. Available: http://www.techspray.com/controls/techspray.tds/tds.ashx?id=59, accessed on Oct 3, 2014.

[31] "R-2183 - Technical Data Sheet" [online]. Available: http://www.silicone-polymers.co.uk/pdfMaster/R-2183P.pdf, accessed on Oct. 3, 2014.

[32] "HT High-Temp Silicone Conformal Coating 2106" [online]. Available: http://www.techspray.com/controls/techspray.tds/tds.ashx?id=63, accessed on Oct. 3, 2014.

[33] "Technical Data Sheet: SolEpoxyTM MH20-01 Black" [online]. Available: http://www.solepoxy.com/Tools/Library/Upload/Project5/MH20-01_Black.pdf, accessed on Oct. 3, 2014.

[34] "Technical Data Sheet: SolEpoxyTM MH20-0686 Epoxy Molding Compound" [online]. Available: http://www.solepoxy.com/Tools/Library/Upload/Project5/MH20-0686_TDS.pdf, accessed on Oct. 3, 2014.

[35] "Technical Data Sheet: SolEpoxyTM MH6-0508NF" [online]. Available: http://www.solepoxy.com/Tools/Library/Upload/Project5/MH6-0508NF.pdf, accessed on Oct. 3, 2014.

[36] "Technical Data Sheet: SolEpoxyTM MH6-78NF" [online]. Available: http://www.solepoxy.com/Tools/Library/Upload/Project5/MH6-78NF.pdf, accessed on Oct. 3, 2014.

[37] "Molding Compounds 'KM-1000, KM-2000(G)' for Super Heat Resistance" [online]. Available: http://www.kyocera-chemi.jp/english/prdct/list/mc/pdf/km1000-km2000_e.pdf, accessed on Oct. 3, 2014.

[38] "P84® Polyimide PTFE/Polyimide Compound" [online]. Available: http://www.hppolymer.com/pdfs/P84-%20Polyimide%20Compound.pdf, accessed on Oct. 3, 2014.

[39] "Molding Compounds 'KM-700 Series' for Rapid Cure General Purpose" [online]. Available: http://www.kyocera-chemi.jp/english/prdct/list/mc/pdf/km727-km757_e.pdf, accessed on Oct. 3, 2014.

[40] "Molding Compounds 'KM-400 Series' for Non-Flammable" [online]. Available: http://www.kyocera-chemi.jp/english/prdct/list/mc/pdf/km450-km470_e.pdf, accessed on Oct. 3, 2014.

[41] "Molding Compounds 'KM-13 Series' for High Insulation" [online]. Available: http://www.kyocera-chemi.jp/english/prdct/list/mc/pdf/km13_e.pdf, accessed on Oct. 3, 2014.

[42] "Molding Compounds 'KM-220(J), KM-350(G)' for Ammonia-Free" [online]. Available: http://www.kyocera-chemi.jp/english/prdct/list/mc/pdf/km220-km350_e.pdf, accessed on Oct. 3, 2014.

[43] "EPM-2422 - Technical Data Sheet" [online]. Available: http://www.silicone-polymers.com/pdfMaster/EPM-2422P.pdf, accessed on Oct. 3, 2014.

[44] "EPM-2482 - Technical Data Sheet" [online]. Available: http://nusil.com/products/ProductProfiles/EPM-2482/EPM-2482P.pdf, accessed on Oct. 3, 2014.

[45] "500°F - 800°F Duraseal+ Silicones" [online]. Available: http://www.cotronics.

com/vo/cotr/pdf/1531.pdf, accessed on Oct. 3, 2014.

[46] "Technical Data Sheet - Master Sil 800 and 801" [online]. Available: http://www.masterbond.com/tds/mastersil-800, accessed on Oct. 3, 2014.

[47] "R-2188 - Technical Data Sheet" [online]. Available: http://nusil.com/products/ProductProfiles/R-2188/R-2188P.pdf, accessed on Oct. 3, 2014.

[48] "Technical Data Sheet - Qsil 550 2-Part Addition Cure Encapsulant" [online]. Available: http://www.acc-silicones.com/TechnicalSheetDownload.ashx?type=tds&id=a557cc06-7674-48d2-968a-bb047b432a5d&locale=en-gb, accessed on Oct. 3, 2014.

[49] "Technical Data Sheet - Qsil 556 2-Part Addition Cure Encapsulant" [online]. Available: http://www.acc-silicones.com/TechnicalSheetDownload.ashx?type=tds&id=b54ed924-456f-4589-9296-f4087705480e&locale=en-gb, accessed on Oct. 3, 2014.

[50] "CF-4721 - Technical Data Sheet" [online]. Available: http://nusil.com/products/ProductProfiles/CF-4721/CF-4721P.pdf, accessed on Oct. 3, 2014.

[51] "Durapot Epoxies - High Performance Casting, Embedding and Encapsulating Compounds" [online]. Available: http://www.cotronics.com/vo/cotr/pdf/860.pdf, accessed on Oct. 3, 2014.

[52] "Tough-Seal Performs" [online]. Available: http://www.keypolymer.com/potting-encapsulating/tough-seal/tough-seal-performs/, accessed on Oct. 3, 2014.

[53] "Products - Examples from Our Catalog of Electronics Products" [online]. Available: http://www.epicresins-electronics.com/products.html, accessed on Oct. 3, 2014.

[54] "Araldite Casting Epoxy System - Araldite® CW 5725 100 pbw / Aradur® HY 5726 28 pbw" [online]. Available: http://www.runtimes.cn/upload/201310/21/20131021133439390 6.pdf, accessed on Oct. 3, 2014.

[55] "Araldite® CY 5825 US Hardener HY 5825 US" [online]. Available: http://krayden.com/tds/hunts_aradur_hy_5825_tds.pdf, accessed on Oct. 3, 2014.

[56] "Advanced Materials - Euremelt® 3413" [online]. Available: http://www.farix.hu/pdf/1389712645.pdf, accessed on Oct. 3, 2014.

[57] "20-2121 Elastomeric Potting & Encapsulating Compound" [online]. Available: http://www.epoxies.com/_resources/common/userfiles/file/20-2121.pdf, accessed on Oct. 3, 2014.

[58] "R-1400 Silicone Glob-Top" [online]. Available: Available: http://nusil.com/products/ProductProfiles/R-1400/R-1400P.pdf, accessed on Oct. 3, 2014.

[59] "Multi-Cure® 9001-E-V3.7 - Resilient, Clear Encapsulant" [online]. Available: http://www.dymax.com/images/pdf/pds/9001-e-v37.pdf, accessed on Oct. 3, 2014.

[60] "Dual-Cure 9103 - Light/Moisture-Cure Clear Encapsulant" [online]. Available: http://www.dymax.com/images/pdf/pds/9103.pdf, accessed on Oct. 3, 2014.

[61] J. Artbauer, "Electric Strength of Polymers," *Journal of Physics D: Applied Physics*, vol. 29, no. 2, pp. 446-456, Feb. 1996.

[62] S. Diaham, M.L. Locatelli, and R. Khazaka, "BPDA-PDA Polyimide: Synthesis, Characterizations, Aging and Semiconductor Device Passivation," in *High Performance Polymers - Polyimides Based - From Chemistry to Applications*, M Abadie ed. InTech, ISBN: 978-953-51-0899-3, DOI: 10.5772/53994, 2002, Ch. 2,

pp. 15-36. Available from: http://www.intechopen.com/books/high-performance-polymers-polyimides-based-from-chemistry-to-applications/bpda-pda-polyimide-synthesis-characterizations-aging-and-semiconductor-device-passivation, accessed on Oct. 3, 2014.

[63] "Data Sheet - Epo-Tek 600", released and discontinued in 2011 by Epoxy Technology, Inc.

[64] "Product Information Sheet - Epo-Tek 390" [online]. Available: http://www.rikei.co.jp/epo-tek/pdf/390.PDF, accessed on Oct. 3, 2014.

[65] M.L. Locatelli, R. Khazaka, S. Diaham, C.D. Pham, M. Bechara, and S. Dinculesc *et al*, "Evaluation of Encapsulation Materials for High-Temperature Power Device Packaging," *IEEE Trans. Power Electronics*, vol. 29, no. 5, pp. 2281-2289, May 2014.

[66] P.R. Dvornic, "Thermal Properties of Polysiloxanes," in *Silicon-Containing Polymers: The Science and Technology of Their Synthesis and Applications*, R. G. Jones, et al. ed. Netherland: Kluwer Academic Publishers, 2000, Ch. 7, pp. 185-212 and references cited therein.

[67] N. Grassie and I.G. MacFarlane, "The Thermal Degradation of Polysiloxanes - 1 Poly(dimethylsiloxane)," *European Polymer Journal*, vol. 14, pp. 875-884, 1978.

[68] G. Camino, S.M. Lomakin, and M. Lageard, "Thermal Polydimethylsiloxane Degradation. Part 2. The Degradation Mechanisms," *Polymer*, vol. 43, pp. 2011-2015, Mar. 2002.

[69] G. Camino, S.M. Lomakin, and M. Lageard, "Polydimethylsiloxane Thermal Degradation, Part 1, Kinetic Aspects," *Polymer*, vol. 42, no. 6, pp. 2395-2402,

Mar. 2001.

[70] J.D. Scofield, J.N. Merrett, J. Richmond, A. Agarwal, and S. Leslie, "Performance and Reliability Characteristics of 1200 V, 100 A, 200ºC Half-Bridge SiC MOSFET-JBS Diode Power Modules," *Proc. of the 2010 International Conference on High Temperature Electronics (HiTEC)*, Albuquerque, NM, May 11-13, 2010.

[71] P.R. Dvornic and M.J. Owen, "Silicon-Containing Dendritic Polymers," in *Advances in Silicon Science*, J. Matisons ed. NY: Springer, 2009, Ch. 17, pp. 345-376.

[72] Y. Luo, Handbook of Bond Dissociation Energies in organic Compounds, FL: CRC Press, 2003, Ch. 1, pp. 1-6.

[73] G. Camino, S.M. Lomakin, and M. Lageard, "Polydimethylsiloxane Thermal Degradation, Part 1, Kinetic Aspects," *Polymer*, vol. 42, pp. 2395-2402, Mar. 2001.

[74] L.J. Durham, C.F. Wurster Jr., and H.S. Mosher, "Peroxide III, The Mechanism for the Thermal Decomposition of n-Butyl Hydroperoxide and n-Butyl 1-Hydroxybutyl Peroxide," *Journal of American Chemistry Society*, vol. 80, no. 2, pp. 332-338, Jan. 1958.

[75] K. Chrissafis and D. Bikiaris, "Can Nanoparticles Really Enhance Thermal Stability of Polymer? Part I: An Overview on Thermal Decomposition of Addition Polymers," *Thermochimica Acta*, vol. 523, pp. 1-24, Aug. 2011.

[76] J. Zhang, S. Feng, and Q. Ma, "Kinetics of the Thermal Degradation and Thermal Stability of Conductive Silicone Rubber Filled with Conductive Carbon

Black," *Journal of Applied Polymer Science*, vol.89, pp.1548-1554, Aug. 2003.

[77] G.B. Sohoni and J.E. Mark, "Thermal Stability of In Situ Filled Siloxane Elastomers," *Journal of Applied Polymer Science*, vol. 45, pp. 1763-1775, Aug. 1992.

[78] A.H. El-Hag, L.C. Simon, S.H. Jayaram, and E.A. Cherney, "Erosion Resistance of Nano-filled Silicone Rubber," *IEEE Trans. Dielectrics and Electrical Insulation*, vol. 13, no. 1, pp. 122-128, Feb. 2006.

[79] L. Yang, S. Qiu, Y. Zhang, and Y. Xu, "Preparation of PDMS/SiO_2 Nanocomposites via Ultrasonical Modification and Miniemulsion Polymerization," *Journal of Polymer Research*, vol. 20, no. 68, pp. 1-6, Dec. 2013.

[80] W. Zhou, S. Qi, C. Tu, and H. Zhao, "Novel Heat-Conductive Composite Silicone Rubber," *Journal of Applied Polymer Science*, vol. 104, no. 4, pp. 2478-2483, Feb. 2007.

[81] L.C. Sim, S.R. Ramanan, H.N. Seetharamu, and T.J. Goh, "Thermal Characterization of Al_2O_3 and ZnO Reinforced Silicone Rubber as Thermal Pads for Heat Dissipation Purposes," *Thermochimica Acta*, vol. 430, no. 1-2, pp. 155-165, Jun. 2005.

[82] Y. Xiong, Q. Shen, F. Chen, G. Luo, K. Yu, and L. Zhang, "High Strength Retention and Dimensional Stability of Silicone/Alumina Composite Panel under Fire," *Fire and Materials*, vol. 36, pp. 254-263, Jun. 2012.

[83] E. Amendola, G. Lupo, C. Petrarca, and A.M. Scamardella, "Alumina Filled Silicone Nanocomposites for Electrical Insulation of Power Rotating Machines,"

International Journal of Applied Electromagnetics and Mechanics, vol. 39, pp. 3-11, 2012.

[84] P. Garg, R.P. Singh, and V. Choudhary, "Pervaporation Separation of Organic Azeotrope Using Poly(dimethyl siloxane)/Clay Nanocomposite Membranes," *Separation and Purification Technology*, vol. 80, no. 3, pp. 435-444, Aug. 2011.

[85] Q. Kong, Y. Hu, L. Song, Y. Wang, Z. Chen, and W. Fan, "Influence of Fe-MMT on Crosslinking and Thermal Degradation in Silicone Rubber/Clay Nanocomposites," *Polymer for Advanced Technologies*, vol. 17, pp. 463-467, Jun. 2006.

[86] L. Yang, Y. Hu, H. Lu, and L. Song, "Morphology, Thermal, and Mechanical Properties of Flame-Retardant Silicone Rubber/Montmorillonite Nanocomposites," *Journal of Applied Polymer Science*, vol. 99, no. 6, pp. 3275-3280, Mar. 2006.

[87] J.W. Kim, M.H. Noh, H.J. Choi, D.C. Lee, and M.S. Jhon, "Synthesis and Electrorheological Characteristics of SAN-Clay Composite Suspensions," *Polymer*, vol. 41, no. 3, pp. 1228-1231, Feb. 2000.

[88] A. Dasari, S. Lim, Z. Yu, and Y. Mai, "Toughening, Thermal Stability, Flame Retardancy, and Scratch-Wear Resistance of Polymer-Clay Nanocomposites," *Australian Journal of Chemistry*, vol. 60, no.7, pp. 496–518, Jul. 2007.

[89] W. Zhou, S. Qi, H. Zhao, and N. Liu, "Thermally Conductive Silicone Rubber Reinforced with Boron Nitride Particle," *Polymer Composites*, vol. 28, no.1, pp. 23-28, Feb. 2007.

[90] N. Roy and A.K. Bhowmick, "Novel in Situ Polydimethylsiloxane-Sepiolite

Nanocomposites: Structure-Property Relationship," *Polymer*, vol. 51, no. 22, pp. 5172-5185, Oct. 2010.

[91] C.P. Wong and R.S. Bollampally, "Thermal Conductivity, Elastic Modulus, and Coefficient of Thermal Expansion of Polymer Composites Filled with Ceramic Particles for Electronic Packaging," *Journal of Applied Polymer Science*, vol. 74, pp. 3396-3403, Dec. 1999.

[92] W. Zhou, C. Wang, Q. An, and H. Ou, "Thermal Properties of Heat Conductive Silicone Rubber Filled with Hybrid Fillers," *Journal of Composite Materials*, vol. 42, no. 2, pp. 173-187, 2008.

[93] B. Adnadjevic and J. Jovanovic, "Investigation of the Effects of NAA-Type Zeolite on PDMS Composites," *Journal of Applied Polymer Science*, vol. 77, no. 6, pp. 1171-1176, Aug. 2000.

[94] C. Lü, Z. Wang, F. Liu, J. Yan, and L. Guo, "Microstructure and Properties of New Polyimide/Polysiloxane Composite Films," *Journal of Applied Polymer Science*, vol. 100, no. 1, pp. 124-132, Apr. 2006.

[95] L.G. Hanu, G.P. Simon, and Y.B. Cheng, "Thermal Stability and Flammability of Silicone Polymer Composites," *Polymer Degradation and Stability*, vol. 91, no. 6, pp. 1373-1379, Jun. 2006.

[96] M.L.Q.A. Kaneko and I.V.P. Yoshida, "Effect of Natural and Organically Modified Montmorillonite Clays on the Properties of Polydimethylsiloxane Rubber," *Journal of Applied Polymer Science*, vol. 108, no. 4, pp. 2587-2596, May 2008.

[97] J. Wang, Y. Chen, and Q. Jin, "Preparation and Characteristics of a Novel

Silicone Rubber Nanocomposite Based on Organophilic Montmorillonite," *High Performance Polymers*, vol. 18, no. 3, pp. 325-340, Jun. 2006.

[98] J. Qu and C.P. Wong, "Effective Elastic Modulus of Underfill Material for Flip-Chip Applications," *IEEE Trans. Components and Packaging Technologies*, vol. 25, no. 1, pp. 53-55, Mar. 2002.

[99] G. Tsagaropoulos and A. Eisenberg, "Dynamic Mechanical Study of the Factors Affecting the Two Glass Transition Behavior of Filled Polymers Similarities and Differences with Random Ionomers," *Macromolecules*, vol. 28, pp. 6067-6077, Aug. 1995.

[100] V.M. Litvinov and H.W. Spiess, "^{2}H NMR Study of Molecular Motions in Polydimethylsiloxane and Its Mixtures with Aerosils," *Die Makromolekulare Chemie*, vol. 192, no. 12, pp. 3005-3019, Dec. 1991.

[101] L. Dewimille, B. Bresson, and L. Bokobza, "Synthesis, Structure and Morphology of Poly(dimethylsiloxane) Networks Filled with in Situ Generated Silica Particles," *Polymer*, vol. 46, pp.4135-4143, Mar. 2005.

[102] S.S. Sternstein and A. Zhu, "Reinforcement Mechanism of Nanofilled Polymer Melts as Elucidated by Nanlinear Viscoelastic Behavior," *Macromolecules*, vol. 35, pp. 7262-7273, Aug. 2002.

[103] D. Pitsa and M.G. Danikas, "Interfaces Features in Polymer Nanocomposites: A Review of Proposed Models," *NANO: Brief Reports and Reviews*, vol. 6, no. 6, pp. 497-508, Oct. 2011.

[104] Z. Chen, Y. Yao, D. Boroyevich, K.D.T. Ngo, M. Paolo, and R. Kaushik, "A 1200V, 60 A SiC MOSFET Multi-Chip Phase-Leg Module for High-

Temperature, High-Frequency Applications", *Proc. of The Applied Power Electronics Conference and Exposition (APEC)*, Long Beach, CA, Mar. 17-21, 2013.

[105] G. Bai, J. Yin, Z. Zhang, G. Lu, and J.D. van Wyk, "High-Temperature Operation of SiC Power Devices by Low-Temperature Sintered Silver Die-Attachment," *IEEE Trans. Advanced Packaging*, vol. 30, no. 3, pp. 506-510, Aug. 2007.

[106] Y. Yao, Z. Chen, D. Boroyevich, and K.D.T. Ngo, "High-Temperature Reliability of Direct-Bond-Copper Substrates with Step-Edges," *Proc. of the International Conference on High Temperature Electronics (HiTEC)*, Albuquerque, NM, May 8-10, 2012.

[107] Z. Chen, D. Boroyevich, R. Burgos, and F. Wang, "Characterization and Modeling of 1.2 kV, 20 A SiC MOSFETs," *Proc. of IEEE Energy Conversion Congress and Exposition (ECCE)*, San Jose, CA, Sept. 20-24, 2009, pp. 1480-1487.

[108] Z. Chen, Y. Yao, M. Danilovic and D. Boroyevich, "Performance Evaluation of SiC Power MOSFETs for High-Temperature Applications," *Proc. of 15th International Power Electronics and Motion Control Conference (EPE-PEMC 2012 ECCE Europe)*, Novi Sad, Serbia, Sept. 3-6, 2012, DS1a.8, pp. 1-9.

[109] A. Lindgren, M. Domeij, and H. Hjort, "1200V 20A SiC BJTs Operating at 250°C," *Proc. of IMAPS International Conference on High Temperature Electronics Network (HiTEN 2011)*, Oxford, United Kingdom, Jul. 18-20, 2011.

[110] J. Schulz-Harder, "Advantages and New Development of Direct Bonded Copper

Substrates," *Micorelectronics Reliability*, vol. 43, pp. 359-365, Mar. 2003.

[111] G. Lei, PhD Dissertation, "Thermomechanical Reliability of Low-Temperature Sintered Attachments on Direct Bonded Aluminum (DBA) Substrate for High-Temperature Electronics Packaging", 2010.

[112] M.K. Schwiebert and W.H. Leong, "Underfill Flow as Viscous Flow between Parallel Plates Driven by Capillary Action," *IEEE Trans. Components, Packaging, and Manufacturing Technology, Part C*, vol. 19, no. 2, pp. 133-137, Apr. 1996.

[113] J.P. Goodelle, J.J. Gilbert, and R.E. Fanucci, "Evaluating Underfill Materials for High Reliability Applications," *Proc. 50th Electronic Components and Technology Conference*, Las Vegas, NV, Aug. 2002, pp. 330-342.

[114] X. Zhang, B. Sun, W. Feng, Q. Zhang, and Q. Li, "Wetting Behavior of Polymer Melts on Bulk Metallic Glasses," *Applied Mechanics and Materials*, vol. 404, no. 25, 2013, pp. 25-31.

[115] Z. Zhang and C.P. Wong, "Recent Advances in Flip-Chip Underfill: Materials, Process, and Reliability," *IEEE Trans. Advanced Packaging*, vol. 27, no. 3, pp. 515-524, Aug. 2004.

[116] S. Han and K.K. Wang, "Study on the Pressurized Underfill Encapsulation of Flip Chips," *IEEE Trans. Components, Packaging, and Manufacturing Technology, Part B*, vol. 20, no. 4, pp. 434-442, Nov. 1997.

[117] S.C. Machuga, S.E. Lindsey, K.D. Moore, and A.F. Skipor, "Encapsulation of Flip Chip Structures," *Proc. Electronics Manufacturing Technology Symposium, 13th IEEE/CHMT International,* Baltimore, MD, Sept. 28-30, 1992, pp. 53-58.

[118] W. Kim, J. Bae, I. Choi, and Y. Kim, "Thermally Conductive EMC (Epoxy Molding Compound) for Microelectronic Encapsulation," *Polymer Engineering and Science*, vol. 39, no. 4, pp. 756-766, Apr. 1999.

[119] E.A. Chowdhury, J. Kolodzey, J.O. Olowolafe, G. Qiu, G. Katulka, and D. Hits *et al*, "Thermally Oxidized AlN Thin Films for Device Insulators," *Applied Physics Letters*, vol. 70, no. 20, pp. 2732-2734, May 1997.

[120] A.L. Brown, M.G. Norton, "Oxidation Kinetics of AlN Powder," *Journal of Materials Science Letters*, vol. 17, no. 18, pp. 1519-1522, Sept. 1998.

[121] P.J. Launer, "Infrared Analysis of Organosilicon Compounds: Spectra-Structure Correlations," in *Silicone Compounds: Register and Review*, B. Arkles *et al*. ed. PA: Petrarch Systems, 1987, pp. 100-103.

[122] L.H. Sperling, *Introduction to Physical Polymer Science*, 4th ed., NJ: John Wiley & Sons, 2006.

[123] J.P. Matinlinna, S. Areva, L.V.J. Lassila, and P.K. Vallittu, "Characterization of Siloxane Films on Titanium Substrate Derived from Three Aminosilanes," *Surface and Interface Analysis*, vol. 36, pp. 1314-1322, Mar. 2004.

[124] "Material Safety Data Sheet - EPM-2422 Part B" [online]. Available: http://www.silicone-polymers.com/pdfMaster/EPM2422B.pdf, accessed on Oct. 3, 2014.

[125] G. Havet and A.I. Isayev, "A Thermodynamic Approach to the Rheology of Highly Interactive Filler-Polymer Mixtures. Part II. Comparison with Polystyrene/Nanosilica Mixtures," *Rheologica Acta*, vol. 42, no. 1-2, pp. 47-55, 2003.

[126] V. Arrighi, J.S. Higgins, A.N. Burgess, and G. Floudas, "Local Dynamics of Poly(dimethyl siloxane) in the Presence of Reinforcing Filler Particles," *Polymer*, vol. 39, no. 25, pp. 6369-6376, 1998.

[127] P. Cassagnau, "Melt Rheology of Organoclay and Fumed Silica Nanocomposites," *Polymer*, vol. 49, pp. 2183-2196, 2008.

[128] D.W. Litchfield and D.G. Baird, "The Rheology of High Aspect Ratio Nano-Particle Filled Liquids," *Rheology Reviews*, pp. 1-60, 2006.

[129] K.A. Lawler, "Viscosity of Aqueous and Cyanate Ester Suspensions Containing Alumina Nanoparticles," Master Thesis, 2009.

[130] O.S. Agimelen and P.D. Olmsted, "Apparent Fracture in Polymeric Fluids under step Shear," accepted by *Physical Review Letter*, 2013, arXiv:1204.4169v3.

[131] J. Mewis and N.J. Wagner, Colloidal Suspension Rheology, NY: Cambridge University Press, 2012.

[132] J. Goldstein, D. Newbury, D. Joy, C. Lyman, P. Echlin, and E. Lifshin *et al*, *Scanning Electron Microscopy and X-Ray Microanalysis*, 3rd ed., NY: Springer, 2003.

[133] A. Patel, T. Cosgrove, J.A. Semlyen, J.R.P. Webster, and J.M.H.M. Scheutjens, "Adsorption Studies of Different End-Functionalised Linear Poly (dimethylsiloxane)," *Colloids and Surfaces A: Physicochemical and Engineering Aspects*, vol. 87, pp. 15-24, Jul. 1994.

[134] R.S. Ndong and W.B. Russel, "Effects of Molecular Weight and Volume Fraction on Rheological Properties of PDMS-Grafted Alumina in PDMS Melts," *Journal of Rheology*, vol. 55, no. 2, pp. 331-351, Mar./Apr. 2011.

[135] J.P. Cohen-Addad and R. Ebengou, "Silica-Siloxane Mixtures. Investigations into Adsorption properties of End-Methylated and End-Hydroxylated Chains," *Polymer*, vol. 33, no. 2, pp. 379-383, 1992.

[136] T. Tanaka, M. Kozako, N. Fuse, and Y. Ohki, "Proposal of a Multi-Core Model for Polymer Nanocomposite Dielectrics," *IEEE Trans. Dielectrics and Electrical Insulation*, vol. 12, no. 4, pp. 669-681, Aug. 2005.

[137] J.B. Peri and R.B. Hannan, "Surface Hydroxyl Groups on γ-Alumina," *Journal of Physical Chemistry*, vol. 64, no. 10, pp. 1526-1530, Oct. 1960.

[138] A.A. Tsyganenko and V.N. Filimonov, "Infrared Spectra of Surface Hydroxyl Groups and Crystalline Structure of Oxides," *Journal of Molecular Structure*, vol. 19, pp. 579-589, Dec. 1973.

[139] C. Morterra, G. Ghiotti, E. Garrone, and F. Boccuzzi, "Infrared Spectroscopic Characterization of the α-Alumina Surface," *Journal of Chemistry Scociety, Faraday Transaction 1*, vol. 72, pp.2722-2734, 1976.

[140] M. Zamora and A. Cordoba, "A Study of Surface Hydroxyl Groups on γ-Alumina," *The Journal of Physical Chemistry*, vol. 82, no. 5, pp. 584-588, Mar. 1978.

[141] M. Digne, P. Sautet, P. Raybaud, P. Euzen, and H. Toulhoat, "Hydroxyl Groups on γ-Alumina Surface: A DFT Study," *Journal of Catalysis*, vol. 211, pp. 1-5, Oct. 2002.

[142] E. McCafferty and J.P. Wightman, "Determination of the Concentration of Surface Hydroxyl Groups on Metal Oxide Films by a Quantitative XPS Method", *Surface and Interface Analysis*, vol. 26, pp. 549-564, Jul. 1998.

[143] V. Coustet and J. Jupille, "High-Resolution Electron-Energy-Loss Spectroscopy of Hydroxyl Groups at the Surface of Bulk Insulating Oxides," *Surface and Interface Analysis*, vol. 22, pp. 280-283, Jul. 1994.

[144] J. van den Brand, P.C. Snijders, W.G. Sloof, H. Terryn, and J.H.W. de Wit, "Acid-Base Characterization of Aluminum Oxide Surfaces with XPS," *Journal of Physical Chemistry B*, vol. 108, pp. 6017-6024, 2004.

[145] T.R. Gengenbach, R.C. Chatelier, and H.J. Griesser, "Characterization of the Ageing of Plasma-Deposited Polymer Films: global Analysis of X-Ray Photoelectron Spectroscopy Data," *Surface and Interface Analysis*, vol. 24, pp. 271-281, Apr. 1996.

[146] J. van den Brand, W.G. Sloof, H. Terryn, and J.H.W. de Wit, "Correlation between Hydroxyl fraction and O/Al Atomic Ratio as Determined from XPS Spectra of Aluminum Oxide Layers," *Surface and Interface Analysis*, vol. 36, pp. 81-88, Jan. 2004.

[147] "Application Note AN # 79: Attenuated Total Reflection (ATR) – A Versatile Tool for FT-IR Spectroscopy" [online]. Available: http://www.bruker.com/fileadmin/user_upload/8-PDF-Docs/OpticalSpectrospcopy/FT-IR/ALPHA/AN/AN79_ATR-Basics_EN.pdf, accessed on Oct. 3, 2014.

[148] "FT-IR Spectroscopy: Attenuated Total Reflectance (ATR)" [online]. Available: http://www.utsc.utoronto.ca/~traceslab/ATR_FTIR.pdf, accessed on Oct. 3, 2014.

[149] W. Weibull, "A Statistical Distribution Function of Wide Applicability," *Journal of Applied mechanics*, vol. 18, pp. 293-297, Sept. 1951.

[150] G. Chen and A.V. Davis, "The Influence of Defects on the Short-Term Breakdown Characteristics and Long-Term DC Performance of LDPE Insulation," *IEEE Trans. Dielectrics and Electrical Insulation,* vol. 7, no. 3, pp. 401-407, Jun. 2000.

[151] R.W. Coppard, J. Bowman, L.A. Dissado, and S.M. Rowland, and R.T. Rakowski, "The Effect of Aluminium Inclusions on the Dielectric Breakdown of Polyethylene," *Journal of Physics D: Applied Physics*, vol. 23, pp. 1554-1561, Dec. 1990.

[152] IEEE Std 930^{TM}-2004, "IEEE Guide for the Statistical Analysis of Electrical Insulation Breakdown Data," Apr. 2005.

[153] G.C. Stone and R.G. van Heeswijk, "Parameter Estimation for the Weibull Distribution," *IEEE Trans. Electrical Insulation*, vol. 4, pp. 253-261, 1977.

[154] L.B. Loeb and J.M. Meek, "The Mechanism of Spark Discharge in Air at Atmospheric Pressure. I," *Journal of Applied Physics*, vol. 11, pp. 438-447, Jun. 1940.

[155] R.S. Dhariwal, J.M.Torres, and M.P.Y. Desmulliez, "Electric Field Breakdown at Micrometre Separations in Air and Nitrogen at Atmospheric Pressure," *IEE Proc. Science, Measurement and Technology*, vol. 147, no. 5, pp. 261-265, Aug. 2002.

[156] "P2SI® 700LM" [online]. Available: http://www.p2si.com/rtm-resins/data sheets/P2SI-700LM-Datasheet.pdf, accessed on Oct. 3, 2014.

[157] "KINEL® SK4525 S5A (Preliminary data)" [online]. Available: http://www.neopreg.ch/index.php?option=com_rsfiles&task=files.download&pat

h=...Home...DataSheets...Kinel...KINEL_SK4525S5A_DS_Eng.PDF&Itemid=69, accessed on Oct. 3, 2014.

[158] "Shin-Etsu Epoxy Molding Compounds: KMC Series" [online]. Available: http://www.shinetsu-encap-mat.jp/e/product/k_s/kmc/, accessed on Oct. 3, 2014.

[159] "Molding Compounds for General Packages" [online]. Available: http://www.kyocera-chemi.jp/english/prdct/list/mcse/pdf/general_e.pdf, accessed on Oct. 3, 2014.

[160] "Molding Compounds for Surface Mount Devices - Standard (Br/Sb) type" [online]. Available: http://www.kyocera-chemi.jp/english/prdct/list/mcse/pdf/smd_stype_e.pdf, accessed on Oct. 3, 2014.

[161] "Molding Compounds for Power Devices" [online]. Available: http://www.kyocera-chemi.jp/english/prdct/list/mcse/pdf/power_e.pdf, accessed on Oct. 3, 2014.

[162] R. Klieber and R. Lerch, "Evaluation of Materials for High Temperature IC Packaging," *Proc. of 15th International Workshop on Thermal Investigations of ICs and Systems*, Leuven, Oct. 7-9, 2009, pp. 117-120.

[163] "High Temperature Potting and Casting Materials" [online]. Available: http://www.aremco.com/wp-content/uploads/2010/11/A04_13.pdf, accessed on Oct. 3, 2014.

[164] "Durapot Ceramics - 3000°F Potting Compounds" [online]. Available: http://www.cotronics.com/vo/cotr/pdf/801.pdf, accessed on Jul. 11, 2014.

[165] B. Grummel, R. McClure, L. Zhou, A.P. Gordon, L. Chow, and Z.J. Shen, "Design Consideration of High Temperature SiC Power Modules," *Proc. of 34th*

Annual Conference of IEEE on Industrial Electronics (IECON), Orlando, FL, Nov. 10-13, 2008, pp. 2861-2866.

[166] J. Schulz-Harder, "Advanced DBC (Direct Bonded Copper) Substrates for High Power and High Voltage Electronics," *Proc. of the 22nd IEEE Semiconductor Thermal Measurement and Management Symposium*, Dallas, TX, Mar. 14-16, 2006, pp. 230-231.

[167] L. Dupont, S. Lefebvre, Z. Khatir, and S. Bontemps, "Evaluation of Substrate Technologies under High Temperature Cycling," *Proc. of the 4th International Conference on Integrated Power Systems (CIPS)*, Naples, Italy, Jun. 7-9, 2006, pp. 1-6.

[168] J. Schulz-Harder, "Direct Copper Bonded Substrates for Semiconductor Power Devices," Technical Note, available: www.electrovac.com.

[169] P. Ning, PhD Dissertation, "Design and Development of High Density High Temperature Power Module with Cooling Systems," 2010.